

**Design of microwave networks with broadband directional couplers**

## Contents

<b>Summary .....</b>	<b>7</b>
<b>Streszczenie.....</b>	<b>8</b>
<b>List of symbols .....</b>	<b>10</b>
<b>1. Introduction.....</b>	<b>11</b>
<b>2. Microwave directional couplers, power dividers and phase shifters .....</b>	<b>18</b>
2.1. Directional couplers and power dividers with directly connected transmission lines 19	
2.2. Directional couplers and phase shifters utilizing coupled transmission lines ..... 26	
2.2.1. Single-section coupled-line directional couplers..... 26	
2.2.2. Multisection coupled-line directional couplers ..... 30	
2.2.3. Broadband phase shifters ..... 32	
2.2.4. Design of coupled-strip-transmission-line directional couplers and phase shifters with improved frequency response..... 33	
2.3. Summary..... 37	
<b>3. Directional couplers in application to balanced and <i>n</i>-way microwave circuits....</b>	<b>38</b>
3.1. Balanced and <i>n</i> -way microwave circuits..... 39	
3.2. Large signal characterization of solid-state devices..... 46	
3.3. Asymmetric coupled-line directional couplers as impedance transformers in balanced and <i>n</i> -way power amplifiers ..... 52	
3.4. Approach to the design of asymmetric coupled-line impedance transforming directional couplers ..... 63	
3.5. Broadband asymmetric coupled-line impedance transforming directional couplers 73	
3.6. Summary..... 78	
<b>4. Broadband Butler matrices utilizing coupled-line directional couplers.....</b>	<b>79</b>
4.1. Butler matrices utilizing single-section coupled-line directional couplers ..... 82	
4.1.1. 4 x 4 Butler matrix ..... 82	
4.1.2. 8 x 8 Butler matrix ..... 87	
4.2. Butler matrices utilizing multisection coupled-line directional couplers ..... 92	
4.3. Butler matrices with the use of 0/180° directional couplers ..... 117	
4.4. Summary..... 123	
<b>5. Design of miniaturized broadband directional couplers .....</b>	<b>125</b>
5.1. Miniaturization techniques in the design of microwave directional couplers ..... 125	
5.2. Design of broadband quasi-lumped directional couplers ..... 131	
5.3. Summary..... 145	
<b>6. Final remarks .....</b>	<b>146</b>
<b>References .....</b>	<b>148</b>

KRZYSZTOF WINCZA

## **Design of microwave networks with broadband directional couplers**

### **Summary**

The monograph focuses on the design of complex microwave networks with the use of broadband coupled-line directional couplers. Three different areas of the design and application of such couplers have been addressed, which are:

1. Design of coupled-line impedance transforming directional couplers.
2. Design of broadband Butler matrices utilizing coupled-line directional couplers.
3. Design of miniaturized directional couplers with the use of quasi-lumped-element technique.

All aspects have been comprehensively researched by the Author over the recent years. In particular, the application of asymmetric coupled-line directional couplers in balanced and  $n$ -way power amplifiers has been described, and the design of such circuits has been shown with the emphasis on their impedance transforming capability. The major advantage of the proposed approach is that it allows to realize both power dividing and impedance matching within a single component. Single-section and multisection impedance transforming directional couplers are analyzed and the achievable impedance transformation ratio for such couplers is derived.

The second issue presented in the monograph concerns the design of broadband Butler matrices. A method for the design of broadband Butler matrices utilizing coupled-line directional couplers is presented, in which multisection symmetrical coupled-line directional couplers are used. The method proposed by the Author of broadband differential phase shifters' realization for applications in such networks, is outlined. It is shown, that the design of broadband Butler matrices with the use of multisection directional couplers requires applying of Schiffman 'C'-sections in order to minimize the phase imbalance of the resulting network. Moreover, a novel arrangement of an  $8 \times 8$  Butler matrix is proposed, that allows for planar fully integrated realization.

Finally, the design method of miniaturized broadband directional couplers, developed by the Author, is described, in which a quasi-lumped-element technique is used. The proposed approach allows for achieving the frequency response of miniaturized couplers comparable to the response of their distributed counterparts. Moreover, the method allows for achieving broad bandwidths, due to its suitability for the design of multisection miniaturized directional couplers.

The presented theoretical analyses have been confirmed by the measurements of a number of manufactured coupled-line networks.

KRZYSZTOF WINCZA

**Projektowanie układów mikrofalowych wykorzystujących szerokopasmowe sprzęgacze kierunkowe**

## Streszczenie

W niniejszej monografii przedstawione zostały zagadnienia związane z projektowaniem złożonych sieci mikrofalowych wykorzystujących szerokopasmowe sprzęgacze kierunkowe. Przedstawione zostały następujące trzy różne aspekty projektowania i zastosowań szerokopasmowych sprzęgaczy o liniach sprężonych:

1. Projektowanie sprzęgaczy o liniach sprężonych transformujących impedancję.
2. Projektowanie szerokopasmowych macierzy Butlera wykorzystujących sprzęgacze o liniach sprężonych.
3. Projektowanie zminiaturyzowanych szerokopasmowych sprzęgaczy kierunkowych z wykorzystaniem techniki elementów quasi skupionych.

Wymienione obszary zostały dogłębnie przeanalizowane przez Autora monografii na przestrzeni ostatnich kilku lat. W szczególności, przeanalizowana została możliwość zastosowania asymetrycznych sprzęgaczy kierunkowych w zrównoważonych wzmacniaczach mocy mikrofalowej oraz w układach z sumowaniem mocy, biorąc pod uwagę możliwy do pozyskania stosunek impedancji obciążenia we wrotach wejściowych i wyjściowych. Główną zaletą zaproponowanych rozwiązań jest możliwość jednoczesnej realizacji funkcji podziału mocy i dopasowania impedancyjnego w jednym układzie. Przeanalizowane zostały zarówno układy jednosekcyjnych jak i wielosekcyjnych asymetrycznych sprzęgaczy kierunkowych i wyprowadzone zostały zależności opisujące możliwy do pozyskania w tych układach stosunek impedancji.

Kolejnym przedstawionym w pracy zagadnieniem jest projektowanie szerokopasmowych macierzy Butlera. Opisana została metoda projektowania takich układów z wykorzystaniem wielosekcyjnych sprzęgaczy kierunkowych o liniach sprężonych. Zaprezentowana została także, opracowana przez Autora, metoda realizacji szerokopasmowych przesuwników fazy o stałym różnicowym przesunięciu fazy wykorzystywanych w układach macierzy Butlera. Przeprowadzone analizy wykazały, że projektowanie szerokopasmowych macierzy Butlera wykorzystujących wielosekcyjne sprzęgacze o liniach sprężonych wymaga zastosowania sekcji 'C' przesuwników fazy Schiffmana w celu minimalizacji rozrównoważenia charakterystyk fazy różnicowej. Dodatkowo, w pracy zaproponowane zostało nowe rozwiązanie układowe pozwalające na realizację w pełni planarnej, zintegrowanej macierzy Butlera 8 x 8.

Ostatnim zagadnieniem przedstawionym w monografii jest metoda projektowania szerokopasmowych zminiaturyzowanych sprzęgaczy kierunkowych, zaproponowana przez Autora, w której znaczne zmniejszenie rozmiaru realizowanych układów pozwala się poprzez zastosowanie techniki elementów quasi skupionych. Opracowana metoda pozwala na realizację miniaturowych sprzęgaczy kierunkowych cechujących się parametrami po-

równywalnymi ze sprzegaczami zrealizowanymi w technice sprężonych linii transmisyjnych. Ponadto, metoda ta umożliwia pozyskanie szerokiego pasma pracy, ze względu na fakt, że pozwala na projektowanie wielosekcyjnych, zminiaturyzowanych sprzegaczy kierunkowych.

Przedstawione w pracy analizy teoretyczne zostały potwierdzone poprzez pomiary wykonanych modeli zaprojektowanych i wykonanych układów mikrofalowych.

## List of symbols

$\beta$	-	phase constant
$\Gamma$	-	reflection coefficient
$\epsilon_0$	-	permittivity of free space
$\mu_0$	-	permeability of free space
$\lambda_0$	-	free space wavelength
$\lambda_g$	-	guided wavelength
$\theta_0$	-	electrical length
$v_{pe}, v_{po}$	-	even, odd mode phase velocity
$\epsilon_r$	-	dielectric constant (relative permittivity)
$\epsilon_{ree}, \epsilon_{reo}$	-	effective dielectric constant (relative permittivity) for even, odd mode
$BW$	-	operational bandwidth
$C$	-	capacitance matrix
$c$	-	free space light velocity
$C$	-	coupling
$C_{1,2}$	-	per unit length capacitance of line 1, 2
$C_e, C_o$	-	per unit length even, odd mode capacitance of coupled lines
$C_m$	-	per unit length mutual capacitance of coupled lines
$D$	-	directivity
$I$	-	isolation
$IL$	-	insertion losses
$k$	-	coupling coefficient
$k_L, k_C$	-	inductive, capacitive coupling coefficient
$L$	-	inductance matrix
$l$	-	length of a coupled-line section
$L_{1,2}$	-	per unit length self inductance of line 1, 2
$L_m$	-	per unit length mutual inductance of coupled lines
$R$	-	impedance ratio of the transformer
$RL$	-	return losses
$S$	-	scattering matrix
$S^{e,o}$	-	scattering matrix for even and mode excitation
$T$	-	transmission
$Z_0$	-	characteristic impedance
$Z_{0e}, Z_{0o}$	-	even, odd mode characteristic impedance
$Z_{T1,2}$	-	1 <sup>st</sup> , 2 <sup>nd</sup> line terminating impedance
$VSWR$	-	voltage standing wave ratio

# 1. Introduction

In the design of microwave circuits, directional couplers and power dividers/combiners constitute an important class of passive components, due to variety of their applications. One can name antenna feeding networks, balanced mixers, balanced amplifiers, reflectometer bridges, six-port networks for complex reflection coefficient measurements, etc. Among directional couplers two general groups of networks can be distinguished, which are: directly connected couplers and power dividers/combiners and coupled-line couplers and power dividers/combiners. These two groups of networks differ by the principle of operation and, therefore, by their properties. In the first group a circuit is formed by a network consisting of a number of directly connected transmission-line sections. A well-known example of such a device, is a branch-line directional coupler, which is – as all the directional couplers in general – a four-port lossless network, in which a signal delivered to the input port is divided with the specified ratio between the coupled and direct ports. At the fourth port – called isolated port – no power is received. The most broadly 3-dB quadrature couplers are used, in which the input power is equally split between the coupled and transmission ports. Additionally, such couplers have unique phase properties, i.e. the signals received at coupled and transmission ports are  $90^\circ$  out-of-phase. Another well-known device belonging to the group of directional couplers having directly connected transmission-lines is a rat-race coupler, in which the phase relation is different from the branch-line coupler. In this case the signals received at the coupled and transmission ports are  $180^\circ$  out-of-phase.

The second group of devices utilizes electromagnetic coupling between transmission lines, which are not directly connected, and the power from the main line is coupled electromagnetically to the second line. The basic component belonging to this group, is a quarterwave-long directional coupler having the property of  $90^\circ$  differential phase characteristic, similarly to the branch-line coupler. The two groups of devices differ in their construction, but what is more important from the application point of view, also significantly differ by their properties. The directly connected transmission-line components feature narrow operational bandwidth, and therefore, are not suited for modern telecommunication applications, where it is required to operate in relatively large bandwidths, or alternatively in multiple bands with the use of single hardware. Such a demand can be met when coupled-line directional couplers are applied. Apart from allowing for broadband operation, they also provide for significant miniaturization, since the area needed for a typical 3-dB branch-line coupler is much greater than the area of its coupled-line counterpart.

The design of coupled-line directional couplers has been a subject of extensive studies over the years, starting from early works [29, 31, 90, 92, 93, 104, 112, 137], where the basic parameters of coupled-line directional couplers have been formulated. The beginning of TEM coupled-line couplers is dated to mid 50s', when two-wire coupled symmetrical lines and coupled striplines have been considered. The development of symmetrical coupled-line couplers, in which the coupled-line structure features symmetry between coupled conductors, led to the description of coupled-line section properties, in terms of even- and odd mode characteristic impedances, which are directly related to the coupling of the coupler and its terminating impedances. It was also shown in [29, 92, 93, 137], that the bandwidth of such couplers can be further increased by a cascade connection of a number of coupled-line sections having appropriately chosen coupling coefficients. Another class of directional couplers offering very broad frequency response is the class of tapered-line couplers, in which the coupling coefficient continuously changes along the coupled lines. Theoretically, tapered-line asymmetric directional couplers have high-pass frequency characteristics, however – in practice – the bandwidth is limited by the discontinuity effects in the region of connection of signal and coupled lines and also by the manufacturing tolerances.

Further, in mid 70s' asymmetric coupled-line structures became of interest of research community, since such components can be easier incorporated into modern microwave integrated circuits and monolithic microwave integrated circuits. In this class of couplers, no symmetry between coupled conductors exists, and the properties of such structures are defined by modal impedances of  $\pi$  and  $c$  modes, and by the respective voltage mode numbers. The theoretical analysis of asymmetric coupled-transmission-lines has been shown in several papers [30, 146, 147, 148, 149, 150]. It has been shown, that such couplers feature neither perfect isolation nor perfect impedance match, unless the two conditions of quasi-ideal coupled-line section realization are fulfilled, i.e. the inductive and capacitive coupling coefficients are equal and the coupled conductors are terminated by appropriate impedances [127]. A lot of attention has been paid to the development of different methods that allow for quasi-ideal asymmetric coupled-line directional coupler realization [41, 125, 126, 130].

The Author has focused at the early stage of his research on the design methods of high-performance broadband couple-line directional couplers, in which capacitive elements are added to the coupled-lines in various cross-sections and to the signal lines. Such an approach allows for significant improvement of the couplers' properties. The capacitive components compensate the parasitic reactances within the coupled-line structures which severely deteriorate their performance, especially their return losses and isolation [63, 64, 65, 69, 71]. Secondly, the methods have been proposed which allow for meeting the conditions of ideal coupler realization in symmetric and asymmetric structures with the use of lumped-element technique [62, 165, 167]. In one of the recent co-authored papers [72] the generalized methods for the design of quasi-ideal symmetric and asymmetric coupled-line sections have been proposed. The presented approach allows for designing directional couplers with improved performance over broad frequency range in arbitrary dielectric structures, in which the inductive coupling coefficient is either greater or smaller than the capacitive one. The developed methods allowed for the design of a number of high-performance single and multisection directional couplers, in both symmetric and asymmetric coupled-line structures [60, 61, 62, 63, 64, 65, 69, 71, 72, 165, 166, 167, 169].

This monograph is focused on the application of broadband high-performance coupled-line sections in complex microwave networks within the three areas of applications, that have been comprehensively investigated by the Author, which are:

1. high power amplifiers,
2. broadband Butler matrices,
3. broadband miniaturized directional couplers.

The design of high-power, solid-state amplifiers operating in a microwave frequency range is most often approached by the use of multiple-transistor power stages, in which the input power is appropriately distributed among the power amplifiers, each having output power being a fraction of the total output power. The total output power is obtained by combining the power from all the amplifier stages with the use of a power combining network. Typically, the components used for the design of power dividing/combining at microwave frequencies are the directly connected branch-line directional couplers, Wilkinson dividers or Gysel-type dividers [54, 75, 171, 175]. Such networks feature relatively large dimensions in a lower frequency range, and also can introduce insertion losses, limiting the maximum output power of an amplifier. The Author has proposed in [179] an alternative approach to the design of power dividing/combining networks, in which asymmetric coupled-line directional couplers are utilized. As it was shown, such couplers are utmost suitable for the design of balanced power amplifiers and corporate networks of  $N$ -way amplifiers, allowing for a size reduction of the resulting network and, what follows directly from the size reduction, allowing for insertion losses minimization. Moreover, it has been shown that such couplers can provide for impedance transformation, apart from splitting/combining microwave signals. By the appropriate design, an asymmetric coupled-line directional coupler can have properties of an ideal directional coupler at a center frequency, when transmission and coupled ports are terminated with impedances lower (or higher), than the source impedance. It is therefore possible to design networks having the output impedance much lower than the source impedance, which is typically required since the solid-state high-power devices usually feature input/output impedances well below  $10 \Omega$ . Impedance transformation within power dividing/combining networks approaches the aspect of miniaturization of amplifier units, and minimization of losses within the network. As it was shown, the coupled-line power transforming directional couplers do not feature the properties of an ideal directional coupler in a wide frequency range, but operate in a frequency range sufficient for such applications, since they offer the bandwidth wider than the branch-line couplers or single-section impedance transformers. It has also been shown that the operational bandwidth can be increased by designing multisection impedance-transforming directional couplers. Such directional couplers combine in a single component the idea of broadband asymmetric multisection directional couplers, described in [92, 93], and multisection impedance transformers, presented in [122].

Another important class of microwave networks, in which high-performance coupled-line sections find broad range of applications are Butler matrices. Such networks have been first introduced in [12] and are widely used in contemporary microwave electronics. Generally, an  $N \times N$  Butler matrix is a multiport network having  $N$  inputs and  $N$  outputs, in which a signal applied to one of its input ports is equally divided into all output ports. Moreover, the signals received at output ports feature phase shifts dependent on the matrix order and the choice of the excitation port. These unique properties result in a broad range of their applications in contemporary communication systems; e.g. as beamforming networks of multibeam antennas [4, 6, 10, 13, 17, 18, 26, 35, 36, 37, 45, 48, 49, 50, 61, 67, 68, 79, 80, 87, 94, 115, 136, 158, 159, 161, 163, 164, 169], in direction finding systems [96, 141], or in multichannel amplifiers [7, 34, 117, 176]. Recently, large attention has been paid to the design of such networks in various structures. Most of the described Butler matrices have

been realized with the use of branch-line couplers developed in different waveguiding structures, such as microstrip, stripline coplanar waveguide, slotline or rectangular waveguide [34, 45, 49, 77, 87, 109, 110, 111, 117, 156]. As it was already mentioned, such networks feature disadvantages of the applied couplers, which is narrow operational band and relatively large space. Wider operational bandwidth can be achieved when multisection branch-line couplers are applied at the expense of much larger occupied area [36, 44, 50]. There are few examples of realization of Butler matrices with the use of coupled-line directional couplers. In [10] a compact 4 x 4 Butler matrix is presented, in which broadside coupled-line directional couplers are used. However, in this design the bandwidth is limited by the application of narrow phase shifters realized as sections of transmission lines.

The Author has researched the possibility of broadband Butler matrices realization for application in multibeam antennas with the use of single-section coupled-line directional couplers and the results are published in a number of papers [61, 67, 158, 159, 161, 163, 164, 169]. In [164, 169] a broadband 4 x 4 Butler matrix, which consists of six single-section coupled-line directional couplers designed in a stripline technique has been described. In this solution a tandem connection of two couplers serves as a transmission-line crossover and provides, together with sections of transmission lines, broadband 45° phase shifters. A similar approach of a broadband 4 x 4 Butler matrix realization can be applied in an asymmetric microstrip structure, as it was shown in [61]. Apart from communication system applications, Butler matrices are used as a basic element of instantaneous direction finding systems, primarily for military applications. In such systems it is required for the networks to operate in a very wide frequency range. The Author has also focused on the design and development of ultrabroadband Butler matrices. In [68] an innovative approach of broadband multi-octave 4 x 4 Butler matrices' realization has been shown, in which multisection symmetrical 3dB/90° directional couplers are applied.

Higher order Butler matrices, such as 8 x 8 or higher, are rarely reported, due to their large complexity, and therefore, difficulties with designing and manufacturing as integrated units. Exemplary designs can be found in [17, 153, 118], where different techniques such as LTCC, CMOS or rectangular waveguide have been applied. An impressive design of an 8 x 8 Butler matrix is presented in [35]. In this work a tandem connection of tapered-line directional couplers having coupling  $C = 8.34$  dB have been used as a broadband 3-dB directional coupler and discretely stepped 6-section F-type Schiffman networks have been used to form the needed phase shifters. The obtained bandwidth of the developed 8 x 8 Butler matrix equals  $BW = 9:1$ . However, the matrix has been designed in a modular fashion, and the modules have been connected with the coaxial cables. A possibility of realization of fully integrated broadband 8 x 8 Butler matrices with the use of coupled-line directional couplers has been also investigated by the Author.

The third aspect addressed in this monograph concerns miniaturization of broadband directional couplers. The problem of size reduction of passive components is especially important at lower frequency ranges, where the size of components becomes significant. Moreover, the size reduction is a primary objective, when a passive component is to be directly used in advanced technologies such as LTCC or MMIC. Miniaturization of microwave circuits is often approached with the use of lumped or semi-lumped-element techniques [15, 39, 157]. Many authors have focused on miniaturization of directly connected transmission-line directional couplers and power dividers. The principles of the design of lumped-element branch-line couplers have been comprehensively investigated, and the design procedures for various realizations of such networks have been shown in [157]. In

[20, 23], rat-race couplers are presented, in which open stubs and coupled-line ‘C’-sections are used, respectively, for providing significant miniaturization. Other designs of miniaturized directly connected transmission-line couplers and power dividers can be found in [19, 85, 86, 107, 113, 128, 129, 142, 151, 154, 174, 177]. Exemplary realizations of similar components in LTCC and MMIC technology can be found in [42, 76, 88, 98, 138], where lumped-element approach is utilized. In this approach sections of transmission lines are substituted by networks consisting of lumped capacitors and inductors.

Since much broader bandwidth can be achieved with the use of coupled-line directional couplers an effort has been made to develop miniaturized versions of such devices. The commonly used approach assume very simple equivalent circuit of coupled lines consisting of only single-section approximation [8, 47, 91, 139, 155]. The obtained performance of such couplers is limited by the assumed equivalent circuit, and is reflected in the poor amplitude characteristics which narrow the coupler’s operational bandwidth.

The Author has focused on the design of miniaturized directional couplers having attractive frequency response comparable with the distributed coupled-line directional couplers [166]. The influence of the number of subsections used for approximation of a coupled-line directional coupler on the resulting performance has been investigated. The performed analysis reveal that three subsections are sufficient for realization of directional couplers having good properties in a wide frequency range, which on the other hand ensures a significant miniaturization of the circuit.

A general description of microwave passive components with directly connected transmission-lines is presented in the second chapter followed by the introduction to the coupled-line directional couplers. The description of modal analysis of symmetrical coupled lines has been shown together with the formulas for inhomogeneous dielectric stratification. Further, multisection coupled-line directional couplers are briefly described showing the possibility of broadening the couplers’ operational bandwidth. The chapter is concluded with a brief overview of the methods investigated by the Author, which allow for the design of coupled-line sections and directional couplers with improved performance.

The third chapter focuses on the design of directional couplers in applications to balanced and  $n$ -way microwave circuits. A general theory of balanced amplifiers is presented showing their main advantages. Subsequently, a method for large-signal characterization of microwave power transistors is described, in which rat-race couplers with sections of shorted transmission lines are used, as input and output tuning circuits. It has been shown, that such a rat-race coupler allow for realization of any passive impedance, therefore, can be utilized as a lossless matching network at the input and output of a power transistor. Further, a novel approach has been presented, in which asymmetric coupled-line 3-dB directional couplers are used as simultaneous power dividers and impedance transformers. It has been shown, that such a coupler can offer the properties of an ideal directional coupler having equal terminating impedances at coupled and transmission ports different than the terminating impedances of the excited and isolated ports. Further analysis reveal that physically realizable impedance transformation ratio is limited, and for the case of a 3-dB directional coupler equals 2. Then it is possible to design 3-dB asymmetric directional couplers transforming simultaneously  $50\ \Omega$  signal source impedance into  $25\ \Omega$  load. Higher transformation ratios can be obtained when corporate networks consisting of appropriately designed 3-dB impedance transforming directional couplers are used. The theoretical considerations have been confirmed by the design of a 4-way power amplifier operating in L-band. Further, an alternative approach to the analysis and design of 3-dB impedance trans-

forming directional couplers having the maximum obtainable impedance ratio has been presented. In this approach coupled-lines are replaced by the appropriate connection of two uncoupled transmission-line sections. Also an exemplary realization is shown, in which the coupler is composed of a coaxial transmission-line section in conjunction with a microstrip section. Finally, the possibility of realization of broadband coupled-line impedance transforming directional couplers is presented. As an example, the design of a two-section directional coupler operating over 3:1 frequency band and having the impedance ratio equal 1.43 is shown.

In the fourth chapter broadband Butler matrices are described and their basic properties and applications are outlined. A brief overview of the developed broadband 4 x 4 Butler matrices utilizing single-section coupled-line couplers have been presented. Two designs in different coupled-line structures are shown, in which a tandem connection of two 3-dB/90° coupled-line directional couplers in conjunction with transmission-line sections of appropriate length are used, for simultaneous realization of a transmission-line crossover and broadband 45° phase shifters. Subsequently, a novel arrangement of an 8 x 8 Butler matrix is proposed, that allows for realization of a fully integrated, planar circuit operating over a broad frequency range. The proposed method has been experimentally verified by measurements of the 8 x 8 Butler matrix operating over 2.5-3.5 GHz frequency range, proving the usefulness of the presented approach. The chapter also describes the realization of broadband Butler matrices in which multisection 3-dB symmetrical directional couplers are utilized. It is shown that in order to extend the idea of broadband 45° phase shifters' realization with the use of a tandem connection of 3-dB couplers, it is required to apply phase correcting networks consisting of multisection coupled-line Schiffman 'C'-sections in conjunction with transmission-line sections. A class of 4 x 4 Butler matrices being a connection of multisection 3dB/90° symmetrical coupled-line directional couplers has been investigated, and tables giving normalized even-mode impedances of the phase correction networks needed for respective coupled-line couplers have been provided. The proposed concept has been experimentally verified by two designs of 4 x 4 Butler matrices utilizing three-section directional couplers, and an ultrabroadband Butler matrix operating within 1.8 – 12 GHz frequency range designed with the use of five-section directional couplers. The presented concept has been also extended on 8 x 8 broadband Butler matrices and confirmed by the design of an 8 x 8 Butler matrix with the use of five-section directional couplers. Finally, Butler matrices consisting of tapered-line directional couplers have been considered.

The fifth chapter presents the results of Author's investigation on the design of miniaturized directional couplers having the properties of coupled-line distributed couplers. The proposed design method allows for significant miniaturization for structures, in which the achievable inductive coupling coefficient is much greater than the nominal coupling of the designed coupler. The proposed approach is based on quasi-lumped technique, in which coupled-inductors are realized as short sections of tightly-coupled transmission lines, while the needed self and mutual capacitances are realized as lumped capacitors. The presented method allows one to achieve good properties of the designed couplers over a wide frequency range with significant miniaturization of the circuit. Moreover, the Author has shown that such a technique is suitable for realization of broadband multisection directional couplers.

The Author previously published works related to the design of microwave networks utilizing broadband directional couplers are cited in large extend throughout the scope of the monograph [59, 60, 61, 68, 164, 166, 168, 179].

The research results presented in this monograph have been in large part financially supported by the Polish Ministry of Science and Higher Education under the following research grants:

1. Research grant no. 0464/T02/2010/70, *Microwave coupled-line circuits - design, optimization and applications in modern telecommunication devices and systems*, realized at the AGH University of Science and Technology under the supervision of the Author.
2. Research grant no. N515361936, *Broadband microwave Butler matrices designed in coupled stripline techniques*, realized at the Wroclaw University of Technology with the Author's substantial contribution.
3. Research grant no. 4999/B/T02/2011/40, *Miniaturized microwave broadband directional couplers designed with the use of quasi-lumped technique*, realized at the AGH University of Science and Technology under the supervision of the Author.

## **2. Microwave directional couplers, power dividers and phase shifters**

Directional couplers and power dividers find broad applications in microwave networks and systems. They perform a variety of functions, such as splitting and combining power in mixers, sampling power of sources for level control, separating incident and reflected signals in network analyzers, or dividing power among a number of loads. Generally two types of networks can be distinguished:

1. connected-line couplers and power dividers,
2. coupled-line couplers and power dividers.

The chosen realization technique implies the properties of designed components, especially the operational bandwidth. The most simple and well-known among power dividers is the Wilkinson power divider, which belongs to the first type of networks. The basic Wilkinson power divider operates in relatively narrow band, but a modification in which more than one section of transmission line pairs is applied allows for the bandwidth broadening. Such elements can also be designed with the use of coupled-line sections, which also improve the operational bandwidth. In case of directional couplers a significant difference in frequency response is observed between the couplers realized with the use of connected-line technique and the ones designed with the use of coupled-line technique. The first group of couplers, among which a branch-line coupler is the most common example, features narrow operational bandwidth which can be also enhanced by applying a multisection branch-line coupler at the expense of significant increase of the couplers' dimensions, and therefore, insertion losses. Significant improvement of operational band is achieved when coupled-line directional couplers are used. A single-section of coupled lines can constitute a directional coupler having operational bandwidth up to one frequency octave, which can be further enhanced by designing multisection coupled-line directional couplers.

In this Chapter a brief introduction to the connected-line couplers and power dividers has been shown and the properties of both 3-dB Wilkinson power dividers and directional couplers have been described. Further, an analysis of a coupled-line section has been presented and its utilization for designing single-section and multisection symmetrical as well as asymmetrical directional couplers and phase shifters, has been outlined. Finally, the conditions of ideal coupler realization in symmetric and asymmetric coupled-line structures have been described and exemplary designs of single-section 3-dB and 8.34-dB directional couplers realized in symmetric stripline technique and a three-section 3-dB directional coupler designed in multilayer microstrip techniques, have been shown.

## 2.1. Directional couplers and power dividers with directly connected transmission lines

Power dividers and directional couplers are passive microwave components used for power division and power combining. A signal applied to the input port is divided by the coupler/divider into two or more signals of lower power. Typically the power divider is a 3-port lossy or lossless component and take the form of T-junction, but also dividers with greater number of ports can be pointed out for  $n$ -way power splitting, whereas, a directional coupler is a 4-port component.

The simplest type of power divider is a T-junction which is a 3-port network having one input and two output ports. The scattering matrix of a 3-port network has nine independent elements:

$$[S] = \begin{bmatrix} S_{11} & S_{12} & S_{13} \\ S_{21} & S_{22} & S_{23} \\ S_{31} & S_{32} & S_{33} \end{bmatrix} \quad (2.1)$$

For a passive circuit that contains no anisotropic materials its  $S$  matrix must be symmetric ( $S_{ij} = S_{ji}$ ) and the circuit must be reciprocal. It is also desirable that the circuit does not introduce power losses, which means that the T-junction should be lossless and matched at all ports. However, it can be easily shown that it is impossible to construct a 3-port network that is lossless, reciprocal and matched at all ports.

If all ports of the network are matched then all diagonal elements of its  $S$  matrix are zero, and taking into account reciprocal properties, the  $S$  matrix takes form

$$[S] = \begin{bmatrix} 0 & S_{12} & S_{13} \\ S_{12} & 0 & S_{23} \\ S_{13} & S_{23} & 0 \end{bmatrix} \quad (2.2)$$

If the circuit is also lossless then its  $S$  matrix has to be unitary [120], which leads to the following conditions [120]

$$|S_{12}|^2 + |S_{13}|^2 = 1 \quad (2.3)$$

$$|S_{12}|^2 + |S_{23}|^2 = 1 \quad (2.4)$$

$$|S_{13}|^2 + |S_{23}|^2 = 1 \quad (2.5)$$

$$S_{13}^* S_{23} = 0 \quad (2.6)$$

$$S_{23}^* S_{12} = 0 \quad (2.7)$$

$$S_{12}^* S_{13} = 0 \quad (2.8)$$

Equations (2.6 – 2.8) show that at least two of the three parameters ( $S_{12}$ ,  $S_{13}$ ,  $S_{23}$ ) must be zero which is inconsistent with one of the three equations (2.3 – 2.5). It implies that a three-port network cannot be lossless, reciprocal, and matched at all ports. By relaxing one of these three conditions physically realizable circuit can be achieved. If the 3-port network is allowed to be lossy, it can be reciprocal and matched at all ports. The most common example of such a device is the Wilkinson power divider, shown in Fig. 2.1. In this element, output signals are in-phase and have equal amplitude, and also the output ports are ideally isolated at the center frequency. The circuit is composed of two  $\lambda_g/4$  transmission-line sections having characteristic impedance equal  $\sqrt{2}Z_0$  and a lumped resistor connecting the output ports and having value  $2Z_0$ , where  $Z_0$  is the terminating impedance of all three ports of the divider. The frequency response of the Wilkinson power divider is shown in Fig. 2.2.  $S$  matrix of such an element has the following form [120]:

$$[S] = \frac{1}{\sqrt{2}} \begin{bmatrix} 0 & -j & -j \\ -j & 0 & 0 \\ -j & 0 & 0 \end{bmatrix} \quad (2.9)$$

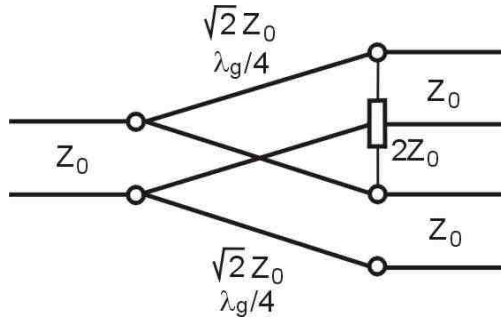


**Fig. 2.1.** Equivalent transmission-line circuit of the Wilkinson power divider.

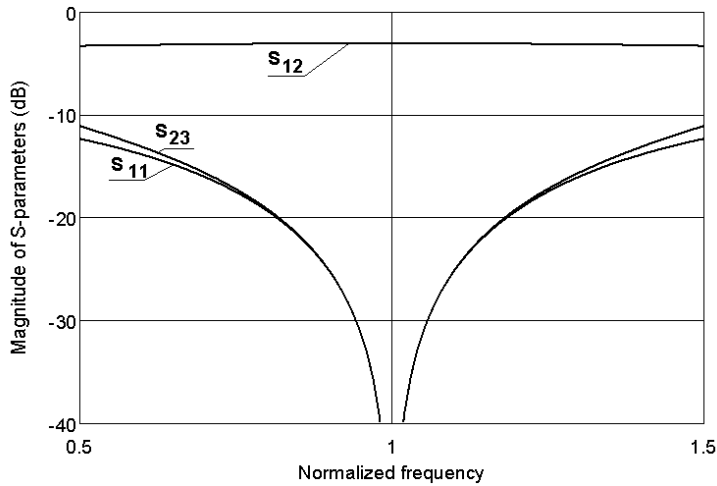


**Fig. 2.2.** Frequency response of an equal-split Wilkinson power divider.

In case of a four-port reciprocal network, which is matched at all ports, its  $S$  matrix has the following form

$$[S] = \begin{bmatrix} 0 & S_{12} & S_{13} & S_{14} \\ S_{12} & 0 & S_{23} & S_{24} \\ S_{13} & S_{23} & 0 & S_{34} \\ S_{14} & S_{24} & S_{34} & 0 \end{bmatrix} \quad (2.10)$$

If the network is lossless, the equations result from the unitarity or energy conservation condition [120]. Considering the multiplication of row 1 and row 2, and multiplication of row 3 and row 4:

$$S_{13}^* S_{23} + S_{14}^* S_{24} = 0 \quad (2.11)$$

$$S_{14}^* S_{13} + S_{24}^* S_{23} = 0 \quad (2.12)$$

When multiplying (2.11) by  $S_{24}^*$  and multiplying (2.12) by  $S_{13}^*$  and subtracting the two, the following expression is obtained

$$S_{14}^* \left( |S_{13}|^2 - |S_{24}|^2 \right) = 0 \quad (2.13)$$

Similarly, the multiplication of row 1 and row 3 and the multiplication of row 4 and row 2, gives

$$S_{12}^* S_{23} + S_{14}^* S_{34} = 0 \quad (2.14)$$

$$S_{14}^* S_{12} + S_{34}^* S_{23} = 0 \quad (2.15)$$

When multiplying (2.14) by  $S_{12}$  and multiplying (2.15) by  $S_{34}$  and subtracting the two, the following formula is obtained

$$S_{23} \left( |S_{12}|^2 - |S_{34}|^2 \right) = 0 \quad (2.16)$$

One way for (2.13) and (2.16) to be met is if  $S_{14} = S_{23} = 0$ , which results in a directional coupler circuit. Then the self-products of the rows of the unitary  $S$  matrix (2.10) yield the following equations

$$|S_{12}|^2 + |S_{13}|^2 = 1 \quad (2.17)$$

$$|S_{12}|^2 + |S_{24}|^2 = 1 \quad (2.18)$$

$$|S_{13}|^2 + |S_{34}|^2 = 1 \quad (2.19)$$

$$|S_{24}|^2 + |S_{34}|^2 = 1 \quad (2.20)$$

which imply that  $|S_{13}| = |S_{24}|$  (using (2.17 – 2.18)) and  $|S_{12}| = |S_{34}|$  (using (2.19 – 2.20)). Choosing the phase references on three of the four ports as  $S_{12} = S_{34} = \alpha$ ,  $S_{13} = \beta e^{j\theta}$  and  $S_{24} = \beta e^{j\phi}$ , where  $\alpha$  and  $\beta$  are real and  $\theta$  and  $\phi$  are phase constants to be determined (one of which is still free to choose), further simplification is achieved. The dot product of rows 2 and 3 of the  $S$  matrix gives

$$S_{12}^* S_{13} + S_{24}^* S_{34} = 0 \quad (2.21)$$

which yields a relation between the phase constants as

$$\theta + \phi = \pi \pm 2n\pi \quad (2.22)$$

There are two particular cases that occur in practice [120]:

1. The symmetrical coupler, for which  $\theta = \phi = \pi/2$ . When the phases of the terms having amplitude  $\beta$  are chosen equal, then the scattering matrix has the following form

$$[S] = \begin{bmatrix} 0 & \alpha & j\beta & 0 \\ \alpha & 0 & 0 & j\beta \\ j\beta & 0 & 0 & \alpha \\ 0 & j\beta & \alpha & 0 \end{bmatrix} \quad (2.23)$$

2. The antisymmetrical coupler, for which  $\theta = 0$ ,  $\phi = \pi$ . When the phases of the terms having amplitude  $\beta$  are chosen to be  $180^\circ$  apart, then the scattering matrix has the following form

$$[S] = \begin{bmatrix} 0 & \alpha & \beta & 0 \\ \alpha & 0 & 0 & -\beta \\ \beta & 0 & 0 & \alpha \\ 0 & -\beta & \alpha & 0 \end{bmatrix} \quad (2.24)$$

The two couplers differ only in the choice of reference planes and the amplitudes  $\alpha$  and  $\beta$  are not independent because (2.17 – 2.20) requires that

$$\alpha^2 + \beta^2 = 1 \quad (2.25)$$

Thus, apart from phase references, an ideal directional coupler features only one degree of freedom. The basic operation of an ideal directional coupler is illustrated in Fig. 2.3, which shows the directional coupler's port definitions. Power delivered to port #1 is coupled to

port #3 – the coupled port, with the coupling factor  $|S_{13}|^2 = \beta^2$ , while the remaining input power is delivered to port #2 – the transmission port, with the coefficient  $|S_{12}|^2 = \alpha^2 = 1 - \beta^2$ , and no power is delivered to port #4 – the isolated port. The following three quantities describe the properties of the directional coupler [39]:

$$Coupling = C = 10 \log \frac{P_1}{P_3} = -20 \log \beta \quad [\text{dB}] \quad (2.26)$$

$$Directivity = D = 10 \log \frac{P_3}{P_4} = -20 \log \frac{\beta}{|S_{14}|} \quad [\text{dB}] \quad (2.27)$$

$$Isolation = I = 10 \log \frac{P_1}{P_4} = -20 \log |S_{14}| \quad [\text{dB}] \quad (2.28)$$

The coupling factor indicates the part of the input power that is coupled to the output port, whereas, the directivity is a measure of a coupler's ability to isolate forward and backward waves, as is the isolation. These three quantities are related as

$$I = D + C \quad [\text{dB}] \quad (2.29)$$

The ideal directional coupler has infinite directivity and isolation and both amplitudes  $\alpha$  and  $\beta$  can be determined from the coupling factor  $C$ .

Hybrid couplers are special cases of directional couplers, where the coupling equals 3 dB, which implies that  $\alpha + \beta = 1/\sqrt{2}$ . There are two types of hybrids, i.e. the quadrature hybrid (the branch-line coupler) and the magic-T hybrid (the rat-race coupler). A quadrature coupler consists of four quarter-wave long transmission lines, two of them having characteristic impedance equal  $Z_0$ , the other two equal  $Z_0/\sqrt{2}$  appropriately connected, as shown in Fig. 2.3. The power entering port #1 is evenly divided between ports #2 and #3, with  $90^\circ$  phase shift between these outputs. No power appears in port #4 (the isolated port). Thus, the  $S$  matrix has the following form:

$$[S] = \frac{-1}{\sqrt{2}} \begin{bmatrix} 0 & j & 1 & 0 \\ j & 0 & 0 & 1 \\ 1 & 0 & 0 & j \\ 0 & 1 & j & 0 \end{bmatrix} \quad (2.30)$$

It is seen that the branch-line coupler has a high-degree of symmetry, which means that any port can be used as the input port. The output ports will always be on the opposite side of the junction from the input port, whereas the isolated port will be the remaining port on the same side as the input port. The frequency response of the branch-line coupler is shown in Fig. 2.4.

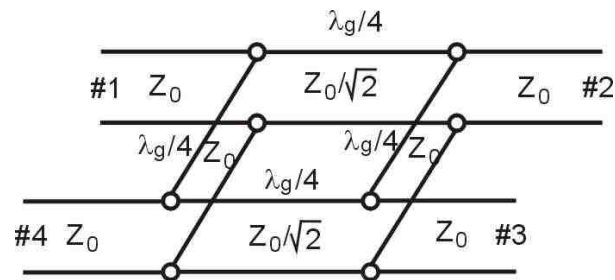


**Fig. 2.3.** Equivalent transmission-line circuit of a 3-dB branch-line coupler.

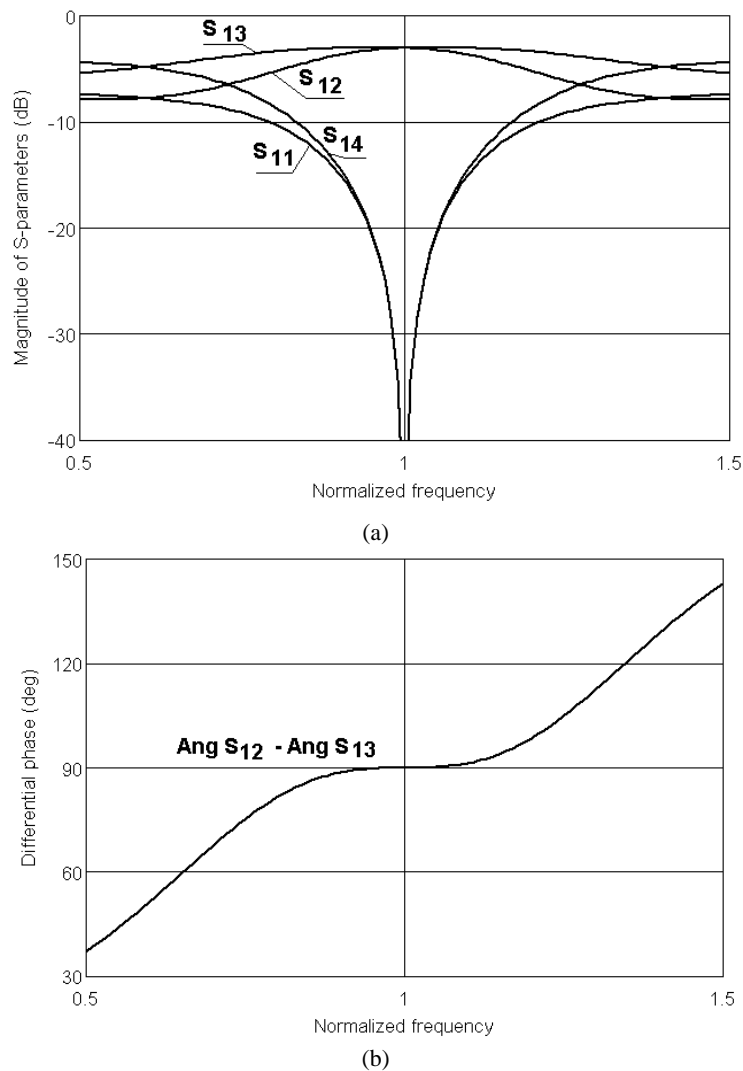
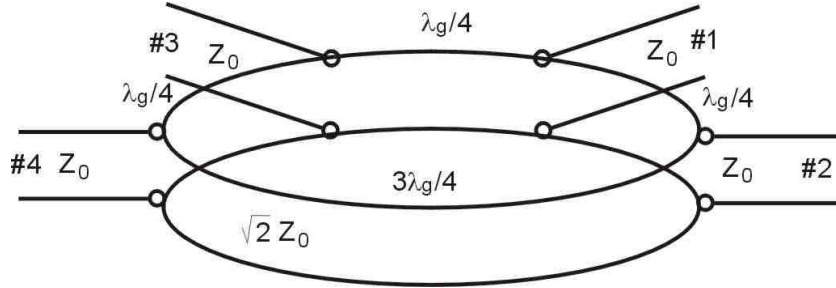


**Fig. 2.4.** Frequency response of a 3-dB branch-line coupler. Amplitude characteristics (a) and differential phase characteristics (b).

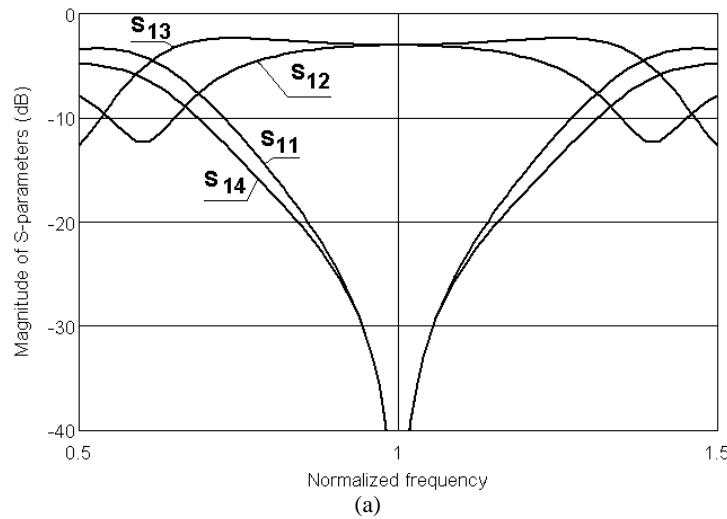
The most common realization of a magic-T hybrid is a rat-race coupler, a four-port network consisting of four sections of transmission lines, having characteristic impedance equal  $\sqrt{2}Z_0$ , three of them being quarter-wave long and the forth having length  $3\lambda_g/4$ , as it is shown in Fig. 2.5. A signal applied to port #1 is evenly split into two in-phase output signals at port #2 and #3, and port #4 is isolated. If the input signal is applied to port #4 it will be equally split into two output signal having  $180^\circ$  phase difference at ports #2 and #3, and port #1 will be isolated. When the coupler operates as a combiner with input signals applied at ports #2 and #3, the sum of the inputs will be formed at port #1, whereas, the difference will be formed at port #4. Hence ports #1 and #4 are referred to as sum and difference ports, respectively. Thus, the scattering matrix of the ideal rat-race coupler, at the center frequency, has the following form [120]:

$$[S] = \frac{-j}{\sqrt{2}} \begin{bmatrix} 0 & 1 & 1 & 0 \\ 1 & 0 & 0 & -1 \\ 1 & 0 & 0 & 1 \\ 0 & -1 & 1 & 0 \end{bmatrix} \quad (2.31)$$

The frequency response of a rat-race coupler is shown in Fig. 2.6.



**Fig. 2.5.** Equivalent transmission-line circuit of a 3-dB rat-race coupler



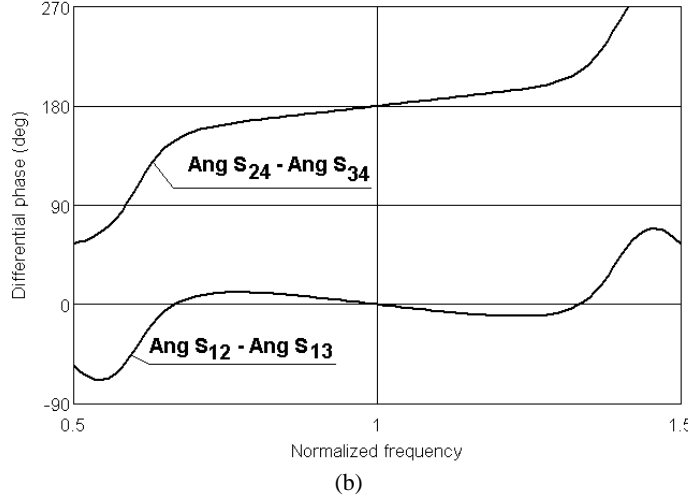


**Fig. 2.6.** Frequency response of a 3-dB rat-race coupler. Amplitude characteristics (a) and differential phase characteristics (b).

## 2.2. Directional couplers and phase shifters utilizing coupled transmission lines

### 2.2.1. Single-section coupled-line directional couplers

Two parallel transmission lines, being in close proximity, so that the electromagnetic fields of both lines influence each other, have the properties of a directional coupler. Due to the proximity of the two transmission lines some part of the power of the excited line appears in the coupled line. Coupling coefficient is a function of physical dimensions and the properties of the coupled-line structure.

Figure 2.7 presents the general case of a three-conductor coupled-line system consisting of two signal conductors placed over a common ground plane [120]. Such a network is described by a capacitance system consisting of capacitances  $C_1$  and  $C_2$  of the first and second line respectively, and a mutual capacitance  $C_m$ . If the geometrical dimensions of the signal lines are identical the resulting self capacitances are equal, i.e.  $C_1 = C_2$ . In this case an even- and odd-mode excitation method can be applied to characterize the coupled-line system. Figure 2.7b shows an even-mode excitation of coupled lines, in which both lines are excited with the in-phase signals of equal amplitudes resulting in an even symmetry of the electric field about the center line. This leads to the equivalent capacitance network where  $C_m$  is effectively open-circuited and the resulting capacitance of either line for even mode is

$$C_e = C_1 = C_2 \quad (2.32)$$

Then the characteristic impedance for the even mode is

$$Z_{0e} = \sqrt{\frac{L}{C_e}} = \frac{\sqrt{LC_e}}{C_e} = \frac{1}{\nu C_e} \quad (2.33)$$

where  $\nu$  is the velocity of propagation in the line and  $L$  is the inductance of the line. Similarly, in the odd-mode excitation, shown in Fig. 2.7c, the two out-of-phase signals of equal amplitudes are applied to the signal conductors resulting in virtual short-circuit in the symmetry about the center lines. This leads to the equivalent capacitance network where  $2C_m$  is effectively in parallel to each of the self capacitances, hence the resulting capacitance of either line for odd mode is

$$C_o = C_1 + 2C_m = C_2 + 2C_m \quad (2.34)$$

Then the characteristic impedance for the odd mode is

$$Z_{0o} = \frac{1}{\nu C_o} \quad (2.35)$$

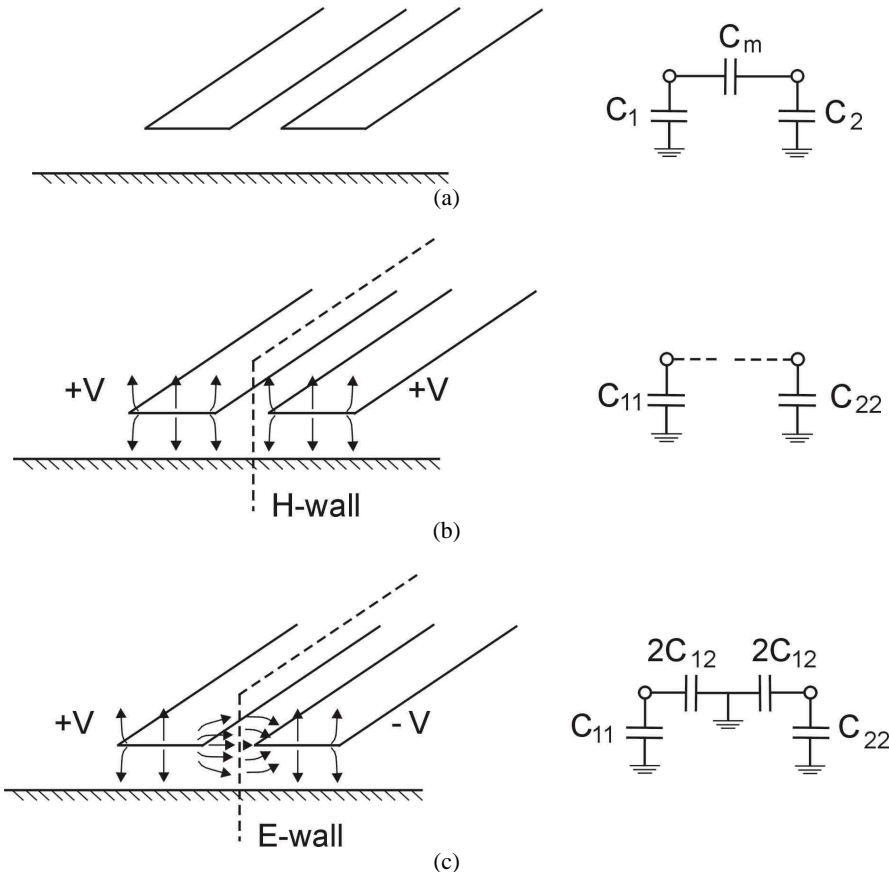


**Fig. 2.7.** A three-conductor coupled-transmission-line system and its equivalent capacitance network (a). Even-mode excitation of coupled lines and the resulting capacitance network (b), and odd-mode excitation of coupled lines and the resulting capacitance network (c) [120].

The properties of a coupled-line section, having electrical length  $\theta$ , can be derived applying the method of analysis of symmetrical networks, as shown in [121]. The resulting  $S$  parameters of the coupled-line section having even- and odd-mode characteristic impedances  $Z_{0e}, Z_{0o}$  is as follows [123]:

$$S_{11} = S_{22} = S_{33} = S_{44} = 0 \quad (2.36)$$

$$S_{14} = S_{41} = S_{23} = S_{32} = 0 \quad (2.37)$$

$$S_{12} = S_{21} = S_{34} = S_{43} = \frac{\sqrt{1-k^2}}{\sqrt{1-k^2} \cos \theta + j \sin \theta} \quad (2.38)$$

$$S_{13} = S_{31} = S_{24} = S_{42} = \frac{j k \sin \theta}{\sqrt{1-k^2} \cos \theta + j \sin \theta} \quad (2.39)$$

where

$$k = \frac{Z_{0e} - Z_{0o}}{Z_{0e} + Z_{0o}} = \frac{C_m}{\sqrt{(C_1 + C_m)(C_2 + C_m)}} \quad (2.40)$$

Moreover, even- and odd mode characteristic impedances are related by

$$\sqrt{Z_{0e} Z_{0o}} = Z_0 \quad (2.41)$$

where  $Z_0$  is the terminating impedance of all ports of the directional coupler.

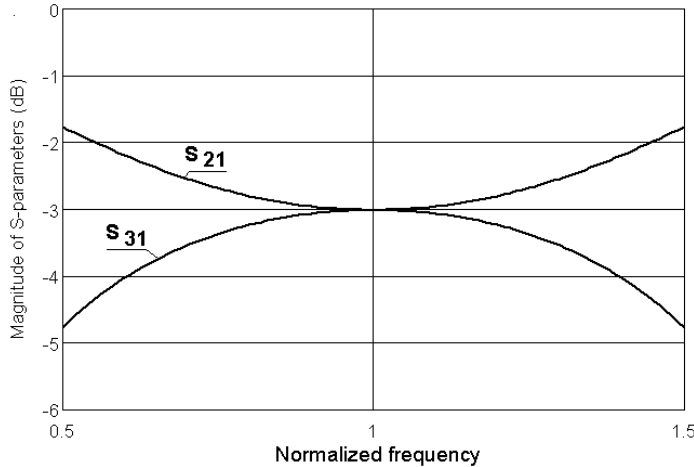


**Fig. 2.8.** Frequency response of a 3-dB coupled-line directional coupler.

The maximum coupling between the coupled lines occurs at the frequency for which  $\theta = 90^\circ$  and equals  $k$ , whereas, the power delivered to the direct port is equal  $\sqrt{1-k^2}$ . Moreover

the differential phase of signals measured at coupled and direct ports is constant and equals  $90^\circ$  at all frequencies. The exemplary frequency response of an ideal 3-dB directional coupler is presented in Fig. 2.8. The presented properties of a coupled-line section have been derived assuming that the phase velocities of both propagating modes are equal, which requires the homogeneity of the dielectric structure of the coupled-line system. In case of inhomogeneous dielectric structure, the even- and odd-mode phase velocities ( $\theta_e$  and  $\theta_o$ ) are different and the following scattering parameters are derived [81]

$$S_{11e,o} = \frac{j(z_{e,o} - y_{e,o})\sin\theta_{e,o}}{M_{e,o}} \quad (2.42)$$

$$S_{21e,o} = \frac{1}{M_{e,o}} \quad (2.43)$$

$$M_{e,o} = 4\cos\theta_{e,o} + j2(z_{e,o} + y_{e,o})\sin\theta_{e,o} \quad (2.44)$$

$$\theta_e = \theta(1+u), \quad \theta_o = \theta(1-u) \quad (2.45)$$

$$z_{e,o} = \frac{Z_{o[e,o]}}{Z_0}, \quad y_{e,o} = \frac{1}{z_{e,o}} \quad (2.46)$$

$$u = \frac{\theta_e - \theta_o}{\theta_e + \theta_o} = \frac{\sqrt{\epsilon_{ree}} - \sqrt{\epsilon_{reo}}}{\sqrt{\epsilon_{ree}} + \sqrt{\epsilon_{reo}}} \quad (2.47)$$

$$S_{11} = \frac{1}{2}(S_{11e} + S_{11o}) \quad (2.48)$$

$$S_{12} = \frac{1}{2}(S_{11e} - S_{11o}) \quad (2.49)$$

$$S_{31} = \frac{1}{2}(S_{21e} + S_{21o}) \quad (2.50)$$

$$S_{41} = \frac{1}{2}(S_{21e} - S_{21o}) \quad (2.51)$$

where  $\epsilon_{ree}$ ,  $\epsilon_{reo}$  are the even and odd mode dielectric constants.

Symmetrical couplers represent a very useful but restricted class of coupled lines. In many practical cases, it might be more useful or even necessary to design components using asymmetrical coupled lines. For asymmetrical coupled lines the two normal modes of propagation are known as  $c$ - and  $\pi$ -modes [43, 127, 135, 146, 147, 148]. In such couplers the inductive and capacitive coupling coefficients defined as

$$k_L = \frac{L_m}{\sqrt{L_{11}L_{22}}} \quad (2.52)$$

$$k_c = \frac{C_m}{\sqrt{C_{11}C_{22}}} \quad (2.53)$$

are not equal, and the maximum coupling of the asymmetric directional coupler equals [125]

$$k = \frac{k_L + k_c}{2} \quad (2.54)$$

where  $L_{11}$ ,  $L_{22}$ ,  $L_m$  are self and mutual per unit length inductances of the coupled lines and similarly  $C_{11}$ ,  $C_{22}$ ,  $C_m$  are their self and mutual per unit length capacitances.

### 2.2.2. Multisection coupled-line directional couplers

The described in the above Section single-section coupled-line directional couplers allow for achieving operational bandwidths up to one frequency octave. To achieve a specified coupling over a wider frequency bandwidth, than it is possible with the use of a single-section coupler, a number of coupled-line sections can be cascaded, as shown in Fig. 2.9. Each section is quarter-wave long at the center frequency. By properly choosing the even- and odd-mode impedances of each section, the bandwidth of the coupler can be increased [29, 55, 92, 93, 116, 137]. As it was shown in [145] the multisection directional coupler shown in Fig. 2.9 can be represented by a cascaded connection of transmission-line sections, and the reflection and transmission coefficients of such a circuit give, respectively, coupling and transmission of the multisection directional coupler. The even- and odd-mode impedances of the  $i^{\text{th}}$  section of the multisection coupler are related by (2.41). A multisection coupler can be either symmetrical or asymmetrical. In multisection couplers the term symmetrical is used to denote a coupler that has end-to-end symmetry. A symmetrical coupler utilizes an odd number of sections and the  $i^{\text{th}}$  section is identical to the  $N+1-i^{\text{th}}$  section, as shown in Fig. 2.9b. If the coupler does not have end-to-end symmetry (see Fig. 2.9a), it is referred to as an asymmetrical coupler. An asymmetrical coupler can consist of either even or odd number of sections. The major difference between the two types of multisection couplers is observed when comparing their phase properties. The symmetrical couplers feature, similar to the single-section couplers, constant  $90^\circ$  differential phase characteristic between signals measured at coupled and transmission ports, which results directly from the unitary properties of the scattering matrix [120]. Because of this property, 3-dB symmetrical directional couplers are broadly used in diplexers, multiplexers, directional filters, balanced mixers, Butler matrices, balanced amplifiers, and in other devices where the  $90^\circ$  phase difference property is required. Exemplary coupling responses of two- and three-section asymmetrical directional couplers have been presented in Fig. 2.10.

The synthesis of multisection asymmetrical couplers has been shown by Levy in [92, 93], whereas, the synthesis of multisection symmetrical couplers has been shown by Cristal and Young in [29] and also by Toulios and Todd in [144]. The analytical design expressions used for the synthesis of multisection couplers are very cumbersome even for a small number of sections. For aiding designers, Levy has prepared design tables for equal-ripple asymmetrical couplers for various values of coupling and bandwidth for up to six sections

[93]. For equal-ripple and maximally flat symmetrical couplers, Cristal and Young presented similar tables for couplers having up to nine sections [29].

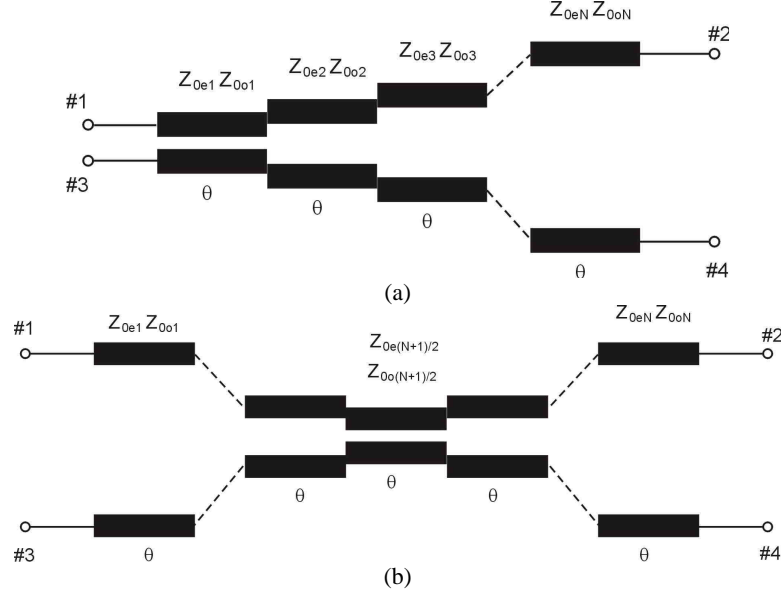


**Fig. 2.9.** Multisection coupled-line directional couplers, asymmetrical (a) and symmetrical (b).

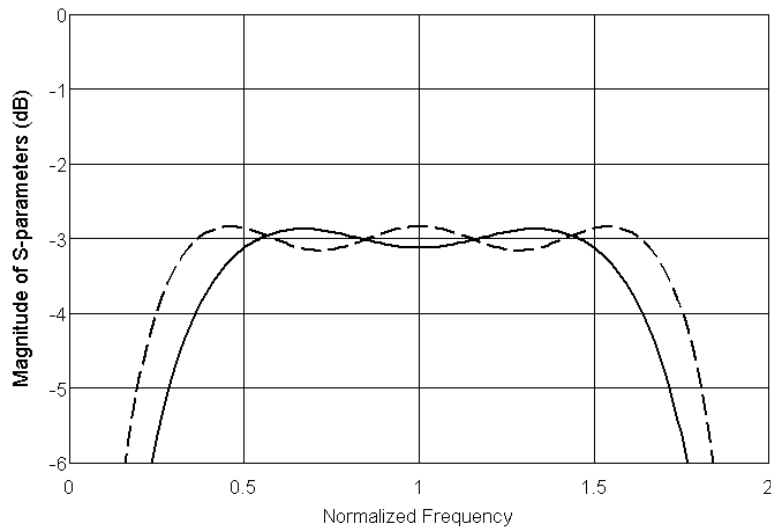


**Fig. 2.10.** Coupling characteristics of a two-section (solid line) and three-section (dashed line) directional couplers having coupling imbalance equal  $\delta C = \pm 0.12$  dB.

### 2.2.3. Broadband phase shifters

It is known that the coupled-line sections can be used for the design of all-pass networks. In particular, it was shown in [84] that two parallel coupled lines of equal length connected at one end, for which the condition (2.41) is fulfilled, constitute a two terminal network (called ‘C’-section) being ideally matched with  $|S_{21}| = 1$ . The phase characteristic of such a section is given by [133]

$$\phi = \arccos \left( \frac{\frac{Z_{0e}}{Z_{0o}} - \tan^2 \theta}{\frac{Z_{0e}}{Z_{0o}} + \tan^2 \theta} \right) \quad (2.55)$$

The phase characteristic of the ‘C’-section has been shown in Fig. 2.11. It is seen that the behavior of the response depends on the coupling  $k$  of the section, being linear for  $k = 0$  and becoming highly non-linear when  $k$  increases. Figure 2.12 presents differential phase characteristics between a section of transmission line having electrical length  $\theta = 270^\circ$  and ‘C’-sections having coupling  $k = 0, 0.5$  and  $0.707$ . It is seen that for certain values of coupling  $k$  the differential phase characteristics becomes equal-ripple with the mean value of  $90^\circ$ , thus, such a ‘C’-section together with a transmission-line section constitutes broadband  $90^\circ$  differential phase shifter [133], with the bandwidth and phase imbalance depending on the coupling  $k$ .

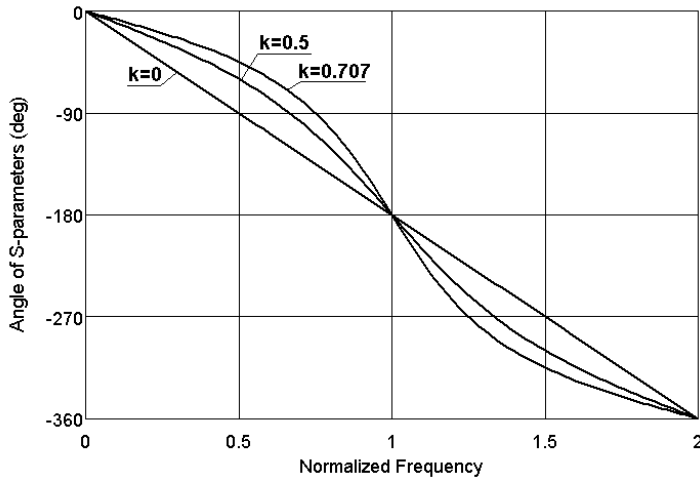


**Fig. 2.11.** Phase characteristic of a ‘C’-section for three different values of coupling coefficient  $k$ .

The presented ‘C’-section in conjunction with a transmission-line section may provide any other differential phase shift over broad frequency range. It was shown in [133, 178] that the bandwidth of the differential phase shifter can be further increased when a network having more than one coupled-line section is employed. In particular, in case of a two-section Schiffman ‘C’-section an equal-ripple differential phase shifter can be designed with the number of ripples increasing into four. This network is suitable for achieving bandwidths of about 3:1. Moreover, in [178] a multisection phase-shift network is analyzed and the following formula is given, describing its phase characteristics

$$\phi_n = \arccos \left( \frac{\rho_1 - (\tan \theta_1)^2}{\rho_1 + (\tan \theta_1)^2} \right) \quad (2.56)$$

where

$$\begin{aligned}\theta'_1 &= \theta_1 + \arctan(\sigma_{12} \tan \theta_2) \\ \theta'_2 &= \theta_2 + \arctan(\sigma_{23} \tan \theta'_3) \\ &\vdots \\ \theta'_{n-1} &= \theta_{n-1} + \arctan(\sigma_{n-1,n} \tan \theta'_n) \\ \theta'_n &= \theta_n \\ \sigma_{i,i+1} &= \frac{Z_{0ei}}{Z_{0e(i+1)}} = \frac{Z_{0o(i+1)}}{Z_{0oi}}\end{aligned}$$

The presented expression allows for calculation of phase characteristics of a multisection phase shifter having coupled-line sections of unequal lengths. By allowing the lengths of the sections to be varied, greater degree of freedom in phase shaping is achieved.

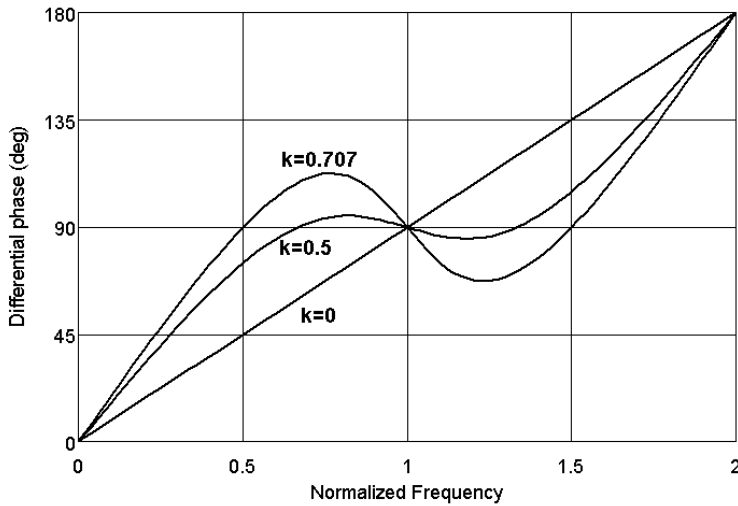


**Fig. 2.12.** Differential phase characteristic between a transmission-line section having electrical length  $\theta = 270^\circ$  and a 'C'-section for three different values of coupling factor  $k$ .

#### 2.2.4. Design of coupled-strip-transmission-line directional couplers and phase shifters with improved frequency response

The coupled-line circuits can be designed in technology of either pure-TEM striplines in homogeneous dielectric medium, or quasi-TEM microstriplines in inhomogeneous dielectric medium, in which normal waves are propagating with different phase velocities. Realistic

zation of ideal, symmetrical coupled-line sections requires that two conditions have to be fulfilled, which are: (i) the product of even and odd mode characteristic impedances of coupled lines equals the square of the terminating impedance (2.41) and (ii) the modal phase velocities are equal. In asymmetric, coupled-line sections two modes, the  $c$  mode and  $\pi$  mode, propagate in the structure. It was shown in [127] that for such a coupled-line section the conditions for an ideal coupler realization are: (i) the ratio of self inductance and self capacitance of the line  $i$  equals the square of the terminating impedance

$$Z_{Ti}^2 = \frac{L_{ii}}{C_{ii}} \quad (2.57)$$

where  $Z_{Ti}$ ,  $i = 1, 2$  – characteristic impedances of terminating lines, and (ii) inductive and capacitive coefficients are equal

$$k_L = k_C. \quad (2.58)$$

It is important to remember that symmetric coupled-lines are the special case of more general asymmetric coupled lines, therefore, the conditions of ideal asymmetric coupled-line section realization are more general, and apply also for the case of symmetric coupled-line sections.

The physical realization of coupled-line directional couplers requires the connection of signal lines to the coupled-lines and in case of multisection couplers the connection of coupled-line sections having different geometrical dimensions. Such connections introduce parasitic reactances that severely deteriorate frequency characteristics of directional couplers, especially their return losses and isolations between respective ports.

To summarize, there are two important aspects that have to be approached when directional couplers having superior performance are to be designed:

1. Equalization of modal phase velocities or inductive and capacitive coupling coefficients.
2. Taking into account parasitic reactances of the transition regions within the directional couplers geometry.

A number of techniques have been reported over the years to approach the first aspect. The known techniques can be divided into four groups:

1. The compensation techniques in which equalization of coupling coefficients is achieved by a proper choice of dielectric layers and coupled-line geometry [46, 51, 60, 65, 126, 130, 167].
2. The compensation techniques in which lumped elements are connected to coupled lines [41, 46, 101, 167]. The presented methods assume the equalization of even and odd mode phase velocities for the center frequency only, which causes that the frequency characteristics deteriorate in wider frequency range. A number of papers follows the idea of a single or multiple element compensation technique presented in [41] with modifications on a type, placement and a number of compensating elements (i.e. lumped capacitors, lumped inductors, step-impedance transformers, complex impedances, coupled spur-lines, interdigital capacitors, feedback transmission-line sections) [73].
3. The compensation techniques in which coupled lines are modified periodically resulting in modal phase velocities' equalization or coupling coefficients' equalization [73].
4. Other compensation techniques such as compensation with the use of delay lines, stepped impedance sections, or compensation using corrugated ground planes [73].

The Author has researched the two aspects concerning the realization of directional couplers having improved performance, and the results can be found in [60, 62, 63, 64, 65, 69, 71, 72, 165, 166, 167, 169]. In [165] the Author has investigated a capacitive compensation method that allows for coupling coefficients equalization in a suspended stripline technique. In this method, compensating elements are equally distributed along coupled lines allowing for appropriate decrease of the capacitive coupling coefficient to the value of the inductive one. The proposed procedure is iterative since it is also desired to achieve appropriate impedance of coupled lines. The method has been also applied for the design of a broadband three-section directional coupler shown in [62]. One of the recent co-authored papers proposes the generalized methods to design quasi-ideal symmetric and asymmetric coupled-line sections [72].

The second aspect, i.e. the problem of discontinuities in coupled-stripline directional couplers and phase shifters has been comprehensively investigated by the Author in [63, 64, 69, 71, 167]. In [63, 64] a method of capacitive compensation of parasitic reactances has been proposed, in which a number of lumped capacitors connected to coupled and signal lines in various cross-sections allow for significant improvement of coupled-line circuits' performance. The proposed method has been successfully applied in various single and multisection directional couplers designed in various dielectric structures.

The usefulness of the proposed in [63] method of parasitic reactances' compensation can be illustrated with the design of 3-dB and 8.34-dB directional couplers in homogeneous stripline technique. Fig. 2.13 shows the chosen, dielectrically homogeneous ( $\epsilon_r = 3.38$ ) structure, in which the directional couplers have been designed, and consists of two 1.524 mm thick laminates between which a thin laminate layer has been placed, having thickness  $h = 0.152$  mm. The initial dimensions of the coupled lines of both types of couplers have been calculated using Linpar software [38] which are:  $w = 0.62$  mm and  $offset = 0.18$  mm for the 3-dB directional coupler and  $w = 1.36$  mm and  $offset = 1.66$  mm for the 8.34-dB directional coupler.

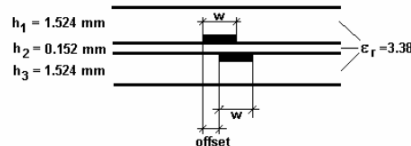


**Fig. 2.13.** Cross-sectional view of the stripline coupled lines used for the design of high-performance directional couplers.

The final layouts of the couplers have been found with the use of electromagnetic optimization, where the capacitive elements' dimensions have been established. Measured results of the developed directional couplers are presented in Fig. 2.14 and Fig. 2.15. Exceptionally good parameters have been obtained in terms of return losses, isolations and coupling-transmission imbalance. Figure 2.16 presents a picture of the inner laminate layer on which the traces of the couplers are etched. In both cases the capacitive elements, which improve the couplers' performance, are visible.

An exemplary design, where the methods allowing for coupling coefficients equalization have been utilized is shown in [167], in which a three-section, 3-dB directional coupler is realized in a multilayer microstrip technique. In the presented design three different compensating techniques have been simultaneously used, i.e. equalization of inductive and capacitive coupling coefficients by the proper selection of dielectric structure and coupled-

line geometry and by adding capacitive elements between coupled lines, and finally the capacitive compensation of parasitic reactances introduced by the transition regions. The applied techniques allow for achieving an excellent performance of the coupler, as it is seen in Fig. 2.17. The designed coupler features coupling imbalance  $\delta C = \pm 0.2$  dB over two-octave frequency range having isolations and return losses as low as -28 dB. Figure 2.18 presents a picture of the manufactured coupler.

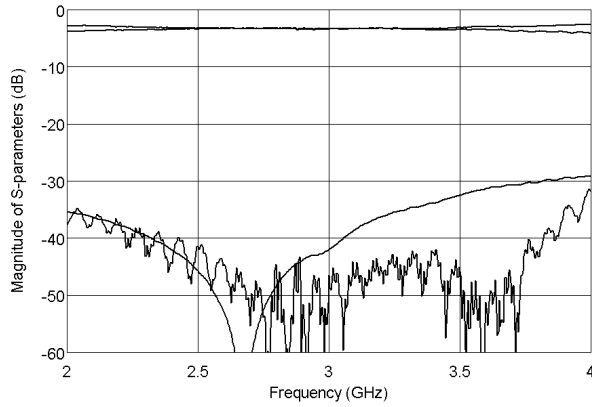


**Fig. 2.14.** Measured frequency response of the designed 3-dB directional coupler.

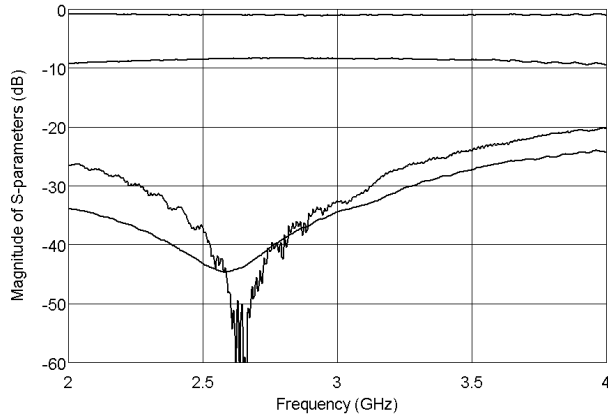


**Fig. 2.15.** Measured frequency response of the designed 8.34-dB directional coupler.



**Fig. 2.16.** Pictures of the inner laminate layer on which the traces of the couplers are etched. 3-dB directional coupler (a) and 8.34-dB directional coupler (b).

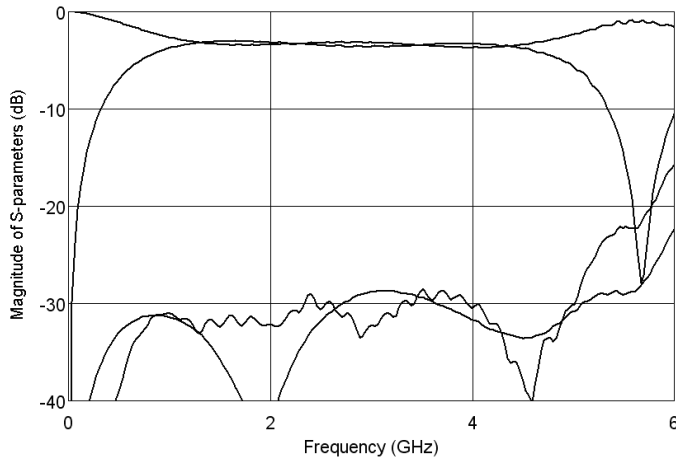


**Fig. 2.17.** Measured amplitude characteristics of the designed 3-dB directional coupler [167].

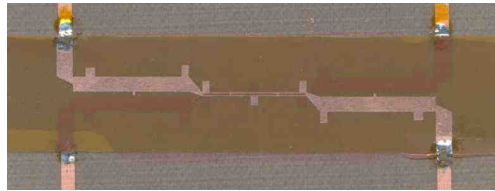


**Fig. 2.18.** Photograph of the developed 3-dB directional coupler with compensating capacitances visible [167].

### 2.3. Summary

The chapter presents a brief introduction to basic passive microwave components such as directional couplers, power divider and phase shifters. At first connected-line devices are presented, followed by circuits utilizing sections of coupled lines. As it was shown, the devices designed in a connected-line technique feature narrower operational bandwidth than the coupled-line circuits. A basic theory of coupled-lines has been outlined from which conditions to realize an ideal coupled-line section, are derived. Finally, the two main aspects in the design of high-performance coupled-line circuits have been presented:

1. Equalization of modal phase velocities or inductive and capacitive coupling coefficients in case of couplers designed in symmetric and asymmetric structures, respectively.
2. Compensation of parasitic reactances of transition regions within coupled-line circuits.

The Author has investigated both phenomena and as a result a compensation method of parasitic reactances of the transition regions, broadly described in co-authored papers [63, 64] have been proposed. Also methods of inductive and capacitive coupling coefficients' equalization have been presented in the following co-authored papers [72, 165].

### **3. Directional couplers in application to balanced and $n$ -way microwave circuits**

One of the primary applications of 3-dB directional couplers and power dividers is the signal distribution in balanced circuits and  $n$ -way networks. The examples of high-power balanced amplifiers can be found in [54, 75, 95, 108, 143, 171, 175]. In [171] the most conventional approach has been presented, where branch-line 3-dB directional couplers have been used as power splitter and combiner. Similar design has been shown in [108], where a Wilkinson power divider has been utilized, together with meandered transmission line sections for proper phase adjustment. Another type of power dividers, i.e. Gysel power dividers [54, 175] together with a 90°-long sections of transmission lines have been utilized for realization of the 1.5 kW amplifier operating in L-band, in which eight 300W transistors are used in the final power stage. An example of a balanced amplifier in which coupled-line 3-dB directional couplers are used has been presented in [75], where commercially available semi-rigid cable with two internal wires is utilized to realize a coupled-line section.

This section shows the methods of the design of balanced and  $n$ -way power amplifiers with the use of asymmetric coupled-line directional couplers, in which coupled-line sections are used to simultaneously provide equal power division between direct and coupled ports, and to provide impedance transformation in both direct and coupled ports [179]. Such a solution allows to design high-power amplifiers with reduced both size and losses within the power splitting/combining network. While the impedance transformation is achieved at the first and every following stage of the  $n$ -way power divider, the microwave power is distributed by a network having lower (typically) impedance. In case of stripline realization it provides for wider conducting strips and, therefore, for lower attenuation. Moreover, the decreased impedance can be brought close to the input/output impedance level of the applied semiconductors, and therefore, simpler matching networks can be designed. The large content of the Author's work published in [179] is cited in this section.

In section 3.1 the basic properties of balanced circuits have been described, followed by the exemplary application in balanced mixers and switches. Further,  $n$ -way power dividing/combining networks have been briefly outlined and a multichannel network has been presented. In the next section, a method for large signal measurements of transistor reflection coefficients, with the use of 3-dB/0/180° directional couplers has been shown [59]. The utilization of asymmetric coupled-line directional couplers in application to balanced circuits has been theoretically investigated in Sections 3.3 and 3.4 and a limitation for impedance ratio transformation  $Z_1/Z_2 \leq 2$  has been derived. This limitation can be overcome by

expanding a simple balanced circuit into a larger  $n$ -way network, in which the transformation ratio can be increased up to  $Z_1/Z_2 \leq n$ . The theoretical investigations have been verified by measurements of the designed impedance-transforming directional couplers, balanced, and 4-way networks. Also, the measured results of a 4-way power amplifier are shown, in which the developed power splitters/combiners are successfully utilized. Moreover, the concept of impedance-transforming directional couplers has been extended in section 3.5 into multisection directional couplers, which results in significant enhancement of the operational bandwidth.

### 3.1. Balanced and $n$ -way microwave circuits

A balanced circuit, shown schematically in Fig. 3.1, consists of two 3-dB directional couplers/power dividers between which two identical two-port networks are inserted. Such a circuit is often used in microwave technique, due to its advantageous features, for the design of amplifiers, voltage-controlled PIN-diode attenuators, modulators, power switches and diplexers [58]. In general, the principal advantage of such a circuit is an ideal impedance match of its input port in the operating frequency range of the directional coupler/power dividers. The impedance match is independent from the inserted two-port networks, under the condition however, that the two-port networks are identical. Such a balanced circuit can be regarded as a cascade connection of three four-port networks, in which the middle network is a compound of two identical two-port networks. Having the scattering matrix of a two-port network as [66]:

$$[S^N] = \begin{bmatrix} S_{11}^N & S_{12}^N \\ S_{21}^N & S_{22}^N \end{bmatrix} \quad (3.1)$$

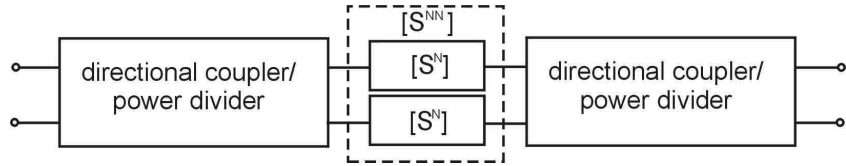
and assuming the identity of both two-port networks, the following scattering matrix of the four-port network can be written:

$$[S^{NN}] = \begin{bmatrix} S_{11}^N & 0 & S_{12}^N & 0 \\ 0 & S_{11}^N & 0 & S_{12}^N \\ S_{21}^N & 0 & S_{22}^N & 0 \\ 0 & S_{21}^N & 0 & S_{22}^N \end{bmatrix} \quad (3.2)$$

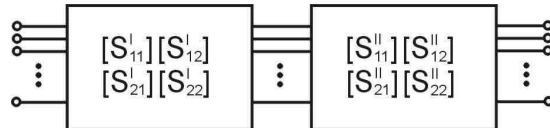
The scattering matrix of a complete balanced circuit can be calculated as a cascade connection of the four-port networks. Generally, the scattering matrix of the connection of two  $n$ -port networks can be calculated as follows [66]:

$$[S] = \begin{bmatrix} S_{11}^I + S_{12}^I (I - S_{11}^H S_{22}^I)^{-1} S_{11}^H S_{21}^I & S_{12}^I (I - S_{11}^H S_{22}^I)^{-1} S_{12}^H \\ S_{21}^H (I - S_{22}^I S_{11}^H)^{-1} S_{21}^I & S_{22}^H + S_{21}^H (I - S_{22}^I S_{11}^H)^{-1} S_{22}^I S_{12}^H \end{bmatrix} \quad (3.3)$$

where the quantities in the formula are block  $S$  matrices of  $n$ -port networks as shown in Fig. 3.2.

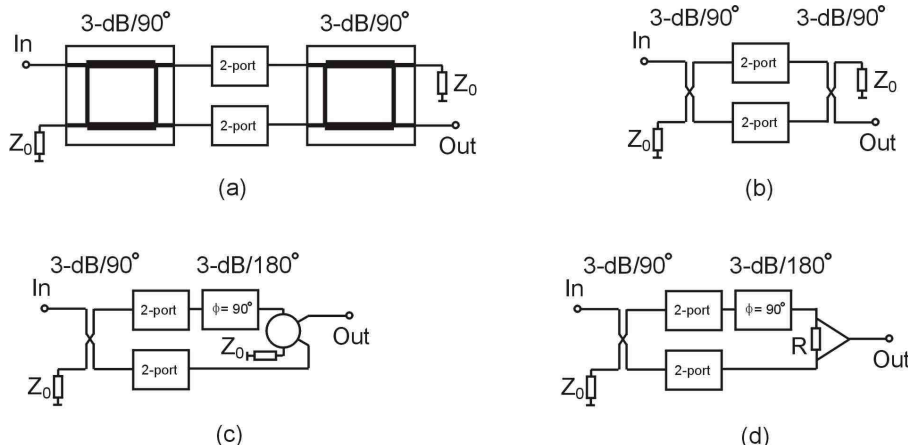


**Fig. 3.1.** Schematic diagram of a balanced circuit.



**Fig. 3.2.** Schematic diagram of a cascade connection of two  $n$ -port networks.

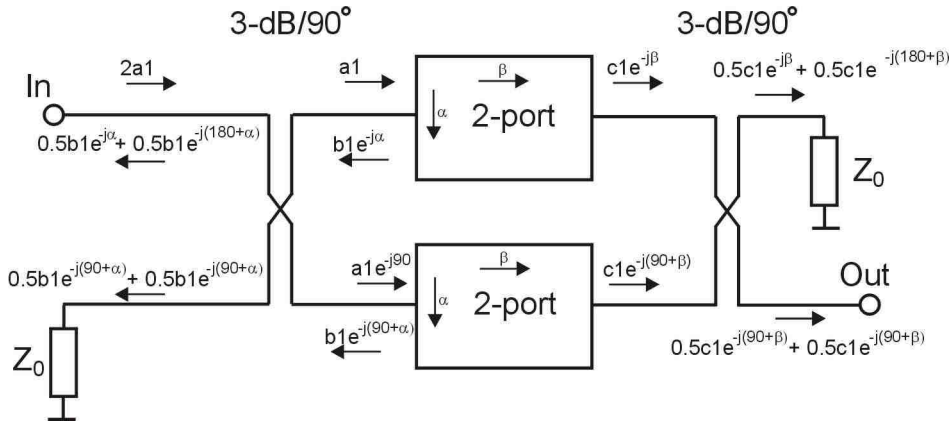
Balanced circuits can be designed with the use of different types of directional couplers and power dividers, and their combination. Figure 3.3 presents basic configurations with the use of branch-line directional couplers (Fig. 3.3a), coupled-line directional couplers (Fig. 3.3b), a coupled-line directional coupler in conjunction with a rat-race coupler (Fig. 3.3c) and a coupled-line directional coupler in conjunction with a Wilkinson power divider (Fig. 3.3d). In the last two presented circuits  $90^\circ$  constant phase shifters are required for proper operation.



**Fig. 3.3.** Balanced networks composed of (a) two branch-line directional couplers, (b) two coupled-line directional couplers, (c) a coupled-line directional coupler and a rat-race coupler in conjunction with a  $90^\circ$  phase shifter, and (d) a coupled-line directional coupler and a Wilkinson power divider in conjunction with a  $90^\circ$  phase shifter [66].

The principle of operation of a balanced circuit has been outlined in Fig. 3.4. The presented circuit consists of two coupled-line 3-dB/ $90^\circ$  directional couplers and two identical 2-port networks. The input and output ports have been distinguished, however, taking into account the reciprocity of the circuit, any port can play a role of an input port, as long as the 2-port

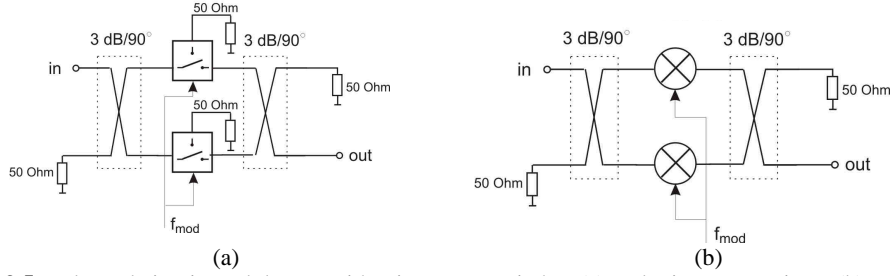
networks are also reciprocal. The incident and reflected waves have been schematically shown in the picture with the special attention to their respective phase relations, which play a crucial role in the principle of balanced circuits operation. A wave of magnitude  $2a_1$  is incident upon the input port of the circuit and is being split between coupled and transmitted ports of the input directional coupler. Waves with equal amplitude and with the phase difference of  $90^\circ$  are incident upon the 2-port networks and reflected with additional phase shift  $\alpha$ . Both reflected waves are again incident upon the ports of the input directional coupler and are directed to the load  $Z_0$  and the input port. The directional coupler introduces additional  $90^\circ$  phase shift of the reflected signals resulting in their out-of-phase cancellation at the input port, and their in-phase addition at the port where a load  $Z_0$  is applied, hence, no reflected power appears at the input port. The waves propagating through the 2-port networks acquire some additional, but identical in both channels, phase shifts  $\beta$ . The waves  $c_1$  are, similarly as the waves  $b_1$ , incident upon the ports of the output directional coupler, where an additional  $90^\circ$  phase shift is introduced. Due to similar mechanism as described for the input directional coupler, the waves are added at the output port, and they cancel out in the port where the load  $Z_0$  is connected. In the presented circuit, assuming ideal directional couplers and lossless 2-port networks, no insertion losses are introduced and all power delivered into the input port is being split between the output port and the load  $Z_0$  connected to the input directional coupler [120].



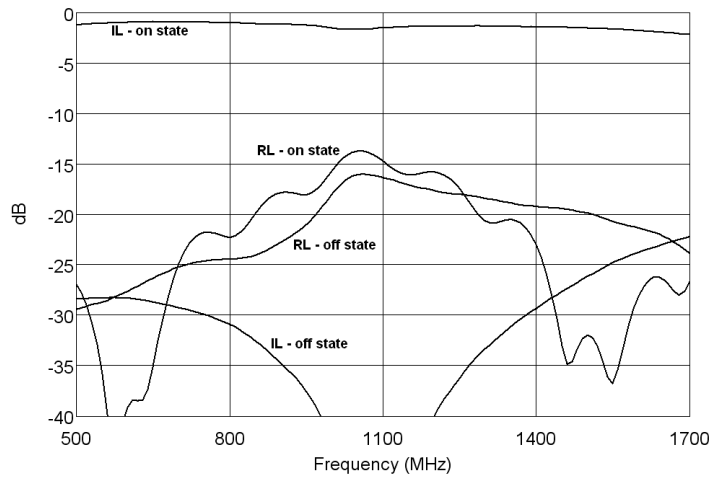
**Fig. 3.4.** Schematic diagram of a balanced circuit showing the principles of operation.

An example of coupled-line couplers' applications in the design of balanced modulators with the use of monolithic mixers and switches is presented in [60]. Figure 3.5 presents schematic diagrams of the developed modulators. Two types of modulators have been considered, i.e. the modulator 'A' which utilizes microwave switches and the modulator 'B' with monolithic microwave mixers. Both circuits have been developed on a cost-effective FR4 laminate.

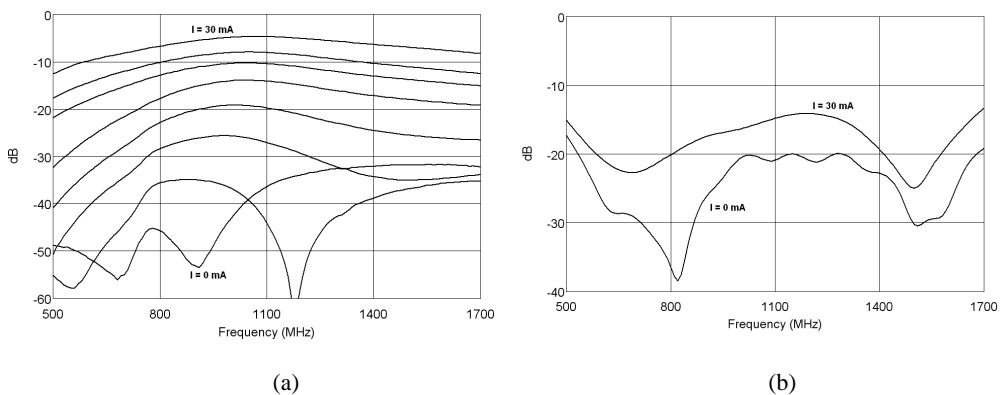
Results of measurements of the 'A' modulator are shown in Fig. 3.6. As it is seen the circuit features low insertion losses  $IL = 1$  dB @ 850 MHz and high isolation  $I > 30$  dB. The return losses in both states are better than 15 dB.



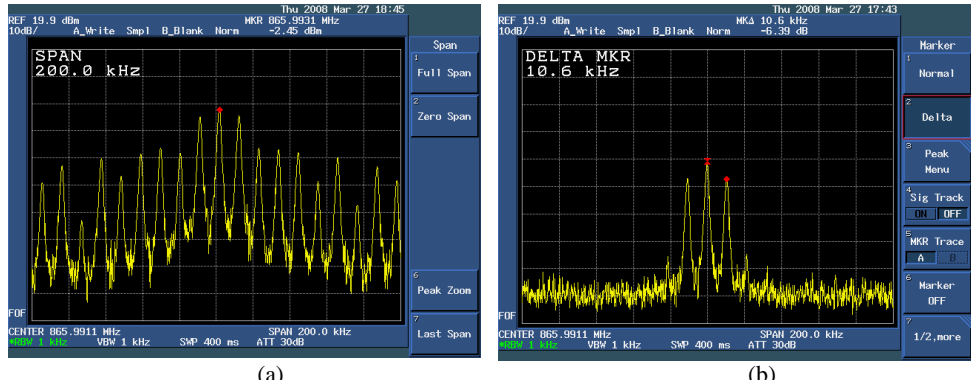
**Fig. 3.5.** Balanced circuit modulators; with microwave switches (a) and microwave mixers (b) [60].



**Fig. 3.6.** Insertion losses  $IL$  and return losses  $RL$  of the designed modulator with the use of microwave switches. Results of measurements for ‘on’ and ‘off’ state of the modulator [60].

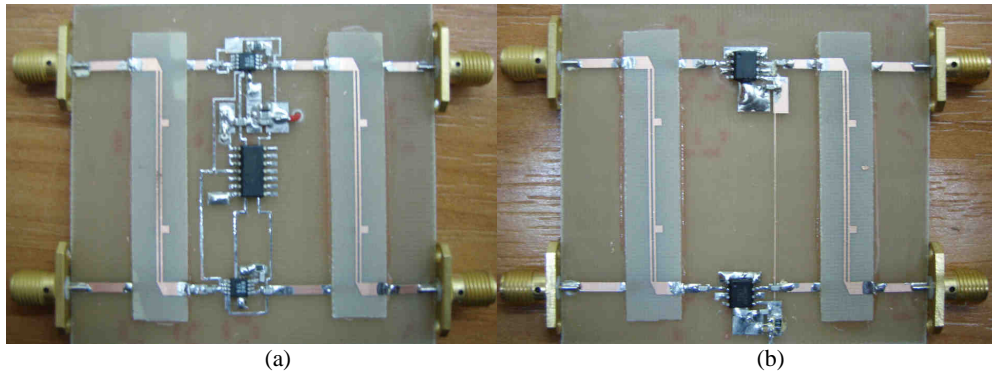


**Fig. 3.7.** Results of measurements of the modulator designed with the use of microwave mixers. Insertion losses (a) and return losses (b) for various values of modulation current [60].



**Fig. 3.8.** Spectrum of the modulated signals obtained with the use of the modulator consisting of microwave switches (a) and microwave mixers (b) [60].

Measurement results of the modulator ‘B’ are shown in Fig. 3.7 for various values of modulation current. The lowest insertion losses on the level of 5 dB @ 865 MHz are achieved with a total current (taken by both mixers) reaching  $I = 30$  mA, whereas isolation exceeding 40 dB can be achieved for current  $I = 0$  mA. As in the previous case the developed modulator features return losses better than 15 dB.



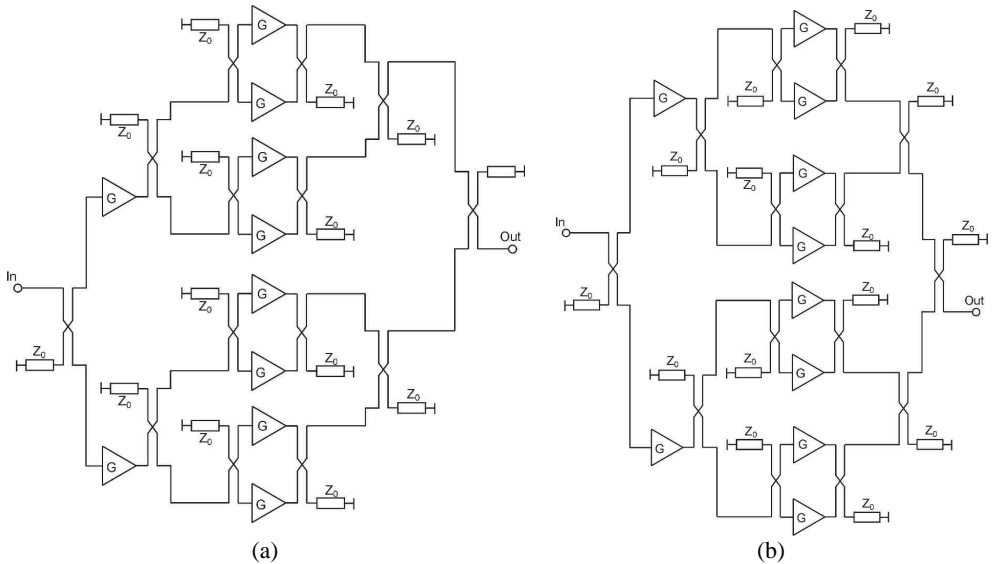
**Fig. 3.9.** Balanced circuit modulators with microwave switches (a) and microwave mixers (b) [60].

Fig. 3.8 presents frequency spectrum of a modulated signal obtained with the use of both types of modulators. In case of the modulator ‘A’ multi-component spectrum results from a switching operation of the modulator, whereas in case of the modulator ‘B’ classic single tone AM modulation is seen. Pictures of the developed modulators are shown in Fig. 3.9.

The described balanced circuits are often used for the design of balanced amplifiers. In a microwave amplifier design, the primary goal is to achieve a constant gain and good input matching over the desired frequency range. As it is shown in [120] the conjugate matching gives the maximum gain only over the relatively narrow band, whereas designing for less than the maximum gain improves the gain bandwidth, at the expense of poor impedance match of input and output ports of the amplifier. The application of a balanced circuit solves the problem of a broadband amplifier design offering a number of advantages [120]:

1. The individual amplifier stages can be optimized for gain flatness or noise figure without the concern for input and output matching.
2. The stability of the amplifier is improved while the reflections are absorbed in the couplers' terminations.
3. Degradation of gain by only 6 dB is observed when a single section of the amplifier fails.
4. The amplifier can operate in a broad bandwidth limited only by the bandwidth of the used directional coupler.
5. The maximum output power increases by 3 dB in comparison with the maximum power of a single stage.

Following the idea of balanced circuit amplifiers more complex networks consisting of a number of directional couplers or power dividers can be realized. Such circuits allow to design high-power amplifiers, in which the maximum output power is increased by  $N$ , where  $N$  is the number of used output stages. The exemplary topologies of 8-way power amplifiers are shown in Fig. 3.10.



**Fig. 3.10.** 8-way power amplifiers, uniform topology power stage (a), and nonuniform topology power stage (b).

Once designing an  $n$ -way power dividers/combiners a care has to be taken to the phase relation between the signals within the structure, in order to ensure proper combining the microwave power at the output port. There are two possible approaches in the design of  $n$ -way power dividers and combiners. The first relies directly on the principle of a balanced circuit shown in Fig. 3.4, i.e. the same scheme is repeated at every stage of dividing and combining the power, resulting in identical dividing and combining networks (Fig. 3.10a). The other approach is shown in Fig. 3.10b. In this topology two types of couplers are used, one being a mirror image of the other. The goal is to minimize the insertion losses of the combining network at the expense of increasing the insertion losses of the power divider. Such a modification allows to obtain the maximum output power at the expense of the gain

needed to ensure it, but in practice higher gain is less troublesome than higher output power.

Another type of an  $n$ -way amplifier that utilizes directional couplers is a multichannel amplifier. Figure 3.11 presents an exemplary four-channel amplifier with the input and output networks consisting of four directional couplers connected in a Butler-matrix-type arrangement. Such a circuit is well-suited for applications in low-noise receivers of focal arrays in multibeam reflector antennas. The power introduced to any one of its input ports is divided equally between the output ports of the input network, but with various phase delays. If the divided output power is fed into the identical output network – attached back-to-back – the power is recombined in the second matrix and the total power appears at a single port diagonally opposite the input port. Figure 3.12 presents a picture of the developed four-channel amplifier with the use of monolithic integrated circuits, the input and output matrices are designed in a multilayer microstrip technology [176].

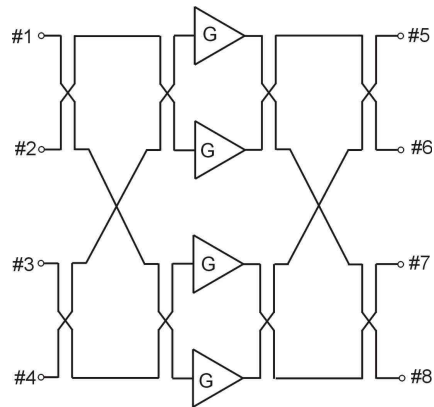


**Fig. 3.11.** Schematic diagram of a four-channel amplifier.

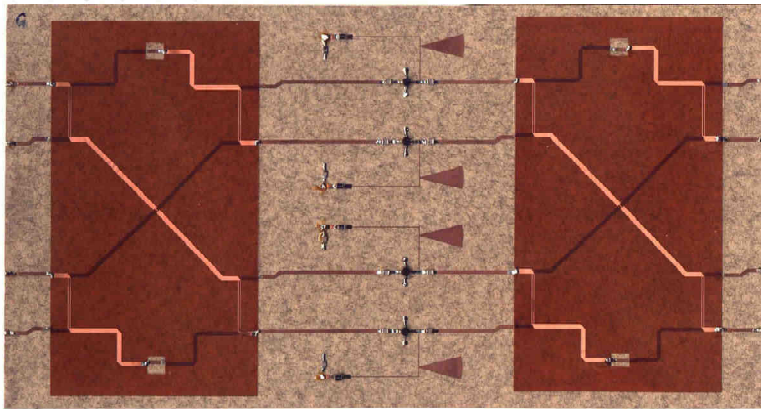


**Fig. 3.12.** Picture of the designed four-channel amplifier\*.

---

\* Courtesy of prof. Krzysztof Sachse, Microwave Theory and Techniques Division, Wroclaw University of Technology, Poland.

### 3.2. Large signal characterization of solid-state devices

The presented in previous section concepts of  $n$ -way power amplifiers require introduction of amplifiers into the power dividing/combining networks. Moreover, it is desired to minimize reflections within the amplifier network and to maximize the output power of each single amplifier unit. In order to achieve that, however, it is required to measure input and output impedances of the device used for the amplifier design. Typically, in the design of a low-power amplifier, the small-signal transistors' parameters are measured with the use of a vector network analyzer. Such an approach is inadequate in the design of a high-power amplifier, since the active device operates in a highly nonlinear regime. The commonly used technique for measuring transistors' impedance under large-signal operation is a load pull technique. In this procedure the high-power transistor's input and output are simultaneously matched in an iterative process, whereas, the output power is controlled aiming to its maximization. Such a class of techniques is widely described in literature [32, 103, 134]. In most cases the key elements used for tuning the system, i.e. changing the input and output impedance of the network take a form of a manual or automated tuner, in which one or more probes is/are coupled to a transmission line and both position and coupling of probes can be changed [152, 140].

In [59] the Author proposed a concept of applying two 3dB/180° directional couplers, which together with two shorted transmission lines serve as a source and load pull tuners. The content of [59] is cited in this section in a large extent. The presented concept has its origin in a rectangular waveguide technique, where a magic-T network with two shorted waveguide sections (E-H tuner) is used to obtain impedance match at a center frequency.

The proposed in [59] measurement set-up, which can be used for determining input and output impedances of a transistor under large signal conditions is presented in Fig. 3.11. It consists of a signal source, input and output matching networks, an active element to be matched (DUT) and a power meter. The input and output matching networks consist of rat-race couplers in conjunction with two sections of shorted transmission lines connected to ports #2 and #4, as it is schematically shown in Fig. 3.13. By adjusting the length of shorted transmission lines the impedance seen at the matching networks' inputs can be changed.

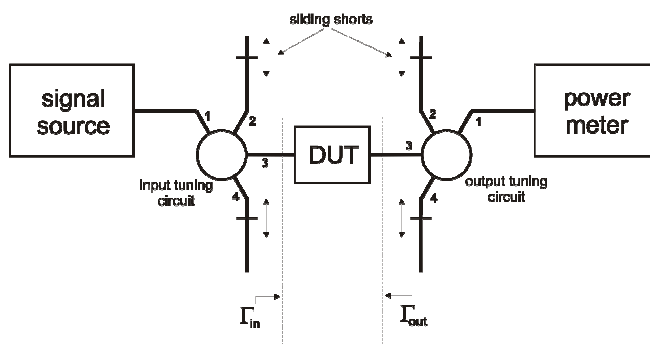


**Fig. 3.13.** Schematic diagram of a set-up for source and load pull measurement technique with rat-race couplers as matching networks [59].

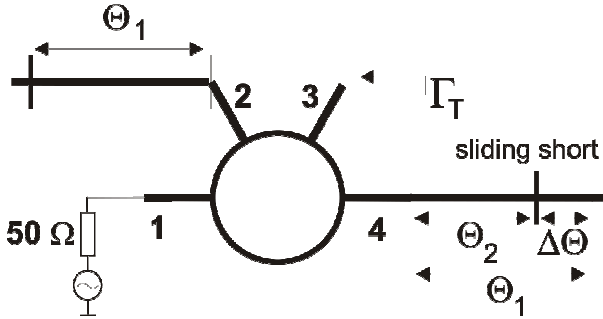


**Fig. 3.14.** A rat-race coupler with two shorted transmission lines as a matching network [59].

The behavior of such a matching network can be described by examining  $S$ -parameters of an ideal rat-race coupler. Taking into account the ports order shown in Fig. 3.14, the scattering matrix (2.31) has the following form

$$S = \frac{j}{\sqrt{2}} \begin{bmatrix} 0 & -1 & 0 & 1 \\ -1 & 0 & -1 & 0 \\ 0 & -1 & 0 & -1 \\ 1 & 0 & -1 & 0 \end{bmatrix} \quad (3.4)$$

Termination of port #1 with  $50 \Omega$  matched load leads to the following  $S$  matrix

$$S = \begin{bmatrix} 0 & \frac{-j}{\sqrt{2}} & 0 \\ \frac{-j}{\sqrt{2}} & 0 & \frac{-j}{\sqrt{2}} \\ 0 & \frac{-j}{\sqrt{2}} & 0 \end{bmatrix} \quad (3.5)$$

By connecting shorted sections of  $50 \Omega$  transmission lines having the reflection coefficient

$$\Gamma_{l1,2} = e^{-j2\Theta_{l1,2}} \quad (3.6)$$

to ports #2 and #3, the  $S$  matrix is reduced in the following manner

$$S = \begin{bmatrix} \frac{-\Gamma_{l1}}{2} & \frac{-j}{\sqrt{2}} \\ \frac{-j}{\sqrt{2}} & 0 \end{bmatrix} \quad (3.7)$$

$$S = \Gamma_T = -\frac{\Gamma_{l1}}{2} - \frac{\Gamma_{l2}}{2} \quad (3.8)$$

$$\Theta_2 = \Theta_1 + \Delta\Theta \quad (3.9)$$

Finally assuming (3.9) the reflection coefficient of a matching network can be expressed as:

$$\Gamma_r = -\frac{1}{2}(e^{-j2\Theta_1} + e^{-j2\Theta_2}) = -\frac{1}{2}e^{-j2\Theta_1}(1 + e^{-j2\Delta\Theta}) \quad (3.10)$$

The analysis of (3.10) shows that any impedance of a passive network can be realized for  $\Theta_1, \Delta\Theta \in (0, \pi)$ . The displacement of a reflection coefficient in the Smith chart as a function of transmission line lengths  $\Theta_1$  and  $\Delta\Theta$  is shown in Fig. 3.15. It can be seen that by changing one of the variables, for instance  $\Delta\Theta$ , one can change the reflection coefficient value along the circle marked  $O_1$ , whereas, the other variable corresponds to the shift of the  $O_1$  circle center. Within the range of 0 to  $\pi$  the reflection coefficient travels full circle for one of the variables ( $\Delta\Theta$ ) and the circle center performs full turn around the Smith chart for the other ( $\Theta_1$ ), allowing to realize any desired reflection coefficient.

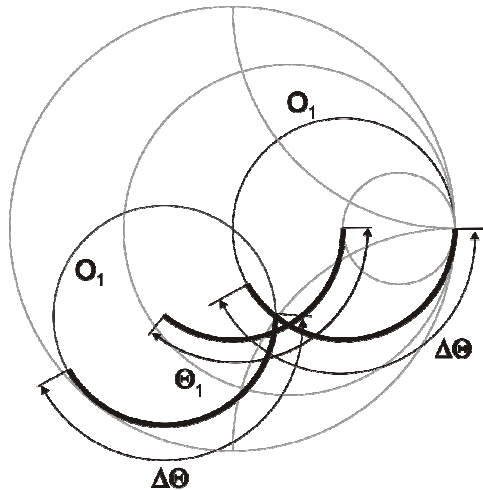


**Fig. 3.15.** Reflection coefficient of a rat-race coupler matching network with reflection coefficient displacement as a function of shorted line lengths  $\Theta_1$  and  $\Delta\Theta$  [59].

The presented concept of large-signal  $S$ -parameters measurements can be illustrated with the design of a 4W-power amplifier operating at 1.43 GHz [59]. The rat-race coupler has been designed on 0.8mm thick FR4 laminate and transmission line sections have been manufactured as finite ground microstrip lines allowing for applying sliding elements shorting the transmission line strips to the ground. Fig. 3.16 presents the measured minimum and maximum VSWR of the manufactured network. The VSWR ratio for the manufactured network equals 18:1 and allows for achieving impedance on the level of  $Z = 2.7 \Omega$ , which is sufficient for majority of power transistors. The limitation of VSWR ratio in the presented case is caused by relatively high losses of the chosen FR4 laminate and can be improved by careful design of the matching network with the use of low-loss dielectric substrates.

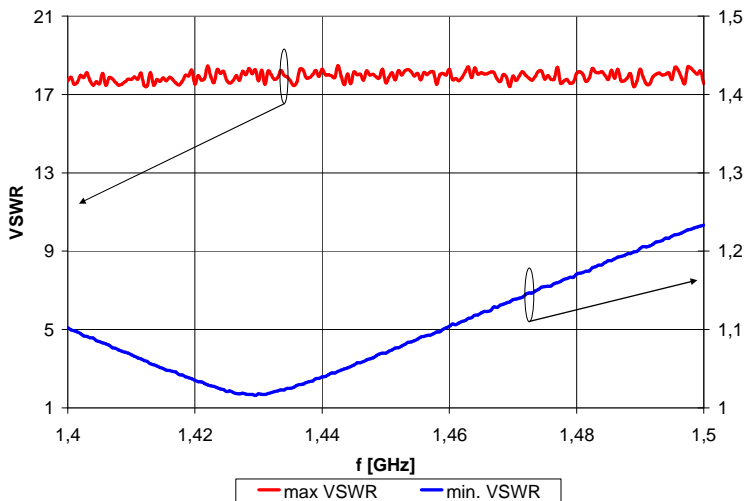


**Fig. 3.16.** Measured min. and max. VSWR of a rat-race coupler matching network shown schematically in Fig. 3.14 [59].

The matching network has been tested while designing a power amplifier operating at 1.43 GHz with the use of a MW6S004NT1 N-channel enhancement-mode lateral MOSFET transistor from Freescale Semiconductor. By the procedure of manual tuning, the input and output impedances of a transistor (together with a mounting fixture) have been determined and output power reaching 6 W has been measured. The manufactured measurement set-up is shown in Fig. 3.17. The measured value of the input and output reflection coefficients (impedances) have been shown in Table 3.1, in comparison with the small signal reflection coefficients given in the transistor specification. Based on the measured impedance values the power amplifier shown in Fig. 3.18 has been designed and manufactured. Figure 3.19 presents the input and output matching networks of the developed amplifier and measured results are shown in Fig. 3.20 and Fig. 3.21 for different bias conditions. It is seen that the output power reaching 6 W has been achieved with the gain equal 15 dB.

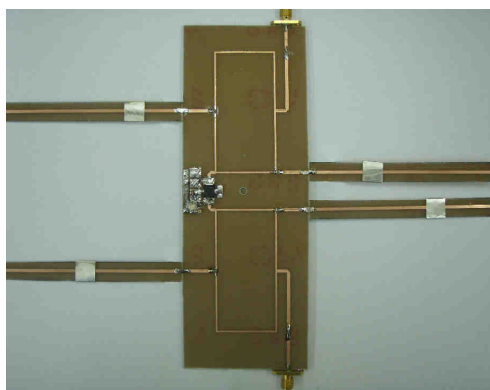


**Fig. 3.17.** Picture of a manufactured measurement setup with power transistor, input and output rat-race coupler matching networks and bias circuitry [59].

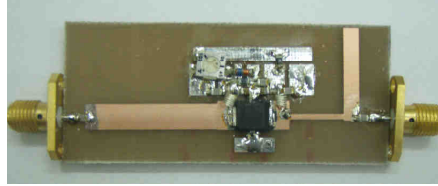


**Fig. 3.18.** Picture of the manufactured single-stage power amplifier [59].

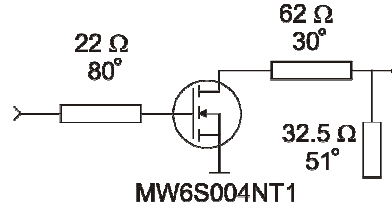


**Fig. 3.19.** Diagram schematic of input and output matching networks of the designed single-stage power amplifier [59].

The proposed technique has been also applied in the design of a two-stage power amplifier. The input and output matching networks remained unchanged and a new intermediate matching network has been found. Figure 3.22 shows a schematic diagram of the designed amplifier and the obtained measurement results are presented in Fig. 3.23. The obtained output power equals 6 W with the gain exceeding 30 dB.

**Table 3.1**  
**Measured input and output reflection coefficients (impedances) in comparison with small signal reflection coefficients given in the transistor specification [59]**

	small signal	measured*
input reflection coefficient	$ \Gamma  = 0.95$ Ang $ \Gamma  = -179^\circ$ $Z = 1.25-j0.65\Omega$	$ \Gamma  = 0.66$ Ang $ \Gamma  = -167.2^\circ$ $Z = 10.2-j5.34\Omega$
output reflection coefficient	$ \Gamma  = 0.866$ Ang $ \Gamma  = -132.4^\circ$ $Z = 4.35-j22.45\Omega$	$ \Gamma  = 0.65$ Ang $ \Gamma  = +145^\circ$ $Z = 11.6+j14.9\Omega$

\*Values measured together with the transistor fixture.

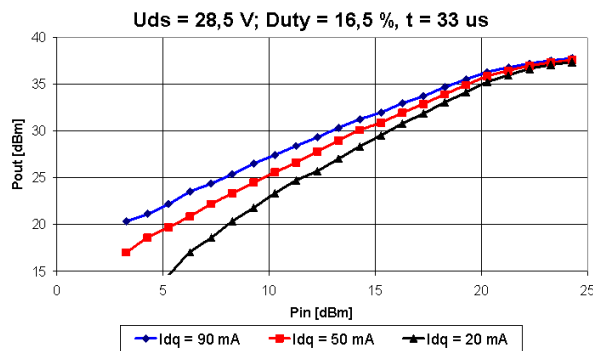


**Fig. 3.20.** Measured output power vs. input power of the manufactured power amplifier. Three curves are shown for three different values of transistor's drain quiescent current [59].

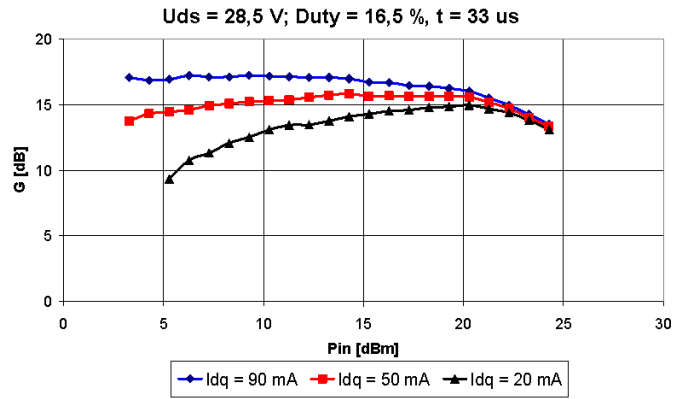


**Fig. 3.21.** Measured gain vs. input power of the manufactured power amplifier. Three curves are shown for three different values of transistor's drain quiescent current [59].

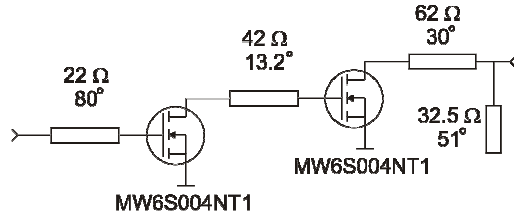


**Fig. 3.22.** Diagram schematic of input, intermediate and output matching networks of the designed two-stage power amplifier [59].

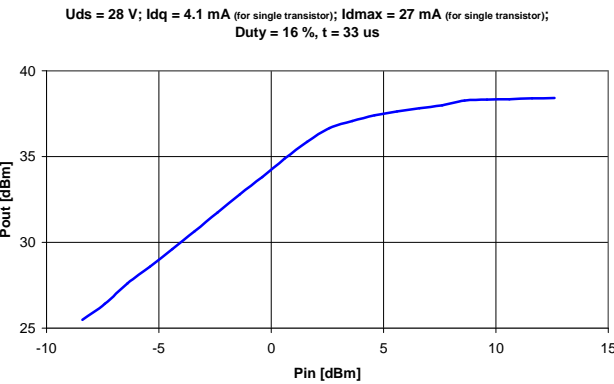


**Fig. 3.23.** Measured output power vs. input power of the manufactured two-stage [59].

### 3.3. Asymmetric coupled-line directional couplers as impedance transformers in balanced and $n$ -way power amplifiers

As it was shown in section 3.1, coupled-line directional couplers are the key components of balanced circuits and  $n$ -way power divider/combiners. On the other hand the impedances of high-power microwave active elements are small in comparison with  $Z_0$  – typically equal  $50 \Omega$  - as shown in section 3.2. It would be, therefore, desirable to develop directional couplers having the properties of both power dividers and impedance transformers. As it was shown in [30] an asymmetric coupled-line section offers the possibility of impedance transformation in a sense that, when appropriately designed, each line of the section can be terminated with the different impedances defined by (2.57). Therefore, the asymmetric coupled-line section can be used as an impedance transformer, where partial power defined by coupling  $C$  of the asymmetric coupled-line section (directional coupler) is delivered to the load having different impedance than the source impedance. Such a section cannot be straightforwardly applied into the balanced circuit, since the impedances at the coupled and direct ports would have different values. On the other hand both symmetrical and asymmetric coupled-line sections can be used for the design of two-port impedance transformers as it was theoretically presented in [119]. In [22] a simple solution has been presented allowing for size reduction of a multisection stepped quarter-wave transformer by replacing sections of quarter-wave-long transmission lines by meandered sections, in which coupling between appropriate arms has been considered. In [5, 82, 172] impedance transformers have been considered, in which meandered coupled-line sections have been utilized. A coupled-line section can also be used in the design of matching circuits of microwave power amplifiers. In [1] an exemplary design of a millimeter-wave monolithic amplifier design is presented, in which coupled-line sections have been used to design matching circuits for both gate and drain, utilizing the idea presented in [120].

A method of utilization of asymmetric coupled-line sections having the properties of simultaneous power division and impedance transformation in the direct and coupled ports, developed by the Author in [179], is described below.

Let us consider, the most simple circuit that allows for impedance transformation, which is a quarter-wave-long section of a transmission line, as shown in Fig. 3.24a.

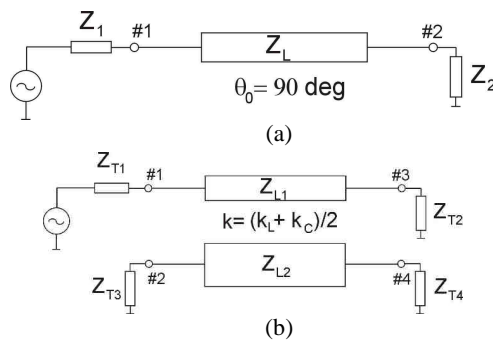


**Fig. 3.24.** Schematic diagram of a single-section quarter-wave transformer (a) and an asymmetric coupled-line quarter-wave transforming directional coupler (b) [179].

The impedance of the line depends on the values of terminating impedances  $Z_1$  and  $Z_2$  as follows

$$Z_L = \sqrt{Z_1 Z_2} \quad (3.11)$$

Similarly, a section of asymmetric coupled lines, shown in Fig. 3.24b, can be used as an impedance transformer. In this case a similar relation for the main-line impedance  $Z_{L1}$  should hold

$$Z_{L1} = \sqrt{Z_{T1} Z_{T2}} \quad (3.12)$$

Let us define the impedance ratio of the transformer as

$$\frac{Z_{T1}}{Z_{T2}} = R \quad (3.13)$$

Since it is desired to obtain power split and the impedance transformation simultaneously, and moreover, the impedance of the loads to which the power is transmitted should be equal, i.e.  $Z_{T2} = Z_{T3}$ , the impedance  $Z_{L2}$  of the coupled line is calculated as follows

$$Z_{L2} = \sqrt{Z_{T3} Z_{T4}} = \sqrt{Z_{T2} \frac{Z_{T2}}{R}} \quad (3.14)$$

The above relation has been derived assuming, that in order to obtain ideal match of all ports (at the center frequency) it is necessary to provide the same impedance transformation  $R$  in both lines of the coupled-line section. The terminating impedance of the isolated ports  $Z_{T4}$  is then calculated in the following manner

$$Z_{T4} = \frac{Z_{T2}}{R} \quad (3.15)$$

Let us examine the capacitance matrix of an ideal asymmetric coupled-line section in homogeneous dielectric medium having  $\epsilon_r = 1$  (the phase velocity of the propagating waves equals  $c$  – free space light velocity). The values of the capacitance matrix elements for the coupled-line section described by  $Z_{L1}$ ,  $Z_{L2}$ ,  $k$ ,  $c$  are defined as follows

$$C_{11} = \frac{1}{c Z_{L1}} \quad (3.16)$$

$$C_{22} = \frac{1}{c Z_{L2}} \quad (3.17)$$

$$C_m = k \sqrt{C_{11} C_{22}} \quad (3.18)$$

The capacitances of the coupled conductors, shown in Fig. 3.25a are expressed as

$$C_1 = C_{11} - C_m, \quad C_2 = C_{22} - C_m \quad (3.19)$$

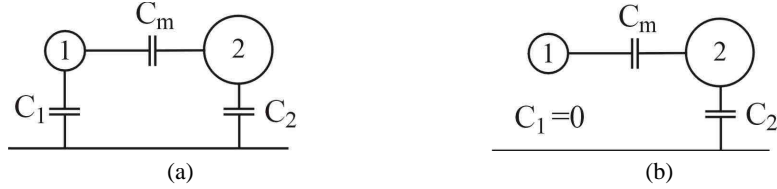
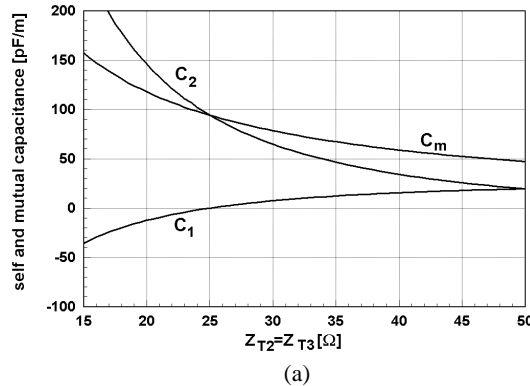
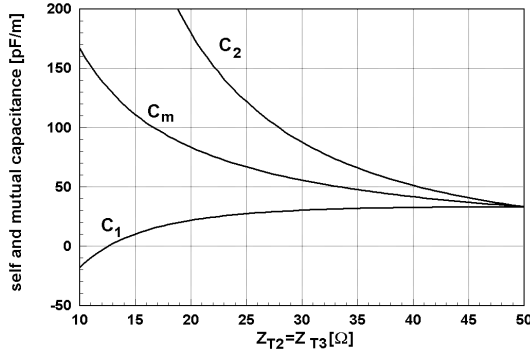


**Fig. 3.25.** Schematic diagram of the cross-section of an asymmetric coupled-line system (a) and the same system in which  $C_1 = 0$  (b) [179].

Values of capacitances  $C_1$ ,  $C_2$  and  $C_m$  for the ideal asymmetric coupled-line section vs. load impedance at direct and coupled ports  $Z_{T2} = Z_{T3}$  have been plotted in Fig. 3.26a, assuming source impedance  $Z_{T1} = 50 \Omega$ ,  $C = 3 \text{ dB}$  ( $k = 0.707$ ) and  $\epsilon_r = 1$ . It is important to notice that the capacitance  $C_1$  of the direct line decreases with the increase of impedance ratio  $R$  taking negative values for large values of  $R$ . Fig. 3.26b shows similar calculations, in which the coupling  $C = 6 \text{ dB}$  of the coupled-line section has been assumed. As in the previous case the capacitance of the direct line  $C_1$  takes negative values for greater  $R$ , different however, than in the first case. The relation between the coupling  $C$  ( $k$ ) and the impedance ratio can be derived for the simple case of homogeneous coupled lines.



(a)



(b)

**Fig. 3.26.** Calculated self and mutual capacitances of an asymmetric coupled-line section assuming  $Z_{T1} = 50 \Omega$  and uniform dielectric medium ( $\epsilon_r = 1$ ) versus  $Z_{T2} = Z_{T3}$  for the case of coupling  $C = 3 \text{ dB}$  (a) and  $C = 6 \text{ dB}$  (b) [179].

To derive the relation let us first note that the greatest value of  $R$  is obtained when  $C_1 = 0$ , which is the boundary of physical realization of the circuit. Substituting that condition into (2.57) the following expressions for 1<sup>st</sup> and 2<sup>nd</sup> line impedance are obtained

$$Z_{T1} = \sqrt{\frac{L_{11}}{C_{11}}} \xrightarrow{C_1=0} \sqrt{\frac{L_{11}}{C_m}} \quad (3.20)$$

$$Z_{T2} = \sqrt{\frac{L_{22}}{C_{22}}} = \sqrt{\frac{L_{22}}{C_2 + C_m}} \quad (3.21)$$

Let us now calculate the inductance matrix also assuming  $C_1 = 0$

$$\begin{aligned} L &= \epsilon_0 \mu_0 C^{-1} = \epsilon_0 \mu_0 \frac{1}{C_{11} C_{22} - C_m^2} \begin{bmatrix} C_{22} & C_m \\ C_m & C_{11} \end{bmatrix} \xrightarrow{C_1=0} \\ &\rightarrow \epsilon_0 \mu_0 \frac{1}{C_m C_{22} - C_m^2} \begin{bmatrix} C_{22} & C_m \\ C_m & C_m \end{bmatrix} = \epsilon_0 \mu_0 \begin{bmatrix} \frac{C_{22}}{C_2 C_m} & \frac{1}{C_2} \\ \frac{1}{C_2} & \frac{1}{C_2} \end{bmatrix} \end{aligned} \quad (3.22)$$

Applying calculated  $L_{11}$  and  $L_{22}$  into (3.20) and (3.21), the following expressions for line impedances are obtained:

$$Z_{T1} = \sqrt{\frac{L_{11}}{C_m}} = \sqrt{\frac{\epsilon_0 \mu_0 C_{22}}{C_2 C_m^2}} \quad (3.23)$$

$$Z_{T2} = \sqrt{\frac{L_{22}}{C_{22}}} = \sqrt{\frac{\epsilon_0 \mu_0}{C_2 (C_2 + C_m)}} \quad (3.24)$$

Calculating the impedance ratio  $R$  from (3.13), (3.23) and (3.24) one obtains:

$$R = \frac{Z_{T1}}{Z_{T2}} = \sqrt{\frac{C_{22}}{C_2 C_m^2} C_2 (C_2 + C_m)} = \frac{C_{22}}{C_m} \quad (3.25)$$

On the other hand the coupling of coupled lines  $k$  in this case equals:

$$k = k_C = \frac{C_m}{\sqrt{C_{11} C_{22}}} \xrightarrow{C_1=0} \frac{C_m}{\sqrt{C_m C_{22}}} = \sqrt{\frac{C_m}{C_{22}}} \quad (3.26)$$

Therefore, the limitation on the impedance ratio is expressed by the simple formula, derived by comparing (3.25) and (3.26):

$$R = \frac{1}{k^2} \quad (3.27)$$

The above presented limitation on impedance transformation with the use of coupled-line sections states that, for the case of an equal-split ( $C = 3$  dB) directional coupler and the same terminating impedances of the transmission and coupled ports, the maximum physically realizable impedance ratio equals  $R = 2$ . Calculated frequency characteristics of such a

3-dB ideal coupled-line section with impedance transformation  $R = 2$  are presented in Fig. 3.27. It is seen that the section is ideally matched at the center frequency and has equal power split. The return losses of the coupled-line section have been additionally compared to the return losses of a single-section quarter-wave-long transmission-line transformer having  $R = 2$ , shown in Fig. 3.24a, and it is seen that the coupled-line circuit operates in a broader frequency range than the single section transformer. Finally, it is interesting to test the asymmetric coupled-line section in application to the balanced circuit. Fig. 3.28 presents a schematic diagram of a balanced circuit consisting of two identical 3-dB asymmetric coupled-line sections for the case of maximum attainable impedance transformation  $R = 2$ . The impedance within the balanced circuit equals  $Z_{T2,3} = 25 \Omega$  (assuming source impedance  $Z_{T1} = 50 \Omega$ ) and the impedance of the termination of the isolated port  $Z_{T4} = 12.5 \Omega$ . Calculated frequency characteristics of the regarded balanced circuit are presented in Fig. 3.29. As it is seen the circuit is matched in a wider bandwidth than a single-section transmission-line transformer and has theoretically no losses from input to output. It is important to note that in  $n$ -way power dividers the impedance ratio can be easily increased to the value  $R_{total} = n$  by the appropriate connection of several 3-dB directional couplers, each transforming the impedance with the ratio  $R = 2$ .

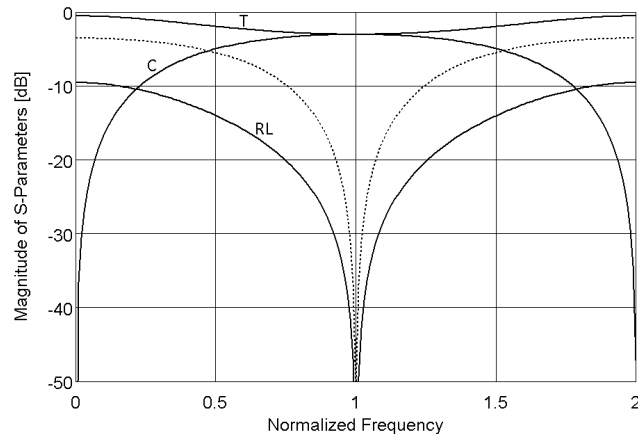


**Fig. 3.27.** Calculated frequency characteristics of an asymmetric coupled-line section for which  $C = 3$  dB,  $R = 2$  (solid lines), in comparison with the return losses of a single-section quarter-wave transmission-line transformer for which  $R = 2$  [179].

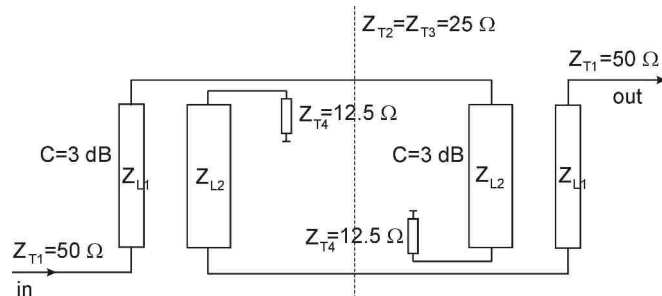


**Fig. 3.28.** Schematic diagram of a balanced circuit consisting of two asymmetric 3-dB directional couplers providing impedance transformation with the ratio  $R = 2$  [179].

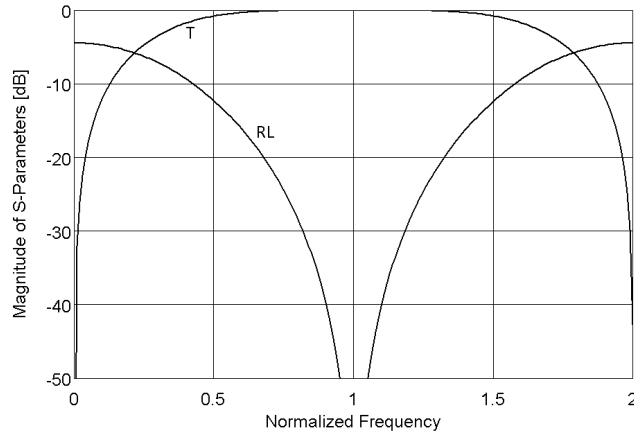


**Fig. 3.29.** Calculated frequency characteristics of a balanced circuit shown schematically in Fig. 3.28 [179].

To verify the theoretical analysis a 3-dB coupled-line directional coupler has been designed and manufactured. To achieve the maximum ratio of the transformed impedances  $R = 2$  the coupled-line structure shown in Fig. 3.30 has been chosen which allows to minimize the capacitance  $C_1$  of the upper stripline, while it is shielded from the ground plane by the wide lower stripline. It is important to underline that the minimization of the  $C_1$  capacitance ensures maximum impedance ratio  $R$ . The assumed input impedance is equal  $Z_{T1} = 50 \Omega$ , whereas, the impedances at the coupled and transmission ports are equal  $Z_{T2,3} = 25 \Omega$ . The chosen structure has been analyzed with the use of a spectral domain method [131]. The obtained results are shown in Table 3.2. Note, that a very low value of  $C_1 = 1.2 \text{ pF/m}$  has been obtained providing for impedance ratio  $R = 1.96$ . The designed coupler has been manufactured and measured with the use of quarter-wave impedance transformers applied to the coupled and transmission ports, as shown schematically in Fig. 3.31. Figure 3.32 presents the measured S parameters in comparison with the simulated ones. It is seen that a very good agreement has been achieved in terms of power splitting and impedance match. Figure 3.33a shows a photograph of the manufactured directional coupler. The application of the designed coupler in balanced circuits has been tested, as shown in Fig. 3.28. The manufactured network is shown in Fig. 3.33b and its measured results are shown in Fig. 3.34. The achieved insertion losses are equal 0.6 dB.

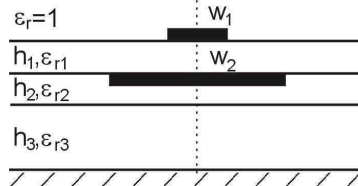


**Fig. 3.30.** Cross-sectional view of the dielectric structure used for the design of 3-dB asymmetric coupled-line impedance-transforming directional couplers [179].

**Table 3.2**

Parameters of the coupled-line section for which  $R = 2$ , designed in the structure shown in Fig. 3.30, having  $h_1 = 0.051$  mm,  $\epsilon_{r1} = 3.4$ ,  $h_2 = 0.04$  mm,  $\epsilon_{r2} = 3.38$ ,  $h_3 = 0.508$  mm,  $\epsilon_{r3} = 3.38$  and  $w_1 = 0.36$  mm,  $w_2 = 3.15$  mm [179]

parameter	value
$C_{11}$ [pF/m]	220.9
$C_{22}$ [pF/m]	438.6
$C_m$ [pF/m]	219.7
$C_1$ [pF/m]	<b>1.2</b>
$C_2$ [pF/m]	218.9
$L_{11}$ [nH/m]	282.4
$L_{22}$ [nH/m]	148.4
$L_m$ [nH/m]	145.9
$k_L$	0.71
$k_C$	0.705
$k$	0.707
$Z_{T1}$ [ $\Omega$ ]	50
$Z_{T2,3}$ [ $\Omega$ ]	25.5
$Z_{T4}$ [ $\Omega$ ]	13.27
$Z_{L1}$ [ $\Omega$ ]	35.7
$Z_{L2}$ [ $\Omega$ ]	18.4
$\epsilon_{effc}$	2.94
$\epsilon_{eff\pi}$	2.75

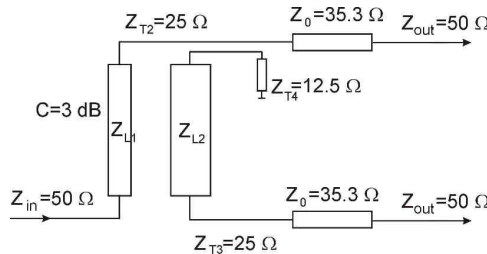


**Fig. 3.31.** Schematic diagram of a 3-dB asymmetric coupled-line 50/25  $\Omega$  impedance-transforming directional coupler with additional single-section impedance transformers connected to the direct and coupled ports [179].

Similarly, a 3-dB directional coupler has been designed for impedance transformation from  $Z = 25 \Omega$  to  $Z = 12.5 \Omega$  (Fig. 3.33c). The parameters of the designed coupler are shown in Table 3.3. Figure 3.35 presents a schematic diagram of the circuit developed for measurements of the directional coupler. Measured results in comparison with the theoretical ones are presented in Fig. 3.36. The comment is needed, that the condition for the maximum impedance ratio has been derived for the homogeneous medium, which is not the case in the chosen multilayer microstrip structure. In the following section a theoretical analysis is given, which shows that, when the higher-impedance line is decoupled from the ground plane, the condition (3.27) converts into the condition stating that the impedance-transforming ratio equals the inverse product of the inductive and capacitive coupling coefficients.

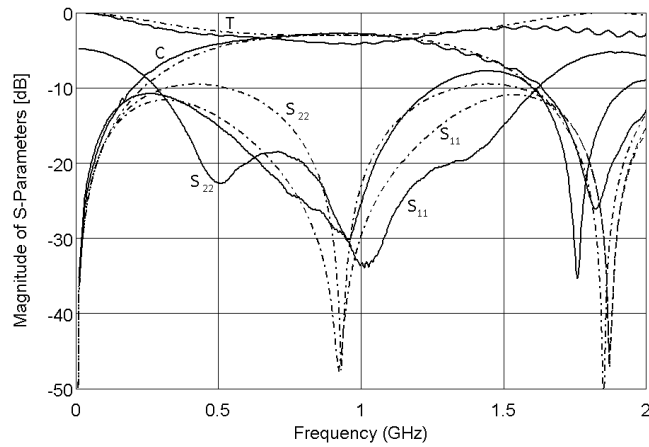


**Fig. 3.32.** Calculated (dashed line) and measured (solid line) frequency characteristics of a 3-dB asymmetric coupled-line 50/25  $\Omega$  impedance-transforming directional coupler with additional single-section impedance transformers connected to the direct and coupled ports, as shown in Fig. 3.31 [179].

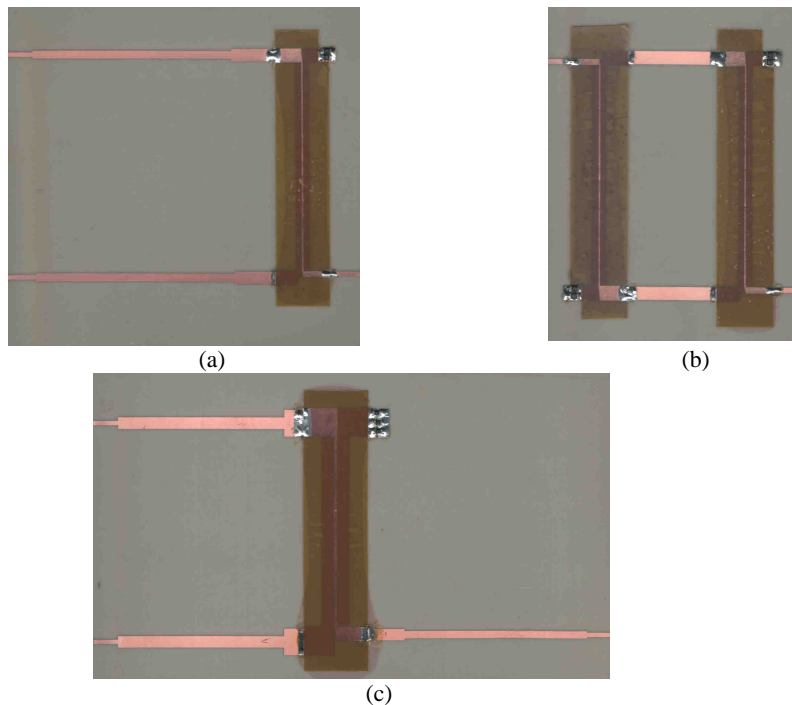


**Fig. 3.33.** Pictures of the manufactured circuits. (a) the 3-dB directional coupler for 50 to 25  $\Omega$  impedance transformation, (b) the balanced circuit consisting of two such 3-dB directional couplers and (c) the 3-dB directional coupler for 25 to 12.5  $\Omega$  impedance transformation [179].

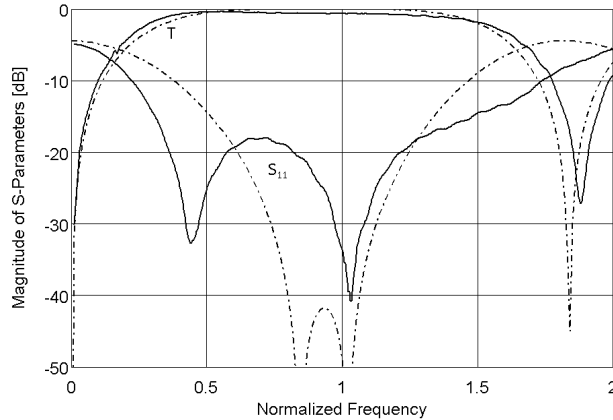


**Fig. 3.34.** Calculated (dashed line) and measured (solid line) frequency characteristics of the balanced network (shown in Fig. 3.28) consisting of two 3-dB asymmetric coupled-line impedance-transforming directional couplers presented in Fig. 3.32 [179].

**Table 3.3**

Parameters of the coupled-line section for which  $R = 2$ , designed in the structure shown in Fig. 3.30, having  $h_1 = 0.051$  mm,  $\epsilon_{r1} = 3.4$ ,  $h_2 = 0.04$  mm,  $\epsilon_{r2} = 3.38$ ,  $h_3 = 0.508$  mm,  $\epsilon_{r3} = 3.38$  and  $w_1 = 0.95$  mm,  $w_2 = 7.2$  mm [179]

parameter	value
$C_{11}$ [pF/m]	440
$C_{22}$ [pF/m]	883.9
$C_m$ [pF/m]	439.3
$C_1$ [pF/m]	<b>0.7</b>
$C_2$ [pF/m]	444.6
$L_{11}$ [nH/m]	145.9
$L_{22}$ [nH/m]	77
$L_m$ [nH/m]	76.3
$k_L$	0.72
$k_C$	0.70
$k$	0.71
$Z_{T1}$ [ $\Omega$ ]	25.5
$Z_{T2,3}$ [ $\Omega$ ]	12.75
$Z_{T4}$ [ $\Omega$ ]	6.7
$Z_{L1}$ [ $\Omega$ ]	18.2
$Z_{L2}$ [ $\Omega$ ]	9.3
$\epsilon_{effc}$	3.08
$\epsilon_{eff\pi}$	2.78

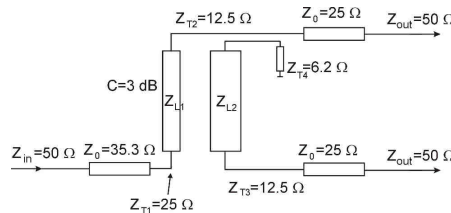


**Fig. 3.35.** Schematic diagram of a 3-dB asymmetric coupled-line 25/12.5  $\Omega$  impedance-transforming directional coupler with additional single-section impedance transformers connected to the input, direct and coupled ports [179].

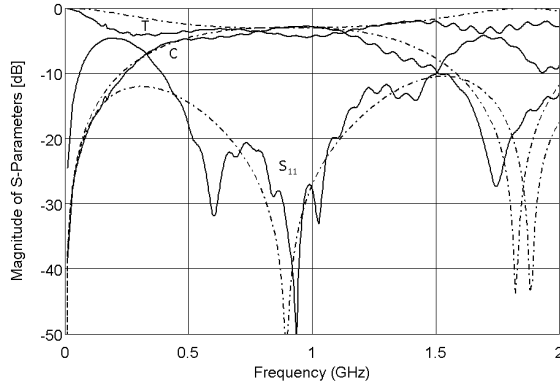


**Fig. 3.36.** Calculated (dashed line) and measured (solid line) frequency characteristics of the 3-dB asymmetric coupled-line  $25/12.5 \Omega$  impedance-transforming directional coupler with additional single section impedance transformers connected to the input, direct and coupled ports, as shown in Fig. 3.35 [179].

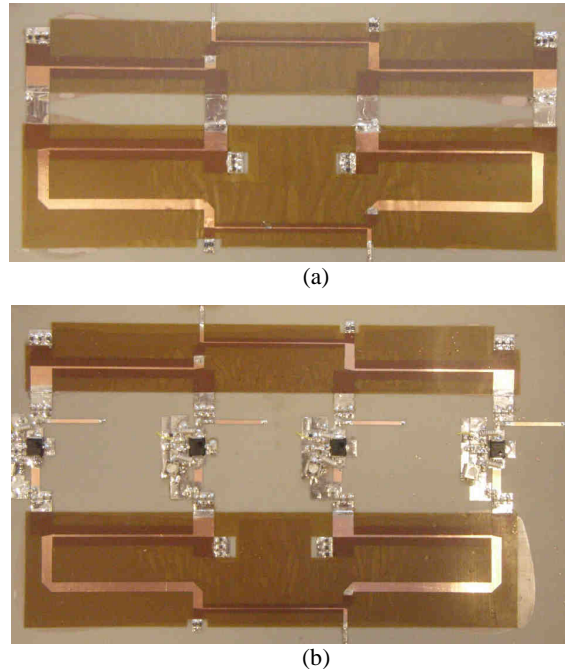


**Fig. 3.37.** Photograph of the developed 4-way power divider/combiner in a back-to-back connection (a), and the 4-way power amplifier (b) [179].

Both designed couples have been used to design a 4-way power divider, the picture of which in a back-to-back connection is presented in Fig. 3.37a. Such a network allows for equal power split and impedance transformation with  $R_{total} = 4$ . The calculated and measured frequency responses of the back-to-back connection are shown in Fig. 3.38, where a very good agreement between the obtained results is observed.

The designed 4-way power splitter/combiner has been applied in a 4-way power amplifier, shown in Fig. 3.37b, in which a 4W N-channel MOSFET transistor (MW6S004NT1 from Freescale Semiconductor) as an active element has been used. The large signal input and output impedances have been measured with the use of the method presented in section 3.2 and the results are:  $Z_{in} = 2.82 - j2.83 \Omega$ ,  $Z_{out} = 11.1 - j6.51 \Omega$ . As it is seen, the measured output impedance is very close to the output impedance of the designed power splitting/combining network. The input impedance of the transistor is lower than the feeding network, but a simple matching circuit has been designed for the center operating frequency  $f_0 = 0.92$  GHz. The measured output power versus input power is presented in Fig. 3.39, and one can noticed that the expected power exceeding  $4 \times 4 = 16$  W has been obtained.

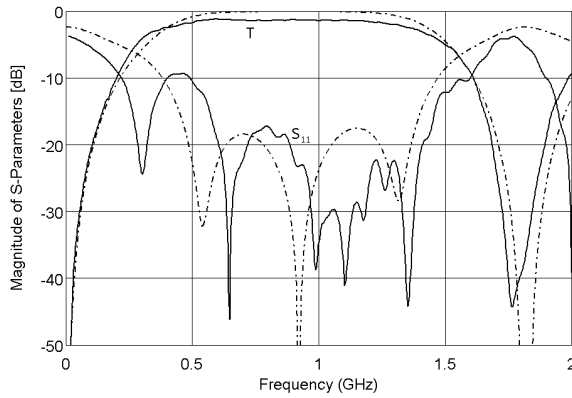


**Fig. 3.38.** Calculated (dashed line) and measured (solid line) frequency characteristics of the 4-way 50/12.5  $\Omega$  impedance transforming power divider/combiner in a back-to-back connection consisting of the developed asymmetric 3-dB directional couplers [179].

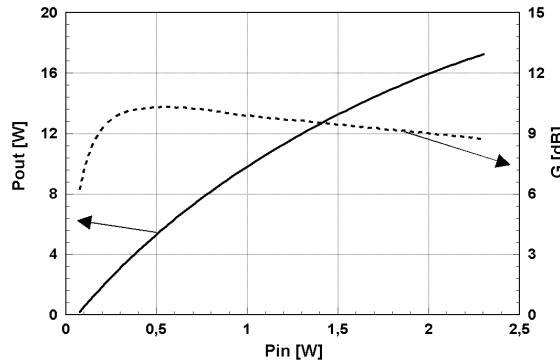


**Fig. 3.39.** Measured output power (solid line) and gain (dashed line) characteristics vs. input power of the developed 4-way power amplifier [179].

### 3.4. Approach to the design of asymmetric coupled-line impedance transforming directional couplers

The presented in previous section analysis of impedance transforming coupled-line couplers has shown that the maximum impedance transformation ratio equals  $R = 2$ . In this case the self-capacitance of one of the coupled lines equals zero. Since in practical applications the maximum value of the impedance transformation is of the greatest interest, it is worth to further examine the methods of analysis and design of such transformers. Figure 3.40 shows an exemplary cross-section of coupled-transmission lines, in which the inner conductor is completely enclosed by the outer conductor, satisfying therefore, the condition  $C_1 = 0$ , and allowing to obtain  $R = 2$ . Such a coupled-line section can be regarded as a connection of two transmission lines, as shown schematically in Fig. 3.41.

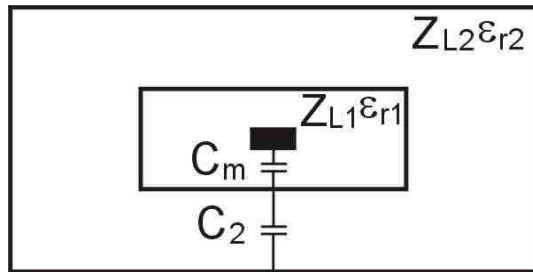


**Fig. 3.40.** Two coupled lines having inner conductor shielded by outer conductor.

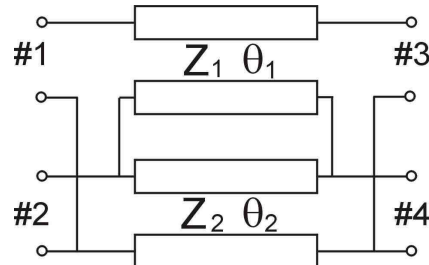


**Fig. 3.41.** Schematic diagram of an impedance transforming directional coupler realized as a connection of two transmission lines.

In order to calculate the impedances  $Z_1$  and  $Z_2$  of the transmission-line connection having the properties corresponding to the properties of a 3-dB coupled-line section with impedance transformation ratio  $R = 2$ , per-unit-length capacitance and inductance matrices have been considered. It is evident, from Fig. 3.40, that the capacitance matrix of the coupled transmission lines has the following form

$$C = \begin{bmatrix} C_m & -C_m \\ -C_m & C_2 + C_m \end{bmatrix} \quad (3.28)$$

Let us assume, that the medium of propagation is homogeneous, i.e.  $\epsilon_{r1} = \epsilon_{r2} = \epsilon_r$ , and the phase velocity of the propagating waves equals  $v$ . The self and mutual capacitances can be defined by line impedances as follows:

$$C_m = \frac{1}{vZ_1} = \frac{\sqrt{\epsilon_r}}{cZ_1} \quad (3.29)$$

$$C_2 = \frac{1}{vZ_2} = \frac{\epsilon_r}{cZ_2} \quad (3.30)$$

$$C_{11} = \frac{1}{vZ_1} = \frac{\sqrt{\epsilon_r}}{cZ_1} \quad (3.31)$$

$$C_{22} = \frac{1}{vZ_2} + \frac{1}{vZ_1} = \frac{\sqrt{\epsilon_r}}{cZ_2} + \frac{\sqrt{\epsilon_r}}{cZ_1} \quad (3.32)$$

The inductance matrix can be calculated from (3.22):

$$L = \frac{1}{v^2} C_0^{-1} \quad (3.33)$$

where  $C_0$  is the capacitance matrix of the coupled lines for which the phase velocities of propagating waves equal  $c$ , i.e. the conductors are placed in an homogeneous free-space dielectric medium. In such a case the components of  $C_0$  are calculated as follows:

$$C_{0m} = \frac{1}{cZ_1\sqrt{\epsilon_r}} \quad (3.34)$$

$$C_{02} = \frac{1}{cZ_2\sqrt{\epsilon_r}} \quad (3.35)$$

$$C_{011} = \frac{1}{cZ_1\sqrt{\epsilon_r}} \quad (3.36)$$

$$C_{022} = \frac{1}{cZ_1\sqrt{\epsilon_r}} + \frac{1}{cZ_2\sqrt{\epsilon_r}} \quad (3.37)$$

and components of  $L$  matrix as:

$$L_{11} = \frac{1}{c^2} \frac{C_{022}}{C_{02}C_{0m}} = \frac{Z_1\sqrt{\epsilon_r} + Z_2\sqrt{\epsilon_r}}{c} \quad (3.38)$$

$$L_{22} = L_m = \frac{1}{c^2} \frac{1}{C_{02}} = \frac{Z_2 \sqrt{\epsilon_r}}{c} \quad (3.39)$$

Having found the  $L$  and  $C$  matrix components of the coupled lines described by the impedances of equivalent circuit composed of two uncoupled lines, the two sets of impedances, i.e.  $Z_1, Z_2$  and  $Z_{L1}, Z_{L2}$  can be related using (2.52, 2.53) and (2.57):

$$Z_{L1} = \sqrt{\frac{L_{11}}{C_{11}}} = \sqrt{\frac{L_{11}}{C_m}} = \sqrt{Z_1(Z_1 + Z_2)} \quad (3.40)$$

$$Z_{L2} = \sqrt{\frac{L_{22}}{C_{22}}} = Z_2 \sqrt{\frac{Z_1}{Z_1 + Z_2}} \quad (3.41)$$

From (3.40, 3.41)  $Z_1$  and  $Z_2$  can be found:

$$Z_1 = \sqrt{Z_{L1}(Z_{L1} - Z_{L2})} \quad (3.42)$$

$$Z_2 = Z_{L2} \sqrt{\frac{Z_{L1}}{Z_{L1} - Z_{L2}}} \quad (3.43)$$

From (3.42, 3.43) the impedances  $Z_1$  and  $Z_2$  of uncoupled transmission lines are found to be equal  $Z_1 = Z_2 = 25\Omega$ . The presented considerations assumed the homogeneous dielectric medium. Note that in such a case the impedances  $Z_1$  and  $Z_2$  are not affected by the change of the medium, i.e. by the change of its dielectric constant. In case of inhomogeneous dielectric media when  $\epsilon_{r1} \neq \epsilon_{r2}$ , relations (3.40, 3.41) modify as follows:

$$Z_{L1} = \sqrt{Z_1 \left( Z_1 + Z_2 \sqrt{\frac{\epsilon_{r2}}{\epsilon_{r1}}} \right)} \quad (3.44)$$

$$Z_{L2} = Z_2 \sqrt{\frac{Z_1 \sqrt{\frac{\epsilon_{r2}}{\epsilon_{r1}}}}{Z_1 \sqrt{\frac{\epsilon_{r2}}{\epsilon_{r1}}} + Z_2}} \quad (3.45)$$

In this case the impedance  $Z_2$  can be expressed as:

$$Z_2 = \sqrt{\frac{\epsilon_{r1}}{\epsilon_{r2}}} \frac{Z_{L1}^2 - Z_1^2}{Z_1} \quad (3.45)$$

and  $Z_1$  can be found from the following equation:

$$Z_1^4 + Z_1^2 \left( \frac{\epsilon_{r1} - \epsilon_{r2}}{\epsilon_{r1}} Z_{L2}^2 - 2Z_{L1}^2 \right) + Z_{L1}^4 - Z_{L1}^2 Z_{L2}^2 = 0 \quad (3.46)$$

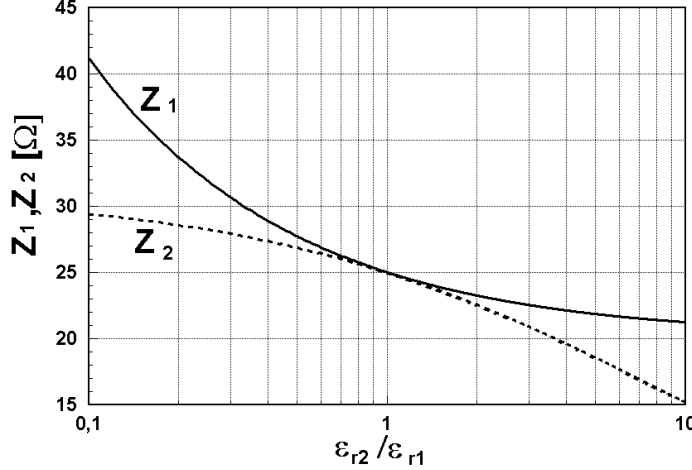


**Fig. 3.42.** Impedances  $Z_1$  and  $Z_2$  of the transmission lines shown in Fig. 3.41 assuming inhomogeneous dielectric media vs. dielectric constant ratio calculated using (3.45) and (3.46).

Also the limitation on the impedance transformation ratio  $R$  can be derived for inhomogeneous coupled lines with the use of the uncoupled-line approach. The derivation is similar to the previously shown (3.16 – 3.27) and (3.27), being the final conclusion that for homogeneous coupled lines the maximum impedance transformation ratio  $R$  is equal the inverse of squared coupling coefficient  $k$ . In this case the capacitance and inductance matrices can be written as follows:

$$C = \begin{bmatrix} C_m & -C_m \\ -C_m & C_2 + C_m \end{bmatrix} \quad (3.47)$$

$$C_0 = \begin{bmatrix} \frac{C_m}{\epsilon_{r1}} & -\frac{C_m}{\epsilon_{r1}} \\ -\frac{C_m}{\epsilon_{r1}} & \frac{C_2 + C_m}{\epsilon_{r2}} \end{bmatrix} \quad (3.48)$$

$$L = \frac{1}{c^2} [C_0]^{-1} = \frac{1}{c^2} \frac{\epsilon_{r1} \epsilon_{r2}}{C_m C_2} \begin{bmatrix} \frac{C_2 + C_m}{\epsilon_{r2}} & -\frac{C_m}{\epsilon_{r1}} \\ -\frac{C_m}{\epsilon_{r1}} & \frac{C_2 + C_m}{\epsilon_{r2}} \end{bmatrix} = \frac{1}{c^2} \begin{bmatrix} \frac{\epsilon_{r2} + \epsilon_{r1}}{C_2} & \frac{\epsilon_{r2}}{C_2} \\ \frac{\epsilon_{r2}}{C_2} & \frac{\epsilon_{r2}}{C_2} \end{bmatrix} \quad (3.49)$$

$$Z_{T1} = \frac{1}{c} \sqrt{\frac{\epsilon_{r1} + \epsilon_{r2}}{C_m^2 + C_2 C_m}} \quad (3.50)$$

$$Z_{T2} = \frac{1}{c} \sqrt{\frac{\epsilon_{r2}}{C_2(C_2 + C_m)}} \quad (3.51)$$

$$k_c = \sqrt{\frac{C_m}{C_2 + C_m}} \quad (3.52)$$

$$k_L = \sqrt{\frac{\epsilon_{r2}C_m}{\epsilon_{r1}C_2 + \epsilon_{r2}C_m}} \quad (3.53)$$

$$R = \frac{Z_{T1}}{Z_{T2}} = \sqrt{\frac{(\epsilon_{r1}C_2 + \epsilon_{r2}C_m)(C_2 + C_m)}{\epsilon_{r2}C_m^2}} = \frac{1}{k_L k_c} \quad (3.54)$$

The derived limitation (3.54) states that in case of inhomogeneous coupled lines, in which the higher-impedance line is completely decoupled from the ground plane, the maximum impedance-transformation ratio equals the inverse product of inductive and capacitive coupling coefficients. The derived limitation also proves the presented in section 3.3 design approach, in which the designed impedance-transforming directional couplers have been designed in a multilayer microstrip technique. In each of the two couplers, the higher-impedance coupled-lines were practically decoupled from the ground plane, and the impedance transformation ratios found from (3.54) equals  $R = 1.997$  and  $R = 1.984$  in case of the coupler shown in Table 3.2 and Table 3.3, respectively.

The analysis of the circuit presented in 3.41 can be performed with the use of the method of analysis of symmetrical  $n$ -port networks with the use of in-phase and out-of-phase excitations [122, 123]. The conversion of the circuit into two even- and odd-mode excited subcircuits is presented in Fig. 3.42. In order to apply this method of analysis, it is required to assume that all terminating impedances are equal, so that the symmetry plane can be constituted. The 4-port network simplifies into two 2-port networks with open-ended and short-ended transmission-line stubs. The impedances of the stubs  $Z_{s1}$  and  $Z_{s2}$  are defined as:

$$Z_{s1}^o = jZ_1 \tan\left(\frac{\theta_1}{2}\right) \quad (3.55)$$

$$Z_{s2}^o = jZ_2 \tan\left(\frac{\theta_2}{2}\right) \quad (3.55)$$

for the network with odd-mode excitation, and

$$Z_{s1}^e = -jZ_1 \cot\left(\frac{\theta_1}{2}\right) \quad (3.56)$$

$$Z_{s2}^e = -jZ_2 \cot\left(\frac{\theta_2}{2}\right) \quad (3.57)$$

for the network with even-mode excitation.

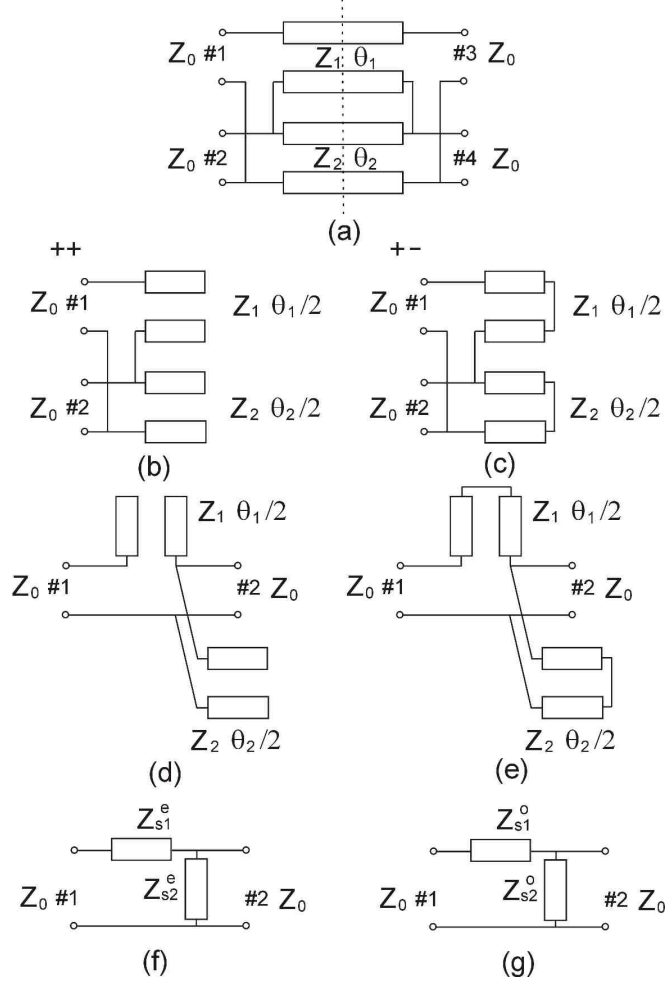


**Fig. 3.43.** Schematic diagram of an impedance transforming directional coupler with the symmetry plane indicated (a), even- and odd-mode excitation equivalent sub-circuits (b) and (c) respectively, and their reconfigured versions (d) - (g).

The resulting scattering matrices for even- and odd-mode excitations are

$$S^{e,o} = \begin{bmatrix} \frac{\frac{Z_{s1}^{e,o}}{Z_{s2}^{e,o}} + \frac{Z_{s1}^{e,o}}{Z_0} - \frac{Z_0}{Z_{s2}^{e,o}}}{2 + \frac{Z_{s1}^{e,o}}{Z_{s2}^{e,o}} + \frac{Z_{s1}^{e,o}}{Z_0} + \frac{Z_0}{Z_{s2}^{e,o}}} & \frac{2}{2 + \frac{Z_{s1}^{e,o}}{Z_{s2}^{e,o}} + \frac{Z_{s1}^{e,o}}{Z_0} + \frac{Z_0}{Z_{s2}^{e,o}}} \\ \frac{-\frac{Z_{s1}^{e,o}}{Z_{s2}^{e,o}} + \frac{Z_{s1}^{e,o}}{Z_0} - \frac{Z_0}{Z_{s2}^{e,o}}}{2 + \frac{Z_{s1}^{e,o}}{Z_{s2}^{e,o}} + \frac{Z_{s1}^{e,o}}{Z_0} + \frac{Z_0}{Z_{s2}^{e,o}}} & \frac{2}{2 + \frac{Z_{s1}^{e,o}}{Z_{s2}^{e,o}} + \frac{Z_{s1}^{e,o}}{Z_0} + \frac{Z_0}{Z_{s2}^{e,o}}} \end{bmatrix} \quad (3.58)$$

The scattering matrix of the 4-port network can be found from [123]:

$$\begin{aligned}
S_{11} &= \frac{1}{2}(S_{11}^e + S_{11}^o) \\
S_{12} &= \frac{1}{2}(S_{11}^e - S_{11}^o) \\
S_{13} &= \frac{1}{2}(S_{12}^e + S_{12}^o) \\
S_{14} &= \frac{1}{2}(S_{12}^e - S_{12}^o) \\
S_{33} &= \frac{1}{2}(S_{22}^e + S_{22}^o) \\
S_{34} &= \frac{1}{2}(S_{22}^e - S_{22}^o)
\end{aligned} \tag{3.59}$$

and the remaining parameters are found from the symmetry condition as

$$\begin{aligned}
S_{41} &= S_{14} & S_{31} &= S_{13} & S_{11} &= S_{22} & S_{33} &= S_{44} & S_{12} &= S_{21} \\
S_{13} &= S_{24} & S_{23} &= S_{14} & S_{31} &= S_{42} & S_{32} &= S_{41} & S_{34} &= S_{43}
\end{aligned} \tag{3.60}$$

The scattering matrix of the network shown in Fig. 3.43a described by (3.55 – 3.60) has been derived assuming equal terminating impedances  $Z_0$  of the 4-port network. In order to examine the properties of the impedance transforming network, the scattering matrix needs to be renormalized, so that each port is terminated with the proper impedance, as shown in Fig. 3.24b. The renormalization of  $S$  matrix terminating impedances has been shown in [14, 89]

$$S' = A^{-1}(S - \Gamma^+)(I - \Gamma S)^{-1}A^+ \tag{3.61}$$

where  $\Gamma$  and  $A$  are the diagonal matrices with their  $i^{\text{th}}$  diagonal components being  $r_i$  and  $(1 - r_i^*)\sqrt{|1 - r_i r_i^*|}/|1 - r_i|$ , respectively. The  $^+$  indicates the complex conjugate transposed matrix and  $r_i$  are reflection coefficients of the new terminating impedances  $Z_{Ti}'$  with respect to  $Z_i^*$ . The calculated frequency responses of the network for different dielectric constants  $\epsilon_{r1}$  and  $\epsilon_{r2}$  are shown in Fig. 3.44, whereas, Fig. 3.45 shows the values of transmission, coupling and isolation of the considered network vs. dielectric constant ratio  $\epsilon_{r2}/\epsilon_{r1}$ , calculated at the center frequency.

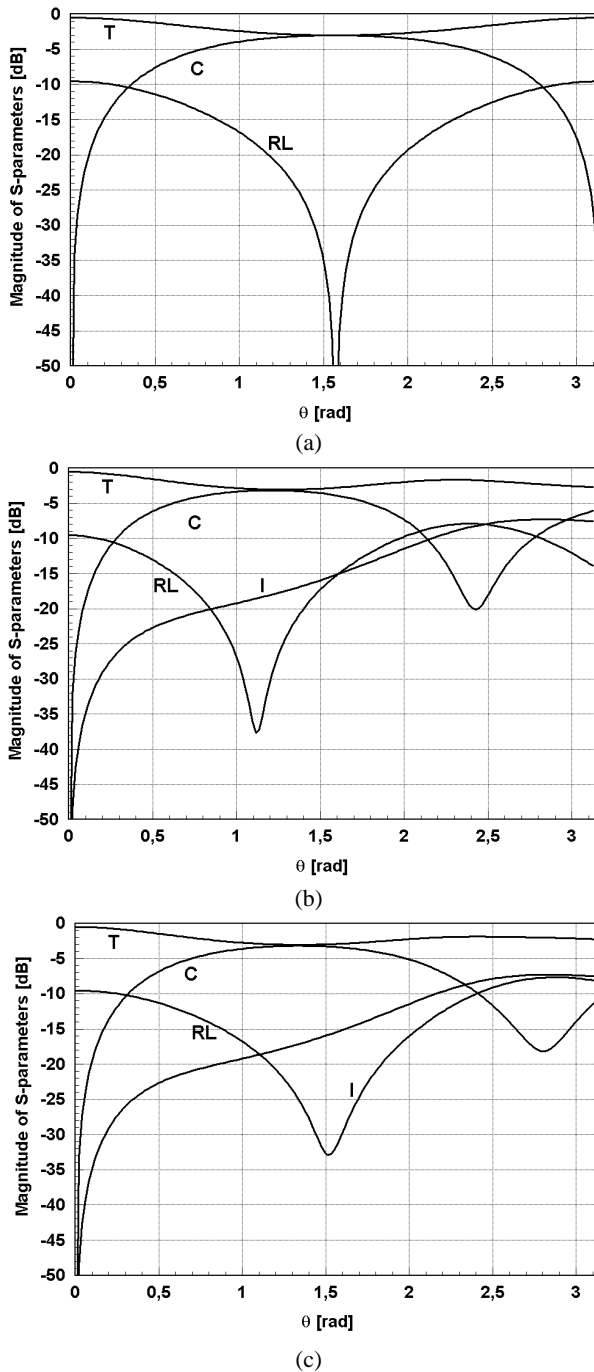


**Fig. 3.44.** Frequency characteristics of the impedance-transforming network shown in Fig. 3.40 and Fig. 3.41 vs. electrical length in free space, for three different dielectric properties, i.e.:  $\epsilon_{r1} = \epsilon_{r2} = 1$  (a),  $\epsilon_{r1} = 1, \epsilon_{r2} = 2$  (b) and  $\epsilon_{r1} = 2, \epsilon_{r2} = 1$  (c).

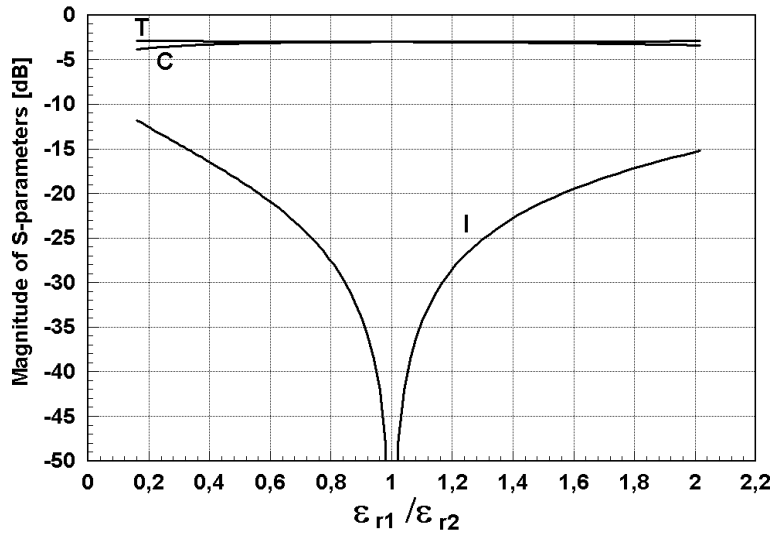


**Fig. 3.45.** Transmission, coupling and isolation of the impedance-transforming network shown in Fig. 3.40 and Fig. 3.41 vs. dielectric constant ratio, calculated for  $\theta = 90^\circ$  (in free space).

From the presented in Fig 3.44 and 3.45 calculation results of parameters of the impedance transforming network, it is seen that, similarly, as in the case of directional couplers, the inhomogeneity degrades the isolation and the transmission and coupling imbalance of the resulting coupler at the center frequency. It is important to note, however, that since the lines are not coupled electromagnetically but connected directly, the compensation of dielectric constant inequality may be achieved by adjusting the lines' physical length, so that both lines have equal electrical length at the center frequency.

The major advantage of the modified network having two uncoupled lines is its design simplicity. Figure 3.46 shows two possible ways of physical realization of the impedance-transforming network with two uncoupled lines, which are: a shielded stripline on a dielectric sheet over a ground layer (Fig. 3.46a), and a coaxial line placed on a dielectric sheet over a ground layer (Fig. 3.46b). The design procedure reduces to the calculation of impedances and effective dielectric permittivity of wire microstrip line, symmetric stripline and finite thickness microstrip line. For all cases either formulas can be found [27], or they can be calculated numerically using standard commercially available numerical software [38].

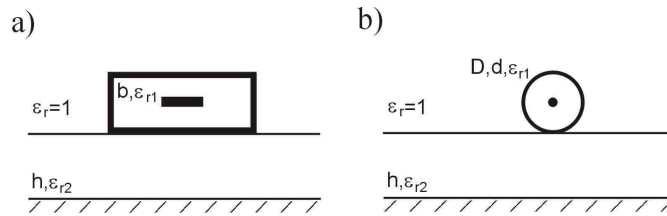


**Fig. 3.46.** Cross-sectional view of a shielded stripline on a dielectric sheet over a ground layer and a coaxial line placed on a dielectric sheet over a ground layer.

The approach to the design of impedance transforming directional couplers with the use of the idea of two-uncoupled lines, has been verified experimentally with the cross-section shown in Fig. 3.46b, in which a coaxial transmission line is placed on a dielectric sheet. The impedances of both lines have to be equal  $Z_1 = Z_2 = 25 \Omega$  as found from (3.42 – 3.43). In order to realize a section of a coaxial transmission line having the characteristic impedance equal  $25 \Omega$ , a commercially available semi-rigid cable can be utilized. In the design, a cable having the impedance of  $25 \Omega$ ,  $\epsilon_{r1} = 2.05$ , and outer diameter  $D = 2.3$  mm has been chosen. The second transmission line has been designed on ARLON 25 laminate with the dielectric constant  $\epsilon_{r2} = 2.05$  and thickness  $h = 1.52$  mm. In order to obtain the impedance of the line equal  $25 \Omega$ , the cross-section has to be modified by introducing additional strip as shown in Fig. 3.47, to decrease the impedance of the wire-microstrip-line. The width of a standard stripline conductor having impedance  $Z = 25 \Omega$  on the chosen dielectric substrate equals  $w = 9.23$ , which is by far wider than the outer diameter of the coaxial line. This causes that the former can be neglected while designing the geometry, hence, the standard formulas for microstrip line calculation can be applied. The assembled model of the coaxial-microstrip impedance transforming directional coupler is shown in Fig. 3.48. The coupler has been realized together with single-section impedance transformers, as shown in Fig. 3.31. As it is seen the coaxial line has been meandered in order to compensate effective dielectric constant inequality ( $\epsilon_{r1} = 2.05$ ,  $\epsilon_{r2} = 2.9$ ). The measured frequency characteristics are shown in Fig. 3.49.

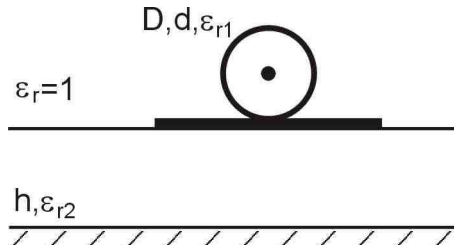


**Fig. 3.47.** Cross-sectional view of the coaxial-microstrip line.

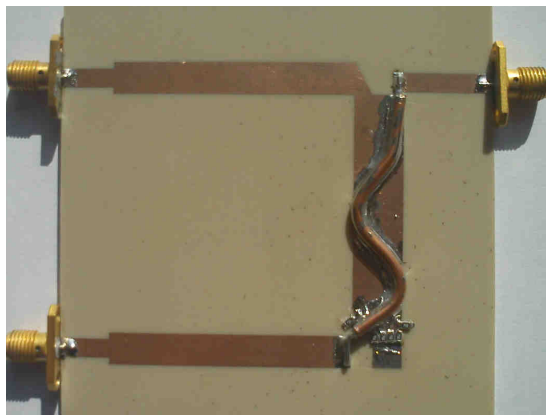


**Fig. 3.48.** Picture of the developed coaxial-microstrip line impedance-transforming directional coupler.

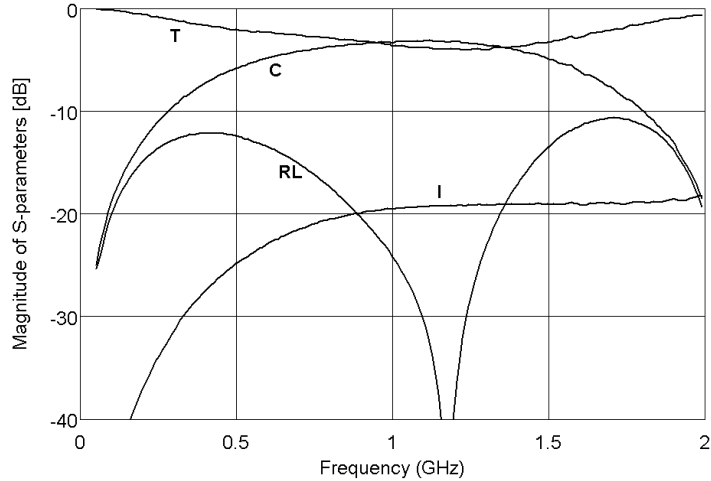


**Fig. 3.49.** Measured frequency characteristics of the 3-dB coaxial-microstrip coupled-line 50/25  $\Omega$  impedance-transforming directional coupler with additional single-section impedance transformers connected to the direct and coupled ports, as shown in Fig. 3.31.

The measured results are in a good agreement with the theoretical ones. The poor isolation and imbalance of coupling-transmission characteristic are caused by the mismatch at the isolated ports, where the terminating impedance  $Z = 12.5 \Omega$  has been connected, composed of six SMD resistors having resistance  $R = 75 \Omega$ .

### 3.5. Broadband asymmetric coupled-line impedance transforming directional couplers

The presented in sections 3.3 and 3.4 single-section impedance transforming directional couplers feature relatively narrow operational bandwidth. As it was shown in section 2.2.2, the operational bandwidth of a coupled-line directional coupler can be increased when multisection directional couplers are designed [29, 92, 93, 137]. Similarly, in order to increase the operational bandwidth of an impedance transformer, a cascade connection of quarter-wave-long sections can be used – instead of a single-section quarter-wave-long transmission line – which constitutes a multisection transformer [25, 27, 28, 122].

In this section the design of broadband two-section impedance-transforming directional couplers is presented, and appropriate formulas allowing for calculation of per-unit-length impedances and capacitances of each section are derived. Also, the appropriate formulas for the design of two-section impedance transformers and asymmetrical directional couplers are briefly presented after [102] and [92], respectively.

The idea of a two-section broadband impedance transforming directional coupler follows directly the method developed for the design of a two-section quarter-wave impedance transformer, so that the impedances of direct-feed lines of coupled-line sections are equal to the impedances of the corresponding two-section transformer. Figure 3.50 shows schematic-

cally, a two-section transformer in which the impedances  $Z_{L11}$  and  $Z_{L12}$  of the quarter-wave transmission lines are calculated from the corresponding values of VSWR:

$$Z_{L11} = \frac{Z_{T1}}{\nu_1}, \quad Z_{L12} = \frac{Z_{L11}}{\nu_2} \quad (3.62)$$

The VSWR values for a Chebyshev transformer are found from [102]:

$$\nu_1 = \sqrt{\sqrt{C^2 + R} + C}, \quad \nu_2 = \frac{R}{\nu_1^2} \quad (3.63)$$

where:

$$C = \frac{(R-1)\mu_0^2}{2(2-\mu_0^2)} \quad (3.64)$$

$$\mu_0 = \sin\left(\frac{\pi w_q}{4}\right) \quad (3.65)$$

$$w_q = 2 \frac{(f_2 - f_1)}{(f_2 + f_1)} \quad (3.66)$$

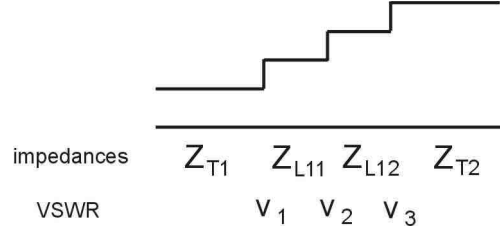


**Fig. 3.50.** Schematic diagram of a two-section impedance transformer [102].

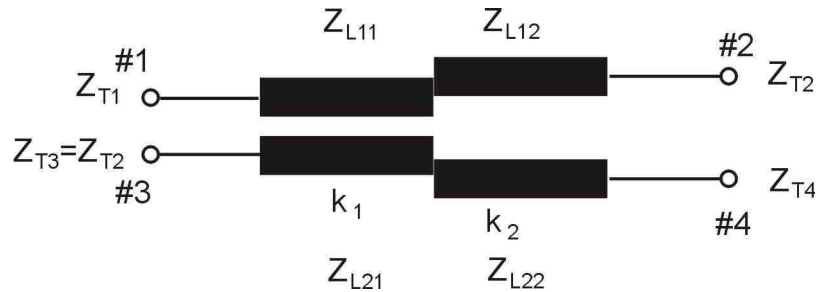


**Fig. 3.51.** Schematic diagram of a two-section impedance-transforming directional coupler.

A schematic diagram of a two-section impedance-transforming directional coupler has been presented in Fig. 3.51. The impedances of the directly-feed line  $Z_{L11}$  and  $Z_{L12}$  equal to the impedances found from (3.62). Since the limiting condition (3.27) holds for each section of the directional coupler separately, it is obvious, that in case of a two-section 3-dB directional coupler, the impedance transforming ratio  $R$  needs to be lower than 2, since in such a directional coupler coupling  $k > 0.707$  ( $> 3\text{dB}$ ) is required for the tight-coupled section. The coupled-line sections' impedances  $Z_{L21}$  and  $Z_{L22}$  are calculated for each section individually, as shown in section 3.3 for a single-section impedance-transforming directional coupler. The coupling coefficients for both sections of the directional coupler, having equal-ripple response of coupling frequency characteristic are expressed as [92]:

$$k_{1,2} = \frac{z_{0e1,2}^2 - 1}{z_{0e1,2}^2 + 1} \quad (3.67)$$

where:

$$z_{0e1} = \frac{a+1}{c}, \quad z_{0e2} = z_{0e1}d \quad (3.68)$$

$$\begin{aligned} a &= \sqrt{1+\beta^2-h^2} + \sqrt{\beta^2-h^2} \\ c &= \sqrt{1+\beta^2-(\beta+h)\sqrt{1+\beta^2}+\beta h} + \\ &\quad + \sqrt{1+\beta^2+(\beta+h)\sqrt{1+\beta^2}+\beta h-\sqrt{2\beta(\beta+h)}} \\ d &= \sqrt{1+\beta^2-h^2} - \sqrt{\beta^2-h^2} \end{aligned} \quad (3.69)$$

$$\beta = \cosh(J)h \quad (3.70)$$

$$h = \frac{1}{\sqrt{\cos(H)^2 - \cosh(J)^2}} \quad (3.71)$$

$$H = 0.5 \sinh^{-1}(10^{C(dB)/10} \sinh(2J)) \quad (3.72)$$

$$J = 2 \cosh^{-1}\left(\frac{1}{\cos(\theta_0)}\right) \quad (3.73)$$

$C$  is the mean coupling of the directional coupler and  $\theta_0$  is the electrical length of the section at the lower cut-off frequency of the directional coupler. Having found the impedance values for both sections from (3.62 - 3.66) and coupling coefficients from (3.67 - 3.73) the per-unit-length parameters of each section can be calculated as:

$$C_{11}^{1,2} = \frac{1}{ck_{1,2}} \frac{1}{Z_{L11,12} \sqrt{\frac{1}{k_{1,2}^2} - 1}} \quad (3.74)$$

$$C_{22}^{1,2} = \frac{1}{ck_{1,2}} \frac{1}{Z_{L21,22} \sqrt{\frac{1}{k_{1,2}^2} - 1}} \quad (3.75)$$

$$C_{12}^{1,2} = \frac{1}{c} \frac{1}{\sqrt{Z_{L11,12} Z_{L21,22} \left( \frac{1}{k_{1,2}^2} - 1 \right)}} \quad (3.76)$$

$$[L] = \frac{1}{c} [C]^{-1} \quad (3.77)$$

Figure 3.52 shows the calculated frequency characteristics of a two-section impedance-transforming directional coupler designed with the presented procedure. In the presented example the input impedance of the directional coupler has been chosen to be equal  $Z_{T1} = 50 \Omega$  and the output impedance  $Z_{T2} = 35 \Omega$ , the isolated port has been terminated with the impedance  $Z_{T4} = 24.5 \Omega$ . The bandwidth for the impedance transformer has been chosen  $f/f_0 = 0.8 - 1.2$ , for which the following values of impedances of transmission-line sections have been found  $Z_{L11} = 45.53 \Omega$  and  $Z_{L12} = 38.44 \Omega$ . The corresponding impedances for the coupled lines are  $Z_{L21} = 31.85 \Omega$  and  $Z_{L22} = 26.88 \Omega$ . The coupling coefficients for both sections have been chosen  $k_1 = 0.815$  and  $k_2 = 0.271$ . From (3.74 – 3.77) the following values of per-unit-length inductances and capacitance have been found:  $C_{11} = 126.3 \text{ pF/m}$ ,  $C_{22} = 180.5 \text{ pF/m}$ ,  $C_{21} = -123 \text{ pF/m}$ ,  $L_{11} = 261.5 \text{ nH/m}$ ,  $L_{22} = 183.1 \text{ nH/m}$ ,  $L_{21} = 178.3 \text{ nH/m}$ .

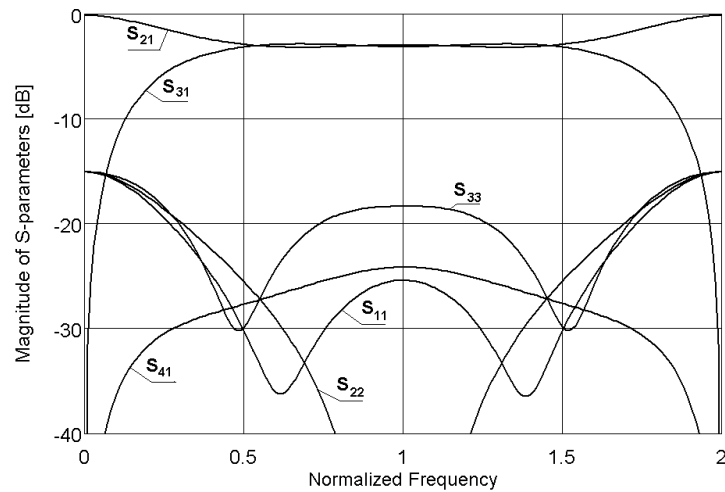


**Fig. 3.52.** Calculated S-parameters of a two-section impedance-transforming directional coupler with impedance ratio  $R = 1.43$ .

The designed directional coupler features equal-ripple coupling characteristic, in which the return losses at the input port and isolation are better than 25 dB. The application of such a

coupler into balanced circuit requires phase compensation, since as it was mentioned in section 2.2, asymmetrical directional couplers do not feature the constant  $90^\circ$  differential phase characteristic. The method for compensation of differential phase characteristic has been shown in Fig. 3.53, where a  $90^\circ$ -long section of a transmission line has been added to the coupled port. The resulting differential phase characteristic is shown in Fig. 3.54, and the phase imbalance for the designed coupler does not exceed  $\delta\phi = \pm 15^\circ$ . The frequency response of the resulting balanced circuit are shown in Fig. 3.55, as it is seen proper transmission has been obtained in a broad frequency range of over two octaves!

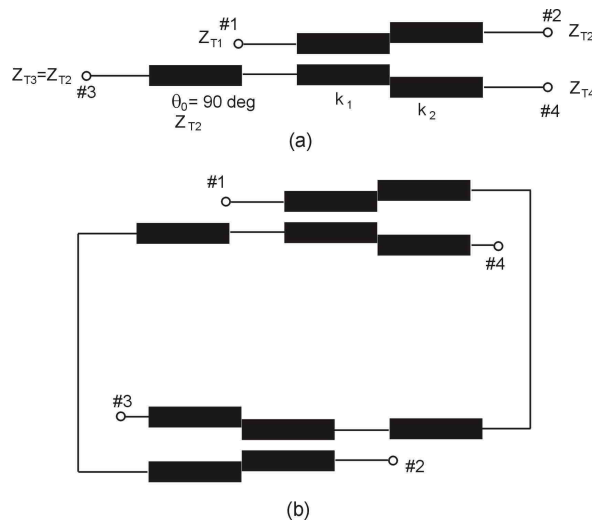


**Fig. 3.53.** Schematic diagram of a two-section impedance-transforming directional coupler with a transmission-line section used for phase compensation (a), and a balanced circuit composed of two such directional couplers (b).

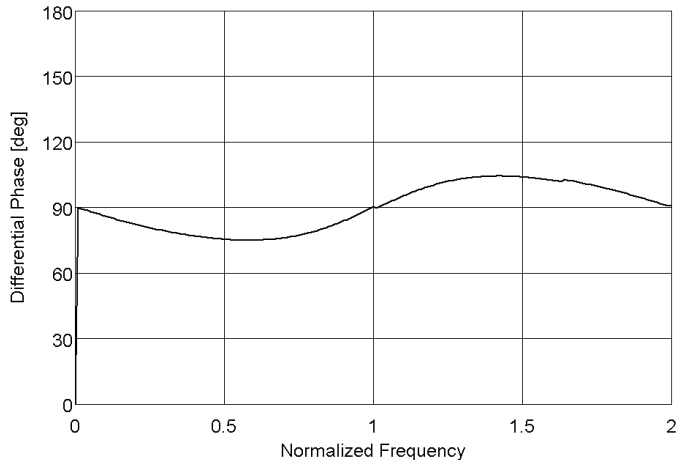


**Fig. 3.54.** Differential phase characteristic of a two-section impedance-transforming directional coupler with a transmission-line section used for phase compensation.

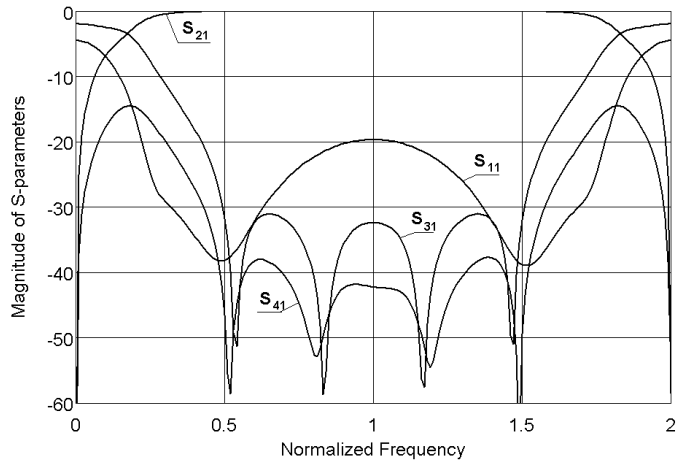


**Fig. 3.55.** Calculated  $S$ -parameters of a balanced circuit composed of two two-section impedance-transforming directional couplers, shown in Fig 3.52 – 3.54.

### 3.6. Summary

The Chapter presents a novel method for the design of balanced circuits and  $n$ -way power splitter/dividers, in which a new class of impedance-transforming coupled-line directional couplers is used to provide simultaneous power splitting/combing and impedance transformation. At first, a method of large-signal reflection coefficient measurement with the use of 3-dB/0/180° directional couplers, recently proposed by the Author [59] has been described. Secondly, it was shown that, by the application of asymmetric 3-dB directional couplers, it is possible to simultaneously provide power split and impedance transformation, in such a way that the impedances seen at direct and coupled ports are equal [179]. It was also shown that to achieve ideal match at all ports both lines need to serve as transforming sections with the same impedance ratio  $R$ . Moreover, it is proved that the maximum achievable impedance transforming ratio  $R$  is dependant on the coupling  $C$  of the used directional coupler and in case of a 3-dB directional coupler  $R_{max} = 2$  for homogeneous dielectric medium [179]. The theoretical investigation has been supported by experiments, in which two different 3-dB directional couplers having  $R = 2$  have been designed and measured. The first coupler has been designed to transform the impedance from 50 to 25  $\Omega$  and the second from 25 to 12.5  $\Omega$ . These two couplers have been used in a design of a 4-way power splitting/combing network, which has been successfully tested in a 4-way power amplifier [179]. Moreover, in section 3.4, a novel approach to the design of asymmetric impedance-transforming directional couplers has been presented, in which the coupler has been represented as a connection of two uncoupled transmission-line sections. The theoretical analysis has been verified by an exemplary realization of a coaxial microstrip impedance-transforming directional coupler. Finally, the concept of impedance-transforming directional couplers has also been used in the design of broadband two-section directional couplers having the impedance transforming ratio equal  $R = 1.43$ . The design coupler provides both equal power split, with amplitude imbalance less than 0.15 dB, and impedance transformation within over two-octave frequency range.

## **4. Broadband Butler matrices utilizing coupled-line directional couplers**

The Butler matrices are well-known and commonly used networks that allow for generation of multiple beams from a linear array [12, 136]. It is due to the fact that beams generated with the use of such networks feature an adequate level of overlapping and the networks themselves are lossless and relatively easy in realization. In general an  $N \times N$  Butler matrix is a network having  $N$  input and  $N$  output ports, in which a signal applied to one of the input ports is equally divided into  $N$  output ports. Moreover, the resulting phase offset of output signals between the respective output ports is constant and depends on the choice of the input ports. These unique properties of Butler matrices result in a broad range of their applications in modern-day communications; e.g. as beamforming networks of multibeam antennas [4, 10, 17, 18, 26, 35, 37, 45, 52, 53, 80, 136, 159], in direction finding systems [96, 141], or in multichannel amplifiers [7, 34, 117, 176]. Among other networks allowing for multiple-beam generation are: Blass matrices [9, 106], Nolen [97] matrices and Rotman matrices [124]. The most commonly used are  $4 \times 4$  Butler matrices, which are composed of four 3-dB/90° directional couplers in conjunction with two 45° phase shifters. There has been significant effort devoted to realization of  $4 \times 4$  Butler matrices designed as a connection of 3-dB branch-line couplers in a microstrip technique [33, 36, 48, 49, 77, 87, 156]. In [49] a dual-polarization, multibeam antenna integrated with Butler matrix has been shown, in which eight branch-line couplers have been utilized, two of which connected in a tandem connection, realize a transmission-line crossover. As described in section 2 branch-line couplers feature narrow bandwidth, so do the Butler matrices composed of such couplers. The resulting bandwidth of a  $4 \times 4$  Butler matrix composed of a basic branch-line coupler presented in Fig. 2.3 does not exceed 6.6%, in which return losses are better than 20 dB. The amplitude imbalance of such a matrix equals  $\pm 0.22$  dB and the phase imbalance is less than  $\pm 1^\circ$ . One way to increase the bandwidth of a Butler matrix it to employ multisection branch-line couplers, as it was shown, e.g. in [50], however, in such a solution the size of the resulting network radically increases. In [77] it was shown that the operational bandwidth can be increased by adding sections of transmission-lines half-wave-long at the center frequency. Also realizations of Butler matrices operating in two separate frequency ranges are reported [26]. Apart from microstrip technique, Butler matrices can be realized in a coplanar-waveguide technique [110, 111]. In [110] a Butler matrix realized as a connection of two branch-line couplers and two coplanar-waveguide couplers has been presented. The coplanar-waveguide couplers utilize electromagnetic coupling via slot in a common ground plane, therefore, in the resulting circuit the transmission-line crossovers

are avoided. Few realization of Butler matrices in rectangular waveguide [45, 117] and slot-line [109] are reported. The bandwidth of Butler matrices can be significantly increased together with the size reduction, when coupled-line directional couplers are applied. An exemplary realization has been shown in [10], where a connection of four coupled-line directional couplers realized in a symmetric stripline technique has been considered. In the presented solution, a significant size reduction of the circuit has been obtained, however, the bandwidth is limited by the fact that the phase shifters are realized as sections of transmission lines having appropriate lengths.

Butler matrices can also be utilized in multichannel amplifiers, as it was shown in section 3.1 [6, 7, 176]. In [34] the application of a Butler matrix for multichannel switching of high-power microwave signal has been presented, in which  $N$  phase shifters have been connected between two Butler matrices.

The most simple Butler matrix is constituted by a single 3-dB/90° directional coupler. By connecting radiating elements into the coupled and transmission ports two radiating beams can be generated simultaneously, placed symmetrically along the line perpendicular to the line connecting radiating elements [169]. Phase progression of the signals exciting radiating elements equals  $\pm 90^\circ$  and the scattering matrix of the 2 x 2 Butler matrix is represented by (2.30). Higher order Butler matrices are created by the appropriate connection of two Butler matrices of order  $N-1$  and by the addition of  $N/2$  phase shifters and  $N/2$  directional couplers. A 4 x 4 Butler matrix has been presented in Fig. 4.1 and consists of four 3-dB/90° directional couplers and two 45° phase shifters. Scattering matrix of such a network can be expressed as [169]:

$$S = \frac{1}{2} \begin{bmatrix} 0 & 0 & 0 & 0 & e^{-j\frac{\pi}{4}} & e^{-j\frac{\pi}{2}} & e^{-j\frac{3\pi}{4}} & e^{-j\pi} \\ 0 & 0 & 0 & 0 & e^{-j\frac{3\pi}{4}} & e^{-j0} & e^{-j\frac{5\pi}{4}} & e^{-j\frac{\pi}{2}} \\ 0 & 0 & 0 & 0 & e^{-j\frac{\pi}{2}} & e^{-j\frac{5\pi}{4}} & e^{-j0} & e^{-j\frac{3\pi}{4}} \\ 0 & 0 & 0 & 0 & e^{-j\pi} & e^{-j\frac{3\pi}{4}} & e^{-j\frac{\pi}{2}} & e^{-j\frac{\pi}{4}} \\ e^{-j\frac{\pi}{4}} & e^{-j\frac{3\pi}{4}} & e^{-j\frac{\pi}{2}} & e^{-j\pi} & 0 & 0 & 0 & 0 \\ e^{-j\frac{\pi}{2}} & e^{-j0} & e^{-j\frac{5\pi}{4}} & e^{-j\frac{3\pi}{4}} & 0 & 0 & 0 & 0 \\ e^{-j\frac{3\pi}{4}} & e^{-j\frac{5\pi}{4}} & e^{-j0} & e^{-j\frac{\pi}{2}} & 0 & 0 & 0 & 0 \\ e^{-j\pi} & e^{-j\frac{\pi}{2}} & e^{-j\frac{3\pi}{4}} & e^{-j\frac{\pi}{4}} & 0 & 0 & 0 & 0 \end{bmatrix} \quad (4.1)$$

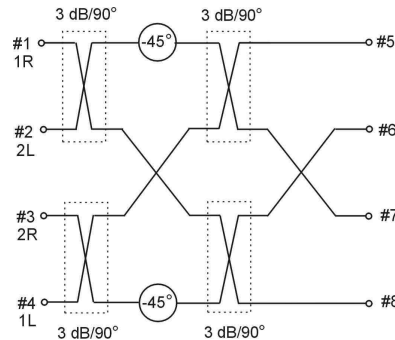


**Fig. 4.1.** Schematic diagram of a 4 x 4 Butler matrix.

Similarly an  $8 \times 8$  Butler matrix is created from a  $4 \times 4$  Butler matrix, as shown in Fig. 4.2. The matrix consists of two  $4 \times 4$  Butler matrices, in which  $45^\circ$  phase shifters have been replaced with  $22.5^\circ$  and  $67.5^\circ$  phase shifters, and additional four  $45^\circ$  phase shifters and four 3-dB directional couplers are added. The scattering matrix of an  $8 \times 8$  Butler matrix takes the form:

$$S = \frac{1}{\sqrt{8}} \begin{bmatrix} 0 & A \\ A^T & 0 \end{bmatrix} \quad (4.2)$$

where:

$$A = \begin{bmatrix} e^{-j\frac{5\pi}{8}} & e^{-j\frac{3\pi}{4}} & e^{-j\frac{7\pi}{8}} & e^{-j\pi} & e^{-j\frac{9\pi}{8}} & e^{-j\frac{5\pi}{4}} & e^{-j\frac{11\pi}{8}} & e^{-j\frac{3\pi}{2}} \\ e^{-j\frac{9\pi}{8}} & e^{-j\frac{\pi}{4}} & e^{-j\frac{11\pi}{8}} & e^{-j\frac{\pi}{2}} & e^{-j\frac{13\pi}{8}} & e^{-j\frac{3\pi}{4}} & e^{-j\frac{15\pi}{8}} & e^{-j\pi} \\ e^{-j\frac{3\pi}{4}} & e^{-j\frac{11\pi}{8}} & e^{-j0} & e^{-j\frac{5\pi}{8}} & e^{-j\frac{7\pi}{4}} & e^{-j\frac{11\pi}{8}} & e^{-j\frac{5\pi}{8}} & e^{-j\frac{9\pi}{8}} \\ e^{-j\frac{7\pi}{4}} & e^{-j\frac{15\pi}{8}} & e^{-j0} & e^{-j\frac{7\pi}{8}} & e^{-j\frac{\pi}{4}} & e^{-j\frac{11\pi}{8}} & e^{-j\frac{7\pi}{8}} & e^{-j\frac{5\pi}{8}} \\ e^{-j\frac{11\pi}{8}} & e^{-j\frac{7\pi}{8}} & e^{-j\frac{\pi}{2}} & e^{-j\frac{\pi}{8}} & e^{-j\frac{7\pi}{4}} & e^{-j\frac{11\pi}{8}} & e^{-j\frac{7\pi}{8}} & e^{-j\frac{5\pi}{8}} \\ e^{-j\frac{15\pi}{8}} & e^{-j\frac{7\pi}{8}} & e^{-j\frac{\pi}{4}} & e^{-j\frac{7\pi}{8}} & e^{-j\frac{\pi}{2}} & e^{-j\frac{11\pi}{8}} & e^{-j\frac{7\pi}{8}} & e^{-j\frac{5\pi}{8}} \\ e^{-j\frac{19\pi}{8}} & e^{-j\frac{15\pi}{8}} & e^{-j\frac{5\pi}{4}} & e^{-j\frac{5\pi}{8}} & e^{-j0} & e^{-j\frac{11\pi}{8}} & e^{-j\frac{11\pi}{8}} & e^{-j\frac{3\pi}{4}} \\ e^{-j\frac{15\pi}{8}} & e^{-j\frac{11\pi}{8}} & e^{-j\frac{7\pi}{4}} & e^{-j\frac{7\pi}{8}} & e^{-j\frac{\pi}{2}} & e^{-j\frac{11\pi}{8}} & e^{-j\frac{7\pi}{4}} & e^{-j\frac{9\pi}{8}} \\ e^{-j\frac{11\pi}{8}} & e^{-j\frac{7\pi}{8}} & e^{-j\frac{7\pi}{4}} & e^{-j\frac{9\pi}{8}} & e^{-j\pi} & e^{-j\frac{7\pi}{8}} & e^{-j\frac{3\pi}{4}} & e^{-j\frac{5\pi}{8}} \end{bmatrix} \quad (4.3)$$

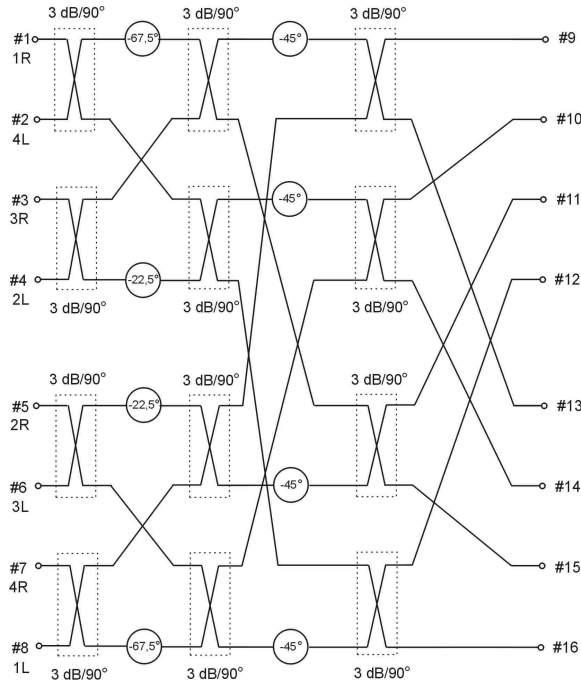


**Fig. 4.2.** Schematic diagram of an  $8 \times 8$  Butler matrix.

The procedure of creating Butler matrices of higher order has been described in [80, 100, 105].

The chapter presents the Author's theoretical and experimental investigations regarding the design of 4 x 4 and 8 x 8 broadband Butler matrices. At first, the previously published designs of broadband 4 x 4 Butler matrices utilizing single-section coupled-line directional couplers and realized in symmetric stripline and asymmetric multilayer microstrip techniques have been presented. Afterwards, a novel approach to the design of an 8 x 8 Butler matrix is shown, allowing for realization of a fully planar integrated network. Section 4.2 describes the method of broadband 4 x 4 Butler matrices' realization with the use of multisection symmetrical 3-dB/90° directional couplers. The large content of the Author's work published in [61, 68, 164] is cited in this section. The new concept of broadband 4 x 4 Butler matrices' realization has been experimentally verified by the design of three different 4 x 4 Butler matrices, the measurements of which are also presented. Moreover, the method developed for the design of broadband 4 x 4 Butler matrices has been extended on the design of 8 x 8 Butler matrices, which has also been experimentally verified. Finally, 4 x 4 Butler matrices utilizing 3-dB/0/180° directional couplers are considered in the last section.

## **4.1. Butler matrices utilizing single-section coupled-line directional couplers**

### **4.1.1. 4 x 4 Butler matrix**

It is known that single-section coupled-line directional couplers allow for achieving operational bandwidth up to one frequency octave. In [61] and [164] the Author has shown the designs of one-octave 4 x 4 Butler matrices realized in homogenous symmetric stripline and asymmetric microstrip technologies. In both cases the presented in Fig. 4.1 Butler matrix has been designed as a connection of six 3-dB/90° single-section coupled-line directional couplers. In these designs two of the couplers constitute a 0-dB coupler, which together with two sections of 135°-long transmission lines realizes a transmission line crossover and two broadband 45° differential phase shifters [164]. The developed Butler matrices have been designed without the last crossovers at the outputs (#6 and #7 in Fig. 4.1), which need to be separately designed for integration in multibeam antennas [160, 162]. Moreover, the approach of utilizing a tandem connection of two 3-dB/90° couplers allows to avoid the inter-layer connections, which can be realized as plated-trough-holes or with the use of electromagnetic coupling. The compensated 3-dB coupled-line directional couplers have been used as basic elements of the designed Butler matrices. First of the couplers has been developed with the use of the dielectric structure shown in Fig. 2.13. Figure 4.3 shows the measured results of the manufactured coupler [164]. The second one has been developed in a dielectric structure shown in Fig. 4.4. The three-strip multilayer microstrip structure has been selected to allow for compensation of inductive and capacitive coupling coefficients necessary for realization of a quasi-ideal coupled-line section [65, 125]. The measured frequency characteristics are presented in Fig. 4.5. Exceptionally good electrical performance of the coupler has been achieved with the use of the compensation method of parasitic reactances connected with the transition regions in coupled-lines, developed by the Author [63].

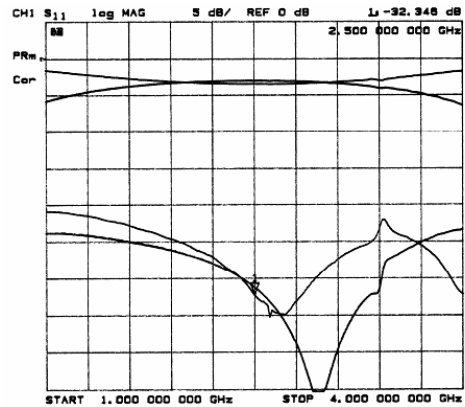


**Fig. 4.3.** Measured amplitude characteristics of the high-performance 3dB/90° coupled-line directional coupler designed in a dielectric structure shown in Fig. 2.13 [164].

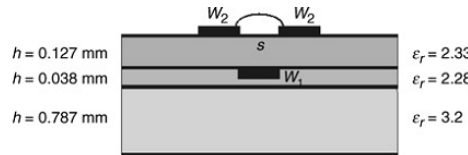


**Fig. 4.4.** Cross-sectional view of multilayer-microstrip coupled-lines used for the design of the 3-dB directional coupler and the 4 x 4 Butler matrix [65].

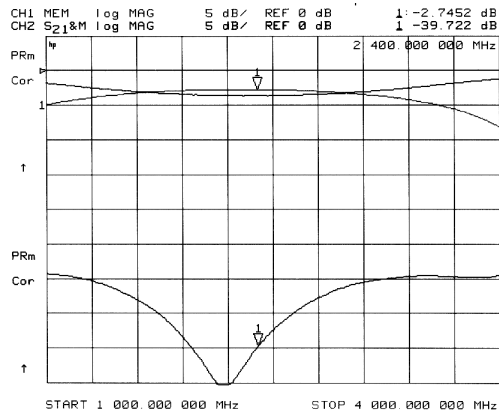


**Fig. 4.5.** Measured amplitude characteristics of the high-performance 3dB/90° coupled-line directional coupler designed in a dielectric structure shown in Fig. 4.4 [65].

Figure 4.6 presents the measured frequency responses of the 4 x 4 Butler matrix developed in a symmetric stripline technique. The manufactured matrix operates within 2 – 3 GHz frequency range, in which the amplitude imbalance is less than  $\pm 0.4$  dB and the differential phase ripple does not exceed  $\pm 4^\circ$ . Moreover, the matrix features very good impedance match and high isolation between the respective ports, which has been achieved by the use of the applied technique of parasitic reactances' compensation [63]. Figures 4.7 and 4.8 show the photographs of the developed matrix.

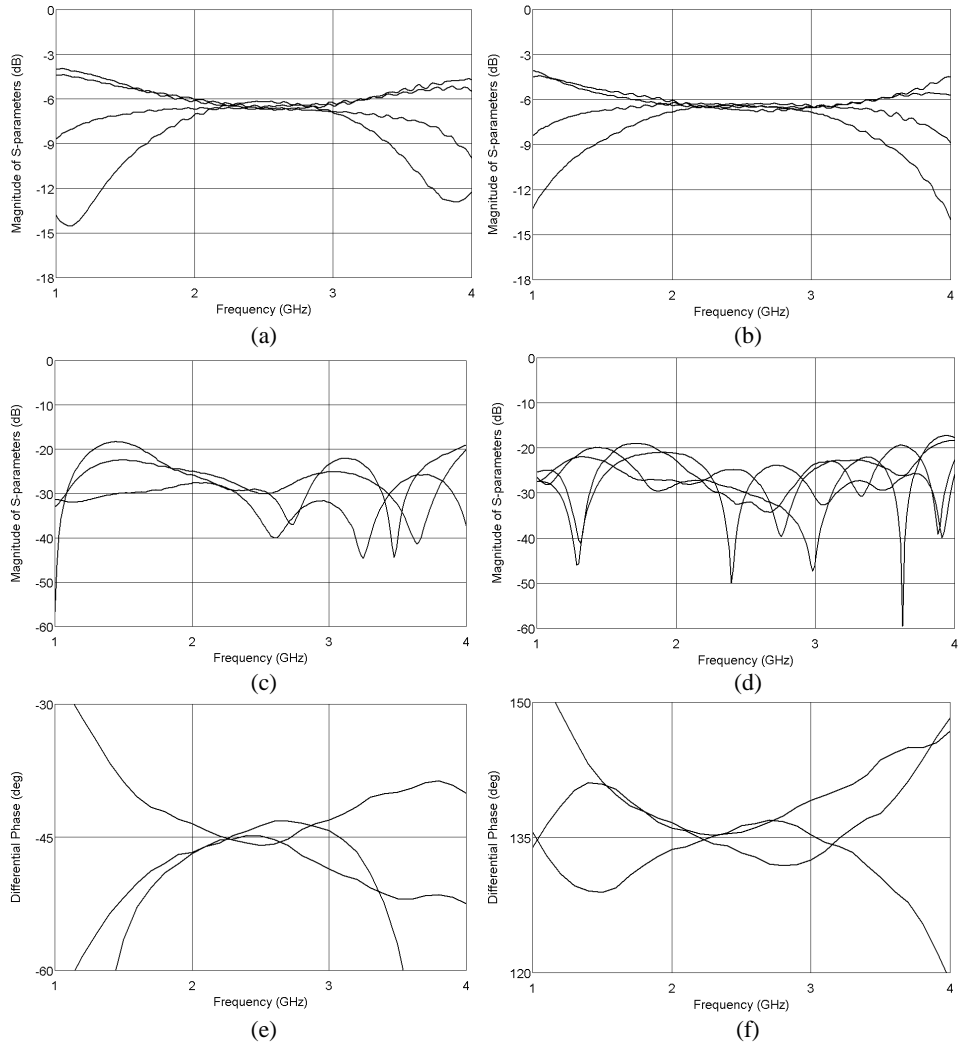


**Fig. 4.6.** Measured frequency characteristics of the developed  $4 \times 4$  Butler matrix designed in a symmetric stripline technique with the use of the directional coupler shown in Fig. 4.3. Transmissions when port #1 is fed (a), transmissions when port #2 is fed (b), isolations (c), return losses (d) and differential phase characteristics when port #1 is fed (e) and when port #2 is fed (f) [169].

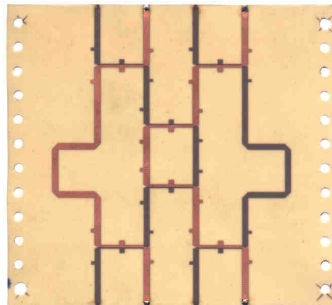


**Fig. 4.7.** A photograph of the inner layer of the developed 4 x 4 Butler matrix in a symmetric stripline technique. [169].

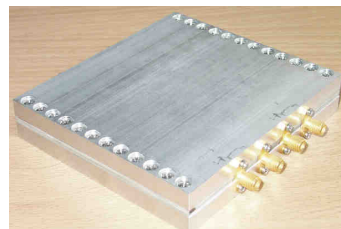


**Fig. 4.8.** A photograph of the assembled model of the developed 4 x 4 Butler matrix in a symmetric stripline technique [169].

The 4 x 4 Butler matrix designed in a multilayer microstrip technique with the use of the directional coupler shown in Fig. 4.4 is presented in Fig. 4.9, whereas, its measured frequency responses are plotted in Fig. 4.10. One can see that the matrix features slightly larger amplitude imbalance due to the larger imbalance of the applied directional coupler. The matrix operates within 1.5-3.1 GHz frequency range, in which the amplitude imbalance is less than  $\pm 1\text{dB}$  and the differential phase ripple does not exceed  $\pm 6^\circ$ . Also in this case the matrix features exceptionally good return losses and isolations between respective ports which are better than 25 dB.

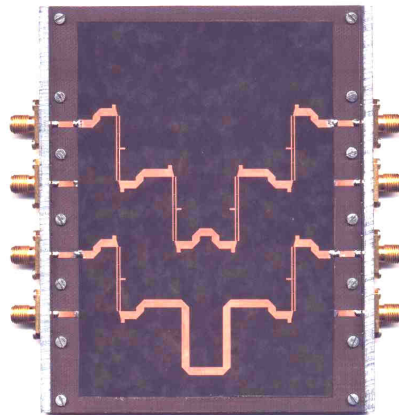


**Fig. 4.9.** A photograph of the developed 4 x 4 Butler matrix in an asymmetric multilayer microstrip technique [61].

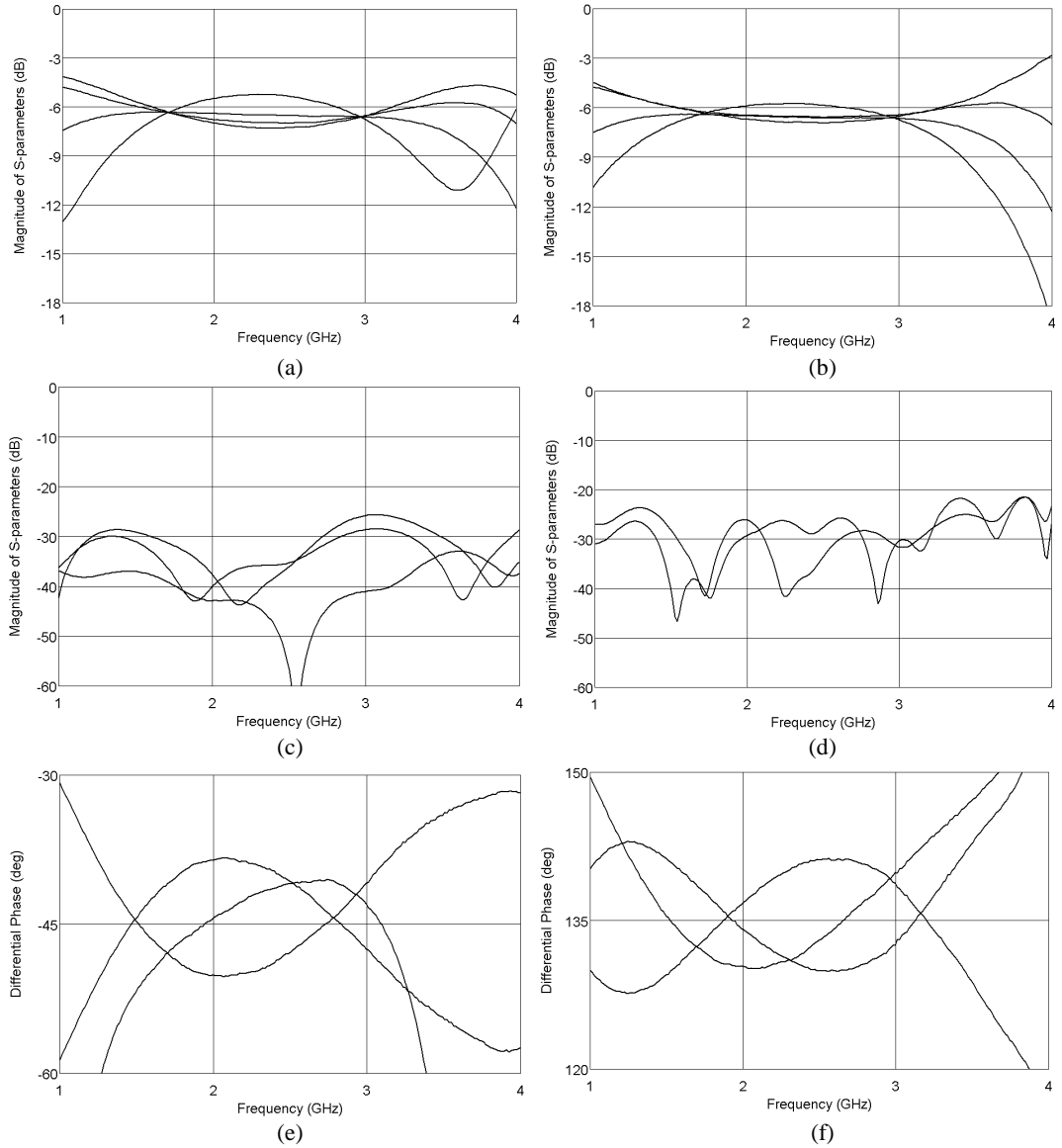
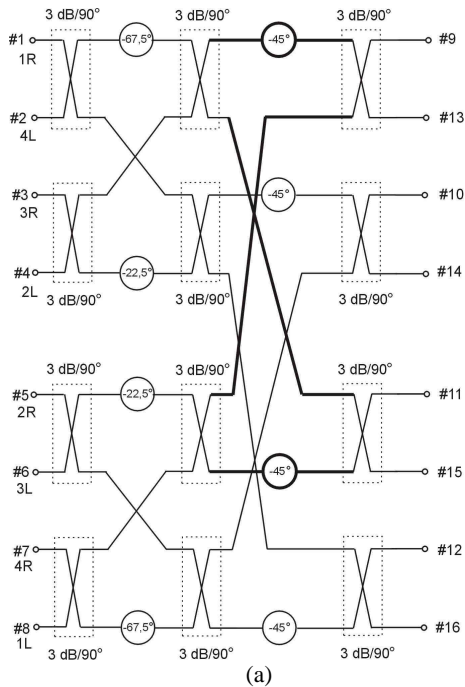


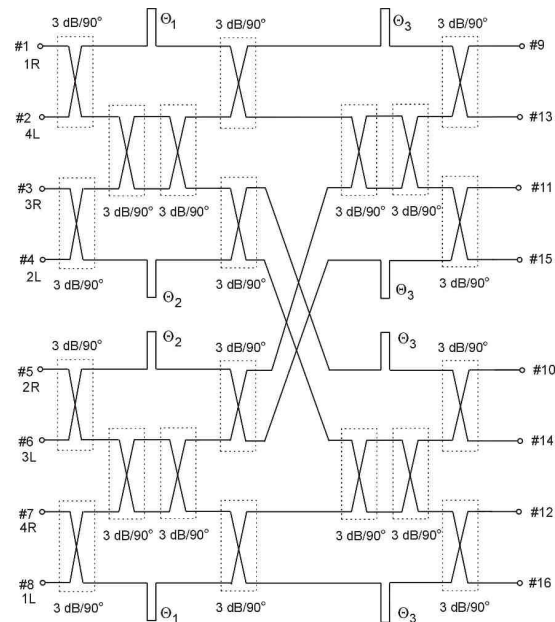
**Fig. 4.10.** Measured frequency characteristics of the developed  $4 \times 4$  Butler matrix designed in an asymmetric multilayer microstrip technique with the use of the directional coupler shown in Fig. 4.5. Transmissions when port #1 is fed (a), transmissions when port #2 is fed (b), isolations (c), return losses (d) and differential phase characteristics when port #1 is fed (e) and when port #2 is fed (f) [169].

### 4.1.2. 8 x 8 Butler matrix

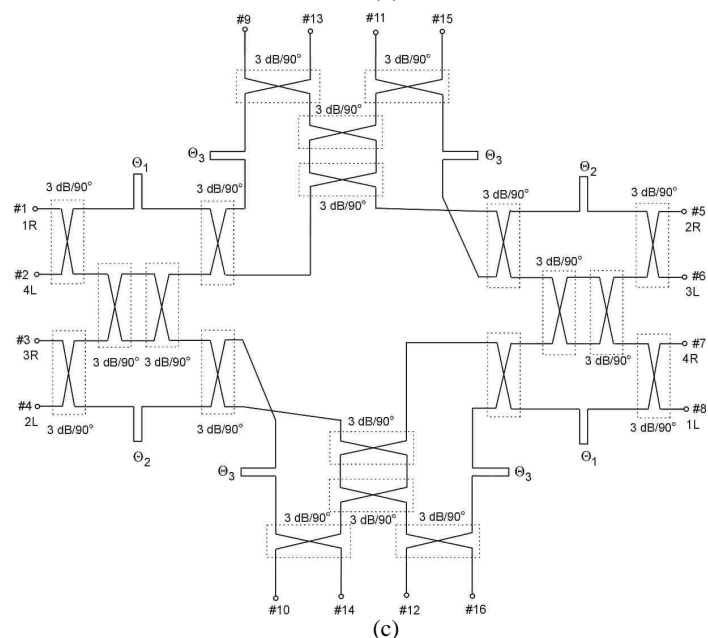
8 x 8 and higher order Butler matrices are very seldom reported, due to their large complexity, and therefore, difficulty in designing and manufacturing as integrated units. An exemplary realization of an 8 x 8 Butler matrix can be found in [153], where a compact multilayer design has been shown in LTCC technology, having 40 layers appropriately stacked and folded. Another example of an 8 x 8 Butler matrix realization can be found in [117], where a planar matrix operating within Ka-band is presented, designed in a rectangular waveguide technique. One of the recent papers [17] reports the realization of an 8 x 8 Butler matrix in CMOS technology operating at 5.5 GHz, in which branch-line couplers designed with the use of a lumped-element technique, are applied. Among reported broadband 8 x 8 Butler matrices impressive results have been presented in [35], where a Butler matrix utilizing tapered-line directional couplers and operating in a frequency range of  $f_u/f_l = 9:1$  has been presented. The matrix has been designed in a modular fashion, and the modules have been connected with coaxial cables. The needed broadband phase shifters have been realized with the use of multisection Schiffman phase shifters.

In this Section a novel arrangement of an 8 x 8 Butler matrix is presented, which allows for a planar fully integrated design. A schematic diagram of an 8 x 8 Butler matrix is shown, after [136], in Fig. 4.11a with the exception of transmission-line crossings at the output of the matrix (the numeration of the output ports corresponds to the numeration of the original Butler matrix). The matrix consists of twelve 3-dB/90° directional couplers, two 67.5°, two 22.5° and four 45° phase shifters, additionally multiple crossings of inner connecting lines between components are needed, which complicates the physical realization. The idea of realization of a fully planar integrated Butler matrix is in detail explained in Fig. 4.11b – Fig. 4.11d.





(b)



(c)

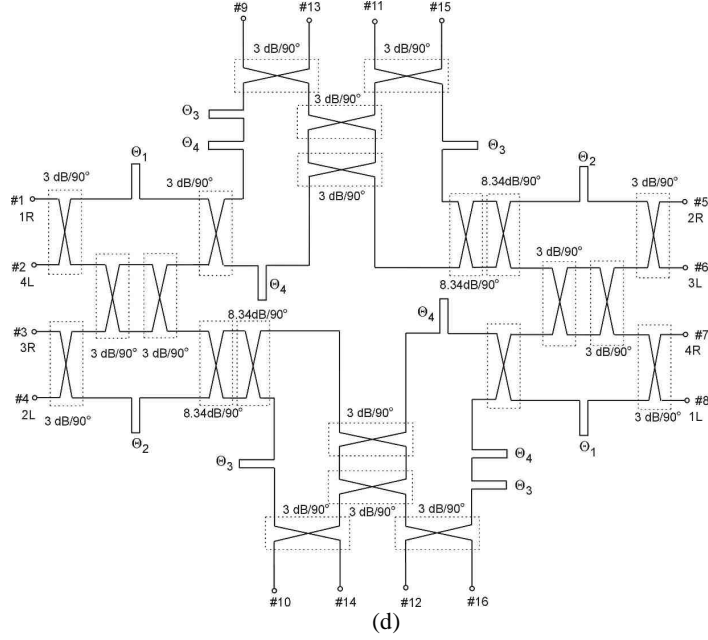


**Fig. 4.11.** Schematic diagram of the  $8 \times 8$  Butler matrix. Original arrangement a), network with phase shifters as a tandem connection of 3-dB/90° directional couplers and sections of transmission lines b), the rearranged network with only two crossovers c), the final matrix arrangement suitable for integrated planar realization d).

As a first step all the phase shifters have been realized using the method presented in [164]. The needed  $67.5^\circ$  and  $22.5^\circ$  phase shifters together with crossovers of transmission lines have been realized as a tandem connection of two 3-dB/90° directional couplers and two transmission lines having electrical lengths  $\theta_1 = 157.5^\circ$  and  $\theta_2 = 112.5^\circ$  (see Fig. 4.11b). The phase imbalance of such a phase shifter does not exceed  $\pm 7.5^\circ$  in an octave frequency range. The four  $45^\circ$  phase shifters have been realized in a similar manner. A sub-circuit with two  $45^\circ$  phase shifters and a corresponding transmission line crossover, marked with bolded lines in Fig. 4.11a, is replaced by a tandem connection of two 3-dB/90° directional couplers and two transmission lines having electrical lengths  $\theta_3 = 135^\circ$ , as shown in Fig. 4.11b. The phase difference of such  $45^\circ$  phase shifters does not exceed  $\pm 3^\circ$ .

In the resulting circuit four transmission-line crossovers remain to be resolved (see Fig. 4.11b). This is done by the rearrangement of the four subsections of the matrix, as shown in Fig. 4.11c. Such a rearrangement reduces the number of transmission-line crossovers into two, as it is seen in Fig. 4.11c. The last remaining crossovers can be eliminated by replacing each of the two 3-dB/90° directional couplers with a tandem connection of two 8.34-dB/90° directional couplers. Such a tandem connection is nearly equivalent to the original 3-dB/90° directional coupler, having, however, interchanged coupling and transmission ports and slightly reduced bandwidth. In order to ensure proper phase relations of the entire network four sections of transmission lines having electrical length equal  $\theta_4 = 90^\circ$  have been introduced in the corresponding channels. The final arrangement of the  $8 \times 8$  Butler matrix, presented in Fig. 4.11d, allows for its fully integrated planar realization, at the expense of having the input and output ports scattered around the network.

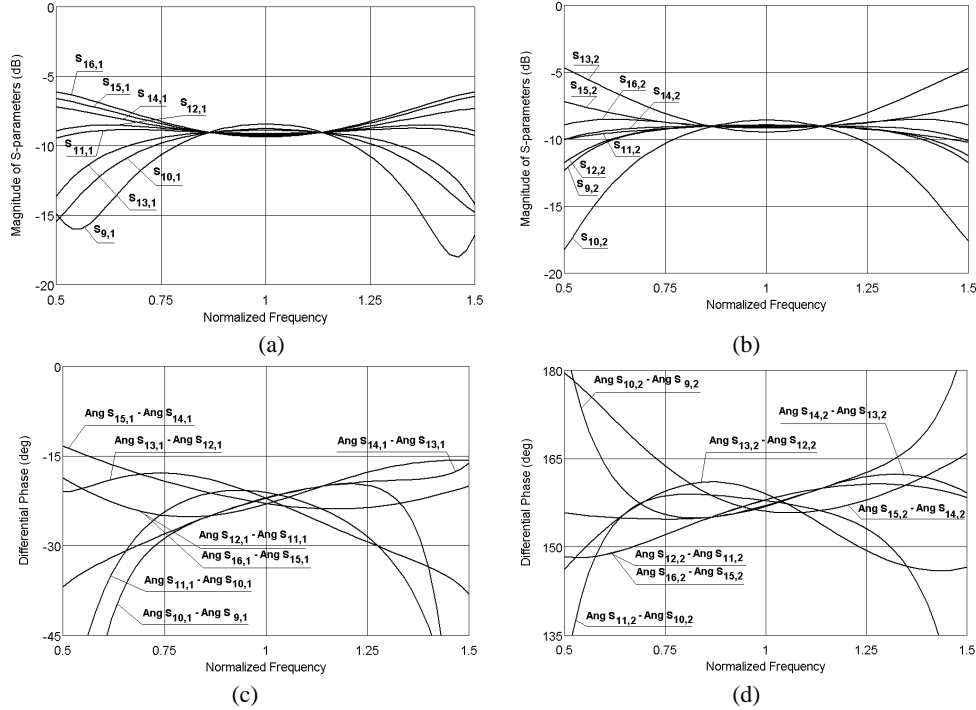


**Fig. 4.12.** Frequency response of an ideal  $8 \times 8$  Butler matrix shown in Fig. 4.11d. Amplitude characteristics when port #1 is fed a), amplitude characteristics when port #2 is fed b), differential phase characteristics when port #1 is fed c), differential phase characteristics when port #2 is fed d).

The theoretical performance of the  $8 \times 8$  Butler matrix shown in Fig. 4.11d, has been calculated and the results are presented in Fig. 4.12. Ideal coupled-line directional couplers with  $Z_{0e} = 122.7 \Omega$  (3-dB directional coupler with the amplitude imbalance of  $\delta C = \pm 0.1$  dB) and  $Z_{0e} = 75.4 \Omega$  (8.34-dB directional coupler giving the amplitude imbalance of its tandem connection equal  $\delta C = \pm 0.1$  dB) have been assumed for the calculations. The resulting Butler matrix operates in a frequency range of 1.5:1 ( $f/f_0 = 0.79 - 1.2$ ) with the maximum amplitude imbalance  $\pm 0.45$  dB and the maximum phase ripple less than  $\pm 5^\circ$ .

The  $8 \times 8$  Butler matrix has been experimentally tested with the use of the developed 3-dB and 8.34-dB directional couplers shown in Fig. 2.14 – 2.16. The measured results of the entire  $8 \times 8$  Butler matrix are presented in Fig. 4.13. The obtained results are in a very good agreement with the theoretical ones. The measured amplitude imbalance equals  $\pm 0.45$  dB and the maximum phase error is less than  $\pm 7.5^\circ$  in the frequency range of 2.5 – 3.5 GHz. The return losses are better than 20 dB and isolations better than 25 dB within the operational bandwidth. Figure 4.14 shows a picture of the center laminate layer with the traces of the network etched. As it is seen the matrix is fully planar with no need of inter-layer connections.

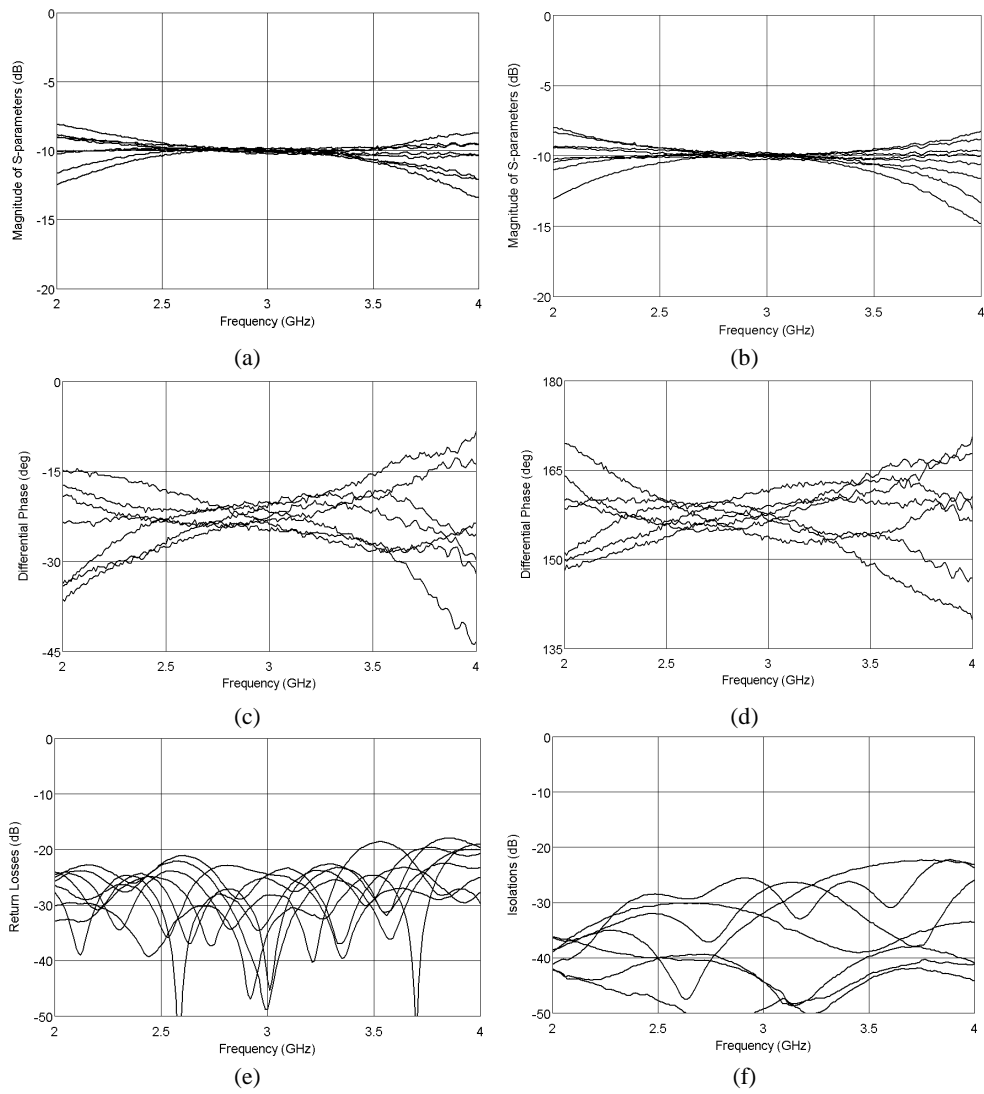


**Fig. 4.13.** Measured frequency response of the designed broadband fully integrated 8 x 8 Butler matrix. Amplitude characteristics when port #1 is fed a), amplitude characteristics when port #2 is fed b), differential phase characteristics when port #1 is fed c), differential phase characteristics when port #2 is fed d), return losses e) and isolations f).

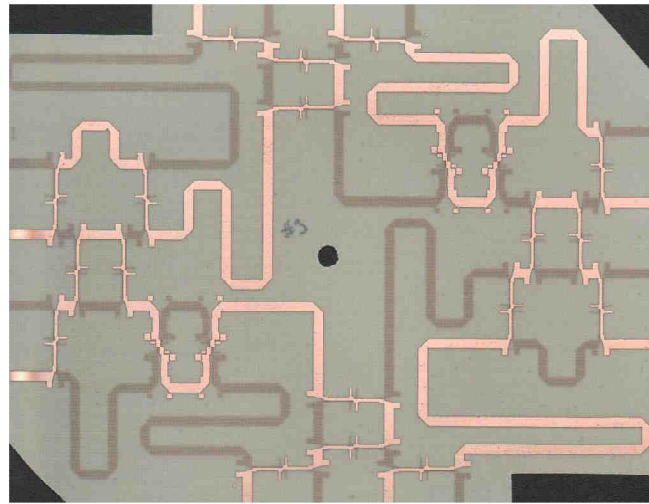


**Fig. 4.14.** Picture of the inner laminate layer on which the traces of the  $8 \times 8$  Butler matrix were etched.

## 4.2. Butler matrices utilizing multisection coupled-line directional couplers

The presented in section 4.1 Butler matrices offer operational bandwidths up to one frequency octave. The limitation of the achievable bandwidth is a result of the employment of single-section coupled-line directional couplers. As it was mentioned in section 2.2.2, wider bandwidths can be obtained with the use of multisection coupled-line directional couplers. In [68], the Author has proposed a new class of broadband  $4 \times 4$  Butler matrices, which consists of multisection symmetrical 3-dB/90° coupled-line directional couplers and phase correction networks. A large content of [68] has been cited in this section.

In section 4.1 two exemplary realizations of single-octave  $4 \times 4$  Butler matrices have been presented, each composed of six 3dB/90° directional couplers [164]. A tandem connection of two of the six directional couplers serves as a transmission-line crossover, and together with 135°-long transmission lines, as two broadband 45° phase shifters. This configuration works well in case of single-section 3dB/90° directional couplers but cannot be straightforwardly applied for realization of broadband  $4 \times 4$  Butler matrices consisting of multisection 3dB/90° directional couplers. This is due to the fact that the tandem connection of two multisection 3dB/90° directional couplers together with the reference lines does not exhibit broadband 45° differential phase characteristics. Figure 4.15 presents a differential phase characteristic between a tandem connection of two three-section symmetrical 3dB/90° directional couplers and a 315°-long reference line (dashed line). It can be seen, that the characteristic inclines – resulting in a large overall differential phase imbalance. To overcome the described difficulty, the Author has proposed in [68] a modified circuit in which a coupled-line ‘C’-section 90° long at  $f_0$  (introduced by Schiffman in [133]) is added. This modification allows to obtain equal-ripple differential phase characteristics in a wide frequency range. The modified schematic diagram of the proposed broadband  $4 \times 4$  Butler

matrix is presented in Fig. 4.16. The network consists of six three-section symmetrical 3-dB/90° coupled-line directional couplers. The middle network (as shown in Fig. 4.16) consists of a tandem connection of two directional couplers and two coupled-line ‘C’-sections together with sections of transmission lines. The calculated amplitude and differential phase characteristics of the Butler matrix shown in Fig. 4.16, are presented in Fig. 4.17. For these calculations a three-section coupled-line coupler with coupling ripple  $\delta C = \pm 0.29$  dB has been considered and the achieved parameters of the Butler matrix are: maximum amplitude imbalance  $\delta C_{max} = 1$  dB and phase ripple  $\delta\phi = \pm 6^\circ$ . The normalized modal characteristic impedances of the coupled-line ‘C’-section are:  $Z_{0e} = 1.218 \Omega$  and  $Z_{0o} = 0.821 \Omega$ , whereas, transmission-line sections are 315°-long (at  $f_0$ ). The obtained bandwidth of the Butler matrix equals  $BW = 4.38$  and is equal to the bandwidth of the applied directional coupler.

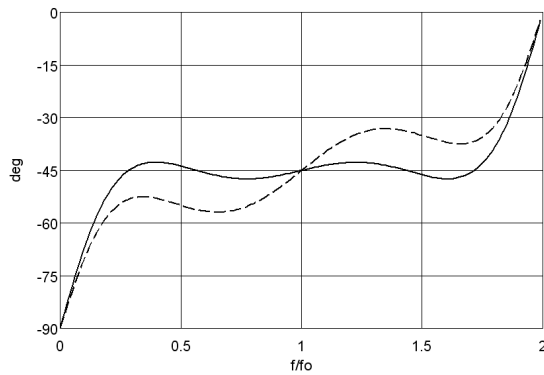


**Fig. 4.15.** Differential phase characteristics between transmission of a tandem connection of two three-section symmetrical 3-dB/90° coupled-line directional couplers and a section of transmission line with (solid line) and without (dashed line) a ‘C’-section of coupled-lines [68].

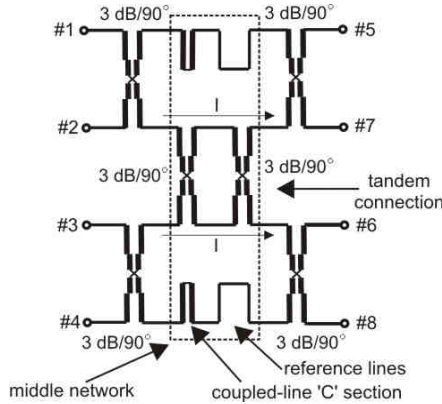


**Fig. 4.16.** Generic schematic of a broadband 4x4 Butler matrix consisting of three-section symmetrical coupled-line directional couplers. Two of the couplers constitute a broadband transmission line crossover and, together with coupled-line ‘C’-sections and reference lines, broadband 45° phase shifters [68].

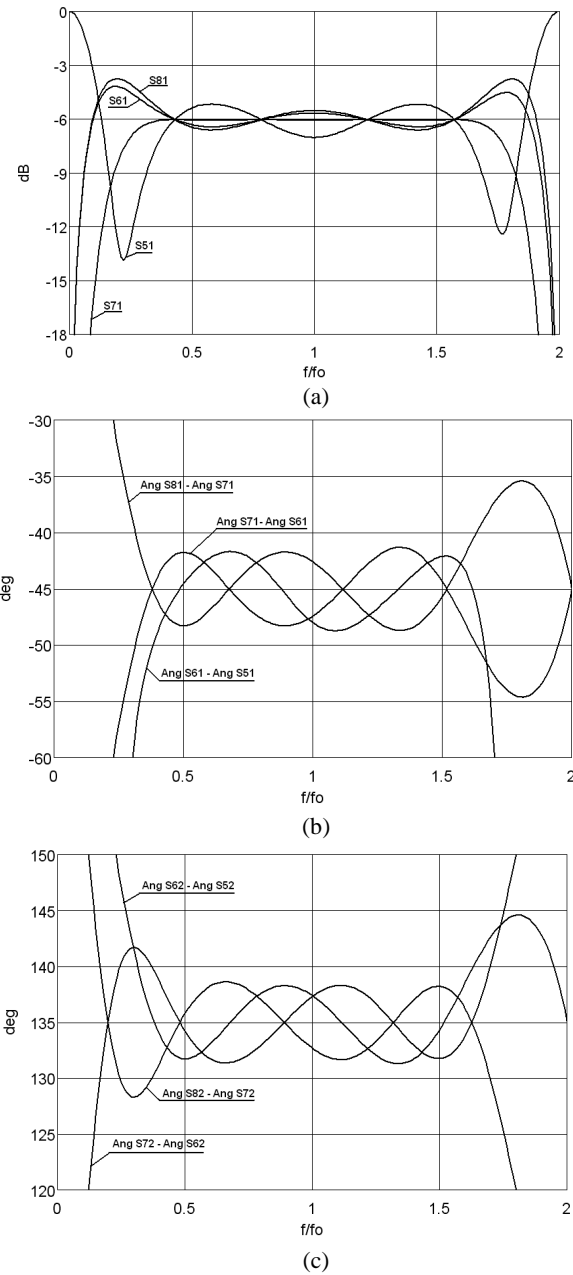


**Fig. 4.17.** Frequency characteristics of a 4x4 Butler matrix being a connection of six three-section symmetrical 3-dB/90° coupled-line directional couplers having coupling imbalance  $\delta C = \pm 0.29$  dB, two phase correction networks and two 315°-long transmission lines. Transmissions when port #1 is fed (a), differential phase characteristics when port #1 is fed (b) and differential phase characteristics when port #2 is fed (c) [68].

Figure 4.18 presents the comparison between the bandwidth of the middle network (dashed line) and the bandwidth of the used directional couplers alone (solid lines). Moreover, it should be underlined, that the amplitude imbalance of the couplers has a direct influence on the amplitude characteristic of a crossover being their tandem connection as presented in Fig. 4.19 and determines the isolation level of the crossover (isolation  $I$  has been schematically marked in Fig. 4.16). The analysis of such broadband Butler matrices shows, that the limited isolation  $I$  of the crossover deteriorates overall amplitude and phase characteristics of the networks [68]. Figure 4.20 shows the differential phase characteristics of the Butler matrix shown in Fig. 4.16, in which the isolation  $I$  is assumed ideal, i.e.  $I = 0$ . It is seen, that the resulting differential phase characteristics have an equal-ripple character with smaller imbalance and two of the three characteristics are identical. This phenomena has been utilized in a concept of  $4 \times 4$  Butler matrix realization having a modified middle network – also proposed by the Author in [68].

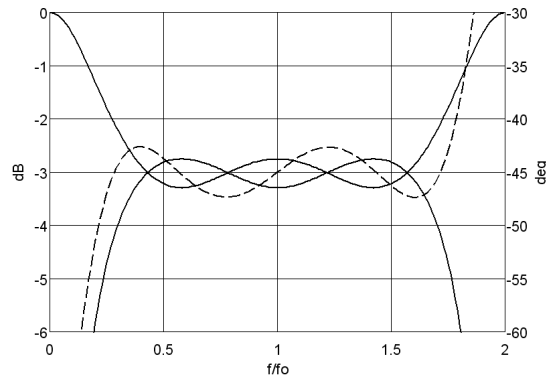


**Fig. 4.18.** Transmission and coupling (solid lines) of a three-section symmetrical 3-dB/90° directional coupler and differential phase characteristic (dashed line) between transmission of a tandem connection of two three-section symmetrical 3-dB/90° coupled-line directional couplers and a section of transmission line together with a 'C'-section of coupled-lines [68].

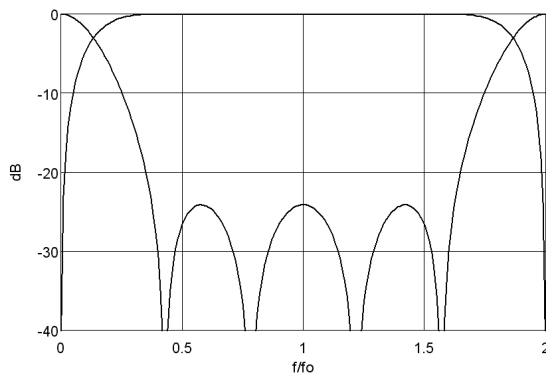


**Fig. 4.19.** Transmission and isolation of a crossover being a connection of six three-section symmetrical 3dB/90° coupled-line directional couplers having coupling ripple  $\delta C = \pm 0.29$  dB [68].

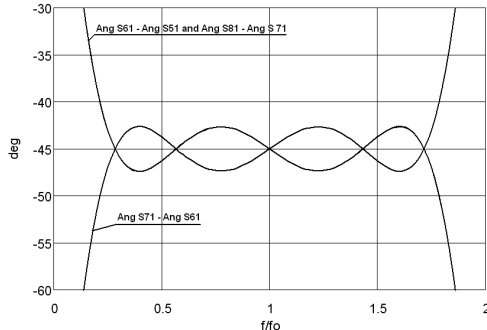


**Fig. 4.20.** Differential phase characteristics of a  $4 \times 4$  Butler matrix being a connection of six three-section symmetrical 3-dB/ $90^\circ$  coupled-line directional couplers having coupling ripple  $\delta C = \pm 0.29$  dB and two phase correction networks in which the isolation  $I$  (Fig. 4.16) is assumed ideal ( $I = 0$ ) [68].

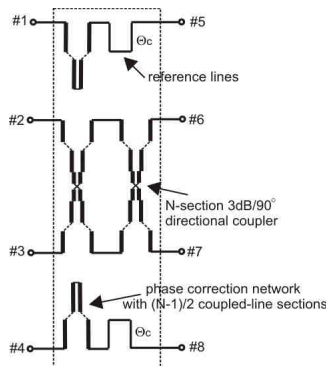


**Fig. 4.21.** Generic schematic of a middle network consisting of  $N$ -section symmetrical coupled-line directional couplers, two  $(N-1)/2$ -section coupled-line phase correction networks and reference lines [68].

The idea of broadband  $4 \times 4$  Butler matrix realization with the use of three-section symmetrical 3-dB/ $90^\circ$  directional couplers can be extended on broadband  $4 \times 4$  Butler matrices consisting of multisection symmetrical directional couplers. In such networks, if the number of coupled-line sections of a directional coupler applied in a crossover changes, then an appropriate change of the number of coupled-line sections has to be introduced to the phase correction network. A schematic diagram of a middle network, in which an  $N$ -section directional coupler is applied, is shown in Fig. 4.21. The number of 'C'-sections used within the phase correction network increases with the increase of the coupled-line sections of the directional coupler and can be expressed as follows:

$$N_p = \frac{N_c - 1}{2} \quad (4.4)$$

where:  $N_p$  – number of coupled-line sections of the phase correction network,  $N_c$  – number of sections of the directional coupler. The electrical length of the reference line can be found from:

$$\Theta_c = N_p \cdot 180^\circ + 135^\circ \quad (4.5)$$

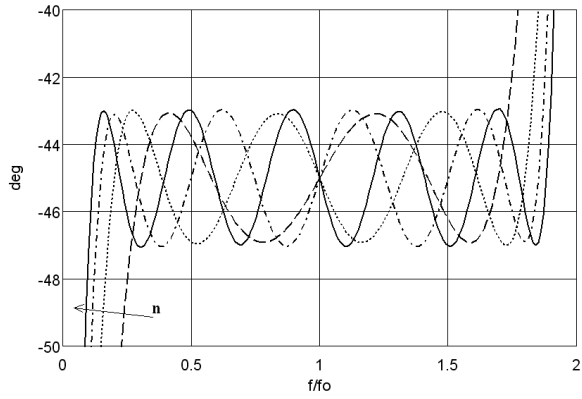


**Fig. 4.22.** Differential phase characteristics of a middle network (Fig. 4.21) for the case of three-, five-, seven- and nine-section directional couplers ( $\delta C = \pm 0.2$  dB). The phase correction networks' number of sections and normalized impedance for each section were selected to obtain equal-ripple characteristics [68].

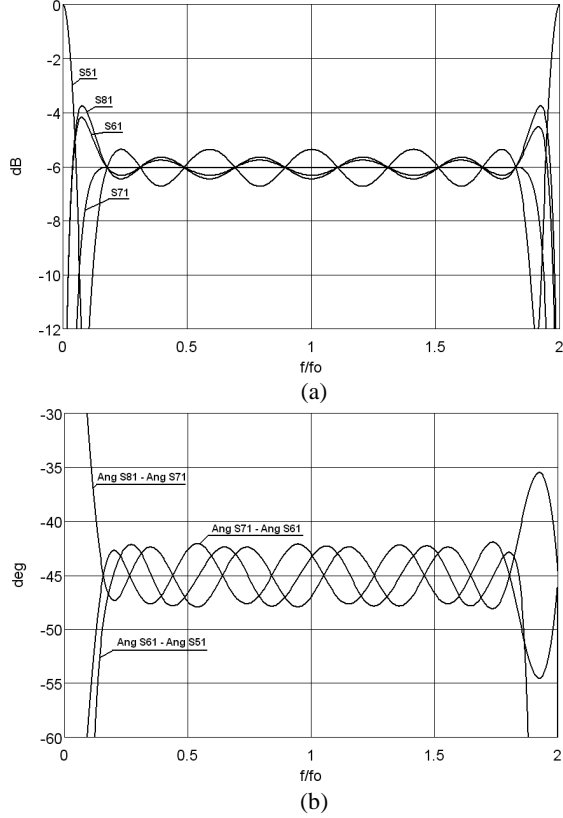


**Fig. 4.23.** Frequency characteristics of a  $4 \times 4$  Butler matrix being a connection of six nine-section symmetrical 3-dB/90° coupled-line directional couplers having coupling ripple  $\delta C = \pm 0.2$  dB, two phase correction networks, and two  $855^\circ$ -long transmission lines. Transmissions (a) and differential phase characteristics (b) [68].

**Table 4.1**

**Normalized even-mode characteristic impedances of phase-compensation networks, parameters of middle networks and parameters of 4 x 4 Butler matrices designed with the use of 3-, 5-, 7-, and 9-section 3-dB symmetrical directional couplers [68]**

	n = 3 $\Theta_c = 315^\circ$		n = 5 $\Theta_c = 495^\circ$		n = 7 $\Theta_c = 675^\circ$		n = 9 $\Theta_c = 855^\circ$	
I	$\delta C = \pm 0.1$ dB		$I = 32.6$ dB		$\delta\varphi = \pm 1.1^\circ$		$\delta C_{max} = 0.34$ dB	
BW	3.03063		4.93114		6.9531		$\delta\varphi_{max} = 2.0^\circ$	
n	$Z_{0e} [\Omega]^*$ coupler	$Z_{0e} [\Omega]$ phase comp. network	$Z_{0e} [\Omega]^*$ coupler	$Z_{0e} [\Omega]$ phase comp. network	$Z_{0e} [\Omega]^*$ coupler	$Z_{0e} [\Omega]$ phase comp. network	$Z_{0e} [\Omega]^*$ coupler	$Z_{0e} [\Omega]$ phase comp. network
1	1.1713	1.161	1.0785	1.049	1.0524	1.025	1.0411	1.015
2	3.2598	-	1.3272	1.343	1.1840	1.126	1.1202	1.067
3	-	-	3.9761	-	1.5675	1.521	1.2948	1.212
4	-	-	-	-	4.6118	-	1.7486	1.687
5	-	-	-	-	-	-	5.1824	-
II	$\delta C = \pm 0.2$ dB		$I = 26.5$ dB		$\delta\varphi = \pm 2.0^\circ$		$\delta C_{max} = 0.7$ dB	
BW	3.83085		6.29714		8.8860		11.528	
n	$Z_{0e} [\Omega]^*$ coupler	$Z_{0e} [\Omega]$ phase comp. network	$Z_{0e} [\Omega]^*$ coupler	$Z_{0e} [\Omega]$ phase comp. network	$Z_{0e} [\Omega]^*$ coupler	$Z_{0e} [\Omega]$ phase comp. network	$Z_{0e} [\Omega]^*$ coupler	$Z_{0e} [\Omega]$ phase comp. network
1	1.2077	1.196	1.1092	1.073	1.0795	1.042	1.0659	1.031
2	3.4124	-	1.4402	1.41	1.2358	1.167	1.1636	1.101
3	-	-	4.2102	-	1.6579	1.599	1.3626	1.271
4	-	-	-	-	4.9066	-	1.8569	1.795
5	-	-	-	-	-	-	5.5265	-
III	$\delta C = \pm 0.4$ dB		$I = 20.3$ dB		$\delta\varphi = \pm 3.5^\circ$		$\delta C_{max} = 1.4$ dB	
BW	5.17521		8.55845		12.0666		15.627	
n	$Z_{0e} [\Omega]^*$ coupler	$Z_{0e} [\Omega]$ phase comp. network	$Z_{0e} [\Omega]^*$ coupler	$Z_{0e} [\Omega]$ phase comp. network	$Z_{0e} [\Omega]^*$ coupler	$Z_{0e} [\Omega]$ phase comp. network	$Z_{0e} [\Omega]^*$ coupler	$Z_{0e} [\Omega]$ phase comp. network
1	1.2703	1.254	1.1626	1.115	1.1279	1.077	1.1114	1.062
2	3.6656	-	1.5454	1.510	1.3175	1.238	1.2339	1.158
3	-	-	4.5749	-	1.7936	1.741	1.4654	1.363
4	-	-	-	-	5.3561	-	2.0171	1.956
5	-	-	-	-	-	-	6.0465	-
IV	$\delta C = \pm 0.6$ dB		$I = 16.6$ dB		$\delta\varphi = \pm 5.1^\circ$		$\delta C_{max} = 2.2$ dB	
BW	6.45616		10.69292		15.0578		19.475	
n	$Z_{0e} [\Omega]^*$ coupler	$Z_{0e} [\Omega]$ phase comp. network	$Z_{0e} [\Omega]^*$ coupler	$Z_{0e} [\Omega]$ phase comp. network	$Z_{0e} [\Omega]^*$ coupler	$Z_{0e} [\Omega]$ phase comp. network	$Z_{0e} [\Omega]^*$ coupler	$Z_{0e} [\Omega]$ phase comp. network
1	1.3296	1.304	1.1213	1.153	1.1750	1.108	1.1562	1.089
2	3.9058	-	1.6384	1.597	1.3906	1.296	1.2978	1.205
3	-	-	4.9092	-	1.9117	1.845	1.5553	1.436
4	-	-	-	-	5.7643	-	2.1555	2.080
5	-	-	-	-	-	-	6.5176	-
V	$\delta C = \pm 0.8$ dB		$I = 13.9$ dB		$\delta\varphi = \pm 6.5^\circ$		$\delta C_{max} = 3.0$ dB	
BW	7.77966		12.88720		18.1270		23.421	
n	$Z_{0e} [\Omega]^*$ coupler	$Z_{0e} [\Omega]$ phase comp. network	$Z_{0e} [\Omega]^*$ coupler	$Z_{0e} [\Omega]$ phase comp. network	$Z_{0e} [\Omega]^*$ coupler	$Z_{0e} [\Omega]$ phase comp. network	$Z_{0e} [\Omega]^*$ coupler	$Z_{0e} [\Omega]$ phase comp. network
1	1.3897	1.350	1.2655	1.185	1.2232	1.140	1.2023	1.120
2	4.1564	-	1.7301	1.663	1.4625	1.354	1.3611	1.255
3	-	-	5.2536	-	2.0268	1.949	1.6427	1.511
4	-	-	-	-	6.1843	-	2.2903	2.206
5	-	-	-	-	-	-	7.0031	-
VI	$\delta C = \pm 1$ dB		$I = 11.7$ dB		$\delta\varphi = \pm 8.5^\circ$		$\delta C_{max} = 3.9$ dB	
							$\delta\varphi_{max} = 19.7^\circ$	

$BW$	9.2036		15.2404		21.4147		27.644	
$n$	$Z_{0e} [\Omega]^*$ coupler	$Z_{0e} [\Omega]$ phase comp. network						
1	1.4527	1.414	1.3199	1.225	1.2739	1.174	1.2510	1.155
2	4.4312	-	1.8246	1.746	1.5366	1.411	1.4266	1.302
3	-	-	5.6297	-	2.1456	2.046	1.7325	1.579
4	-	-	-	-	6.6440	-	2.4299	2.312
5	-	-	-	-	-	-	7.5360	-

\*coupler values are taken from [29].

where:  $\delta C$  – directional couplers' coupling characteristic ripple,  $BW$  – bandwidth of directional couplers and Butler matrices,  $I$  – crossover isolation,  $\delta\varphi$  - differential phase ripple of middle networks,  $\delta C_{max}$  – Butler matrices' maximum amplitude imbalance,  $\delta\varphi_{max}$  - Butler matrices' differential phase maximum imbalance.

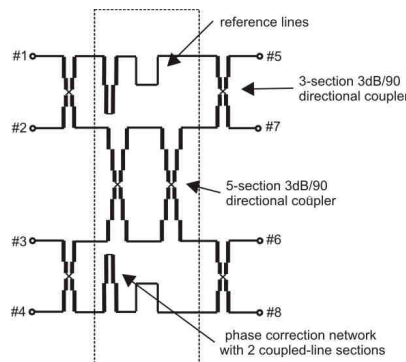


**Fig. 4.24.** A broadband  $4 \times 4$  Butler matrix consisting of three-section symmetrical coupled-line directional couplers with improved amplitude and phase characteristics. The middle network consists of a tandem connection of two five-section symmetrical 3-dB/90° coupled-line directional couplers, two two-section coupled-line phase correction networks and reference lines [68].

The comparison of differential phase characteristics for the case of 3-, 5-, 7- and 9-section directional couplers with the coupling ripple  $\delta C = \pm 0.2$  dB is presented in Fig. 4.22. It is seen that in each case equal-ripple characteristics have been obtained. Figure 4.23 presents the amplitude and differential phase characteristics of a  $4 \times 4$  Butler matrix consisting of nine-section coupled-line couplers having coupling ripple  $\delta C = \pm 0.2$  dB. The normalized even-mode characteristic impedances of the phase correction networks are  $Z_{0e1} = 1.031 \Omega$  and  $Z_{0e2} = 1.101 \Omega$ ,  $Z_{0e3} = 1.271 \Omega$ ,  $Z_{0e4} = 1.795 \Omega$  and the transmission line sections are 855°-long (at  $f_0$ ). It is seen that the obtained bandwidth of the Butler matrix exceeds one frequency decade which confirms the possibility of ultrabroadband  $4 \times 4$  Butler matrix realization with the use of the method proposed in [68]. The following parameters of the  $4 \times 4$  Butler matrix have been found: maximum amplitude imbalance  $\delta C_{max} = 0.7$  dB and phase imbalance  $\delta\varphi = \pm 4.1^\circ$ . In Table 3.1 the results of numerical analysis of broadband multisection  $4 \times 4$  Butler matrices are shown [68]. The normalized even-mode characteristics impedances are given for one-, two-, three- and four-section phase correction networks needed respectively for three-, five-, seven- and nine-section coupled-line couplers. Values of the couplers' normalized even-mode characteristics impedances are taken from [29]. The table also provide the obtained parameters of respective middle networks such as: length of the necessary section of the reference transmission line  $\Theta_c$ , the crossover

isolation  $I$  and the differential phase imbalance  $\delta\varphi$ . Moreover, the resulting Butler matrix parameters for each case are given, which are: the maximum amplitude imbalance  $\delta C_{max}$  and the maximum differential phase imbalance  $\delta\varphi_{max}$ .

**Table 4.2**

**Normalized even-mode characteristic impedances of phase-compensation networks, parameters of middle networks and parameters of 4 x 4 Butler matrices designed with the use of 3-section 3-dB symmetrical directional couplers and 5-section 3-dB symmetrical directional couplers used in the middle network [68]**

	coupler applied in a middle network	phase compensation network	middle network	Butler matrix
I	$\delta C = \pm 0.02 \text{ dB}$ $BW = 3.111$		$\Theta = 495^\circ$ $I = 46.7 \text{ dB}$ $\delta\varphi = \pm 0.4^\circ$	$\delta C_{max} = 0.22 \text{ dB}$ $\delta\varphi_{max} = 0.5^\circ$
$n$	$Z_{0en} [\Omega]$	$Z_{0en} [\Omega]$		
1	1.043	1.021		
2	1.279	1.250		
3	3.640	-		
I	$\delta C = \pm 0.054 \text{ dB}$ $BW = 4.115$		$\Theta = 495^\circ$ $I = 38.1 \text{ dB}$ $\delta\varphi = \pm 0.7^\circ$	$\delta C_{max} = 0.32 \text{ dB}$ $\delta\varphi_{max} = 0.8^\circ$
$n$	$Z_{0en} [\Omega]$	$Z_{0en} [\Omega]$		
1	1.062	1.036		
2	1.331	1.302		
3	3.828	-		
I	$\delta C = \pm 0.12 \text{ dB}$ $BW = 5.254$		$\Theta = 495^\circ$ $I = 31.2 \text{ dB}$ $\delta\varphi = \pm 1.3^\circ$	$\delta C_{max} = 0.9 \text{ dB}$ $\delta\varphi_{max} = 2.8^\circ$
$n$	$Z_{0en} [\Omega]$	$Z_{0en} [\Omega]$		
1	1.085	1.053		
2	1.388	1.359		
3	4.032	-		
I	$\delta C = \pm 0.22 \text{ dB}$ $BW = 6.579$		$\Theta = 495^\circ$ $I = 25.9 \text{ dB}$ $\delta\varphi = \pm 2.0^\circ$	$\delta C_{max} = 1.54 \text{ dB}$ $\delta\varphi_{max} = 6.0^\circ$
$n$	$Z_{0en} [\Omega]$	$Z_{0en} [\Omega]$		
1	1.117	1.081		
2	1.454	1.428		
3	4.246	-		
I	$\delta C = \pm 0.38 \text{ dB}$ $BW = 8.145$		$\Theta = 495^\circ$ $I = 21.1 \text{ dB}$ $\delta\varphi = \pm 3.2^\circ$	$\delta C_{max} = 2.28 \text{ dB}$ $\delta\varphi_{max} = 10.6^\circ$
$n$	$Z_{0en} [\Omega]$	$Z_{0en} [\Omega]$		
1	1.155	1.110		
2	1.528	1.500		
3	4.490	-		
I	$\delta C = \pm 0.52 \text{ dB}$ $BW = 9.510$		$\Theta = 495^\circ$ $I = 18.4 \text{ dB}$ $\delta\varphi = \pm 4.1^\circ$	$\delta C_{max} = 2.82 \text{ dB}$ $\delta\varphi_{max} = 14.4^\circ$
$n$	$Z_{0en} [\Omega]$	$Z_{0en} [\Omega]$		
1	1.187	1.134		
2	1.586	1.554		
3	4.684	-		

As it was shown in Fig. 4.20, the parameters of broadband 4 x 4 Butler matrices depend on the isolation of the crossover designed as a tandem connection of two multisection 3-dB/90° coupled-line directional couplers. The limited isolation of such a crossover deteriorates the amplitude and differential phase imbalance of the resulting 4 x 4 Butler matrix. The Butler matrix's characteristics can be improved with the use of a modified structure, in

which the middle network is designed with the use of directional couplers having greater number of sections than the number of sections of the remaining couplers. This solution is schematically shown in Fig. 4.24, where a Butler matrix designed with the use of three-section 3-dB/90° coupled-line directional couplers is shown. As it is seen 5-section coupled-line couplers are used within the middle network, and to achieve 45° equal-ripple differential phase characteristics the phase correction networks consisting of two coupled-line sections are used. The amplitude imbalance of the couplers applied within the middle networks is properly selected in such a way that the couplers operate within the same frequency range as the remaining couplers. Such networks have been also analyzed by the Author in [68]. The obtained numerical results of such 4 x 4 Butler matrices are presented in Table 4.2. Generally, such networks exhibit smaller amplitude and differential phase characteristic imbalance. For example in case of a 4 x 4 Butler matrix designed with the use of directional couplers having coupling ripple  $\delta C = \pm 0.2$  dB the achieved amplitude and differential phase characteristic imbalance equals  $\delta C_{max} = 0.70$  dB,  $\delta\phi_{max} = 4.1^\circ$  for the case of an unmodified Butler matrix and  $\delta C_{max} = 0.32$  dB,  $\delta\phi_{max} = 0.8^\circ$  for the case of a modified Butler matrix.

The presented concept of broadband 4 x 4 Butler matrix realization has been experimentally verified by three different designs, namely:

1. A broadband 4 x 4 Butler matrix designed in a symmetric stripline technique in which as basic elements three-section symmetrical 3-dB directional couplers are used [68].
2. A broadband 4 x 4 Butler matrix designed in an asymmetric multilayer microstrip technique also with the use of three-section symmetrical 3-dB directional couplers [168].
3. An ultrabroadband 4 x 4 Butler matrix designed in a symmetric stripline technique, in which five-section symmetrical 3-dB directional couplers are used.

The first 4 x 4 Butler matrix has been realized with the use of the three-section 3-dB/90° coupled-line directional coupler described by the Author in [65]. As a middle network a tandem connection of two such couplers have been used together with two 315°-long transmission lines and two coupled-line ‘C’-sections having normalized even-mode characteristic impedance equal  $Z_{0e} = 1.218 \Omega$ . The ‘C’-sections have been compensated with the use of the method developed by the Author [63], which allowed for significant improvement of its return losses. Layout of the designed 4 x 4 Butler matrix is shown in Fig. 4.25. Measured amplitude characteristics of the manufactured 4 x 4 Butler matrix in comparison with the characteristics of an ideal Butler matrix are shown in Fig. 4.26. The Butler matrix exhibits wide operational bandwidth equal  $BW = 5$ . The obtained amplitude imbalance does not exceed  $\pm 1$  dB, whereas, both return losses and isolations are better than 20 dB within the entire bandwidth. Fig. 4.27 shows the measured differential phase characteristics in comparison with the ideal ones. The obtained differential phase imbalance does not exceed  $\pm 8^\circ$  and is comparable with the calculated one. Fig. 4.28 presents a photograph of the developed broadband 4 x 4 Butler matrix.

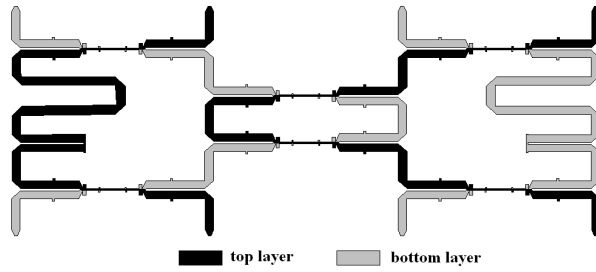


**Fig. 4.25.** Layout of the designed broadband  $4 \times 4$  Butler matrix consisting of six three-section symmetrical 3-dB/90° coupled-line directional couplers, two ‘C’-sections of coupled-lines and reference lines [68].

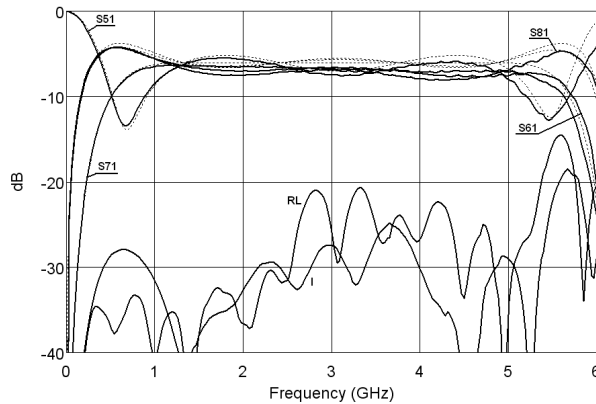


**Fig. 4.26.** Calculated (dashed lines) and measured (solid lines) amplitude characteristics of the developed broadband  $4 \times 4$  Butler matrix consisting of six three-section symmetrical 3-dB/90° coupled-line directional couplers, two ‘C’-sections of coupled-lines and reference lines [68].

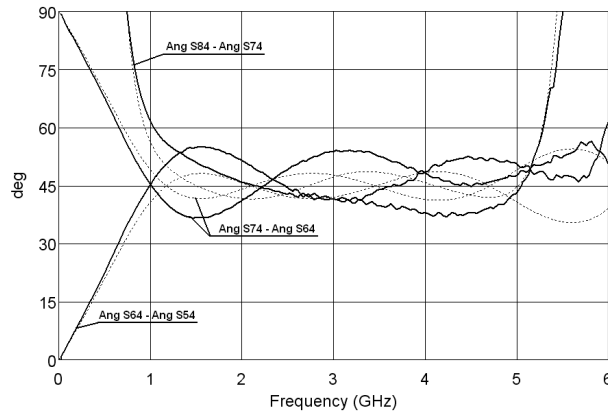


**Fig. 4.27.** Calculated (dashed lines) and measured (solid lines) differential phase characteristics of the developed broadband  $4 \times 4$  Butler matrix consisting of six three-section symmetrical 3-dB/90° coupled-line directional couplers, two ‘C’-sections of coupled-lines and reference lines [68].

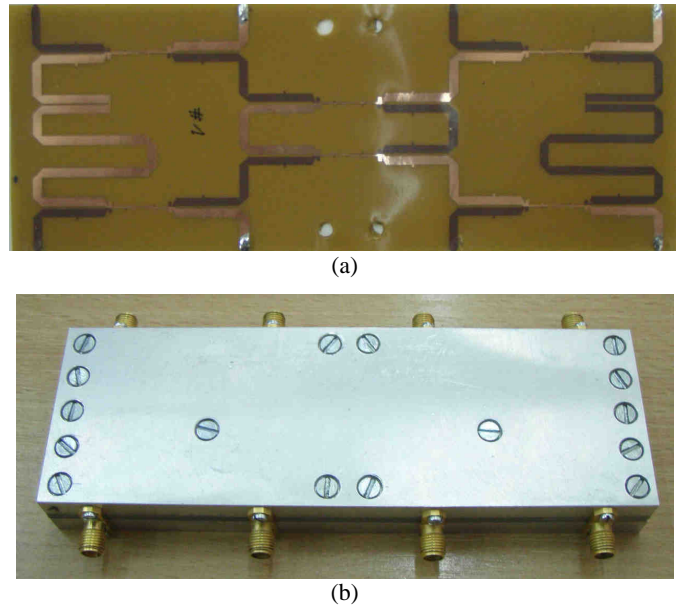


**Fig. 4.28.** Photograph of the developed broadband 4 x 4 Butler matrix. The center laminate in which traces are etched (a) and the assembled model (b) [68].

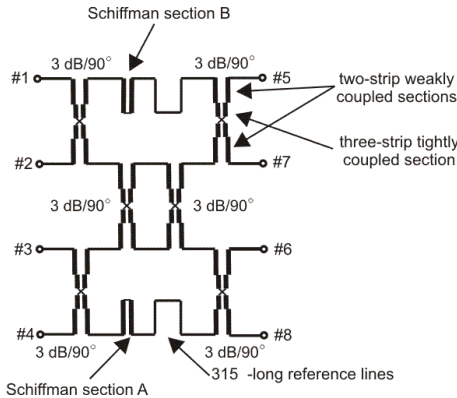


**Fig. 4.29.** Schematic diagram of the broadband 4x4 Butler matrix designed in a microstrip multilayer structure [168].

The second example of a broadband 4 x 4 Butler matrix realization has been presented in [168]. A schematic diagram of the designed Butler matrix is shown in Fig. 4.29. It utilizes the same concept, however, in this case Schiffman ‘C’-sections have to be designed separately, due to the fact that the chosen microstrip structure is asymmetric, as shown in Fig. 4.30. It consists of a thick laminate layer ( $h = 0.787 \text{ mm}$   $\epsilon_r = 3.2$ ) on which a very thin layer ( $h = 0.05 \text{ mm}$   $\epsilon_r = 3.4$ ) has been bonded using prepreg material ( $h = 0.099 \text{ mm}$   $\epsilon_r = 3.38$ ). The traces are etched on both sides of the upper thin dielectric. As a key element of the developed broadband Butler matrix – the high-performance three-section 3-dB multilayer

directional coupler designed with the use of multi-technique compensation has been used [167]. Taking into account the coupler's properties the required Schiffman 'C'-sections have been optimized for which the normalized even-mode impedance has been found to be equal  $Z_{0e} = 1.23 \Omega$ . The required 'C'-sections have been designed and compensated with the use of shunt capacitances connected to coupled-lines, as it was shown in [63]. It is worth mentioning that in this case the compensation technique has been used not only for compensation of parasitic reactances of the transition region between coupled and signal lines, but also, to improve the return losses which deteriorate due to inequality of modal phase velocities in microstrip coupled lines [132]. The calculated results of the broadband 4 x 4 Butler matrix are shown in Fig. 4.31. The achieved amplitude imbalance equals  $\pm 0.7$  dB and the differential phase imbalance equals  $\pm 4^\circ$  within two-octave frequency band (1.12 ÷ 4.5 GHz).

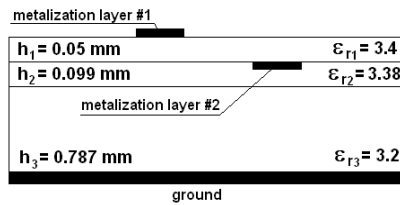


**Fig. 4.30.** Cross-sectional view of a multilayer microstrip structure in which the broadband 4x4 Butler matrix has been designed [168].

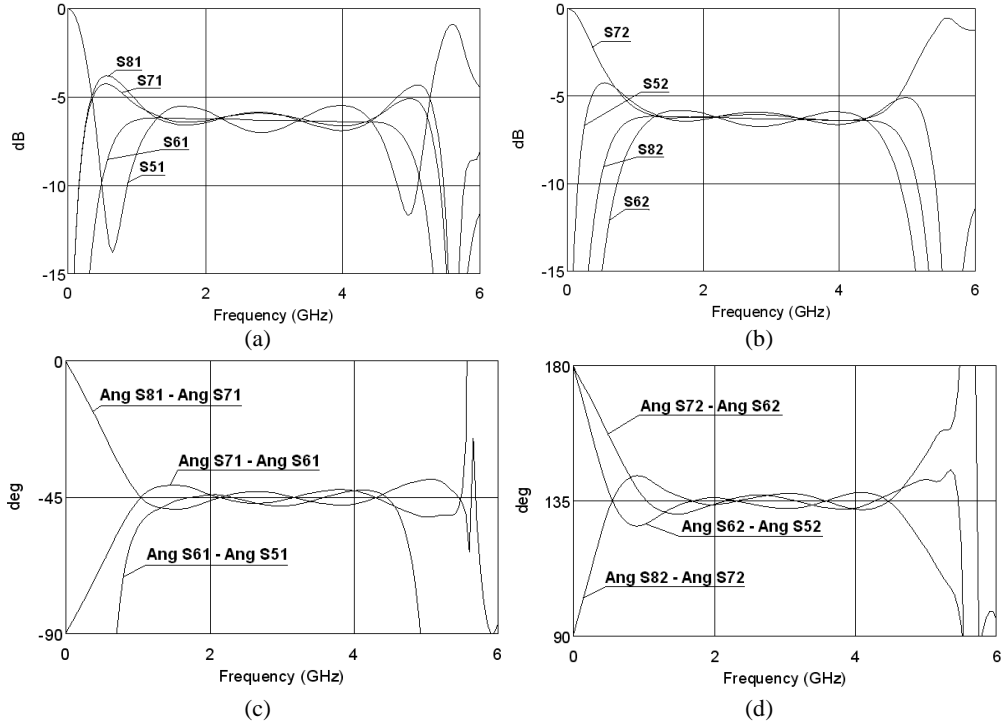


**Fig. 4.31.** Calculated responses of 4x4 Butler matrix. (a) transmissions when port #1 is fed, (b) transmissions when port #2 is fed, (c) differential phase characteristics when port #1 is fed and (d) differential phase characteristics when port #2 is fed [168].

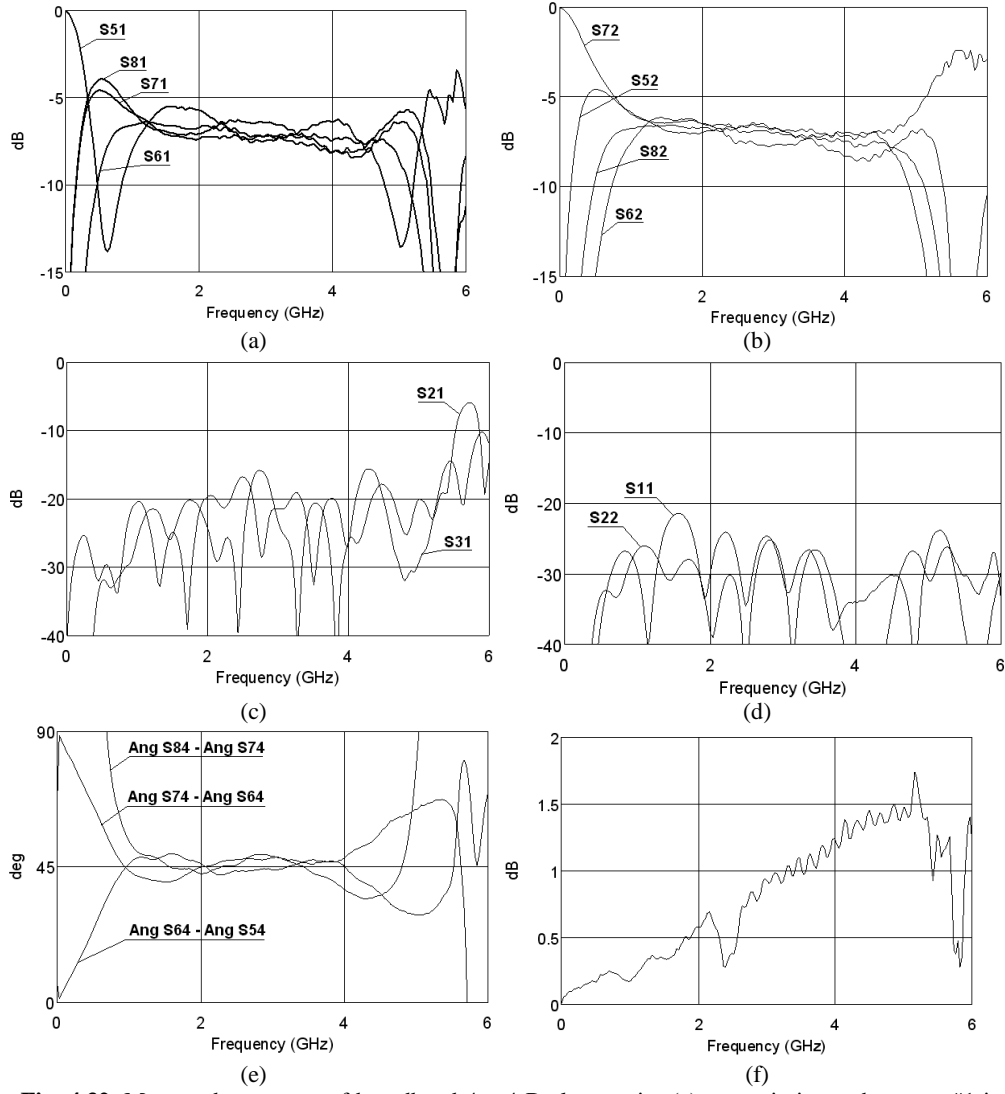


**Fig. 4.32.** Measured responses of broadband 4 x 4 Butler matrix: (a) transmissions when port #1 is fed, (b) transmissions when port #2 is fed, (c) return losses, (d) isolations, (e) differential phase characteristics when port #1 is fed and (f) overall dissipation losses [168].

Measured results of the manufactured Butler matrix are shown in Fig. 4.32. The obtained amplitude and phase imbalance equals  $\pm 0.9$  dB and  $\pm 10^\circ$ , respectively, which is in a good agreement with the calculated results, shown in Fig. 4.31. Moreover, the matrix exhibits good return losses and isolation which are better than 16 dB and 21 dB, respectively. Fig. 4.31f shows the measured overall dissipation losses of the manufactured broadband 4 x 4 Butler matrix, which do not exceed 1 dB for the center frequency of 3 GHz. Layout of the designed Butler matrix is shown in Fig. 4.33, in which two different designs of the ‘C’-sections are seen. Fig. 4.34 presents a picture of the assembled model of the manufactured broadband Butler matrix.

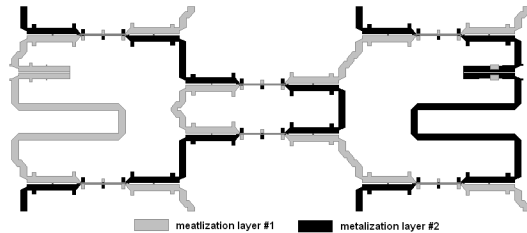


**Fig. 4.33.** Layout of developed broadband 4 x 4 Butler matrix designed in a microstrip multilayer structure [168].

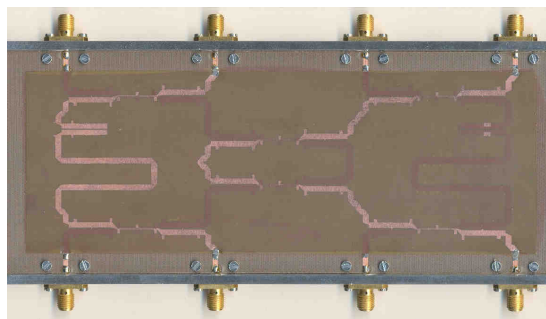


**Fig. 4.34.** Photograph of assembled model of the developed broadband 4 x 4 Butler matrix [168].

The third example shows the design of ultrabroadband 4 x 4 Butler matrix operating from 1.8 up to 12 GHz, which consists of six 5-section 3-dB/90° symmetrical coupled-line directional couplers and two 2-section Schiffman ‘C’-sections. The utilized compensated 5-section symmetrical 3-dB/90° coupled-line directional coupler is presented in [56]. The coupler has been compensated with the method described in [63, 64], which allowed for significant improvement of its amplitude characteristics. However, the applied lumped capacitors, that are used for compensation of parasitic reactances of the transition regions between coupled-line sections modify phase characteristics of the coupler. It is important to stress that due to the fact that the coupler features full symmetry the differential phase characteristics are unchanged and are equal 90° at all frequencies. However, the phase characteristics of the transmission and coupling are changed especially at high frequency range, which influences the differential phase characteristics of the designed Butler matrix. Fig. 4.35a shows the calculated differential phase characteristics of the 4 x 4 Butler matrix consisting of six 5-section coupled-line directional couplers, for which according to [68], the required even-mode characteristic impedances of the coupled-line sections of Schiffman ‘C’-sections equal:  $Z_{0e1} = 70.5 \Omega$ ,  $Z_{0e2} = 53.65 \Omega$ . Each of the sections has 90° electrical length at the center frequency of the coupler. The 4 x 4 Butler matrix features good differential phase characteristics at lower frequency range, whereas, at higher frequencies large imbalance is observed. Further research showed that this deterioration is caused due to the capacitive compensation applied to the directional couplers, and to improve these characteristics modified Schiffman ‘C’-sections have to be applied.

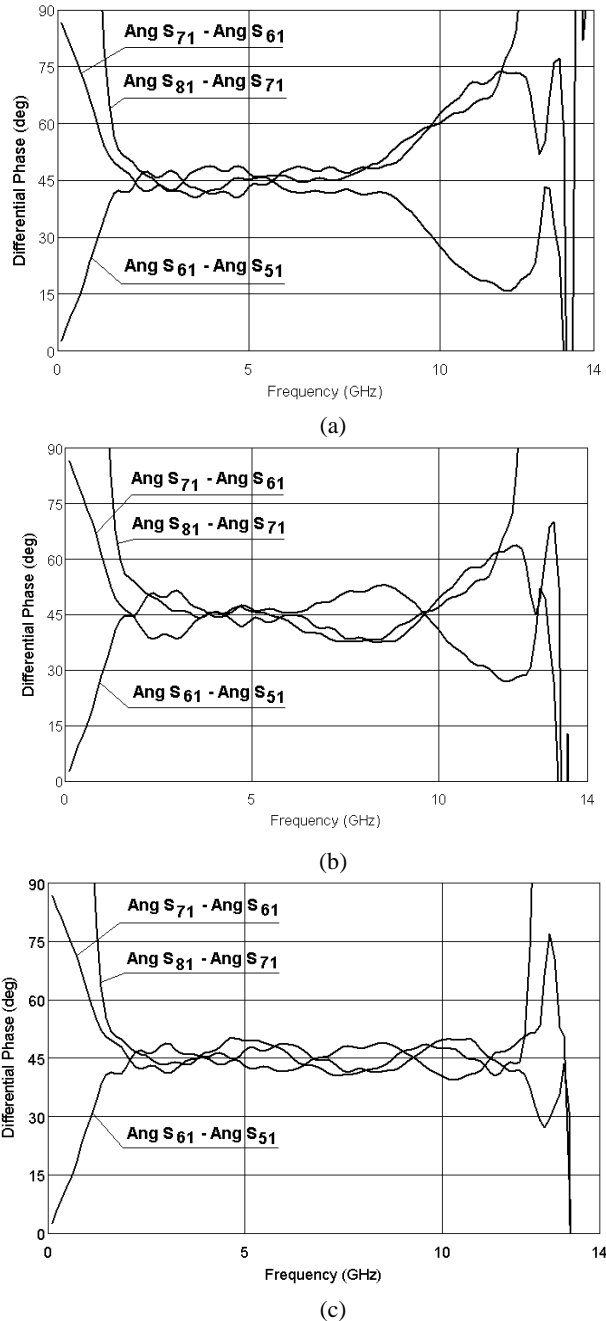


**Fig. 4.35.** Differential phase characteristics when port #1 is fed of the  $4 \times 4$  Butler matrix composed of six compensated 5-section coupled-line directional couplers and Schiffman phase shifters having -  $Z_{0e1} = 70.5 \Omega$ ,  $Z_{0e2} = 53.65 \Omega$ ,  $\Theta = 90^\circ$  (a),  $Z_{0e1} = 79 \Omega$ ,  $Z_{0e2} = 54.3 \Omega$ ,  $\Theta = 90^\circ$  (b) and  $Z_{0e1} = 82 \Omega$ ,  $Z_{0e2} = 55 \Omega$ ,  $\Theta = 71.3^\circ$  (c). Results of circuit analysis.

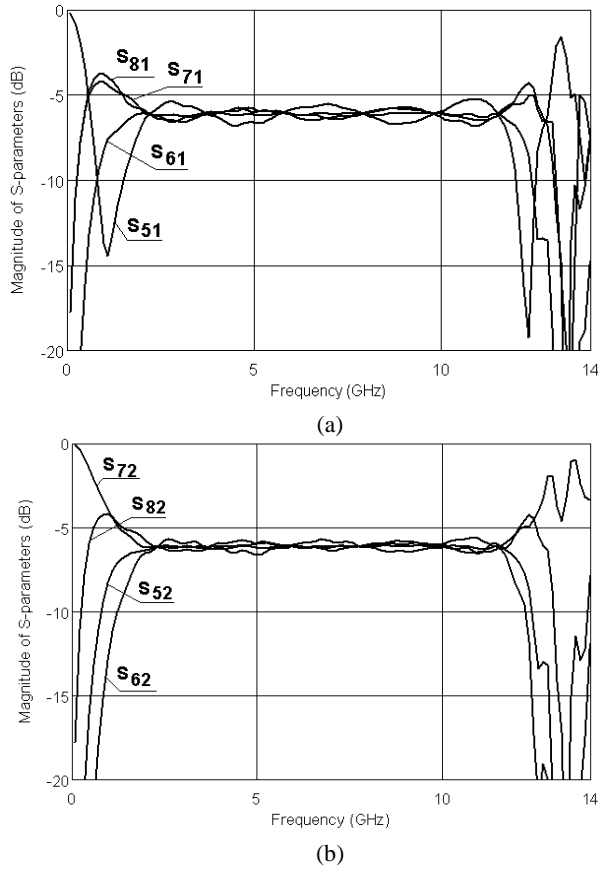


**Fig. 4.36.** Results of electromagnetic calculations the  $4 \times 4$  Butler matrix composed of compensated 5-section coupled-line directional couplers and the modified middle network. Transmissions when port #1 is fed (a), transmissions when port #2 is fed (b).

Fig. 4.35b shows the calculation results of the differential phase of the  $4 \times 4$  Butler matrix, in which the even-mode characteristic impedances of the coupled-line Schiffman ‘C’ sections have been modified to  $Z_{0e1} = 79 \Omega$ ,  $Z_{0e2} = 54.3 \Omega$  and electrical lengths of the reference lines are equal  $500^\circ$ . It is seen that the certain improvement has been achieved, however, the differential phase characteristics of the Butler matrix still feature large imbalance. Further improvement can be achieved when the electrical lengths of the Schiffman ‘C’-sections are modified. Fig. 4.35c shows the differential phase of the  $4 \times 4$  Butler matrix, in which the parameters of the coupled-line sections of Schiffman phase shifters are equal  $Z_{0e1} = 82 \Omega$ ,  $Z_{0e2} = 55 \Omega$ , the sections have electrical length equal  $71.3^\circ$  at the center frequency of the applied coupler, and the reference lines have electrical lengths equal  $588^\circ$ . Such a modification allows for significant improvement of the differential phase characteristics, which feature total imbalance less than  $\pm 5^\circ$ . The designed  $4 \times 4$  Butler matrix with the modified middle network has been analyzed electromagnetically. The calculated amplitude characteristics are shown in Fig. 4.36 and 4.37, and the achieved amplitude imbalance does not exceed  $\pm 1$  dB, whereas, the return losses are better than 15 dB. The calculated differential phases are shown in Fig. 4.38 and feature imbalance equal  $\pm 9^\circ$ .

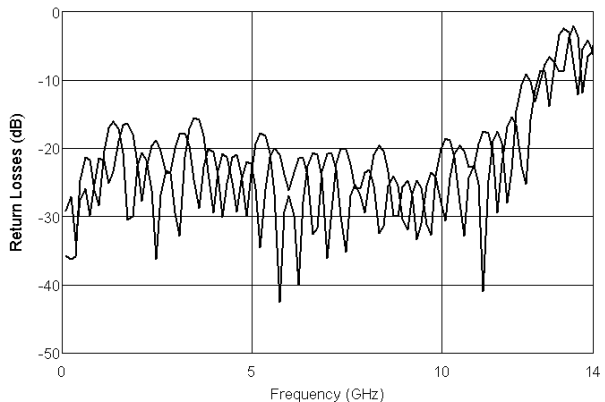


**Fig. 4.37.** Return losses the  $4 \times 4$  Butler matrix composed of compensated 5-section coupled-line directional couplers and the modified middle network. Results of electromagnetic calculations.

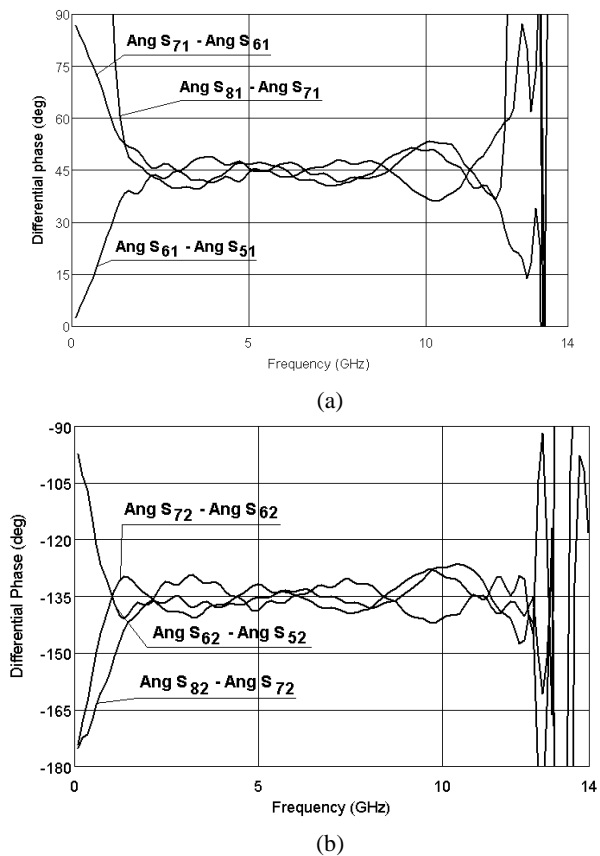


**Fig. 4.38.** Results of electromagnetic calculations the  $4 \times 4$  Butler matrix composed of compensated 5-section coupled-line directional couplers and the modified middle network. Differential phase characteristics when port #1 is fed (a), differential phase characteristics when port #2 is fed (b).

The measured amplitude characteristics of the manufactured matrix are shown in Fig. 4.39 and 4.40. The obtained return losses are better than 12 dB at all input ports which is consistent with the simulated results. The achieved amplitude imbalance is equal  $\pm 1$  dB which corresponds to the simulation results except for the transmissions measured at port #2 within the frequency range between 10.5 - 12 GHz, where the amplitude imbalance is equal  $\pm 2$  dB, due to high reflections within the circuit. Measured differential phase characteristics are shown in Fig. 4.41, and the achieved phase imbalance is equal  $\pm 15^\circ$ . Fig. 4.42 shows a picture of the center laminate layer, in which the traces of the manufactured Butler matrix are visible.

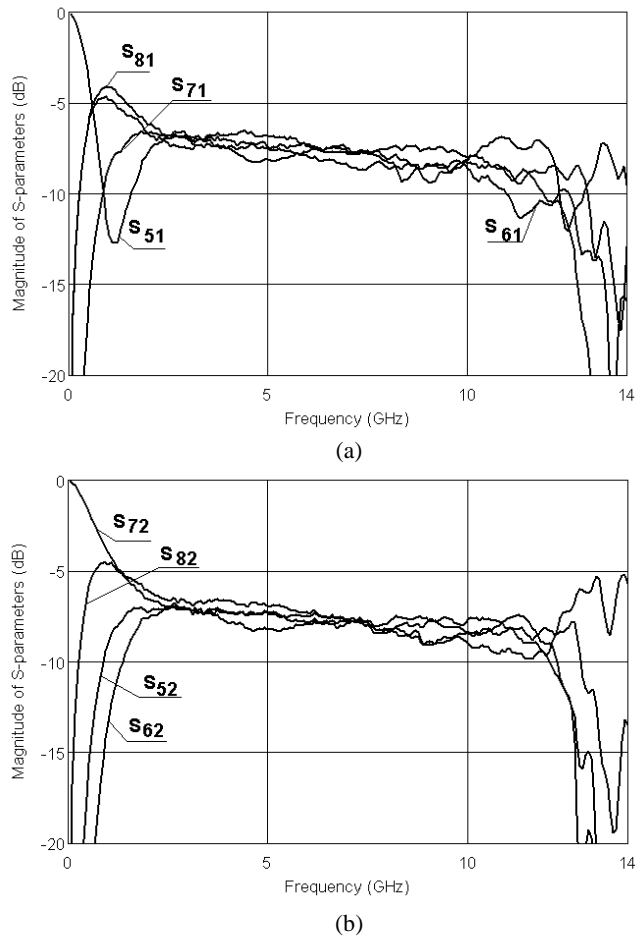


**Fig. 4.39.** Measurement results of the manufactured  $4 \times 4$  Butler matrix. Transmissions when port #1 is fed (a), transmissions when port #2 is fed (b).

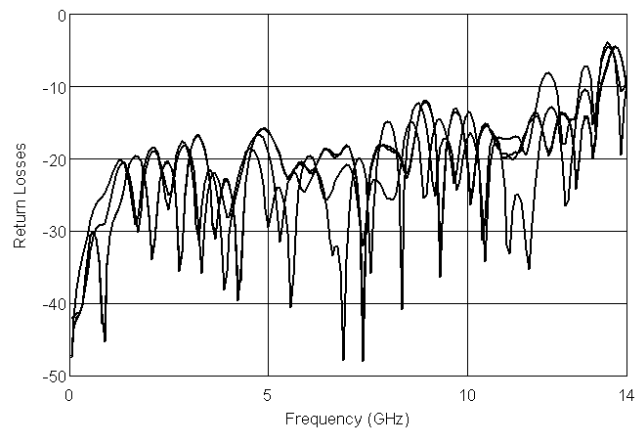


**Fig. 4.40.** Measured return losses of the manufactured 4 x 4 Butler matrix.

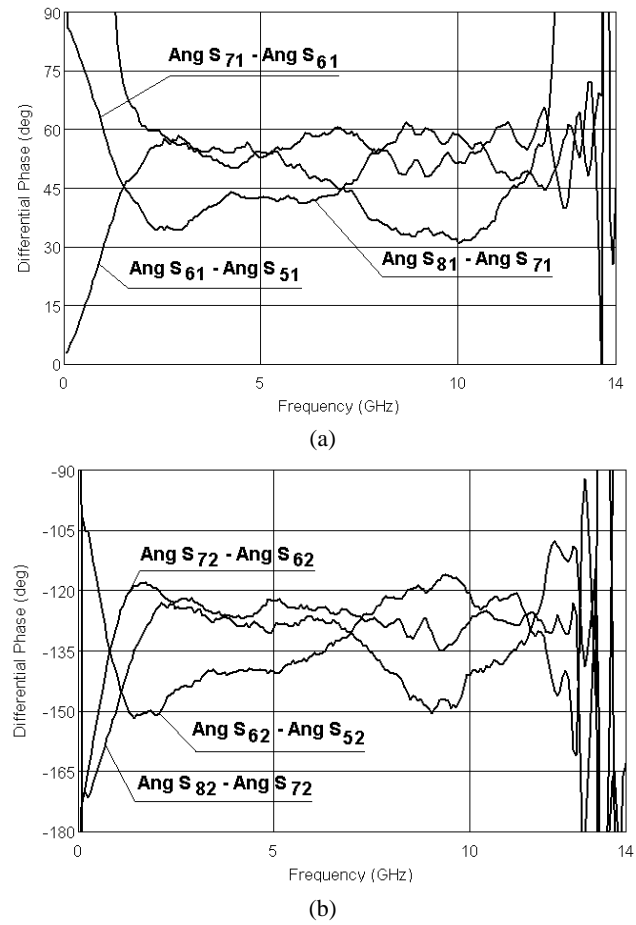


**Fig. 4.41.** Measurement results of the manufactured 4 x 4 Butler matrix. Differential phase characteristics when port 1 is fed (a), differential phase characteristics when port 2 is fed (b).

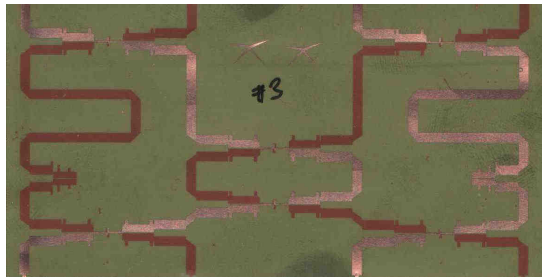


**Fig. 4.42.** Photograph of the center laminate of the ultrabroadband 4x4 Butler matrix.

The concept of the design of broadband 4 x 4 Butler matrices with the use of multisection symmetrical directional couplers and their tandem connections can be extended on realization of higher order Butler matrices. Figure 4.43 shows a schematic diagram of a broadband 8 x 8 Butler matrix, in which four submatrices are distinguished, similarly to the presented in Fig. 4.11 concept of the 8 x 8 Butler matrix realized with the use of single-section coupled-line couplers.

The input of the broadband 8 x 8 Butler matrix is constituted by two identical ‘A’ submatrices which are similar to the presented earlier broadband 4 x 4 Butler matrices. However, in this case the phase correcting networks have to be modified to ensure constant broadband 22.5° and 67.5° phase shifts. This can be achieved by an appropriate modification applied to the middle network, as shown in Fig. 4.43. The 22.5° phase shift can be realized with application of two-section Schiffman ‘C’-section (C2 – phase shifter in Fig. 4.43) and a transmission line having electrical length  $\Theta_2$ , whereas the 67.5° phase shift can be realized with the use of a single-section Schiffman ‘C’-section (C1 – phase shifter in Fig. 4.43) and a transmission line having electrical length  $\Theta_1$ . The calculated results of the differential phase characteristics of such middle networks of the submatrix ‘A’ are shown in Fig. 4.44, in which 5-section symmetrical coupled-line directional couplers having  $Z_{0e1} = 208.1 \Omega$ ,  $Z_{0e2} = 71.36 \Omega$ ,  $Z_{0e3} = 55.17 \Omega$  are used. The even-mode characteristic impedance of the C1 Schiffman ‘C’-section equals  $Z_{0e} = 53.9 \Omega$  and the electrical length of the transmission line section  $\Theta_1 = 697.5^\circ$ , whereas the even-mode characteristic impedances of the C2 Schiffman ‘C’-section equal  $Z_{0e1} = 94.9 \Omega$ ,  $Z_{0e2} = 60.1 \Omega$  and the electrical length of the transmission line section  $\Theta_2 = 472.5^\circ$ . The achieved differential phase imbalance equals  $\pm 1.5^\circ$  and  $\pm 6.5^\circ$  for the 22.5° and 67.5° phase shifters, respectively. The corresponding differential phase characteristics of the ‘A’ submatrix with the described middle network are shown in Fig. 4.45. The obtained differential phase imbalance for all ports does not exceed the phase imbalance of the 67.5° phase shifter realized with the use of the described middle network, i.e.  $\pm 6.5^\circ$ .

The output part of the broadband 8 x 8 Butler matrix presented in Fig. 4.43 is constituted by two identical ‘B’ submatrices, in which 45° phase shifters are realized in an identical manner as in the case of broadband 4 x 4 Butler matrices.

The concept of a broadband 8 x 8 Butler matrix with the use of 5-section symmetrical 3-dB/90° directional couplers has been verified experimentally. In the design the directional coupler described in [56] has been used. As the ‘B’ matrix, the 4 x 4 Butler matrix presented in Fig. 4.42 has been used in which the two input directional couplers have been removed. In order to design the ‘A’ matrix two different Schiffman ‘C’-sections have been developed. Due to the fact that the required coupling of the tight coupled section within the

C2 Schiffman ‘C’-section is not realizable in a symmetric stripline edge-coupled technique, and the broadside coupled-line technique is not suitable (the necessity of inter-layer connections), the tight coupled section of the C2 Schiffman ‘C’-section has been realized as re-entrant coupled lines. The analysis of such coupled lines can be found in [24].

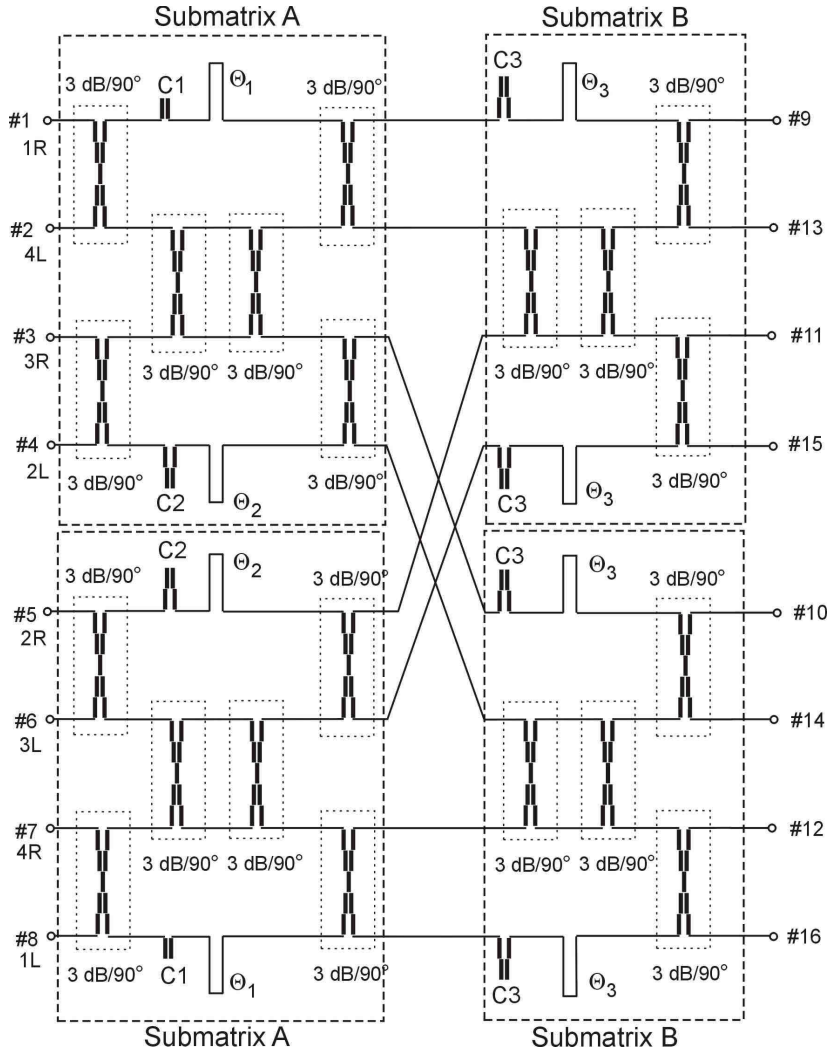


**Fig. 4.43.** Schematic diagram of a broadband 8 x 8 Butler matrix utilizing 5-section symmetrical 3-dB/90° directional couplers.

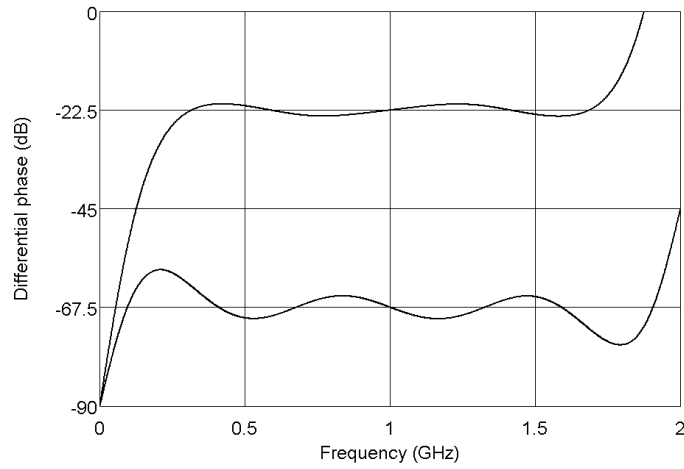


**Fig. 4.44.** Calculated differential phase characteristics between a tandem connection of two 5-section symmetrical coupled-line directional couplers and phase correcting networks showing the realization of broadband 22.5° and 67.5° phase shifters.

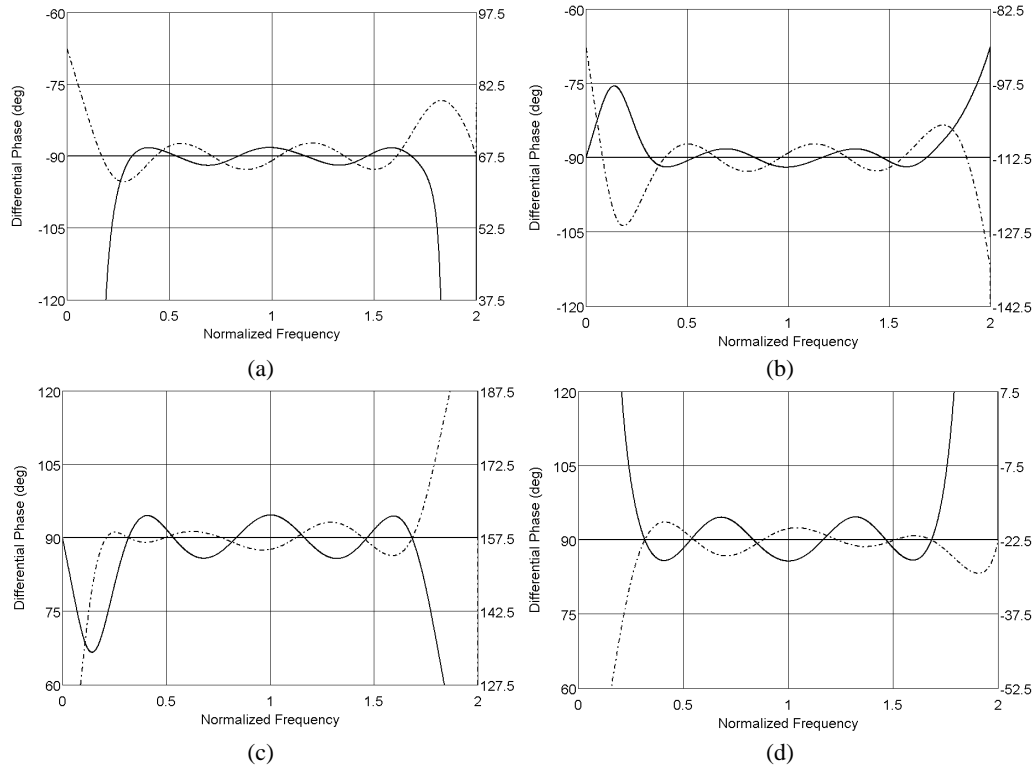


**Fig. 4.45.** Calculated differential phase characteristics of the 'A' submatrix of the 8 x 8 Butler matrix shown in Fig. 4.43. Differential phases when port #1 is fed (a), port #2 is fed (b), port #3 is fed (c), port #4 is fed (d). Solid lines refer to left axes, dashed lines refer to right axes.

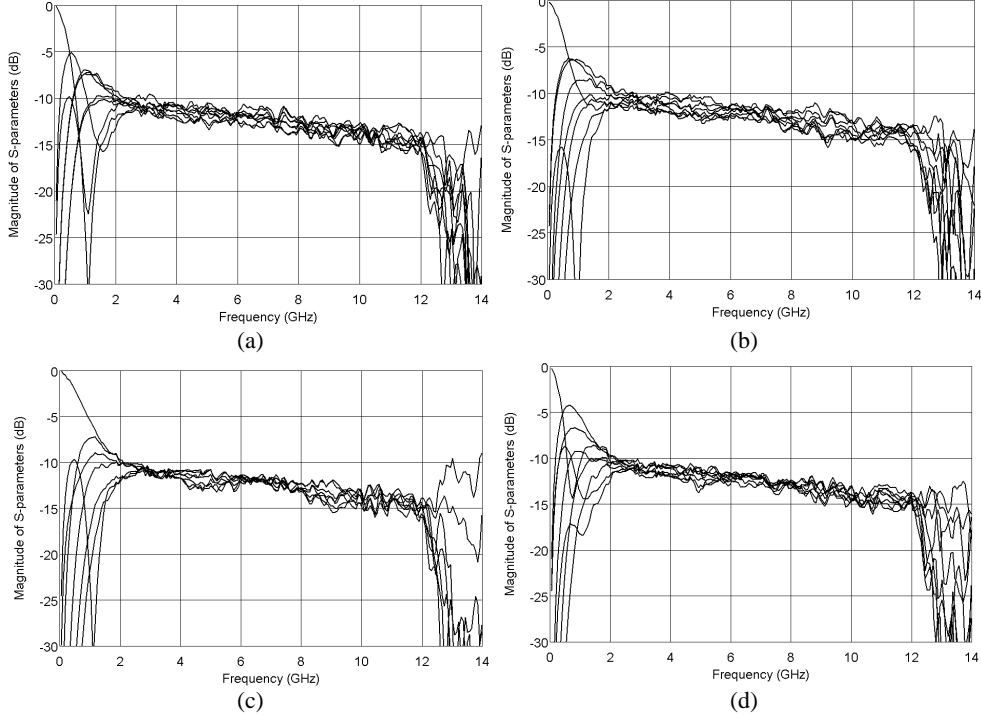


**Fig. 4.46.** Frequency responses of the ultrabroadband  $8 \times 8$  Butler matrix calculated with the use of the measurement results of the ‘A’ and ‘B’ submatrices. Amplitude characteristics when port #1 is fed a), port #2 is fed b), port #3 is fed c), and port #4 is fed d).

The final coupling coefficients of all phase compensating coupled-line sections and their electrical lengths have been modified taking into account the actual parameters of the designed 5-section 3-dB directional couplers obtained from electromagnetic analysis, similarly to the method described in the case of  $4 \times 4$  Butler matrix presented in Fig. 4.42. The following parameters have been obtained:  $Z_{0e} = 63.04 \Omega$  and  $\Theta_0 = 70.81^\circ$  for the C1 Schiffman ‘C’-section and  $Z_{0el} = 106.1 \Omega$ ,  $\Theta_{01} = 83.92^\circ$ ,  $Z_{0e2} = 59.62 \Omega$ ,  $\Theta_{02} = 93.48^\circ$  for the C2 Schiffman ‘C’-section. The electrical lengths of the transmission line sections  $\Theta_1$  and  $\Theta_2$  remain unchanged, i.e.  $\Theta_1 = 697.5^\circ$  and  $\Theta_2 = 472.5^\circ$ .

Both submatrices ‘A’ and ‘B’ have been manufactured, and their measured results have been used to calculate frequency response of the broadband  $8 \times 8$  Butler matrix. The obtained results are shown in Fig. 4.46 and 4.47. The achieved amplitude imbalance does not exceed  $\pm 1.5$  dB for all ports, and the phase imbalance is less than  $\pm 14^\circ$ . Figure 4.48 presents pictures of the center laminates of both manufactured submatrices.

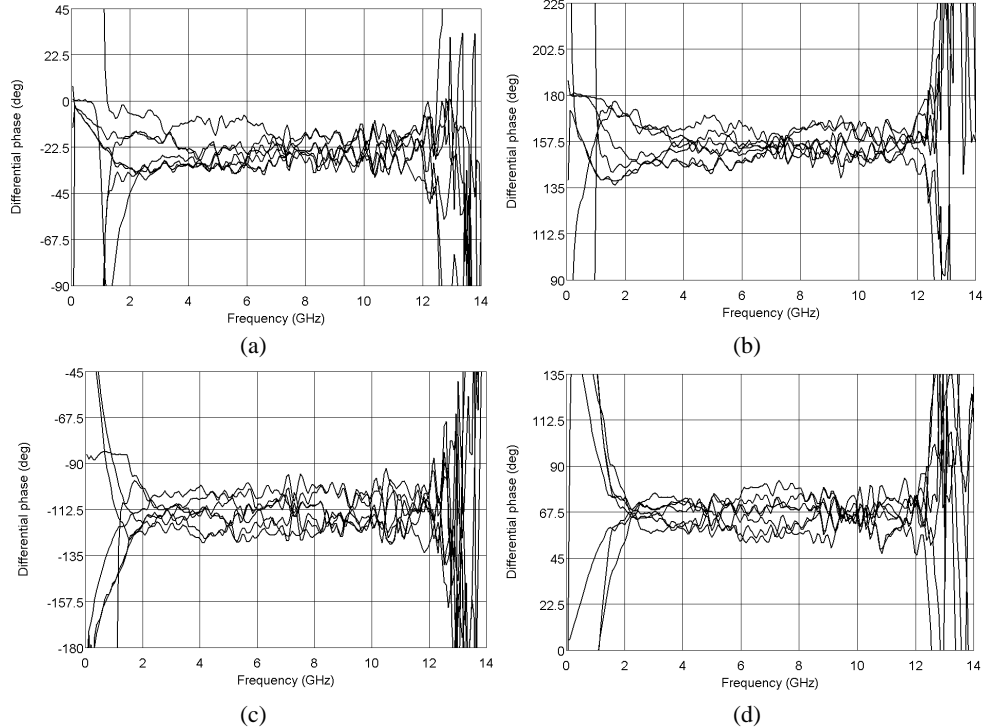


**Fig. 4.47.** Frequency responses of the ultrabroadband  $8 \times 8$  Butler matrix calculated with the use of the measurement results of the ‘A’ and ‘B’ submatrices. Differential phase characteristics when port #1 is fed a), port #2 is fed b), port #3 is fed c), and port #4 is fed d).

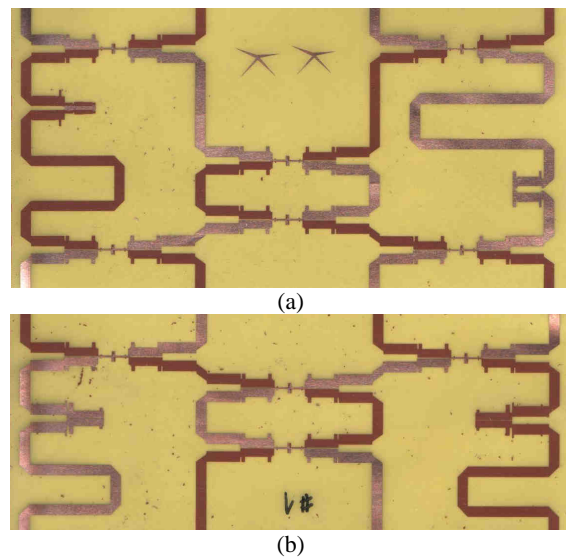


**Fig. 4.48.** Pictures of the center laminates of the manufactured submatrices of the ultrabroadband  $8 \times 8$  Butler matrix. Submatrix ‘A’ (a) and submatrix ‘B’ (b).

### 4.3. Butler matrices with the use of 0/180° directional couplers

The described in previous sections 4 x 4 Butler matrices produce ±45° and ±135° differential phases between adjacent output ports. Another way of achieving constant phase shifts between adjacent outputs of the Butler matrix has been described in [4], in which four 3-dB/0/180° directional couplers are used together with a 90° phase shifter. The resulting phase offsets of such a matrix are equal 0°, 180° and ±90°, thus when connected to a linear antenna array allow for generation four beams: broadside, endfire and two beams symmetrically located on both sides with respect to the broadside beam. An equivalent way of realization of such a network requires the connection of three 3-dB/0°/180° directional couplers and one 3-dB/90° directional coupler, as proposed in [21]. In this case no fixed phase shifters are required. There are few papers describing realizations of such networks. In [170], a method for broadband directional coupler realization with any desired frequency insensitive phase shift is presented, as a connection of a weak coupling directional coupler with 3-dB 0/180° hybrid coupler. In [44], a Butler matrix is proposed in which each hybrid was realized using a three branch-line 90° hybrid augmented by two 45° Schiffman phase shifters at the input side and two reversed 45° Schiffman phase shifters at the output side. The achieved bandwidth equals 26%.

In this section the attention is paid to the design of broadband 4 x 4 Butler matrices utilizing 3-dB/0/180° directional couplers. In order to ensure broadband operation asymmetric tapered-coupled-line couplers are used since they offer theoretically high-pass frequency response [57, 173] and 0/180° differential phase properties when referenced to transmission line sections of appropriate length [40, 74].

Figure 4.49 shows a schematic diagram of a 4 x 4 Butler matrix presented in [21], in which tapered-coupled-line 3-dB 0/180° directional couplers have been applied as hybrid couplers. For further analysis the following formula describing normalized even-mode characteristic impedance distribution of the directional coupler has been considered [64]:

$$\frac{Z_{0e}(x)}{Z_0} = 1 + 5.128 \left( \frac{x}{l} \right)^3 - 0.9 \left( \frac{x}{l} \right)^9 \quad (4.6)$$

The calculated amplitude and phase characteristics of such an ideal directional coupler are shown in Fig. 4.50 and 5.51, respectively. The coupler exhibits high-pass frequency responses allowing for realization of networks with theoretically infinite bandwidth, and features constant 0/180° differential phase characteristics. Figures 4.52 and 4.53 show the calculated amplitude and differential phase characteristics of a 4 x 4 Butler matrix consisting of four such couplers and an ideal 90° phase shifter. The amplitude imbalance equals ±0.6 dB, whereas, the achieved phase ripple equals ±3°. For the purpose of the matrix's physical realization a broadband 90° phase shifter needs to be designed. One of the possible solutions is to employ a multi-section Schiffman phase shifter [133], as shown in Fig. 4.54. To evaluate the matrix's properties a two-section Schiffman phase shifter, having the even-mode impedances of coupled lines equal  $Z_{0e1} = 135 \Omega$ ,  $Z_{0e2} = 68.1 \Omega$ , has been considered, for which the differential phase imbalance equals ±5°. The chosen phase shifter allows for operation of the matrix in the frequency range of 2 – 8 GHz. The differential phase characteristic of the Butler matrix are presented in Fig. 4.55, where it is seen, that the applied phase shifter modifies ±90° differential phase characteristics.

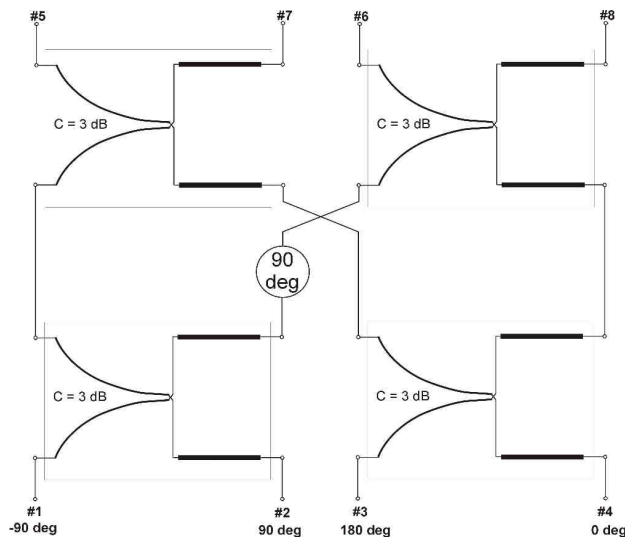


**Fig. 4.49.** Schematic diagram of a broadband 4 x 4 Butler matrix utilizing tapered-coupled-line directional couplers.

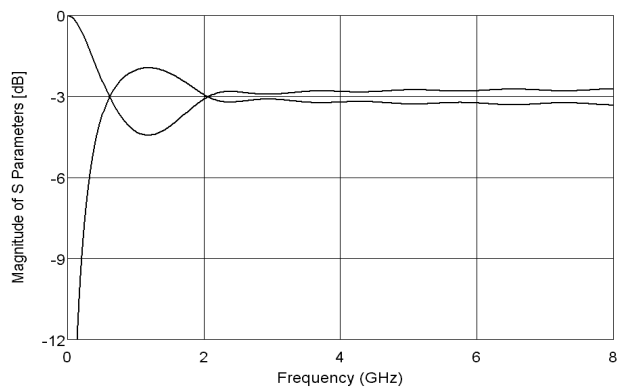


**Fig. 4.50.** Coupling and transmission characteristics of an ideal tapered-coupled-line directional coupler.

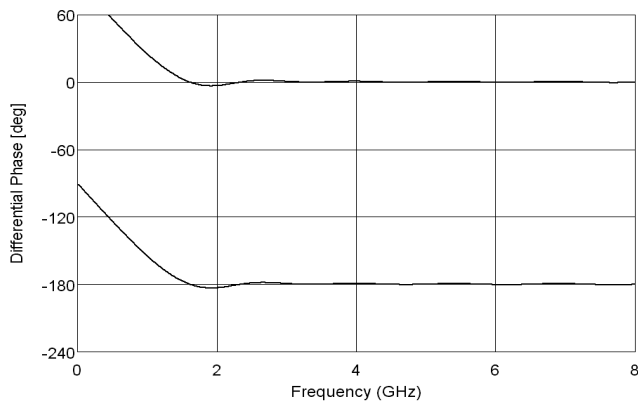


**Fig. 4.51.** Differential phase characteristics of an ideal tapered-coupled-line directional coupler.

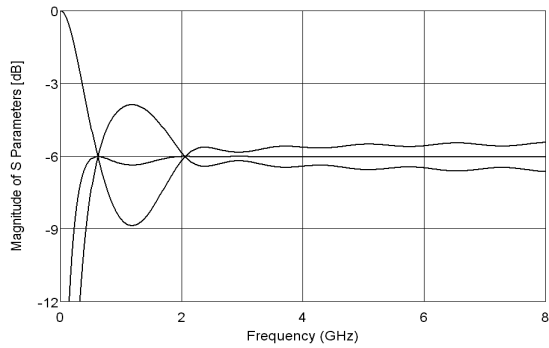


**Fig. 4.52.** Transmissions  $S_{51}$ ,  $S_{61}$ ,  $S_{71}$ ,  $S_{81}$  of an ideal  $4 \times 4$  Butler matrix composed of four tapered-coupled-line directional couplers and an ideal  $90^\circ$  phase shifter.

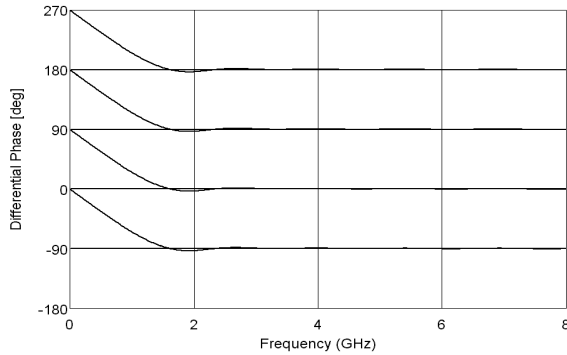


**Fig. 4.53.** Differential phase characteristics of an ideal  $4 \times 4$  Butler matrix composed of four tapered-coupled-line directional couplers and an ideal  $90^\circ$  phase shifter showing the desired  $0^\circ$ ,  $180^\circ$ ,  $\pm 90^\circ$  differential phase shifts.

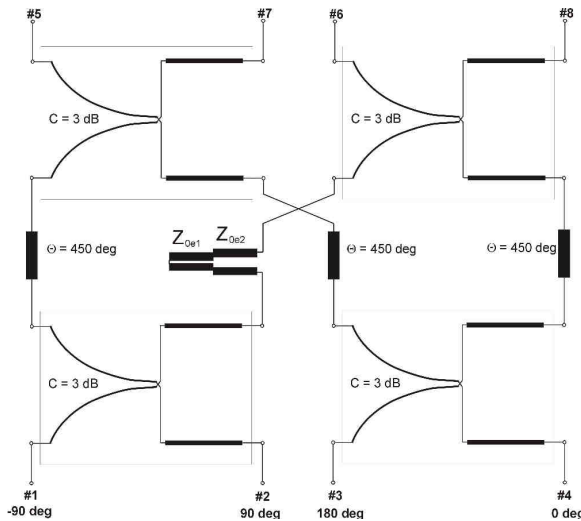


**Fig. 4.54.** Schematic diagram of a broadband  $4 \times 4$  Butler matrix utilizing tapered-coupled-line directional couplers and a two-section type-F Schiffman phase shifter.

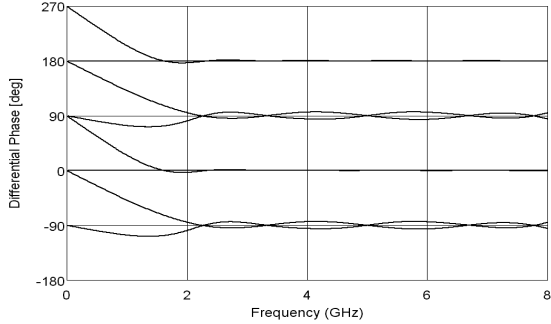


**Fig. 4.55.** Differential phase characteristics of an ideal  $4 \times 4$  Butler matrix composed of four tapered-coupled-line directional couplers and a two-section  $90^\circ$  Schiffman phase shifter showing the desired  $0^\circ, 180^\circ, \pm 90^\circ$  differential phase shifts.

Another way to realize a  $4 \times 4$  Butler matrix that allows for achieving  $0^\circ, 180^\circ$  and  $\pm 90^\circ$  differential phases is shown in Fig. 4.56 [21], where one of the tapered-line couplers is substituted by a broadband 3-dB/ $90^\circ$  directional coupler. The properties of such a network are evaluated assuming the tapered-line directional couplers with the normalized even-mode characteristic impedance distribution given by (4.6) and a 5-section symmetrical 3-dB coupled-line directional coupler.

As a tapered-line directional coupler the coupler presented in [70] and designed in a broadside coupled-stripline technology, has been used. The coupled lines have been etched on a thin CuFlon laminate having thickness  $h = 0.025$  mm and dielectric constant  $\epsilon_r = 2.05$ , which was placed between two thick  $h = 1.575$  mm layers with the same dielectric constant. Figure 4.57 shows the measured frequency characteristics of the tapered-coupled-line directional coupler [70], which exhibits good properties in the frequency range up to 8 GHz. The amplitude imbalance is less than 0.5 dB and isolation and return losses are better than 15 dB. Differential phase characteristics of the manufactured coupler are shown in Fig. 4.58. The achieved phase ripple equals  $\pm 8^\circ$  within 2-8 GHz frequency range. Figure 4.59 presents the picture of the center laminate of the manufactured directional coupler.

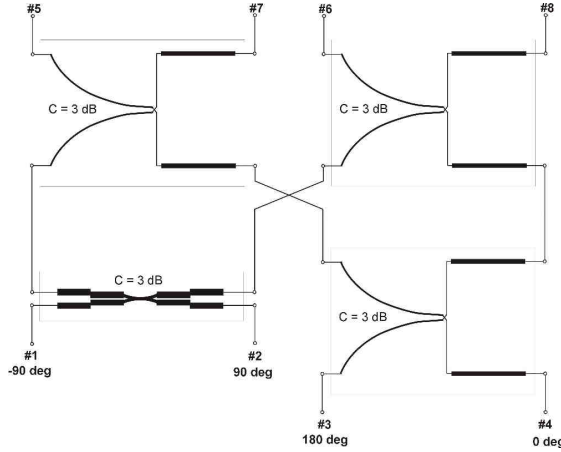


**Fig. 4.56.** Schematic diagram of a broadband  $4 \times 4$  Butler matrix utilizing tapered-coupled-line directional couplers and a two-section type-F Schiffman phase shifter.

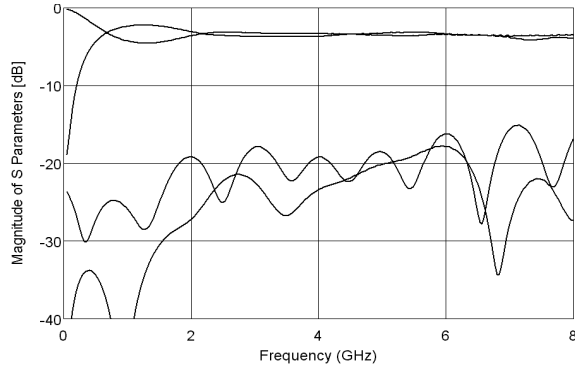


**Fig. 4.57.** Coupling, transmission, isolation and return loss characteristics of the manufactured tapered-coupled-line directional coupler [70].

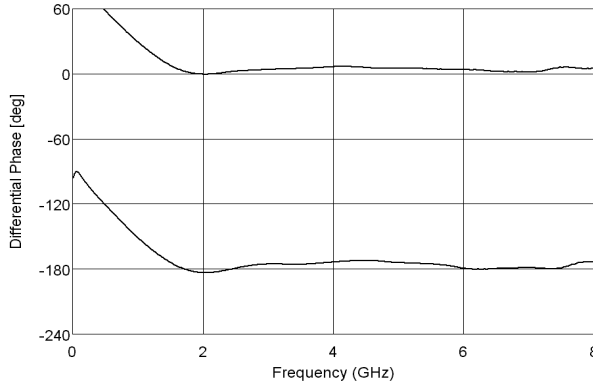


**Fig. 4.58.** Differential phase characteristics of the manufactured tapered-coupled-line directional coupler [70].



**Fig. 4.59.** Photograph of the center laminate of the tapered-line coupler [70].

The needed 5-section 3-dB/90° coupled-line directional coupler has been designed using dielectric structure consisting of a thin CuFlon laminate having thickness  $h = 0.025$  mm and dielectric constant  $\epsilon_r = 2.05$  placed between two thick  $h = 0.787$  mm layers with the same dielectric constant. In this design, a novel approach has been proposed, in which the strongest coupled section is realized as a tapered-line section. The coupling of the tapered-line section changes linearly from the strongest achievable coupling to the nominal coupling of the next section, i.e. from  $Z_{0e} = 262 \Omega$  to  $Z_{0e} = 69.9 \Omega$ . Such an approach allows to minimize the parasitic reactances of the transition region between coupled-line sections. In practice, the tapered-line section has been divided into 20 electrically short subsections. Similarly, the transition regions between weakly coupled sections have been realized as electrically short 5 subsections, in which the coupling coefficient is changing linearly from  $Z_{0e} = 69.9 \Omega$  to  $Z_{0e} = 50.5 \Omega$ . Measurement results of the manufactured directional coupler are shown in Fig. 4.60, and a photograph of the center laminate, where the tapered intersection connections are visible, is shown in Fig. 4.61.

The measured frequency characteristics of both couplers (the tapered-line coupler and the 5-section 3-dB/90° coupler) have been used for calculating the characteristics of the 4 x 4 Butler matrix. The calculated amplitude and differential phase characteristics are shown in Fig. 4.62 and 4.63, respectively. The achieved amplitude imbalance is less than  $\pm 0.5$  dB, whereas, the differential phase ripple equals  $\pm 10^\circ$ .

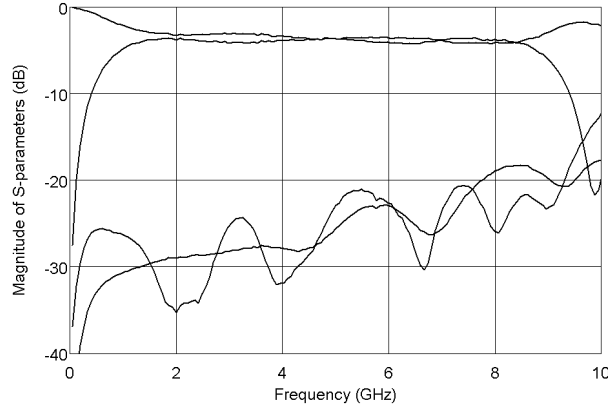


**Fig. 4.60.** Coupling, transmission, isolation and return loss characteristics of the manufactured 5-section 3-dB/90° coupled-line directional coupler with tapered inter-section connections.



**Fig. 4.61.** Photograph of the center laminate of the 3-dB/90° coupled-line directional coupler with tapered inter-section connections.

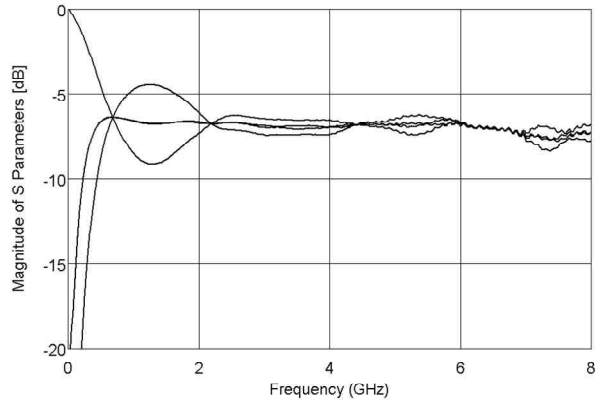


**Fig. 4.62.** Transmissions  $S_{51}$ ,  $S_{61}$ ,  $S_{71}$ ,  $S_{81}$  of a 4 x 4 Butler matrix calculated with the use of the measured responses of the manufactured tapered-coupled-line directional coupler and the 5-section 3dB/90° coupled-line directional coupler with tapered inter-section connections.

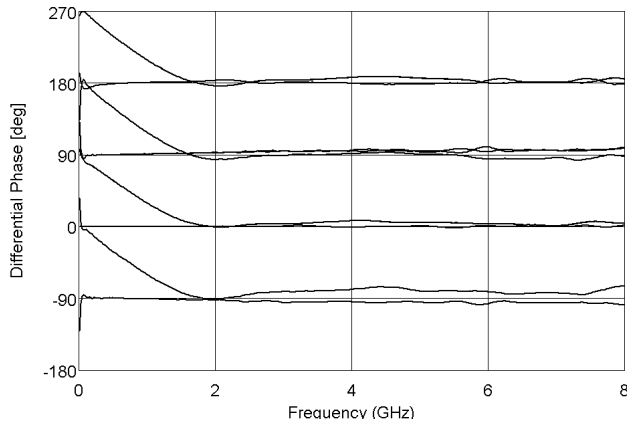


**Fig. 4.63.** Differential phase characteristics calculated with the use of the measured responses of the manufactured tapered-coupled-line directional coupler and the 5-section 3dB/90° coupled-line directional coupler with tapered inter-section connections.

#### 4.4. Summary

The chapter describes methods for the design of broadband Butler matrices utilizing coupled-line directional couplers. Firstly, Butler matrices consisting of single-section coupled-line directional couplers are considered, which allow for achieving the operational bandwidth up to one frequency octave. Two different designs of such 4 x 4 Butler matrices are presented, realized in symmetric stripline and asymmetric microstrip techniques [61, 164]. Furthermore, a novel arrangement of the 8 x 8 Butler matrix is proposed, which allows for realization of a fully planar integrated network having broadband frequency response. In this concept, the broadband operation in terms of differential phase characteristics is ensured by the realization of the selected crossovers as tandem connections of two 3-dB/90° coupled-line directional couplers and reference lines having appropriate electrical lengths. Apart from realization of broadband phase shifters such an approach allows for achieving four crossovers within the center part of the matrix, which can be further reduced into two crossovers by rearranging the circuit, as it has been shown. An arrangement has been proposed in which two final crossovers, to be realized, have been avoided by replacement of typical coupled-line directional couplers with a tandem connection of two 8.34-dB directional couplers.

The approach proposed by the Author in [68] to realize broadband multi-octave 4 x 4 Butler matrices is outlined in Section 4.2. The presented Butler matrices consist of multisection 3-dB/90° symmetrical coupled-line directional couplers and middle networks, which ensure simultaneously a transmission-line crossover and broadband 45° phase shifters. A general analysis of 4 x 4 Butler matrices being a connection of multisection 3dB/90° symmetrical coupled-line directional couplers is presented and tables giving normalized even-mode impedances of the phase correction networks needed for respective coupled-line couplers are provided after [29]. Moreover, the problem of limited isolation of a tandem connection of two directional couplers is outlined and a modified middle network for im-

proving Butler matrices' characteristics proposed by the Author in [68], is shown. In such a network, directional couplers constituting a tandem connection have more sections than the remaining couplers and phase correction networks consist of a greater number of coupled-line sections. This approach allows for significant improvement of both amplitude and differential phase characteristics of the designed Butler matrices.

The presented approach for broadband  $4 \times 4$  Butler matrices' realization has been experimentally verified by three different designs, i.e. the  $4 \times 4$  Butler matrix designed in a symmetric stripline technique with the use of three-section coupled-line directional couplers, similar design in an asymmetric microstrip technique, and the ultrabroadband  $4 \times 4$  Butler matrix designed in a symmetric stripline technique in which 5-section coupled-line directional couplers are used. Moreover, the concept of broadband  $4 \times 4$  Butler matrix realization has been applied to the design of broadband  $8 \times 8$  Butler matrices. An exemplary design with the use of 5-section coupled-line directional couplers is shown, in which a modular approach, based on the division of the network into four submatrices, is applied.

Finally, broadband  $4 \times 4$  Butler matrices utilizing 3-dB/0/180° directional couplers are outlined. The broadband operation of the considered networks is ensured by the application of tapered-line directional couplers having theoretically high-pass frequency response. An exemplary design of such a Butler matrix is shown, which has been realized with the use of three tapered-line directional couplers and a 5-section 3-dB/90° symmetric coupled-line directional coupler.

## **5. Design of miniaturized broadband directional couplers**

In lower microwave frequency range the conventional distributed passive components such as branch-line couplers, Wilkinson power dividers, Gysel power dividers, coupled-line directional couplers, etc. consume large area of a microwave integrated circuit (MIC) or a monolithic microwave integrated circuit (MMIC). Therefore, size reduction techniques of microwave passive components have been the subject of intensive research over the last years. In applications, where size reduction is required, lumped or semi-lumped element devices that require only a small area are very attractive [3, 8, 16, 42, 47, 76, 83, 88, 99, 157]. In addition, a recent rapid development of micromachining technology makes utmost miniaturization of microwave components possible. The development of lumped-element devices is also important in this sense.

In the following section a brief introduction to the miniaturization techniques is presented in application to microwave components utilizing directly-connected transmission lines. The presented techniques allow for significant miniaturization, however, the designed components feature by principle narrow operational bandwidth. The Author has focused on the design of coupled-line directional couplers, which allow for broadband and ultrabroadband operation, as it was shown in the previous chapters. The section 5.2 presents the results of Author's investigation aiming at the development of miniaturization techniques of broadband coupled-line directional couplers. The design technique of quasi-lumped broadband directional couplers proposed in [166] is cited in large extend. The influence of number of subsections in a lumped-element equivalent circuit on the couplers' overall performance has been outlined. The proposed miniaturization technique of coupled-line directional couplers has been experimentally verified by the design of miniature single-section and multisection broadband directional couplers.

### **5.1. Miniaturization techniques in the design of microwave directional couplers**

In the design of passive microwave directional couplers and power splitters in microwave frequency range, the common approach is to utilize distributed networks being a connection of transmission lines in various technologies, or electromagnetically coupled-line sections

in various technologies. The methods allow for realization of many different passive circuits, however, at lower region of microwave frequencies, the resulting circuits suffer from large dimensions. Therefore, over the years techniques for miniaturization of microwave circuits have been developed, which allow for significant reduction of the designed passive components. A conventional approach of branch-line directional couplers' miniaturization has been presented in [85], where a capacitive loaded transmission-line section of a shorter length  $\theta_E$  has been used to replace the original transmission-line section having length  $\theta_A$ , as it is shown schematically in Fig. 5.1. The following equations relate parameters of the two circuits

$$Z_A \sin \theta_A = Z_E \sin \theta_E \quad (5.1)$$

$$\cos \theta_A = \cos \theta_E - \omega C_E Z_E \sin \theta_E \quad (5.2)$$

In [85] an application of the method for the design of a 3-dB three-branch branch-line directional coupler has been shown. The method allowed for 68% size reduction of the miniaturized coupler over the conventional one. A similar approach for the design of a branch-line coupler has been shown in [151], where a further modification of the distributed capacitors in the inner area of the coupler allowed for slight improvement of the size reduction ratio. In this design finger-shaped distributed capacitors have been proposed. Further reduction of the size of the branch-line coupler has been reported in [142], where the distributed capacitive elements  $C_E$  have been replaced by sections of long meandered transmission lines. The achieved size reduction reaches 89%. The open-stab loaded transmission-line-section technique can be also applied in the design of rat-race couplers, as shown in [23], where 12 open-ended transmission-line stubs have been equally distributed on the circumference of the coupler's ring. Another approach to the miniaturization of a rat-race coupler has been presented in [20], where a quarter-wave long transmission-line section is replaced by a cascade connection of two sections of transmission lines and a coupled-line C section. The developed rat-race coupler has been miniaturized to occupy 31% of the area of a conventional rat-race coupler, moreover, it has been optimized to operate in dual frequency range (2.45 GHz and 5.2 GHz). Exemplary applications of the reduced-size branch-line couplers can be found in [50], where the designed miniaturized couplers have been utilized for realization of 4 x 4 Butler matrices operating at 1.8 GHz. Capacitive loading can also be applied in miniaturization of the forward-wave coupled-line directional couplers, as it was shown in [114], where almost 90% miniaturization rate has been reported.

Further miniaturization can be achieved when the distributed element networks are transferred and realized with the use of a lumped-element technique. The principles of the method base on the well-known representation of distributed elements with their equivalent circuits consisting a connection of lumped capacitors and inductors (lossless transmission line). Therefore, a short section of a transmission line can be replaced by the equivalent circuit consisting of an inductor and two shunt capacitors. Following that idea more complex circuits can be designed. Figure 5.3 shows schematic diagrams of the equivalent lumped-element circuits of the well-known rat-race couplers and quadrature couplers [39].

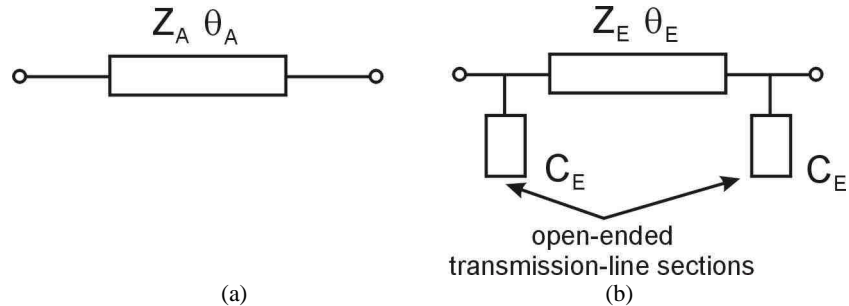


**Fig. 5.1.** Equivalent circuits of an arbitrary transmission line. Conventional transmission line (a) and equivalent circuit with distributed components (b) [85].



**Fig. 5.2.** Concept of miniaturized circuits with the use of the technique described in [85]. Layout of a conventional branch-line coupler (a) and its reduced-size version (b).

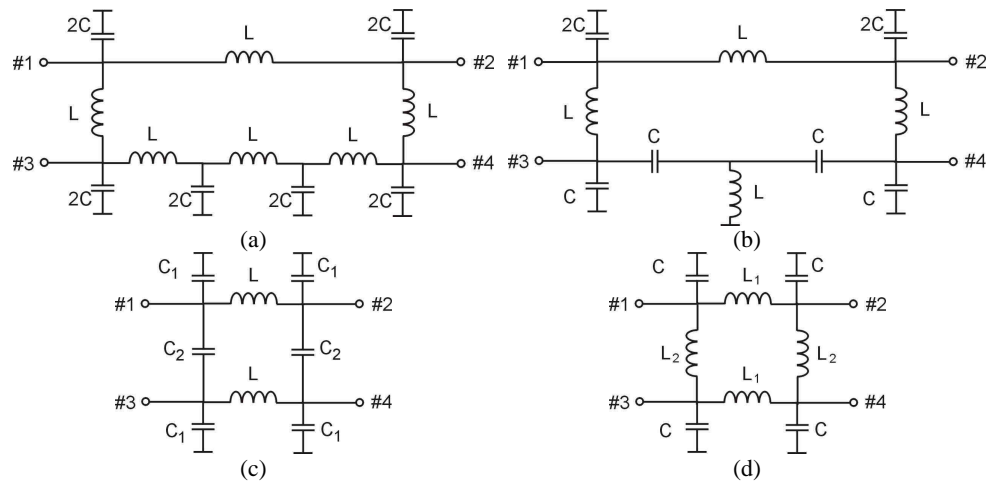


**Fig. 5.3.** Lumped-element equivalent circuits of distributed microwave components. A rat-race coupler (a) and (b), a quadrature coupler (c) and (d) [39].

The circuits consist of appropriately connected  $LC$   $\pi$ -networks in each of their branches replacing sections of transmission lines. In case of rat-race couplers shown in Fig. 5.3a and 5.3b the branches having electrical length greater than  $90^\circ$  consist of multiple  $LC$  sections equivalent to transmission lines.

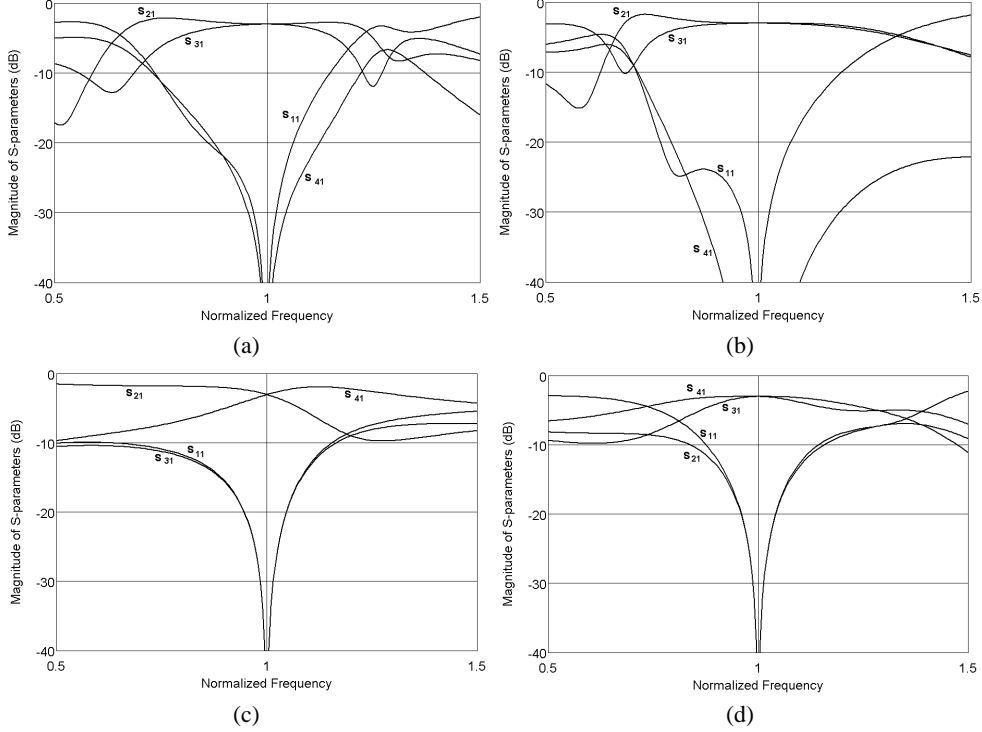


**Fig. 5.4.** Frequency responses of the circuits presented in Fig. 5.3. The rat-race coupler (a) and (b), the quadrature coupler (c) and (d).

The performance of these circuits resembles the performance of their distributed counterparts. The values of the  $L$  and  $C$  elements for the circuits shown in Fig. 5.4 can be calculated with the well-known formulas, i.e. for the rat-race coupler (Fig. 5.4a and 5.4b) as follows:

$$L = \frac{Z_0 \sqrt{2}}{\omega} \quad (5.3)$$

$$C = \frac{1}{\omega Z_0 \sqrt{2}} \quad (5.4)$$

and for the quadrature coupler shown in Fig. 5.4c as follows:

$$C_2 = \frac{1}{\omega Z_0} \quad (5.5)$$

$$L = \frac{Z_0}{\omega \sqrt{2}} \quad (5.6)$$

$$C_1 = \frac{1}{\omega^2 L} - C_2 \quad (5.7)$$

and finally for the quadrature coupler shown in Fig. 5.4d as follows:

$$C = \frac{1 + \sqrt{2}}{\omega Z_0} \quad (5.8)$$

$$L_1 = \frac{Z_0}{\omega} \quad (5.9)$$

$$L_2 = \frac{Z_0}{\omega \sqrt{2}} \quad (5.10)$$

The techniques of miniaturization utilizing the lumped-element approach are well suited to the modern technologies of circuit's realization such as LTCC (*Low Temperature Co-fired Ceramic*) [88, 98, 139, 155] or monolithic technologies [16, 42, 76, 157].

The LTCC technology allows for manufacturing multilayer electronic modules with the use of a ceramic tape (green tape). The typical thicknesses of the tapes offered on the marked range from 100  $\mu\text{m}$  to 200  $\mu\text{m}$ , but also thinner foils with the thickness below 20  $\mu\text{m}$  can be found. The printing of the traces on the layers of ceramic tapes is made with the use of screen printing technique. The layers after printing are stacked and laminated under high pressure of 200 atm. and fired in the temperature of 850°C. The usage of LTCC technology for fabrication of microwave circuits has been noted for several years now. The success of the technology comes from the fact that, despite their relatively high costs, it offers good electrical properties together with the possibility of manufacturing multilayer structures having different microwave components placed on different layers. The main advantages of LTCC technology can be summarized as follows [11]:

- low dielectric constant of the green tapes,  $\epsilon_r$  as low as 3.9,
- low dissipation factor  $\operatorname{tg}\delta \leq 1 \cdot 10^{-3}$  (1 GHz),
- temperature stability of resonant frequency  $T_f < 10 \text{ ppm/K}$ ,
- green tape thickness stability better than 5%,
- low resistivity of the conducting traces, up to 2  $\text{m}\Omega/\text{sq.}$ ,
- possibility of manufacturing precise conducting tracks with the thickness typically 100  $\mu\text{m}$ ,
- possibility of manufacturing conductive connections between layers with the diameter of 100  $\mu\text{m}$ .

There are currently number of companies on the market offering commercial LTCC technology, among which one can name: Barry LTCC, Murata, Schott, Koyocera, SiP Technology, Heraeus, ColdFusion, VTT Electronics each having their own design rules, which are summarized in Table 5.1.

**Table 5.1**

Exemplary design rules and material properties offered currently on the market

Company	Barry LTCC	Murrata	Schott	Koyocera	SiP Technology	Heraeus	Cold-Fusion	VTT Electronics
Minimum thickness [μm]	92	12.5	100	46	300	570	40	40
Dielectric constant	7.4 - 7.8	7.7 - 15.1	7 - 8	5.9 - 7.8	4.4 - 18	7.2	9.1	7.8
Dissipation factor	$2 \times 10^{-3}$ - $6 \times 10^{-3}$		$1 \times 10^{-3}$ - $5 \times 10^{-3}$	$5 \times 10^{-4}$ - $1.5 \times 10^{-3}$	$1 \times 10^{-3}$ - $6 \times 10^{-3}$	$2 \times 10^{-3}$	$2 \times 10^{-3}$	0.15%
Thermal expansion [ppm/°C]	5.8 - 6	5.5-7.2	5 - 6	5.8 - 8	3.5 - 5	5.8	<10	5.8
Minimum track width [μm]	77	75	70	100	60	77	100	150
Minimum via diameter [μm]	89	100	100	100	100	100	200	100
Resistivity mΩ/sq.	3 - 25				2.5 - 5	<3.5	<2	

Figure 5.5 shows a 3-D view of an exemplary design of a branch-line directional coupler having the electrical equivalent circuit shown in Fig 5.3d. The coupler has been designed with the use of AWR Microwave Office electromagnetic simulator with the assumption of the following rules: layer thickness – 87 μm,  $\epsilon_r = 7.7$ , minimum track width 50 μm, minimum via diameter 400 μm (the design rules of the Institute of Electron Technology, Krakow, Poland). As it is seen the circuit consists of four planar inductors having values of 3.3 nH and 2.3 nH and four multilayer capacitors having values 3.1 pF. The coupler has been designed with the use of 5 layers of a green tape and the overall dimensions of the component are less than 5 x 5 mm for the coupler operating at 2.4 GHz. The frequency response of the designed coupler, calculated electromagnetically, are shown in Fig. 5.6 and are in full agreement with the theoretical ones.

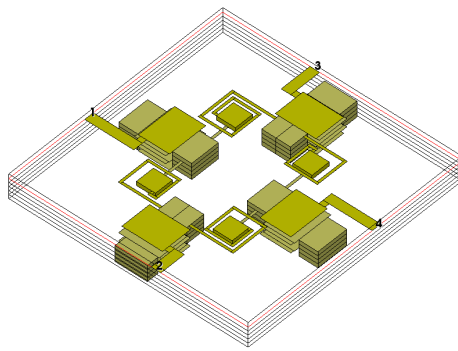


**Fig. 5.5.** A 3-D view of the designed branch-line directional coupler for applications in LTCC technology.

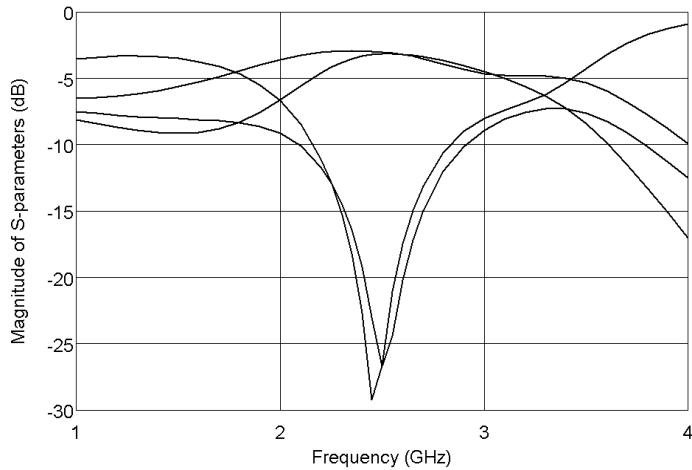


**Fig. 5.6.** Frequency response of the designed branch-line directional coupler for applications in LTCC technology. Results of electromagnetic calculations.

## 5.2. Design of broadband quasi-lumped directional couplers

The presented in section 2.1 directional couplers having directly-connected transmission lines, apart from narrow operational bandwidth, occupy relatively large area, due to large dimensions, i.e. each section of transmission line being at least quarter-wave long, in both planar circuits' dimensions. In term of miniaturization the application of coupled-line directional couplers is a step forward, since such a coupler features extensive dimensions only in one planar direction, while being relatively small in the other direction. Therefore, the occupied area is significantly reduced in comparison to directly-connected directional couplers. Further miniaturization of coupled-line directional couplers can be achieved with the use of the presented in section 5.1 methods applied to directly-connected directional couplers, in which distributed elements are substituted by networks having lumped elements.

A number of papers report investigation results regarding the design of lumped-element coupled-line directional couplers. In [8] and [47] the designs of 3-dB coupled-line directional couplers are presented, where a direct single-section equivalent circuit of coupled lines has been realized in MMIC technology. However, in both presented designs, the simplicity of the assumed equivalent circuits is reflected in poor performance of the transmission-coupling characteristics, which limit the bandwidth of the resulting couplers. In [139] coupled-line directional couplers designed in LTCC technology were presented, in which coupled inductors have been replaced by the connection of uncoupled ones. Also in this case, the proposed modification limits the operational bandwidth of the designed couplers. In [78] a broadband 3-dB directional coupler has been presented, in which transmission-coupling characteristics are in a good agreement with the ones obtained with the standard distributed coupled transmission line technique. The presented approach involves a two subsection equivalent circuit and the coupler has been designed with the use of a planar

spiral transformer technique. Similarly, in [2] a two-subsection equivalent circuit has been employed for the design of a 3-dB directional coupler in GaAs monolithic technology for applications in phase shifters, down-converters and I-Q converters. In [91] an exemplary design of a weak coupling 24 dB directional coupler manufactured using multilayered organic packaging structure is presented. In the presented design, the achieved directivity is low, due to the fact that the obtained isolation is about 25 dB.

In [166] the Author has presented a comprehensive overview regarding the design of quasi-lumped directional couplers having the properties of coupled-line directional couplers, which is cited in a large extend below.

The lumped-element equivalent circuit of a coupled-line directional coupler is shown in Fig. 5.7a. The values of lumped elements can be found once the coupling  $k$  of the directional coupler, the center frequency  $f_0$  and the number of subsections chosen for the realization  $n$  are specified. It is assumed that the conditions of ideal coupler realization (2.57) and (2.58) are met.

At first the expressions for capacitance and inductance elements of the  $[C]$  and  $[L]$  matrices are derived, which describe the properties of coupled lines. These parameters can be found as [166]:

$$C_{11}' = \frac{1}{\sqrt{\nu^2 Z_0^2 (1 - k^2)}} \quad (5.11)$$

$$C_m' = C_{11}' k \quad (5.12)$$

$$C_1' = C_{11}' - C_m' \quad (5.13)$$

$$L_1' = \frac{C_{11}'}{(C_{11}'^2 - C_m'^2) \nu^2} \quad (5.14)$$

Having found the elements of  $[C]$  and  $[L]$  matrices, the values of the directional coupler's elements, shown in Fig. 5.7a can be calculated as

$$C_1 = C_1' \frac{x}{2n} \quad (5.15)$$

$$C_m = C_m' \frac{x}{2n} \quad (5.16)$$

$$L_1 = L_1' \frac{x}{n} \quad (5.17)$$

where  $x = \frac{\nu}{4f_0}$  is the length of the coupler,  $\nu = c$  is the free space velocity of light and

coupling of coupled inductors  $k$  equals the initially chosen coupling  $k$  of the directional coupler  $k_{coupled\ inductors} = k_{directional\ coupler}$ .

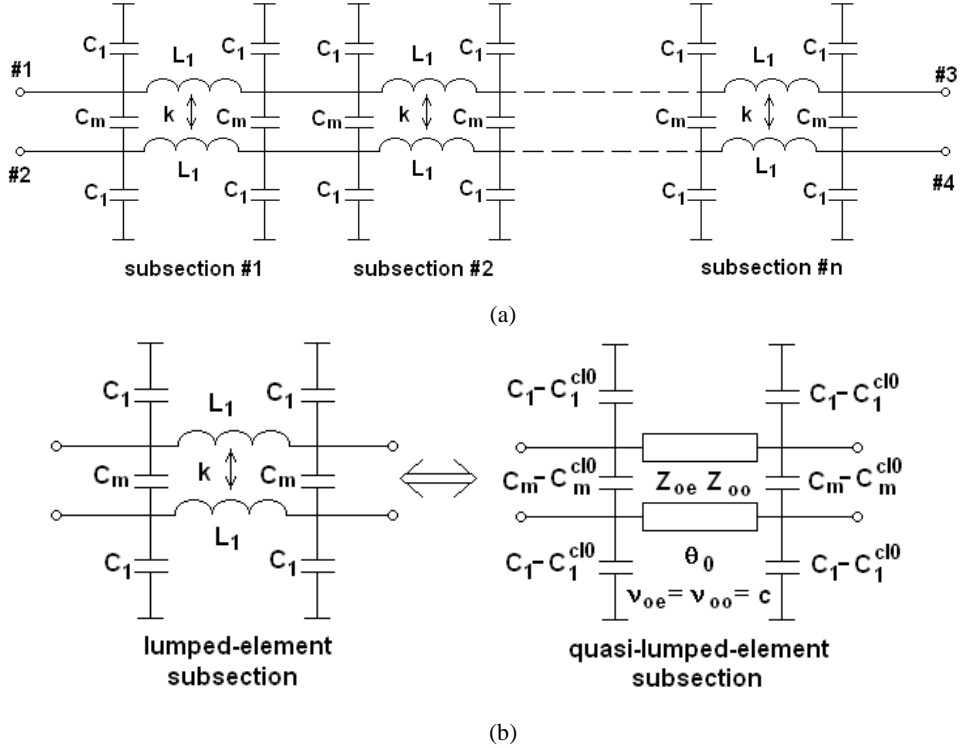


**Fig. 5.7.** Generic schematic of a lumped-element coupled-line directional coupler divided into  $n$  subsections (a) and a quasi-lumped realization of a subsection with the use of the symmetrical coupled-line model (b) [166].

The equivalent circuit of the lumped-element directional coupler's subsection can be also represented in a form shown in Fig. 5.7b, where coupled inductors have been replaced by an electrically short section of coupled lines  $\theta_0 \ll 90^\circ$  at  $f_0$ . Having assumed that the velocities of normal propagating modes equal  $v_{oe} = v_{oo} = c$  and the physical length of the coupled-line section equals  $l$  the even and odd mode characteristic impedances of the coupled-line section can be found as

$$Z_{oe} = \frac{c(L_1 + L_m)}{l} \quad (5.18)$$

$$Z_{oo} = \frac{c(L_1 - L_m)}{l} \quad (5.19)$$

where  $L_m = kL_1$ , and the electrical length of the section equals

$$\theta_0 = \frac{2\pi f_0}{c} l \quad (5.20)$$

Application of such an electrically short coupled-line section provides the required coupled inductors but also contributes to the self and mutual capacitances. Therefore, the cor-

recting capacitances  $C_1^{cl0}$  and  $C_m^{cl0}$  need to be subtracted from original values  $C_1$  and  $C_m$ . These values can be expressed as

$$C_1^{cl0} = \frac{l^2}{2c^2(L_1 + L_m)} \quad (5.21)$$

$$C_m^{cl0} = \frac{L_m l^2}{2c^2(L_1^2 - L_m^2)} \quad (5.22)$$

For these calculations an homogeneous air-filled structure is assumed, since the values of self and mutual inductances of coupled lines are invariant with regard to the dielectric properties. Once the geometry of coupled lines is found in homogeneous medium, it is possible to include dielectric properties, which will modify only correcting capacitances. The new values  $C_1^{cl}$  and  $C_m^{cl}$  can be obtained, knowing the even and odd mode phase velocities ( $v_{oe}$  and  $v_{oo}$ ) for the chosen structure

$$C_1^{cl} = \frac{l^2}{2v_{oe}^2(L_1 + L_m)} \quad (5.23)$$

$$C_m^{cl} = \frac{l^2}{4(L_1^2 - L_m^2)} \left( \frac{(L_1 + L_m)}{v_{oo}^2} - \frac{(L_1 - L_m)}{v_{oe}^2} \right) \quad (5.24)$$

The necessary numerical calculations of the required coupled-line section in a chosen dielectric structure can be performed using numerical software, such as the one presented in [38].

The properties of a lumped-element coupled-line coupler have been investigated by the Author with the use of a schematic diagram shown Fig 5.7a [166]. Figure 5.8 presents the normalized frequency characteristics of a directional coupler for which  $n = 4$  and  $k = 0.707$  ( $C = 3$  dB) are chosen. Identical results are obtained, when each subsection from Fig. 5.7a is substituted with an electrically short coupled-line section and lumped capacitors, as shown in Fig. 5.7b. The values of lumped elements and the coupled-line section parameters have been listed in Table 5.2 (for  $k = 0.707$ ,  $n = 4$ ,  $l = 6.6$  mm,  $f_0 = 1$  GHz).

**Table 5.2**

Values of lumped self and mutual capacitances, self inductances, even and odd mode impedances, and electrical length of the coupled-line section and correcting capacitances for the directional coupler shown in Fig. 5.8 for  $k = 0.707$ ,  $n = 4$ ,  $l = 6.6$  mm,  $f_0 = 1$  GHz [166]

parameter	value
$C_1$ [pF]	0.258
$C_m$ [pF]	0.626
$L_1$ [nH]	4.42
$Z_{0e}$ [ $\Omega$ ]	342.5
$Z_{0o}$ [ $\Omega$ ]	58.79
$\theta_0$ [deg]	7.93
$C_1^{cl0}$ [pF]	0.0321
$C_m^{cl0}$ [pF]	0.0776

Such an approach allows for realization of directional couplers having properties of distributed coupled-line couplers in a wide frequency range. However, the properties of the directional coupler designed with the use of quasi-lumped elements depend on the chosen number of subsections  $n$ , and the higher number of subsections the better approximation of the distributed circuit. It is then worth investigating the influence of the chosen number of subsections  $n$  on the coupler's properties. Figure 5.9 and Fig. 5.10 show respectively, the calculated return losses and isolation of the coupler, in which the number of subsections changes from 1 to 5. The properties of the coupler are very poor for  $n = 1$  but improve rapidly for larger  $n$ . Therefore, broadband operation is ensured by the choice of  $n$  for which return losses and isolation of the directional coupler are acceptable in a wide frequency range (i.e. 0 to  $2f_0$ ). For  $n$  as low as 3 the return losses and isolation of the 3-dB coupler are better than 25 dB, which is sufficient for typical applications. The isolation and return losses can be slightly improved when the  $C_m$  and  $C_1$  parameters are tuned from the theoretical values.

The miniaturization with the use of the presented technique is efficient only, when a dielectric structure is appropriately chosen, so that it is possible to realize a coupled-line section having the inductive coupling  $k_L$  equal to the chosen nominal coupling  $k$  (C in dB) and having the characteristic impedance  $Z_0$  given by (2.41) much higher than  $Z_0$  of the resulting coupler. In practical application the limitations on the coupler's miniaturization come from the minimum thickness of the dielectric layer and the minimum width of the realizable strip. To ensure significant miniaturization of the quasi-lumped coupled-line couplers it is required to select a dielectric structure and technology having:

- large layer thickness ratio, i.e. the thickness of the dielectric layer on which the traces of coupled lines are placed needs to be much smaller than the ground-plane separating layer(s),
- possibility of realization of narrow metallization strips.

To verify experimentally the presented theoretical investigation a single-section 3-dB directional coupler with the coupling imbalance of  $\delta C = \pm 0.6$  dB has been considered [166], and designed having  $n = 4$  and  $f_0 = 1.2$  GHz. Theoretical frequency characteristics of the ideal lumped-element coupler are shown in Fig. 5.11. For further electromagnetic analysis a dielectric structure shown in Fig. 5.12 has been assumed. The structure consists of a thin  $h = 25$   $\mu\text{m}$  laminate layer ( $\epsilon_r = 3.38$ ) on which elements of the coupler are etched.

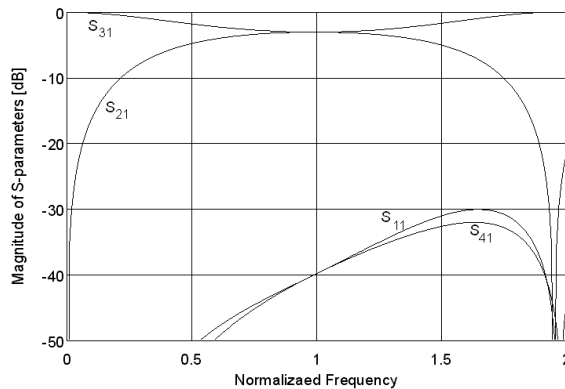


**Fig. 5.8.** Frequency characteristics of the 3-dB directional coupler analyzed using the schematic shown in Fig. 5.7a for which  $n = 4$  [166].

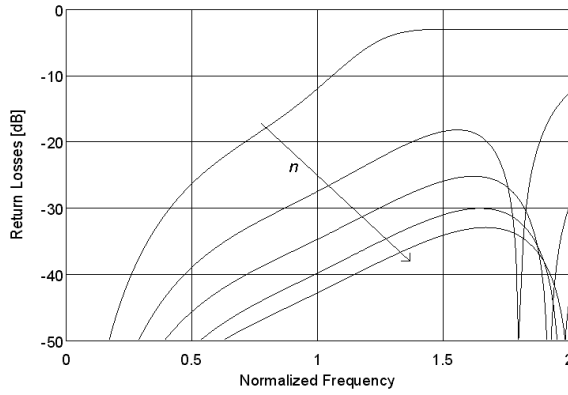


**Fig. 5.9.** Return losses of the 3-dB directional coupler analyzed using the schematic shown in Fig. 5.7a for  $n = 1, 2, 3, 4$  and 5 [166].

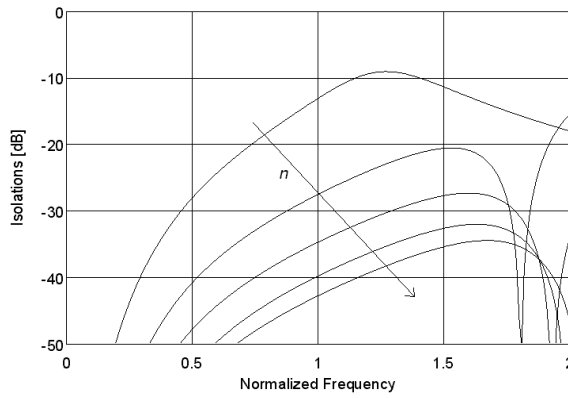


**Fig. 5.10.** Isolation of the 3-dB directional coupler analyzed using the schematic shown in Fig. 5.7a for  $n = 1, 2, 3, 4$  and 5 [166].

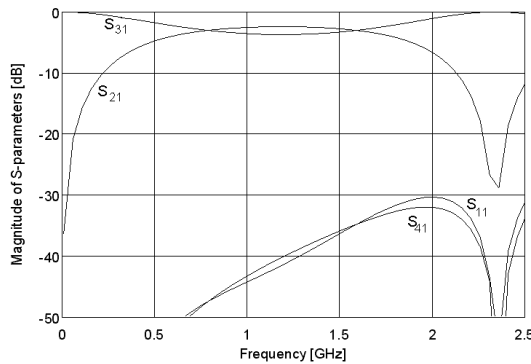


**Fig. 5.11.** Frequency characteristics of the  $3 \pm 0.6$  dB directional coupler analyzed using the schematic shown in Fig. 5.7a for which  $n = 4$  [166].

In order to maximally miniaturize the circuit, the coupled strips' width has been chosen as narrow as possible  $w = 0.09$  mm (technological limitations) to obtain the highest self-inductance per unit length, which gives the shortest length  $l$  of the coupled lines. The dielectric thickness has been chosen to obtain coupling  $k$  per unit length greater than desired. The strip offset was tuned in a way to achieve appropriate coupling. Fig. 5.13 shows the layout of the designed coupler, in which all elements are clearly marked. The electromagnetically calculated frequency response of the designed coupler is shown in Fig. 5.14, whereas, the measured results of the manufactured coupler are presented in Fig. 5.15, Fig. 5.16 and Fig. 5.17. The obtained return losses of the designed coupler are better than 30 dB and isolation is better than 20 dB in a wide frequency range. The measured phase characteristic differs from the theoretical value of  $90^\circ$  by less than  $7^\circ$ , and the dissipation losses are about 0.25 dB measured at the center frequency. Figure 5.18 presents a picture of the etched structure of the quasi-lumped directional coupler.

A very important advantage of the design of quasi-lumped couple-line directional couplers is that the condition of ideal coupler realization – i.e. equalization of inductive and capacitive coupling coefficients – can always be fulfilled! Since the capacitive and inductive elements are independently designed, arbitrary dielectric structure can be chosen. This is opposite to the solutions presented in, e.g. [60, 65, 167], where a special care has had to be taken while choosing the dielectric structure together with coupled-line geometry, in order to achieve good properties of the directional coupler.

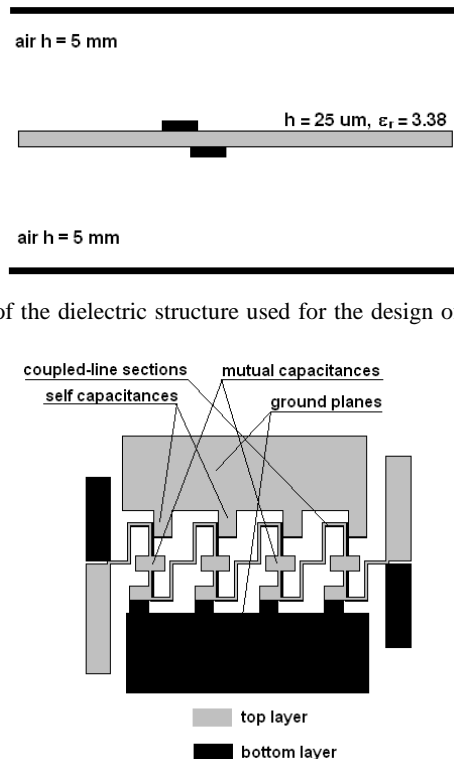


**Fig. 5.12.** Cross-section of the dielectric structure used for the design of quasi-lumped coupled-line directional couplers [166].

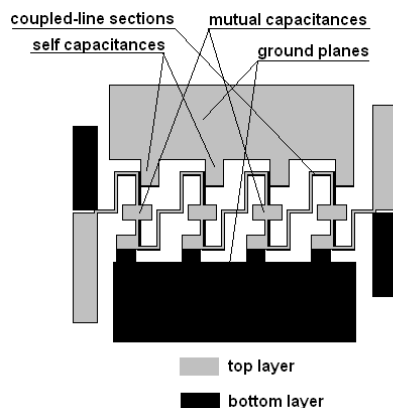


**Fig. 5.13.** Layout of the designed single-section 3-dB directional coupler, the structure of which has been divided into  $n = 4$  subsections [166].

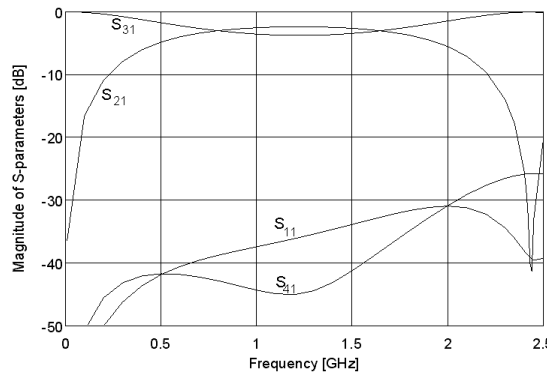


**Fig. 5.14.** Frequency characteristics of the designed  $3 \pm 0.6$  dB directional coupler. Results of electromagnetic analysis [166].

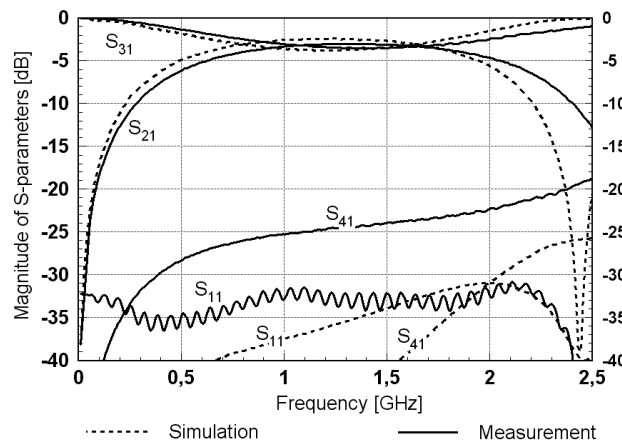


**Fig. 5.15.** Frequency characteristics of the designed  $3 \pm 0.6$  dB directional coupler [166].

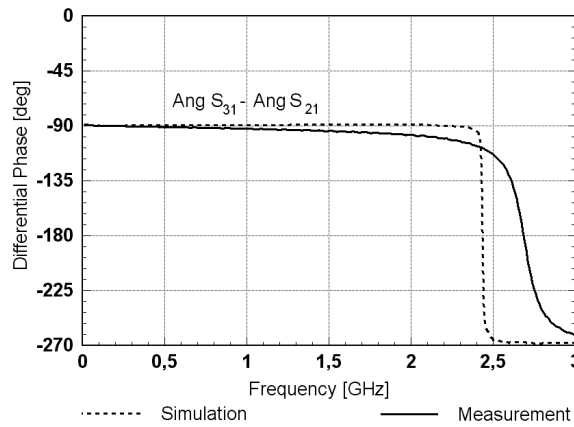


**Fig. 5.16.** Differential phase characteristics of the designed  $3 \pm 0.6$  dB directional coupler [166].

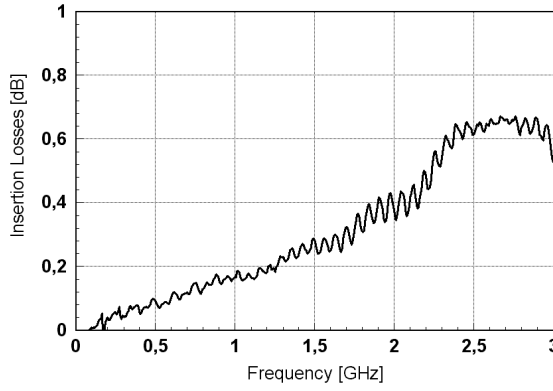


**Fig. 5.17.** Measured dissipation losses of the designed  $3 \pm 0.6$  dB directional coupler [166].

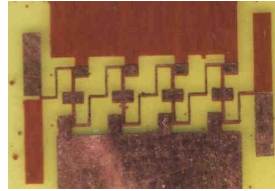


**Fig. 5.18.** Photograph of the thin laminate on which the traces of the designed coupler are etched [166].

The presented procedure has also been verified by the design of a 2.9-dB directional coupler for application in LTCC technology and having the center frequency  $f_0 = 1$  GHz. The design rules offered by Murata have been assumed, being the most attractive, since the minimum layer thickness equals  $12.5\text{ }\mu\text{m}$  (see Table 5.1). The traces were assumed on both sides of the thin  $h = 12.5\text{ }\mu\text{m}$  layer separated from a ground plane by a thick layer  $h = 0.912\text{ mm}$ . The dielectric constant of the green tape is equal  $\epsilon_r = 7.7$ . Assuming  $n = 7$  the following values of inductance and capacitance matrices have been found from (5.11 – 5.14):

$$L' = \begin{bmatrix} 239 & 171.1 \\ 171.1 & 239 \end{bmatrix} [\text{nH/m}], C' = \begin{bmatrix} 95.6 & -68.5 \\ 68.5 & 95.6 \end{bmatrix} [\text{pF/m}],$$

and the values of lumped elements found from (5.15 – 5.17) are  $L_1 = 9.55\text{ nH}$ ,  $L_m = 1.83\text{ nH}$ ,  $C_1 = 0.14\text{ pF}$ ,  $C_m = 0.36\text{ pF}$ . In the next step the inductance and capacitance matrices (denoted as  $L^s$  and  $C^s$ , see Fig. 5.19) of the coupled lines have been found. The coupled lines have been designed to have the minimum realizable width and the needed inductive coupling coefficient  $k = 0.716$ . The following values have been found using [38] for trace width  $w = 100\text{ }\mu\text{m}$  and  $offset = 100\text{ }\mu\text{m}$ :

$$L^s = \begin{bmatrix} 825.8 & 591.4 \\ 591.4 & 825.8 \end{bmatrix} [\text{nH/m}], C^s = \begin{bmatrix} 146.1 & -102.8 \\ -102.8 & 138 \end{bmatrix} [\text{pF/m}],$$

Since the coupled lines in the chosen geometry are asymmetrical, therefore, the resulting values  $L_{11}^s$  is not equal  $L_{22}^s$ , and it is desired to equalize the self inductances, which can be

done by a slight change of the width of one of the lines. This has little practical meaning since in the presented example a change of 1  $\mu\text{m}$  provides for such an equalization. Having found the  $L^s$  matrix values, the length of an electrically short coupled-line subsection can be found as:

$$l = \frac{L_1}{L_{11}^s} \quad (5.25)$$

and is equal to 3.09 mm. Such a section realizes coupled inductors and also contributes to the self and mutual capacitances, therefore, the final capacitances from Fig. 5.19 are found as:

$$C_1^f = C_1 - l(C_{11}^s - C_m^s) \quad (5.26)$$

$$C_2^f = C_1 - l(C_{22}^s - C_m^s) \quad (5.27)$$

$$C_m^f = C_m - lC_m^s \quad (5.28)$$

It is important to note that in this case lumped capacitances connected to both lines have different values, due to the asymmetry of the chosen structure. In the presented example these values are equal:  $C_1^f = 0.078 \text{ pF}$ ,  $C_2^f = 0.09 \text{ pF}$ ,  $C_m^f = 0.2 \text{ pF}$ .

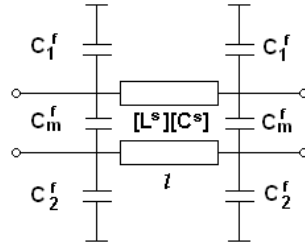


**Fig. 5.19.** Generic schematic of a quasi-lumped coupled-line subsection for asymmetric coupled-line geometry.

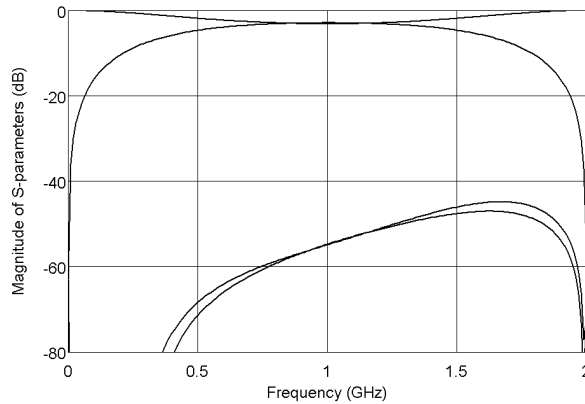


**Fig. 5.20.** Frequency characteristics of the 2.9-dB directional coupler designed using the schematic shown in Fig. 5.7a for which  $n = 7$ .

The calculated theoretical frequency response of the coupler consisting of seven sections shown in Fig. 5.19, are shown in Fig. 5.20, whereas, the results of electromagnetic calculations of the 2.9-dB directional coupler designed for realization in LTCC technology are shown in Fig. 5.21. The designed directional coupler features good electrical properties within a wide frequency range. Figure 5.22 presents a 3-D view of the designed coupler.

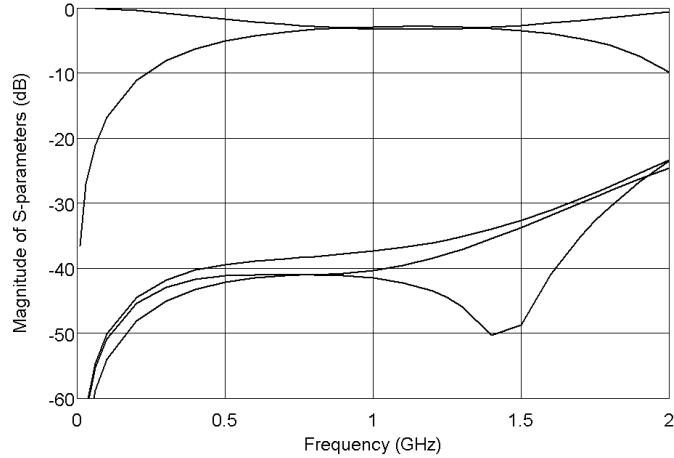


**Fig. 5.21.** Frequency characteristics of the 2.9-dB directional coupler designed for realization in LTCC technology. Results of electromagnetic analysis.

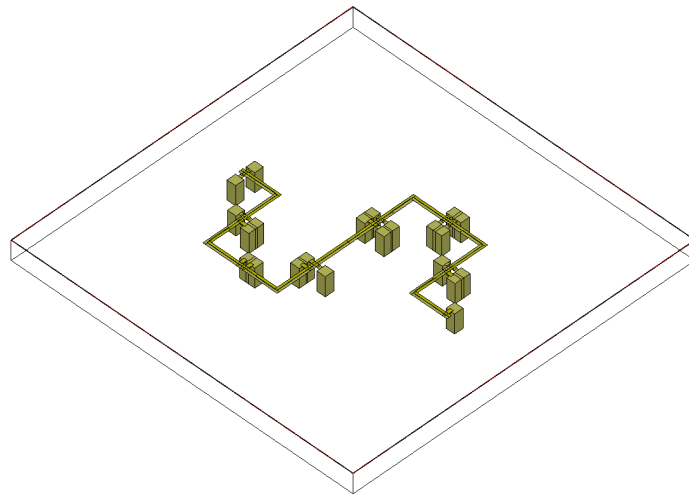


**Fig. 5.22.** A 3-D view of the 2.9-dB coupled-line directional coupler designed for realization in LTCC technology.

The presented miniaturization method can also be applied for realization of directional couplers having frequency response of multisection coupled-line directional couplers presented in section 2.2.2. In this case each section of a multisection directional coupler is

independently designed with the use of the described method. The coupling coefficients  $k$  for each coupled-line section can be taken directly from [29] or [137]. In [166] the Author has shown the design of a two-section asymmetric directional coupler for which a center frequency  $f_0 = 1.4$  GHz, the coupling imbalance of  $\delta C = \pm 0.5$  dB and the number of subsections for each section of the coupler  $n = 3$  have been assumed. The theoretical characteristics of the coupler are presented in Fig. 5.23 and are in agreement with the ones obtained using distributed coupled-line sections regarding the transmission and coupling. The performed analysis of the coupler reveals that the frequency characteristics of the distributed multisection directional coupler differs from the characteristics of the lumped-element multisection directional coupler in a sense that zero-coupling<sup>1</sup> frequency of the former is lower. Further analysis has shown, that the difference depends on the number of applied subsections  $n$ . The larger  $n$  the smaller difference in zero-coupling frequency. For the case of  $n = 2, 3, 4, 5$  the zero-coupling frequency is reduced by the factor of 0.9, 0.955, 0.975, 0.985, respectively.

The two-section 3-dB directional coupler has been designed in the dielectric structure shown in Fig. 5.12. Layout of the designed coupler is presented in Fig. 5.24, in which weakly and strongly coupled sections are indicated. The measured results of the manufactured coupler are presented in Fig. 5.25. The coupling – transmission imbalance of the coupler differs from the theoretical one, since no equal-ripple character is obtained. This can be caused by the manufacturing inaccuracy. To illustrate the influence of manufacturing accuracy on the directional coupler frequency characteristics, a sensitivity analysis has been performed, the results of which are shown in Fig. 5.26 [166]. For the purpose of analysis, the ideal lumped-element directional coupler - shown in Fig. 5.23 - has been assumed with its lumped-element values having normal distribution and deviation equal 2%<sup>2</sup>.

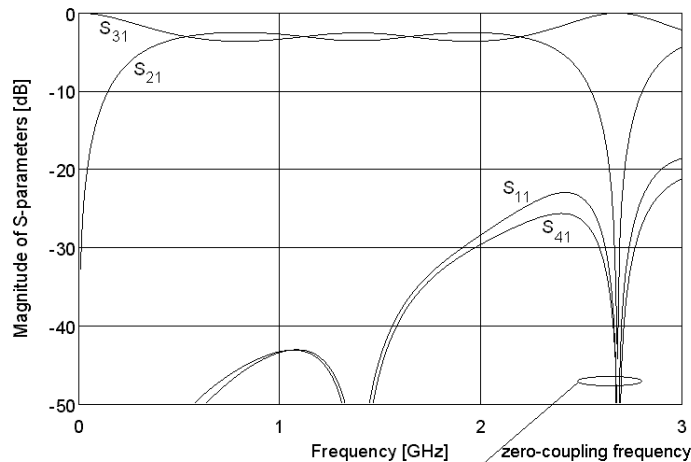


**Fig. 5.23.** Frequency characteristics of a two-section asymmetric  $3 \pm 0.5$  dB directional coupler analyzed using the schematic shown in Fig. 5.7a, in which each of the two sections has been divided into  $n = 3$  subsections [166].

<sup>1</sup> Zero-coupling frequency – the frequency for which coupling equals 0 and transmission equals 1, which corresponds to the frequency at which the electrical length of each section is equal  $180^\circ$  - see Fig. 5.23.

<sup>2</sup> The value has been evaluated based on the manufacturing accuracy equal  $\pm 10\mu\text{m}$  and actual dimensions of the manufactured coupler.

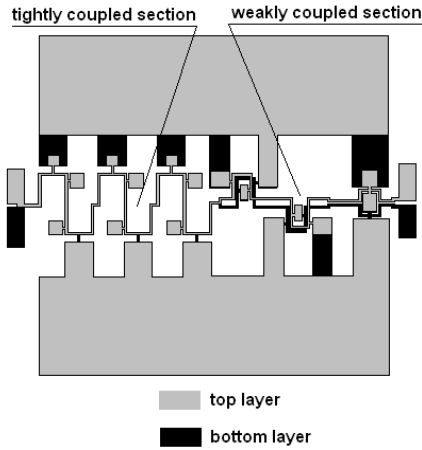


**Fig. 5.24.** Layout of the designed two-section asymmetric  $3 \pm 0.5$  dB directional coupler in which each of the two sections has been divided into  $n = 3$  subsections [166].

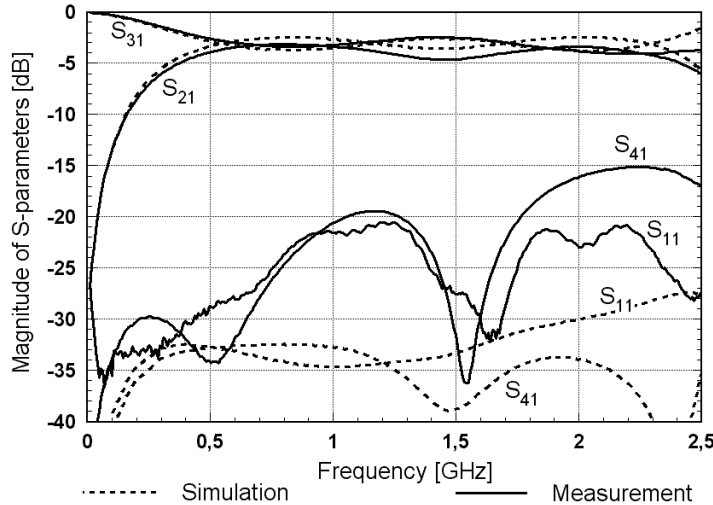


**Fig. 5.25.** Frequency characteristics of the designed two-section asymmetric  $3 \pm 0.5$  dB directional coupler [166].

The measured return losses of the manufactured coupler are better than 20 dB and isolation is better than 15 dB within the frequency range of 0.5 – 2.5 GHz. The phase characteristic in comparison to the theoretical one is shown in Fig. 5.27 and is in a close agreement. Figure 18 shows the measured dissipation losses, which do not exceed 0.4 dB at the center frequency.

It is important to underline that the conditions of ideal coupler realization in case of multisection couplers are even more difficult to be fulfilled in a classic distributed-coupled-line coupler design [167], whereas, they are easily obtained using the presented technique, which is its main advantage next to the possibility of miniaturization [166].

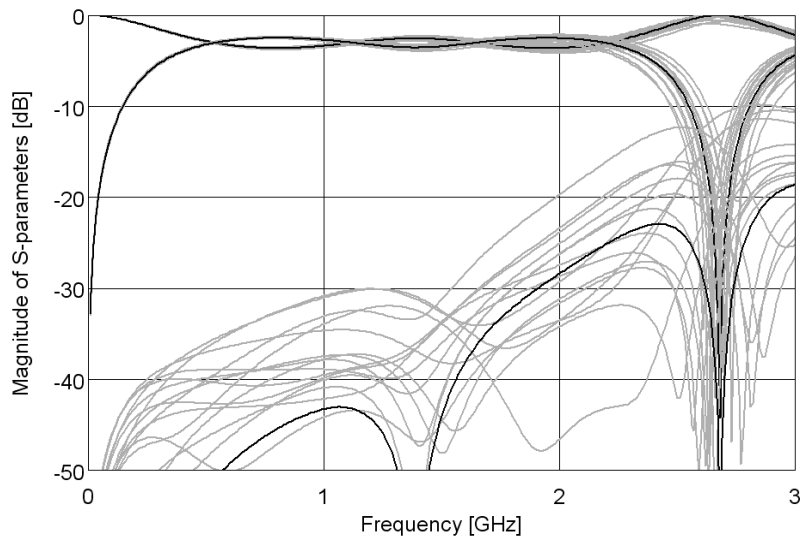


**Fig. 5.26.** Results of sensitivity analysis of transmission, coupling and isolation characteristics of the two-section asymmetric  $3 \pm 0.5$  dB directional coupler shown in Fig. 5.23, in which each of the lumped capacitors' and inductors' values has been assumed to have normal distribution and deviation equal 2% [166].

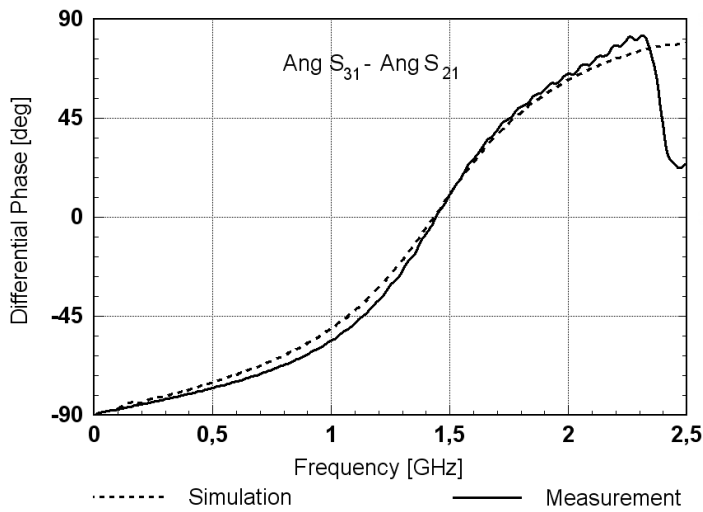


**Fig. 5.27.** Differential phase characteristics of the designed two-section asymmetric  $3 \pm 0.5$  dB directional coupler [166].

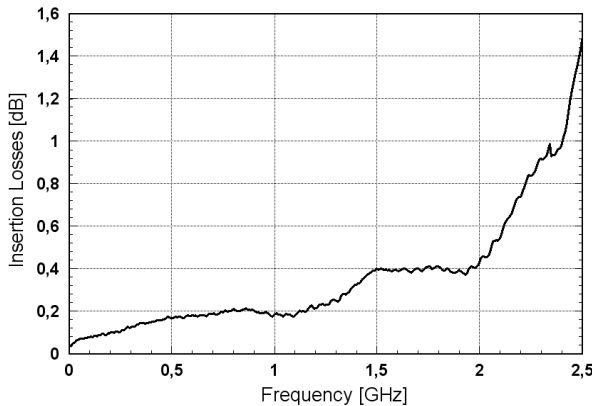


**Fig. 5.28.** Measured dissipation losses of the designed two-section asymmetric  $3 \pm 0.5$  dB directional coupler [166].

### 5.3. Summary

The chapter presents an overview of the known methods of miniaturization of microwave passive components with the use of lumped elements, followed by the Author's investigation on the application of the quasi-lumped technique to the design of broadband directional couplers [166]. The influence of the number of subsections used in a lumped-element equivalent circuit on the couplers' frequency characteristics is shown. The procedure for calculation of capacitors and inductors for arbitrary value of coupling and arbitrary number of subsections has been derived for both symmetric and asymmetric coupled-line structures. The presented analysis has shown that as little as three subsections are sufficient for realization of directional couplers having frequency characteristic comparable with the characteristics of the corresponding distributed-element directional couplers in a wide frequency range.

There are three main advantages of the presented technique, namely:

1. Possibility of miniaturization – the presented technique allows for achieving further miniaturization of already compact coupled-line directional couplers, with no or little performance degradation over a broad frequency range.
2. Possibility of designing directional couplers in commercially available MMIC or LTCC techniques.
3. Finally – which is an important advantage – the possibility of designing coupled-line directional couplers in an arbitrarily chosen dielectric structure. In the designed couplers the conditions of ideal coupled-line coupler realization can be easily fulfilled, and therefore, it is possible to achieve good isolation and good return losses in a wide frequency range.

The presented theoretical analysis have been verified by the design and measurements of the single-section 3-dB and the two-section asymmetric 3-dB directional couplers. Furthermore the design of a single section 3-dB directional coupler suitable for realization in LTCC technology has been shown. The presented designs validate the possibility of realization of wideband coupled-line directional couplers using the quasi-lumped element technique.

## 6. Final remarks

The design of microwave networks has been comprehensively investigated with the emphasis on the three aspects:

1. The design of balanced and  $N$ -way power amplifiers with the use of asymmetric impedance transforming directional couplers.
2. The design of broadband Butler matrices, in which multisection coupled-line directional couplers are utilized.
3. The design of miniaturized directional couplers with the use of quasi-lumped elements having the properties of coupled-line directional couplers.

The research results regarding the design of balanced circuits, in which coupled-line directional couplers are applied have been presented, and reveal that such couplers can be used for simultaneous power split and impedance transformation in a sense that impedances terminating coupled and direct ports are equal and are different than the source impedance terminating the excitation port. Moreover, it has been shown that such couplers posses the properties of an ideal directional coupler at the center frequency, i.e. the isolation and return losses are ideal. The research has shown that a general limitation on impedance transformation in such couplers exists and is equal to the inverse square of the coupling coefficient of the coupled lines. The proposed method has been experimentally tested by the design of the 4-way power amplifier operating in L-band. The obtained measurement results of the manufactured model fully confirmed the usefulness of the proposed method. It was also shown that, for the case of impedance transforming directional couplers, having maximum impedance transforming ratio, it is possible to substitute the coupled-line section with the appropriate connection of two uncoupled lines, which simplifies the design procedure. The presented approach has been comprehensively theoretically investigated, and a practical solution has been proposed, in which the directional couplers is composed of coaxial and microstrip transmission lines. It is important to note that the difference in electrical length of the lines can degrade the couplers parameters, but since the lines are uncoupled it is possible to equalize the electrical length by varying the physical length between the two lines, which leads to the ideal coupler response. Also a method of load-pull and source-pull measurement for evaluation of input and output impedances of power transistors at microwave frequency has been outlined, in which, rat race couplers are used as the input and output matching networks.

Furthermore, the design of broadband Butler matrices has been comprehensively investigated. Initially, the designs of  $4 \times 4$  Butler matrices with the use of single-section coupled-line 3-dB directional couplers have been presented, followed by the design of an  $8 \times 8$  Butler matrix. A new arrangement of the  $8 \times 8$  Butler matrix has been shown, in which the

crossovers of transmission lines being a tandem connection of two 3-dB directional couplers and transmission-line sections provide the needed phase shifts. Moreover, two 0-dB couplers have been used to eliminate the needed two transmission-line crossovers allowing for fully integrated and planar realization. The proposed arrangement of an 8 x 8 Butler matrix has been experimentally tested and the obtained results are in full agreement with the theoretical ones. Further research has shown that the concept used for the design of Butler matrices utilizing single-section coupled-line directional couplers can be extended on Butler matrices designed with the use of multisection symmetrical directional couplers. For such networks, however, phase shift networks consisting of coupled-line ‘C’-sections need to be introduced, in order to achieve small imbalance of differential phase characteristics of the entire matrix. The proposed concept has been successfully verified by the design of 4 x 4 and 8 x 8 Butler matrices utilizing three-section and five-section symmetrical directional couplers in conjunction with single- and two-section coupled-line phase compensating networks. The proposed design method of Butler matrices allows for manufacturing compact networks operating in a very broad frequency range, e.g. the presented 8 x 8 Butler matrix operates in 1.8 – 12 GHz frequency range.

Finally, the possibility of directional couplers’ miniaturization has been investigated. It was shown that by application of a quasi-lumped element technique, it is possible to significantly reduce the directional couplers’ dimensions. The proposed method allows for obtaining the properties of miniaturized directional couplers similar to the corresponding coupled-line couplers, i.e. good return losses and isolation in a wide frequency range. It was shown, that such an approach allows one to design not only a single-section directional couplers, but also broadband multisection directional couplers operating in a wide frequency range. The proposed method has been verified by the design of single and two-section directional couplers. Also, the possibility of application of the developed design procedure in the modern LTCC technology has been shown, by an exemplary design of a compact 3-dB directional coupler.

The large extend of Author’s research results presented in a number of journal and conferences papers has been cited within the content of the text [59, 60, 61, 68, 164, 166, 168, 179].

## References

- [1] Abbasi M., Zirtah H., Angelov I.: Q-, V-, and W-band power amplifiers utilizing coupled lines for impedance matching, in Proc. *IEEE MTT-S Int. Microwave Symp. Dig.*, 2008, pp. 863-866.
- [2] Ali F., Podell A.: A wide-band GaAs monolithic spiral quadrature hybrid and its circuit applications, *IEEE Journal of Solid-State Circuits*, vol. 26, no. 10, pp. 1394-1398, Oct. 1991.
- [3] Ali F., Podell A.: Design and applications of a 3:1 bandwidth GaAs Monolithic spiral quadrature hybrid, *12th Annual Symposium on GaAs Integrated Circuits*, 1990, pp. 279-282.
- [4] Allen J.: A theoretical limitations on the formation of lossless multiple beams in linear arrays, *IRE Trans. Antennas and Propagation*, vol. 9, no. 4, pp. 350-352, July 1961.
- [5] Ang K.S., Lee Ch.H., Leong Y.Ch.: Analysis and design of coupled line impedance transformers, in Proc. *IEEE MTT-S Int. Microwave Symp. Dig.*, 2004, pp. 1951-1954.
- [6] Angelucci A., Audagnotto P., Corda P., Obino P., Piarulli F., Piovano B.: High performance microstrip networks for multibeam and reconfigurable operation in mobile-radio systems, *IEEE Global Telecommunications Conference*, vol. 3, pp. 1717-1721, Nov. 1994.
- [7] Angelucci A., Audagnotto P., Corda P., Piovano B.: Multiport power amplifiers for mobile-radio systems using microstrip Butler matrices, in Proc. *Antennas and Propagation International Symposium Digest*, vol. 1, June 1994, pp. 628-631.
- [8] Avitabile G., Chellini B.: A compact 90° hybrid for MMIC applications, *Microwave and Optical Technology Letters*, vol. 29, no. 6, pp. 392-394, June 2001.
- [9] Blass J.: Multidirectional antenna – a new approach to stacked beams, *IRE International Convention Record*, vol. 8, Part 1, pp. 48-50, March 1960.
- [10] Bona M., Manholm L., Starski J.P.: Low-loss compact Butler matrix for a microstrip antenna, *IEEE Trans. Microwave Theory and Tech.*, vol. 50, pp. 2069-2075, Sept. 2002.

- [11] Golonka L.: *Zastosowanie ceramiki LTCC w mikroelektronice*, (in Polish), *Oficyna Wydawnicza Politechniki Wrocławskiej*, Wrocław 2001.
- [12] Butler J., Lowe R.: Beam-forming matrix simplifies design of electronically scanned antennas, *Electron. Des.*, vol. 9, pp. 170-173, April 1961.
- [13] Caldwell F., Kenney J.S., Ingram M.A.: Design and implementation of a switched-beam smart antenna for an 802.11b wireless access point, *IEEE Radio and Wireless Conference*, pp. 55-58, 2002.
- [14] Carlin H.: The scattering matrix in network theory, *IRE Transactions on Circuit Theory*, vol. 3, no. 2, pp. 88-97, June 1956.
- [15] Caulton M., Hershenov B., Knight S., DeBrecht R.: Status of lumped elements in microwave integrated circuits – present and future, Invited paper, *IEEE Trans. Microwave Theory and Tech.*, vol. 19, no. 7, pp. 588-599, July 1971.
- [16] Caulton M., Hershenov B., Knight S.P., DeBrecht R.E.: Status of lumped-elements in microwave integrated circuits – present and future, *IEEE Trans. Microwave Theory and Tech.*, vol. MTT-19, no. 7, pp. 588-599, July 1971.
- [17] Cetinoneri B., Atesal Y.A., Rebeiz G.M., An 8 x 8 Butler matrix in 0.13 $\mu$ m CMOS for 5-6-GHz multibeam applications, *IEEE Trans. Microwave Theory and Tech.*, vol. 59, no. 2, pp. 295-301, Feb. 2011.
- [18] Chang D.Ch., Jou S.H.: The study of Butler matrix BFN for four beams antenna systems, *IEEE AP International Symposium Dig.*, vol. 4, pp. 176-179, June 2003.
- [19] Chiang Y.Ch., Chen Ch.Y.: Design of a wide-band lumped-element 3-dB quadrature coupler, *IEEE Trans. Microwave Theory and Tech.*, vol. 49, no. 3, pp. 476-479, March 2001.
- [20] Chiou Y.Ch., Kuo J.T., Chan Ch.H.: New miniaturized dual-band rat-race coupler with microwave C-sections, in Proc. *IEEE MTT-S Int. Microw. Symp. Dig.*, 2009, pp. 701 – 704.
- [21] Chow P.E.K., Davies D.E.N.: Wide bandwidth Butler matrix network, *Electronics Letters*, vol. 3, no. 6, pp. 252-253, June 1967.
- [22] Chramiec J., Kitlinski M., Design of quarter-wave compact impedance transformers using coupled transmission lines, *Electronics Letters*, vol. 38, no. 25, pp. 1683-1685, Dec. 2002.
- [23] Chuang M.L.: Miniaturized ring coupler of arbitrary reduced size, *IEEE Microwave and Wireless Components Letters*, vol. 15, no. 1, pp. 16-18, Jan. 2005.
- [24] Cohn S.: The re-entrant cross section and wide-band 3-dB hybrid couplers, *IEEE Trans. Microwave Theory and Tech.*, vol. MTT-11, no. 4, pp. 254-258, July 1963.

- [25] Cohn S.B.: Optimum design of stepped transmission-line transformers, *IRE Trans. Microwave Theory and Tech.*, vol. MTT-3, no. 3, pp. 16–20, April 1955.
- [26] Collado C., De Flavis F.: Dual-band Butler matrix for WLAN systems, *IEEE MTT-S International Symposium Dig.*, pp. 4-7, June 2005.
- [27] Collin R.E.: Foundations for microwave engineering, New York: *John Wiley & Sons Inc.*, 2001, ch. 6.
- [28] Collin R.E.: Theory and design of wide-band multisection quarter-wave transformers, *IRE Trans. Microwave Theory and Tech.*, vol. MTT-3, no. 2, pp. 179–185, Feb. 1955.
- [29] Cristal E.G., Young L.: Theory and tables of optimum symmetrical TEM-mode coupled-transmission-line directional couplers, *IEEE Trans. Microwave Theory and Tech.*, vol. MTT-13, pp. 544-558, Sept. 1965.
- [30] Cristal E.G.: Coupled-transmission-line directional couplers with coupled lines of unequal characteristic impedances, *IEEE Trans. Microwave Theory and Tech.*, vol. MTT-14, no. 7, pp. 337-346, July 1966.
- [31] Cristal E.G.: Re-entrant directional couplers having direct coupled center conductors, *IEEE Trans. Microwave Theory and Tech.*, vol. MTT-14, no. 4, pp. 207–208, April 1966.
- [32] Cusack, J.M., Perlow, S.M., Perlman, B.S.: Automatic load contour mapping for microwave power transistors, *IEEE Trans. Microwave Theory and Tech.*, vol. MTT-22, Dec. 1974, pp. 1146-1152.
- [33] Dall’Omo C., Monediere T., Jecko B., Lamour F., Wolk I., Elkael M.: Design and realization of a 4 x 4 microstrip Butler matrix without any crossing in millimeter waves, *Microwave and Optical Technology Letters*, vol. 38, no. 6, pp. 462-465, Sept. 2003.
- [34] Davis R.S., Schrank H.E.: Applications of the Butler matrix to high-power multichannel switching, *G-MTT Symposium Dig.*, vol. 65, no. 1, pp. 133-138, May 1965.
- [35] De Lillo R.A.: A high performance 8-input, 8-output Butler matrix beamforming network for ultra-broadband applications, in Proc. *IEEE Antennas and Propagation International Symposium Digest*, vol. 1, June 1993, pp. 474-477.
- [36] Denidni T.A., Libar T.E.: Wide band four-port Butler matrix for switched multibeam antenna arrays, *IEEE Proceedings on Personal, Indoor and Mobile Radio Communications*, vol. 3, pp. 2461-2464, Sept. 2003.
- [37] Derneryd A., Johannisson B.: Adaptive base-station antenna arrays, *Ericsson Review*, no. 3, pp. 132-137, 1999.
- [38] Djordjevic A., Harrington R.F., et al.: Matrix parameters for multiconductor transmission lines, Software and User’s Manual, *Artech House*, 1990.

- [39] Dobrowolski J.A.: Technika wielkich częstotliwości (in Polish), *Oficyna Wydawnicza Politechniki Warszawskiej*, Warszawa 2001.
- [40] DuHamel R.H., Armstrong M.E.: The tapered-line magic-T, a wide-band monopulse antenna, *Abstracts of the 15th Annual Symposium on the USAF Antenna R&D Program*, Monticello, Illinois, October 12 – 14, 1965.
- [41] Dydyk M.: Microstrip directional couplers with ideal performance via single-element compensation, *IEEE Trans. Microwave Theory and Tech.*, vol. 47, no. 6, pp. 956-964, June 1999.
- [42] Ellinger F., Vogt R., Bachtold W.: Compact reflective-type phase-shifter MMIC for C-band using a lumped-element coupler, *IEEE Trans. Microwave Theory and Tech.*, vol. 49, no. 5, pp. 913-917, May 2001.
- [43] Emery T., Chin Y., Lee H., Tripathi V.K.: Analysis and design of ideal non symmetrical coupled microstrip directional couplers, in Proc. *IEEE MTT-S Int. Microwave Symp. Dig.*, 1989, pp. 329-332.
- [44] Foti S.J., Macnamara T.: Design of wideband Butler matrices using Schiffman lines, *IEE Colloquium on Multiple Beam Antennas and Beamformers*, pp. 5/1-5/8, Nov. 1989.
- [45] Fragola A., Orefice M., Pirola M.: A modified Butler matrix for taper excitation of scanned arrays, *IEEE AP International Symposium Dig.*, vol. 4, pp. 784-787, July 2001.
- [46] Franti L.F., Paganuzzi G.M.: Wideband high directivity microstrip couplers for microwave integrated circuits, in Proc. *10th European Microwave Conference*, 1980, pp. 377-381.
- [47] Frye R.C., Kapur S., Melville R.C.: A 2-GHz quadrature hybrid implemented in CMOS technology, *IEEE Journal of Solid-State Circuits*, vol. 38, no. 3, pp. 550-555, March 2003.
- [48] Fu K.K., Lai A.K.Y.: FDTD optimization of beam forming network for multibeam antenna, *IEEE AP International Symposium Dig.*, vol. 4, pp. 2028-2031, June 1998.
- [49] Gao S.C., Li L.W., Leong M.S., Yeo T.S.: Integrated multibeam dual-polarised planar array, *IEE Proc. Microwaves, Antennas and Propagation*, vol. 148, no. 3, pp. 174-178, June 2001.
- [50] Gary Kwang T.K, Gardner P.: 4x4 Butler matrix beam forming network using novel reduced size branchline coupler, in Proc. *31st European Microwave Conference*, London, UK, Sept. 2001, pp. 1-4.
- [51] Gilb J.P.K., Balanis C.A.: Improved performance of microstrip couplers through multi-layer substrate, in Proc. *23rd European Microwave Conference*, 1993, pp. 624-626.
- [52] Grau A., Romeu J., De Flaviis F.: On the diversity gain using a Butler matrix in fading MIMO environments, *IEEE/ACES International Conference on Wireless Communications and Applied Computational Electromagnetics*, pp. 478-481, April 2005.

- [53] Grau A., Romeu J., Jofre L., De Flaviis F.: On the MIMO capacity using a Butler matrix with circular arrays in fading indoor environments, *IEEE AP International Symposium Dig.*, vol. 2A, pp. 297-300, July 2005.
- [54] Gruszczyński S., Laska W., Stolarski Z., Zajdel A.: High-power modular transceiver for radar applications, *Signal Processing Symposium*, Wilga Village, Poland, 2005.
- [55] Gruszczyński S., Sachse K.: A coupled-transmission-line multi-section asymmetric 3 dB directional coupler in conjunction with phase compensation networks as a broad-band 3 dB/0°/180° coupler and a sum-difference circuit, *MMS 2002 Mediterranean Microwave Symposium 2002*, June 2002, Caceres, Spain.
- [56] Gruszczyński S., Sachse K.: Compensated broadband five-section directional coupler for application in Butler matrices” in Proc. *XVIII International Conference on Microwaves, Radar and Wireless Communications MIKON 2010*, Vilnius, Lithuania.
- [57] Gruszczyński S., Sachse K.: Improvements to the design of the asymmetric coupled tapered-stripline directional coupler, in Proc. *11th Microcoll 2003*, Sept. 2003, Budapest, Hungary.
- [58] Gruszczyński S., Sachse K.: Wide-band and dual-band directional filters in a practical realization, *MMS 2002 Mediterranean Microwave Symposium*, June 2002, Caceres, Spain.
- [59] Gruszczyński S., Wincza K., Borgosz J.: Application of a rat-race coupler in low-cost load and source pull transistor amplifier design, *Microwave and Optical Technology Letters*, vol. 51, no. 11, pp. 2537-2541, Nov. 2009.
- [60] Gruszczyński S., Wincza K., Borgosz J.: Multilayer surface-mount 3-dB directional coupler for application in balanced modulators, in Proc. *China-Japan Joint Mircowave Conference*, Shanghai, China, 2008, vol. 2, pp. 547-550.
- [61] Gruszczyński S., Wincza K., Sachse K.: Compact broadband Butler matrix in multilayer technology for integrated multibeam antennas, *Electronics Letters*, vol. 43, no. 11, pp. 635-636, May 2007.
- [62] Gruszczyński S., Wincza K., Sachse K.: Design of a broadband low-loss coupled-line multisection symmetrical 3-dB directional coupler in suspended stripline technology, in Proc. *Asia-Pacific Microwave Conference 2010*, Yokohama, Japan, 2010.
- [63] Gruszczyński S., Wincza K., Sachse K.: Design of compensated coupled-stripline 3-dB directional couplers, phase shifters and magic-Ts Part I: Single section coupled line circuits, *IEEE Transactions on Microwave Theory and Techniques*, vol. 54, no. 11, pp. 3986-3994, Nov. 2006.
- [64] Gruszczyński S., Wincza K., Sachse K.: Design of compensated coupled-stripline 3-dB directional couplers, phase shifters and magic-Ts Part II: Broadband coupled-line circuits, *IEEE Transactions on Microwave Theory and Techniques*, vol. 54, no. 9, pp. 3501-3507, Sep. 2006.

- [65] Gruszczyński S., Wincza K., Sachse K.: Design of high-performance three-strip 3-dB directional coupler in multilayer technology with compensated parasitic reactances, *Microwave and Optical Technology Letters*, vol. 49, no. 7, pp. 1656-1659, July 2007.
- [66] Gruchała H.: Układy mikrofalowe z rozdziałem w częstotliwości (in Polish), *Wojskowa Akademia Techniczna*, Warszawa 1999.
- [67] Gruszczyński S., Wincza K., Sachse K.: Reduced sidelobe four-beam N – element antenna arrays fed by 4 x N Butler matrices, *IEEE Antennas and Wireless Propagation Letters*, vol. 5, no. 1, pp. 430-434, Dec. 2006.
- [68] Gruszczyński S., Wincza K.: Broadband 4x4 Butler matrices as a connection of symmetrical multisection coupled-line 3-dB directional couplers and phase correction networks, *IEEE Transactions on Microwave Theory and Techniques*, vol. 54, no. 1, pp. 1-9, Jan. 2009.
- [69] Gruszczyński S., Wincza K.: Broadband multisection asymmetric 8.34-dB directional coupler with improved directivity, in Proc. *Asia-Pacific Microwave Conference 2007*, Bangkok, Tajlandia, 2007.
- [70] Gruszczyński S., Wincza K.: Design of broadband asymmetric 3-dB tapered-line directional couplers, in Proc. *36th European Microwave Conference*, Manchester 2006.
- [71] Gruszczyński S., Wincza K.: Design of high-performance broadband multisection symmetrical 3-dB directional couplers, *Microwave and Optical Technology Letters*, vol. 50, no.3, pp. 636-638, March 2008.
- [72] Gruszczyński S., Wincza K.: Generalized methods for the design of quasi-ideal symmetric and asymmetric coupled-line sections and directional couplers, accepted for publication in *IEEE Transactions on Microwave Theory and Techniques*.
- [73] Gruszczyński S.: Design of quasi-ideal coupled lines and their applications in high-performance directional couplers, *AGH University of Science and Technology Press*, Krakow 2011.
- [74] Gruszczyński S.: Szerokopasmowe układy magicznego T w technice linii paskowych. Analiza, projektowanie i badania eksperimentalne (in Polish), *Rozprawa Doktorska, Instytut Telekomunikacji, Teleinformatyki i Akustyki PWr.*, Wrocław 2006.
- [75] Gryglewski D., Rosołowski D., Wojtasiak W.: A 250 W 2.45GHz-band solid-state pulsed source, in Proc. *XVII International Conference on Microwaves, Radar and Wireless Communications MIKON 2008*, Wroclaw, Poland, May 2006.
- [76] Gupta R.K., Getsinger W.J.: Quasi-lumped-element 3- and 4-port networks for MIC and MMIC applications, in Proc. *IEEE MTT-S Int. Dig.*, 1984, pp. 409-411.
- [77] Hayashi H., Hitko D.A., Sodini Ch.G.: Four-element planar Butler matrix using half-wavelength open stubs, *IEEE Microwave and Wireless Components Letters*, vol. 12, no. 3, pp. 73-75, March 2002.

- [78] Hogerheiden J., Ciminera M., Jue G.: Improved planar spiral transformer theory applied to a miniature lumped element quadrature hybrid, *IEEE Trans. Microwave Theory and Tech.*, vol. 45, no. 4, pp. 543-545, April 1997.
- [79] Hong W., Lin Ch.W., Lin Y.D., Kitazawa T.: Design of a novel planar Butler matrix beamformer with two-axis beam-switching capability, in Proc. *Asia-Pacific Microwave Conference*, vol. 5, pp. 5-9, Dec. 2005.
- [80] Jaeckle W.: Systematic design of a matrix network used for antenna beam steering, *IEEE Trans. Antennas and Propagation*, vol. 15, no. 2, pp. 314-316, March 1967.
- [81] Jaworski G.: Analiza, projektowanie i badania eksperymentalne wybranych biernych mikrofalowych układów scalonych (in Polish), *Rozprawa Doktorska, Instytut Telekomunikacji i Akustyki PW*, Wrocław 1998.
- [82] Jensen T., Zhurbenko V., Krozer V., Meincke P.: Coupled transmission lines as impedance transformer, *IEEE Trans. Microwave Theory and Tech.*, vol. 55, no. 12, pp. 2957-2965, Dec. 2002.
- [83] Jeong Y.S., Kim T.W.: Design and analysis of swapped port coupler and its application in a miniaturized Butler matrix, *IEEE Trans. Microwave Theory and Tech.*, vol. 58, no. 4, pp. 764-770, April 2010.
- [84] Jones E.M.T., Bolljahn J.T.: Coupled-strip-transmission-line filters and directional couplers, *IRE Trans. Microwave Theory and Tech.*, vol. MTT-4, no. 2, pp. 75-81, April. 1956.
- [85] Jung S.Ch., Negra R., Ghannouchi F.M.: A miniaturized double-stage 3dB broadband branch-line hybrid coupler using distributed capacitors, in Proc. *Asia-Pacific Microwave Conference*, 2009, pp. 1323-1326.
- [86] Kopp B.: Asymmetric lumped element power splitters, in Proc. *IEEE MTT-S Int. Microw. Symp. Dig.*, 1989, pp. 333-336.
- [87] Koubeissi M., Decroze C., Monediere T., Jecko B.: Switched-beam antenna based on novel design of Butler matrices with broadside beam, *Electronics Letters*, vol. 41, no. 20, pp. 1097-1098, Sept. 2005.
- [88] Kuo T.S., Lin Y.S., Wang Ch.H., Chen Ch.H.: A compact LTCC branch-line coupler using modified-T equivalent-circuit model for transmission line, *IEEE Microwave and Wireless Components Letters*, vol. 16, no. 2, pp. 90-92, Feb. 2006.
- [89] Kurokawa K.: Power waves and the scattering matrix, *IEEE Trans. Microwave Theory and Tech.*, vol. MTT-13, no. 2, pp. 194-202, March 1965.
- [90] Lange J.: Interdigitated stripline quadrature hybrid, *IEEE Trans. Microwave Theory and Tech.*, vol. MTT-17, no. 12, pp. 1150-1151, Dec. 1969.

- [91] Lee Y.J., Park J.Y.: Fully embedded lumped LC-quadrature hybrid coupler into organic packaging substrate for power sampling, *Microwave and Optical Technology Letters*, vol. 51, no. 3, pp. 845-848, March 2009.
- [92] Levy R.: General synthesis of asymmetric multi-element coupled-transmission-line directional couplers, *IEEE Trans. Microwave Theory and Tech.*, vol. MTT-11, no. 4, pp. 226-237, July 1963.
- [93] Levy R.: Tables for asymmetric multi-element coupled-transmission-line directional couplers, *IEEE Trans. Microwave Theory Tech.*, vol. 12, no. 3, pp. 275-279, May 1964.
- [94] Li W.R., Chu C.Y., Lin K.H., Chang S.F.: Switched-beam antenna based on modified Butler matrix with low sidelobe level, *Electronics Letters*, vol. 40, no. 5, pp. 290-292, March 2004.
- [95] Lim J.S., Eom S.Y., Han J.H., Kim S.H., Lee D.H., Nam S.: A new balanced amplifier using 6-port power divider, *IEEE AP International Symposium Dig.*, pp. 1301-1304, July 2001.
- [96] Lipsky S.E.: DF antenna arrays, *Microwave Passive Direction Finding*, New York: John Wiley & Sons Inc., 1987, ch. 5.
- [97] Lo Y. T., Lee S. W.: *Antenna Handbook*, New York: Van Nostrand Reinhold, 1988.
- [98] Loskot E., Leppavuori S., Kourbanov A., Vendik I., Lapshin A., Jakku E.: A miniaturized branch-line directional coupler on low temperature cofired ceramic board, in Proc. *31st European Microwave Conference*, 2001, pp. 1-4.
- [99] Ma T.G., Cheng Y.T.: Miniaturized broadside coupler using coupled slow-wave artificial lines, *Electronics Letters*, vol. 45, no. 10, pp. 511-512, May 2009.
- [100] Macnamara T.M.: Positions and magnitudes of fixed phase shifters in Butler matrices incorporating 90 degrees hybrids, *IEE Proceedings – Microwaves, Antennas and Propagation*, vol. 135, no. 5, pp. 359-360, Oct. 1988.
- [101] March S.L.: Phase velocity compensation in parallel-coupled microstrip, *IEEE MTT-S Int. Microwave Symp. Dig.*, 1982, pp. 410-412.
- [102] Matthaei G.L., Young L., Jones E.M.T.: *Microwave filters, impedance-matching networks, and coupling structures*, McGraw Hill, New York 1964.
- [103] Maury Microwave Corporation: Measurements of large signal device input impedance during load pull, *Application note 5C-029*, 06 Nov. 1998 Ontario, California, USA, pp. 1-7.
- [104] Mongia R., Bahl I., Bhartia P.: *RF and microwave coupled-line circuits*, Artech House, Boston 1999.
- [105] Moody H.: The systematic design of the Butler matrix, *IEEE Trans. Antennas and Propagation*, vol. 12, no. 6, pp. 786-788, Nov. 1964.

- [106] Mosca S., Bilotti F., Toscano A., Vegni L.: A novel design method for Blass matrix beam-forming networks, *IEEE Trans. Microwave Theory Tech.*, vol. 50, no. 2, pp. 225-232, Feb. 2002.
- [107] Nagi H.S.: Miniature lumped element 180° Wilkinson divider, in Proc. *IEEE MTT-S Int. Microw. Symp. Dig.*, 2003, pp. 55-58.
- [108] Nawaz M.I., Malik Z.Y., Mueed A., Majeed I.: A novel phase-balance technique for corporate structure power combining of high power amplifiers, *Sixth International Bhurban Conference on Applied Sciences and Technology IBCAST*, 2009, pp. 112-117.
- [109] Nedil M., Denidni T.A., Talbi L.: Design and implementation of a new Butler matrix using slot line technology, *IEEE Radio and Wireless Symposium*, pp. 163-166, Jan. 2006.
- [110] Nedil M., Denidni T.A., Talbi L.: Novel Butler matrix using CPW multilayer technology, *IEEE Trans. Microwave Theory and Tech*, vol. 54, no. 1, pp. 499-507, Jan. 2006.
- [111] Nedil M., Denidni T.A., Talbi L.: Novel Butler matrix using CPW multi-layer technology”, *IEEE AP International Symposium Dig.*, vol. 3A, pp. 299-302, July 2005.
- [112] Oliver B.M.: Directional electromagnetic couplers, *Proceedings of the IRE*, vol. 42, no. 11, pp. 1686-1692, Nov. 1954.
- [113] Parisi S.J.: 180° lumped element hybrid, in Proc. *IEEE MTT-S Int. Microw. Symp. Dig.*, 1989, pp. 1243-1246.
- [114] Park J., Lee Y.: Improved capacitive loading method for miniaturization of 0 dB forward-wave directional couplers, *IEEE Microwave and Wireless Components Letters*, no. 99, 2011.
- [115] Peik S.F., Jolley B., Mansour R.R.: High Temperature Superconductive Butler Matrix Beamformer for Satellite Applications, *IEEE MTT-S Int. Microwave Symp. Dig.*, 1999, pp. 1543-1546.
- [116] Person Ch., Carre L., Rius E., Coupez J.Ph., Toutain S.: Original techniques designing wideband 3D integrated couplers, in Proc. *IEEE MTT-S Int. Microwave Symp. Dig.*, 1998, pp. 119-122.
- [117] Piovano B., Accatino L., Angelucci A., Jones T., Capece P., Votta M.: Design and breadboarding of wideband N x N Butler matrices for multiport amplifiers, *SBMO International Microwave Conference*, vol. 1, pp. 175-180, Aug. 1993.
- [118] Piovano B., Accatino L., Muoio F., Caille G., Mongiardo M.: CAD and mechanical realization of planar Ka-band, 8x8 Butler matrices, in Proc. *32nd European Microwave Conference*, Milan, Italy, Sept. 2002.
- [119] Podcameni A.: Symmetrical and asymmetrical edge-coupled-line impedance transformers with a prescribed insertion loss design, *IEEE Trans. Microwave Theory and Tech.*, vol. MTT-34, pp. 1-7, Jan. 1986.

- [120] Pozar D.: *Microwave engineering*, Third edition, New York, *Wiley & Sons*, 2005.
- [121] Reed J., Wheeler G.J.: A method of analysis of symmetrical four port networks, *IRE Trans. Microwave Theory and Tech.*, vol. MTT-4, pp. 246-252, Oct. 1956.
- [122] Riblet H.J.: General synthesis of quarter-wave impedance transformers, *IRE Trans. Microwave Theory and Tech.*, vol. MTT-5, no. 1, pp. 36–43, Jan. 1957.
- [123] Rosłoniec S.: Liniowe obwody mikrofalowe. Metody analizy i syntezy (in Polish), Wydawnictwa Komunikacji i Łączności, Warszawa, 1999.
- [124] Rotman W., Turner R.F.: Wide-angle microwave lens for line source applications, *IEEE Trans. Antennas and Propagation*, vol. 11, no. 6, pp. 623-632, Nov. 1963.
- [125] Sachse K., Sawicki A., Jaworski G.: Novel, multilayer coupled-line structures and their circuit applications, in Proc. *13th Int. Conf. on Microwaves, Radar & Wireless Communications*, pt. 3 (invited paper), Wrocław, Poland, May 2000, pp. 131-155.
- [126] Sachse K., Sawicki A.: Quasi-ideal multilayer two- and three-strip directional couplers for monolithic and hybrid MIC's, *IEEE Trans. Microwave Theory Tech.*, vol. 47, pp. 1873 – 1882, Sept. 1999.
- [127] Sachse K.: The scattering parameters and directional couplers analysis of characteristically terminated asymmetric coupled transmission lines in an inhomogeneous medium, *IEEE Trans. Microwave Theory Tech.*, vol. 38, no. 4, pp. 417-425, April 1990.
- [128] Sakagami I., Tahara M., Fuji M.: Lumped-element type D branch couplers, in Proc. *Asia-Pacific Microwave Conference*, 2009, pp. 2656-2659.
- [129] Sakagami I.: Derivation of two- and three-branch lumped element codirectional couplers and their frequency characteristics, in Proc. *International Symposium on Circuits and Systems, ISCAS 2005*, pp. 5047-5050.
- [130] Sawicki A., Sachse K.: A novel coupled-line conductor-backed coplanar and microstrip directional couplers for PCB and LTCC applications, *IEEE Trans. Microwave Theory Tech.*, vol. 51, No. 6, pp. 1743 – 1751, June 2003.
- [131] Sawicki A., Sachse K.: Lower and upper band calculations on the capacitance of multi-conductor printed transmission line using spectral-domain approach and variational method, *IEEE Trans. Microwave Theory and Tech.*, vol. 34, no. 2, pp. 236-244, Feb. 1986.
- [132] Schiek B., Kohler, J.A.: A method for broad-band matching of microstrip differential phase shifters, *IRE Trans. Microwave Theory and Tech.*, vol. MTT-25, no. 8, Aug. 1977, pp. 666-671.
- [133] Schiffman B.M.: A new class of broadband microwave 90-degree phase shifters, *IRE Trans. Microwave Theory and Tech.*, vol. MTT-4, pp. 232–237, Apr. 1958.

- [134] Schuberth C., Arthaber H., Mayer M.L., Magerl G., Quay R., van Raay F.: Load pull characterization of GaN/SiGaN HEMTs, *International Workshop on Integrated Nonlinear Microwave and Millimeter-Wave Circuits*, Jan. 2006, pp. 180-182.
- [135] Schwindt R., Nguyen C.: Generalized scattering parameters for two coupled transmission-line structures in and inhomogeneous medium, *Microwave and Optical Technology Letters*, vol. 12, no. 6, pp. 335-342, August 1996.
- [136] Shelton J., Kelleher K.: Multiple beams from linear arrays, *IRE Trans. Antennas Propag.*, vol. 9, no. 2, pp. 154-161, March 1961.
- [137] Shelton J.P., Mosko J.A.: Synthesis and design of wideband equal ripple TEM directional couplers and fixed phase shifters, *IEEE Trans. Microwave Theory and Tech.*, vol. MTT-14, pp. 462-473, Oct. 1966.
- [138] Shen T.M., Chen Ch.R., Huang T.Y., Wu R.B.: Design of lumped rat-race coupler in multilayer LTCC, in Proc. *Asia-Pacific Microwave Conference*, 2010, pp. 798-801.
- [139] Song T.Y., Kim J.H., Kim S.H., Lim J.B., Park J.S.: Design of a novel lumped element backward directional coupler based on parallel coupled-line theory, in Proc. *IEEE MTT-S Int. Dig.*, 2002, pp. 213-216.
- [140] Spirito M., Valk P., Mahmoudi R., de Kok M., Tauritz J.L.: A novel method for characterizing RF automated tuners, *58th ARFTG Conference Digest*, Nov. 2001, pp. 1-6.
- [141] Stec B., Chudy Z., Kachel L.: Eight-port planar Butler matrix using circular interferometers systems, *XVI International Conference on Microwaves, Radar and Wireless Communications MIKON 2006*, Kraków, 2006, vol. 1, pp. 313-316.
- [142] Tang Ch.W., Chen M.G., Wu J.W.: Realization of ultra-compact planar microstrip branch-line couplers with high-impedance open stubs, in Proc. *IEEE MTT-S Int. Microw. Symp. Dig.*, 2007, pp. 995 – 998.
- [143] Tanzi N., Dykstra J., Hutchinson K.: A 1-watt doubly balanced 5 GHz flip-chip SiGe power amplifier, *IEEE Symposium on Radio Frequency Integrated Circuits*, 2003, pp. 141-144.
- [144] Toulios P.P., Todd A.C.: Synthesis of symmetrical TEM-Mode directional couplers, *IEEE Trans. Microwave Theory and Tech.*, vol. MTT-13, no. 5, pp. 536-544, Sept. 1965.
- [145] Tresselt C.P.: Design and computed theoretical performance of three classes of equal-ripple nonuniform line couplers, *IEEE Trans. Microwave Theory and Tech.*, vol. MTT-17, pp. 318–230, Apr. 1969.
- [146] Tripathi V. K.: Asymmetric coupled transmission lines in an inhomogeneous medium, *IEEE Trans. Microwave Theory and Tech.*, vol. MTT-23, no. 9, pp. 734-739, Sept. 1975.
- [147] Tripathi V. K.: Equivalent circuits and characteristics on inhomogeneous nonsymmetrical coupled-line two-port circuits, *IEEE Trans. Microwave Theory and Tech.*, vol. MTT-25, no. 2, pp. 140-142, Feb. 1977.

- [148] Tripathi V. K.: Properties and applications of asymmetric coupled line structures in an inhomogeneous medium, in Proc. *5th European Microwave Conference*, 1975, pp. 278-282.
- [149] Tripathi V. K.: The scattering parameters and directional coupler analysis of characteristically terminated three-line structures in an inhomogeneous medium, *IEEE Trans. Microwave Theory and Tech.*, vol. MTT-29, no. 1, pp. 22-26, Jan. 1981.
- [150] Tripathi V.K.: On the analysis of symmetrical three-line microstrip circuits, *IEEE Trans. Microwave Theory and Tech.*, vol. MTT-25, no. 9, pp. 726-729, Sept. 1977.
- [151] Tsai K.Y., Yang H.S., Chen J.H., Chen Y.J.: A miniaturized branch-line coupler using finger-shape distributed capacitors, in Proc. *Asia-Pacific Microwave Conference*, 2010, pp. 1240-1243.
- [152] Tsironis C., Meierer R., Hosein B., Beauchamp T., Jallad R.: MPT, a universal multi-port tuner, *65th ARFTG Conference Digest*, June 2005, pp. 113-117.
- [153] Tudosie G., Vahldieck R., Lu A.: A novel modularized folded highly compact LTCC Butler matrix, in Proc. *IEEE MTT-S Int. Microw. Symp. Dig.*, 2008, pp. 691 – 694.
- [154] Tung W.S., Chiang Y.C.: Wide-band lumped-element directional coupler with an arbitrary coupling coefficient, *IEE Proceedings – Microwaves, Antennas and Propagation*, vol. 151, no. 4, pp. 303-306, August 2004.
- [155] Turalchuk P., Munina I., Kapitanova P., Kholodnyak D., Stoepel D., Humbla S., Mueller J., Hein M.A., Vendik I.: Broadband small-size LTCC directional couplers, in Proc. *40th European Microwave Conference*, 2010, pp. 1162-1165.
- [156] Uehara K., Seki T., Kagoshima K.: A planar sector antenna for indoor high-speed wireless communication terminals, *IEEE AP International Symposium Dig.*, vol. 2, pp. 1352-1355, July 1997.
- [157] Vogel R.W.: Analysis and design of lumped- and lumped-distributed-element directional couplers for MIC and MMIC applications, *IEEE Trans. Microwave Theory and Tech*, vol. 40, no. 2, pp. 253-262, Feb. 1992.
- [158] Wincza K., Gruszczyński S., Sachse K.: Conformal four-beam antenna arrays with reduced sidelobes, *Electronics Letters*, vol. 44, no. 3, pp. 174-175, Jan. 2008.
- [159] Wincza K., Gruszczyński S., Sachse K.: Design of integrated stripline multibeam antenna arrays fed by compact Butler matrices, *IEEE AP International Symposium*, Honolulu, USA, 2007.
- [160] Wincza K., Gruszczyński S., Sachse K.: Improved multilayer crossover for Butler matrix applications, in Proc. *XVI International Conference on Microwaves, Radar and Wireless Communications MIKON 2006*, Cracow, Poland, May 22-24, 2006.
- [161] Wincza K., Gruszczyński S., Sachse K.: Integrated four-beam dual-band antenna array fed by broadband Butler matrix, *Electronics Letters*, vol. 43, no. 1, pp. 7-8, Jan. 2007.

- [162] Wincza K., Gruszczyński S., Sachse K.: Investigations on a strip transmission-line cross-over for Butler matrix applications, *13th Conference on Microwave Techniques – COMITE 2005*, Prague 2005.
- [163] Wincza K., Gruszczyński S., Sachse K.: Reduced sidelobe four-beam antenna array fed by modified Butler matrix, *Electronics Letters*, vol. 42, no. 9, pp. 13-14, April 2006.
- [164] Wincza K., Gruszczyński S.: A Broadband 4x4 Butler matrix for modern-day antennas, in Proc. *35th European Microwave Conference*, Paris, France 2005.
- [165] Wincza K., Gruszczyński S.: Method for the design of low-loss suspended stripline directional couplers with equalized inductive and capacitive coupling coefficients, *Microwave and Optical Technology Letters*, vol. 51, no. 2, pp. 315-319, Feb. 2009.
- [166] Wincza K., Gruszczyński S.: Miniaturized quasi-lumped coupled-line single-section and multi-section directional couplers, *IEEE Transactions on Microwave Theory and Techniques*, vol. 58, no. 11, pp. 2924-2931, Nov. 2010.
- [167] Wincza K., Gruszczyński S.: Three-section symmetrical 3-dB directional coupler in microstrip multilayer technology designed with the use of multi-technique compensation, *Microwave and Optical Technology Letters*, vol. 51, no. 4, pp. 902-906, April 2009.
- [168] Wincza K., Sachse K.: Broadband 4x4 Butler matrix in microstrip multilayer technology designed with the use of three-section directional couplers and phase correction networks, in Proc. *XVIII International Conference on Microwaves, Radar and Wireless Communications MIKON 2010*, Vilnius, Lithuania.
- [169] Wincza K.: Planarne i konforemne układy antenowe z macierzą Butlera jako siecią formowania wielu wiązek. Analiza, projektowanie i badania eksperymentalne (in Polish), *Ph.D. Thesis, Wroclaw University of Technology*, Wroclaw 2007.
- [170] Withers M.J.: Frequency-insensitive phase-shift networks and their use in a wide bandwidth Butler matrix, *Electronics Letters*, vol. 5, no. 20, pp. 496-498, Oct. 1969.
- [171] Wojtasik W., Gruglewski D., Sędek E.: The 100W class A power amplifier for L-band T/R module, in Proc. *XIII International Conference on Microwaves, Radar and Wireless Communications MIKON 2000*, Poland, 2000, pp. 675-677.
- [172] Xiang Z., Xue-guanin L., Hui-ping G., Lv-xia S.: Design of broadband impedance transformers using coupled microstrip transmission lines, in. Proc. *3rd IEEE International Symposium on Microwave, Antenna, Propagation and EMC Technologies for Wireless Communications*, 2009, pp. 994-997.
- [173] Yamamoto S., Azakami T., Itakura K.: Coupled nonuniform transmission line and its applications, *IEEE Trans. Microwave Theory and Tech.* vol. 15, no. 4, pp. 220 – 230, April 1967.
- [174] Yamasaki J., Ohta I., Kawai T., Kokubo Y.: Design of broadband semi-lumped and lumped element quadrature hybrids, in Proc. *IEEE MTT-S Int. Microw. Symp. Dig.*, 2005, pp. 1247 – 1250.

- [175] Zajdel A., Gruszczyński S., Laska W. Kampa J.: High-power L-band pulse amplifier, in Proc. XV Int. Conf. on Microwaves, Radar & Wireless Communications MIKON-2004, Warsaw, Poland.
- [176] Zak T., Sachse K.: An integrated Butler matrix in multi-layer technology for multi-port amplifier applications, in Proc. 14th International Conference on Microwaves, Radar & Wireless Communications, vol. 1, Gdansk, Poland, May 2002, pp. 59-62.
- [177] Zhou Y., Chen Y.: Lumped-element equivalent circuit models for distributed microwave directional couplers, in Proc. International Conference on Microwave and Millimeter Wave Technology ICMMT, 2008, pp. 131-134.
- [178] Schiffman B.M.: Multisection microwave phase-shift network, *IEEE Trans. Microwave Theory and Tech.* vol. 14, no. 4, pp. 229, April 1966.
- [179] Wincza K. Gruszczynski S.: Asymmetric coupled-line directional couplers as impedance transformers in balanced and n-way power amplifiers, accepted for publication in *IEEE Transactions on Microwave Theory and Techniques*.